Department of Precision and Microsystems Engineering

Development of a universal cryogenic test facility

N. Malik

Report no : 2021.034
Coach : C. Ayas
Professor : A. van Keulen
Specialisation : Engineering Mechanics
Type of report : Msc Thesis
Date : 21 June 2021

Development of a universal cryogenic test facility

N. Malik

Development of a universal cryogenic test facility

by

N. Malik

to obtain the degree of Master of Science
at the Delft University of Technology,
to be defended publicly on Date 21 June 2021.

Student number:	4334302	
Project duration:	March 1, 2017 – December 31, 2017	
Thesis committee:	Prof. dr. ir. A. van Keulen,	TU Delft, supervisor
	dr. C. Ayas,	TU Delft, coach
	dr. ir. R.A.J. van Ostayen,	TU Delft, committee member

An electronic version of this thesis is available at `http://repository.tudelft.nl/`.

TU Delft

Abstract

Magnets for High Energy Physics applications built to date are generally superconducting magnets, which operate at cryogenic temperatures. The reliability and safety of the applications are entirely dependent on good design which in turn rely heavily on predictable materials performance. Where at these low temperatures the fracture toughness is of importance to be known (along side mechanical properties such yield and tensile strength). At CERN at the materials and engineering department (EN-MME-MA) a testing facility is being commissioned for the measurement of mechanical at cryogenic temperatures. A tensile test facility has been realised, yet no such set-up is available for fracture toughness measurement.

The aim of this thesis was to develop a test set-up for the measurement of the fracture toughness in order to realise a universal cryogenic testing system, which can be used for both tensile tests and fracture toughness test at low temperatures.

A design for a set-up is proposed for the measurement of the fracture toughness which can be employed within the current cryostat. The design of the tooling and cryostat have been extensively verified using numerical methods taking into account thermal effects (such as conduction and contraction) and the varying material properties at these low temperatures. A modified C(T) specimen is proposed for more robust and reliable set-up. For this modified specimen it is shown with numerical methods that the modification are expected to have a negligible impact on the fracture toughness measurements.

Tests have been performed using the proposed design with four specimen fabricated from two different materials (SS316L and Ti6Al4V), at both room temperature and at 4 K (using liquid helium). The set-up is shown to provide sufficient data for the characterisation of the fracture toughness for both Linear Elastic Fracture Mechanics tests as well as Elastic Plastic Fracture mechanics tests.

Preface

The work of this project will be performed as a fulfilment to the final requirements of the master programme Mechanical Engineering at the TU Delft (faculty 3ME). The project is an assignment from CERN to expand on previous work by adding additional functionality to the current cryogenic tensile test facility.

This document contains the general outline for the design and validation of the universal cryogenic testing system. The goal of the project is to add the functionality to perform fracture mechanics test within the current cryostat at cryogenic temperatures. The current functionality of the cryostat is limited to tensile tests which are typically performed at 4.2 K (boiling point liquid helium).

My gratitude goes out to all the people who've aided me, showed support and extraordinary patience. In particular I'd like to express my gratitude to my two supervisors ir. S. Langeslag & dr. I. Avilles, from the materials section of CERN (EN-MME-MA), and my thesis supervisor at the TU delft prof.dr.ir A. van Keulen.

N. Malik
Delft, May 2020

Contents

1 Introduction

1.1. Project background

With the exception of a few small developmental magnets, all usable magnets for High Energy Physics applications built to date have used the low temperature, high field, Type II superconducting materials. These magnets usually operate at a fixed temperature, depending on it's critical characteristics; generally below the boiling point of liquid helium 4.2 K[27]. These low temperatures are necessary to guarantee the superconducting state of the material, and with that achieve the high magnetic fields required for the application.

These low temperatures required for the application pose significant challenges, materials behaviour is impacted with material properties diverging significantly from those found at room temperature. The reliability and safety of an applications can be assured with a good design which in turn rely heavily on predictable materials performance. Material properties such as the Young's modulus, yield stress, tensile strength and ductility are some of the general mechanical properties used to describe the behaviour of a material, and can be found to be significantly impacted at cryogenic temperatures. With some material exhibiting extremely brittle behaviour for instance. Design of components suited for the loads and conditions subjected to it are dependent on know quantities of these properties. During fabrication processes or under operating conditions a crack like flaw can occur, for a reliable design the behaviour of material in the presence of such a flaw; i.e. the 'fracture toughness' is also necessary to be known.

Within the Mechanical & Materials Engineering -Metallurgy and Metrology section (EN-MME-MM) at CERN, a novel cryogenic testing system has recently been commissioned. The cryogenic tensile testing apparatus is however currently only designed for tensile testing. The measurements of fracture mechanics is a desired additional capability for the cryogenic testing system. In order to perform fracture mechanics tests using the current cryostat a sub-system was designed, verified (using analytical methods and simulations) and subsequently fabricated. The structural components have been verified for the various conditions arising during tests.

1.2. Project goal

The goal of the project is: *the design of a fracture mechanics test facility which can be implemented within the current cryogenic tensile test facility* . The project goal is divided into the following sub-goals:

1. Development, including concept design, final design and production, of an in-house Fracture Mechanics test facility at cryogenic temperatures integrated into the existing tensile system.
   (development of a cryogenic fracture mechanics testing sub-system)
   (a) Design work of the sub-system; specimen, tooling and set-up for measurement system.
   (b) Verification of the design and current cryogenic test facility
   (c) Initiation and monitoring of the production of the designed components.
   (d) Assembly and integration/installation of the sub-system in the testing facility.
2. Validation according to standards, and commissioning of the novel universal test facility.
3. Development of an experimental protocol for standardized fracture toughness measurements at cryogenic temperatures.

1.3. Outline

The materials to be tested are for the purposes of this thesis limited to FCC (such as Austenitic steels) which have excellent ductility and fracture toughness even at cryogenic temperatures, and HCP (such as titanium alloys) which also retain ductile behaviour at cryogenic temperatures (to an extend). Some of these material perform even better at cryogenic temperatures than at room temperature; the expected test loads could be higher than those found for room temperature tests. The limited space and enclosed environment of the cryostat combined with the poses additional constraint on the design of the specimen, tooling and measurement set-up. An additional constrain can be found in the cooling capacity of the coolant available during tests.

The design of the tooling and specimen as described in chapter 2 is set out to take in to consideration these challenges. As a first step the load is estimated using the force displacement curves or maximum load recorded for test results available in literature, wherein materials with high toughness are tested at cryogenic temperatures.

Using these loads the stresses in the design proposed are calculated using analytical methods (section 2.4); showing high stresses in the design. These high stresses are detrimental for the reliability of the set-up, with possible failure of one or more parts upon use, or at the very least significantly limiting the number of test that can be performed before failure can be expected. In addition the plastic deformation caused by these high stresses can also be a source of error in the measurements, where in the instance of the compliance method this deformation can result in a perceived negative crack growth when inferring the crack length[26].

In order to take into account the possibly high stresses a number of design iterations have been performed resulting in the design as proposed in section 2.6, where:

1. In order to limit the stresses and by doing so ensuring the safety and reliability of the set-up a modified design is proposed; which was based on the recommended design from standards. The geometry of the specimen modified at to ensure sufficient strength at the pinned connection. A comparison study is performed to investigate the effect of this modification with regards to the increase in stiffness of the modified specimen with the two standard specimen proposed in the standard ASTM E1820[9] section 3.1.
2. In order to accommodate this modified specimen and the standard specimen geometries whilst ensuring proper alignment with regards to the load application on the specimen a modification of the testing clevis is proposed and implemented. A design verification using a combination of analytical methods and a finite element analysis is performed for the final design of the tooling with the specimen and is included in section 3.2. In addition to verifying the tooling for the estimated load the maximum test load for the tooling is determined.
3. As a proof of concept a total of four tests have been performed using the modified specimen with: two specimen fabricated from Titanium grade 5, and two from Stainless steel 316LN. The tests and interpretation of the test results are included in chapter 4.

1.4. Mechanics and testing methods

In this section a brief introduction is provided for the underlying theory and general testing methods. For a more detailed examination of the theory and testing methods refer to the literature study [17], and the references listed therein (such as [13], [15])

1.4.1. Fracture mechanics

In fracture mechanics two different approaches can be considered: Linear Elastic Fracture Mechanics (LEFM), and Elastic Plastic Fracture Mechanics (EPFM). Where LEFM is well detailed in literature with ample analytical solutions for the stress intensity factor at the crack for a range of loading conditions (example in Figure 1.1). For different crack sizes and specimen geometries see for instance the book by Anderson et al.[6], or Janssen et al.[15]. On of the main disadvantage of LEFM being that it is mainly suited for relatively brittle materials; where no more than small scale yielding occurs. For materials where LEFM is not suited EPFM can allow for a determination of the fracture toughness; taking into account the plasticity at the crack tip.

Within LEFM there are different approaches to determine the fracture toughness:

- Stress intensity approach or energy criterion, which are equivalent for linear elastic materials[6]. (Critical crack extension leading to failure)
- Fatigue Crack Growth Rate

(Incremental crack growth under the influence of cyclic loading)

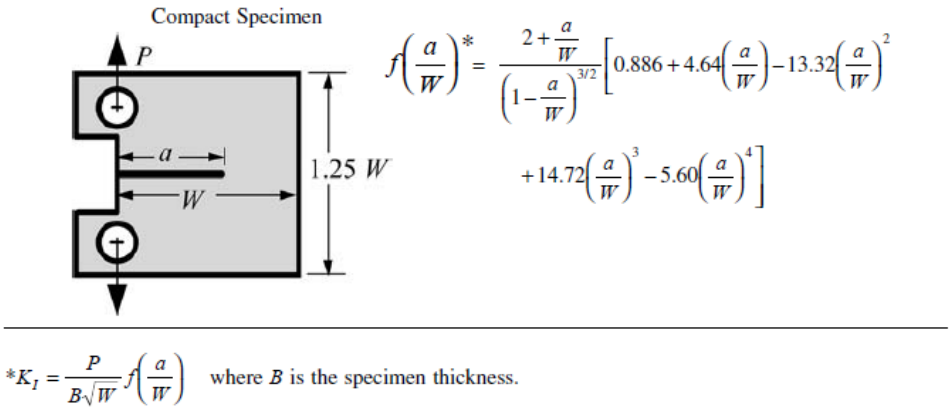

Figure 1.1: Analytical solution for the stress intensity factor (KI) for a compact tensile specimen (C(T)) [6]

Where with EPFM plasticity at the crack tip is considered, making it a suitable method for materials that do not meet the requirements of LEFM. Within EPFM the fracture toughness is typically defined terms of:

- J-integral
- CTOD

The CTOD and the J-integral are both quasi static approaches, and have a unique relationship; both parameters are equally valid and can be considered interchangeable[24]. The EPFM method is however slightly more complex than that of LEFM. The J-integral for instance takes into account the plasticity stored at the crack tip by integrating along a contour as shown in Figure 1.2. This contour needs to be shown to capture all of the plastic behaviour; calculations would need to be repeated with larger contours until the solution converges (as shown using the numerical method in appendix C).

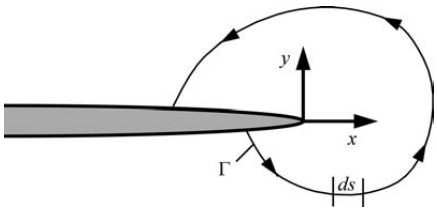

Figure 1.2: Arbitrary integral contour drawn around the crack tip to determine the energy involved with the progression of the crack[6]

Plane stress–strain relation

Regardless of the testing method involved all typically have a requirement with regards to the thickness of the specimen. As most of the methods require complete plane-strain behaviour for the measured value to be considered thickness independent. This as the toughness measured for a plain stress situation can differ from the actual material toughness as illustrated in Figure 1.3.

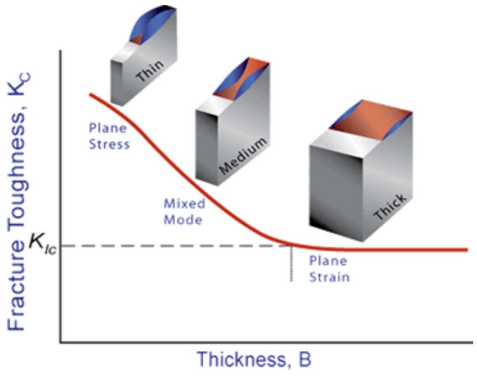

Figure 1.3: Fracture toughness w.r.t. the thickness (image from www.nde-ed.org)

1.4.2. Testing specimen

There are a number testing methods that can be used to determine the toughness depending on the mechanics involved (for both LEFM and EPFM 1.4.1). For the different testing methods a number of specimen geometries are suggested in literature (for example those depicted in Figure 1.4), where certain specimen can be used only for a specific method and some for different testing methods.

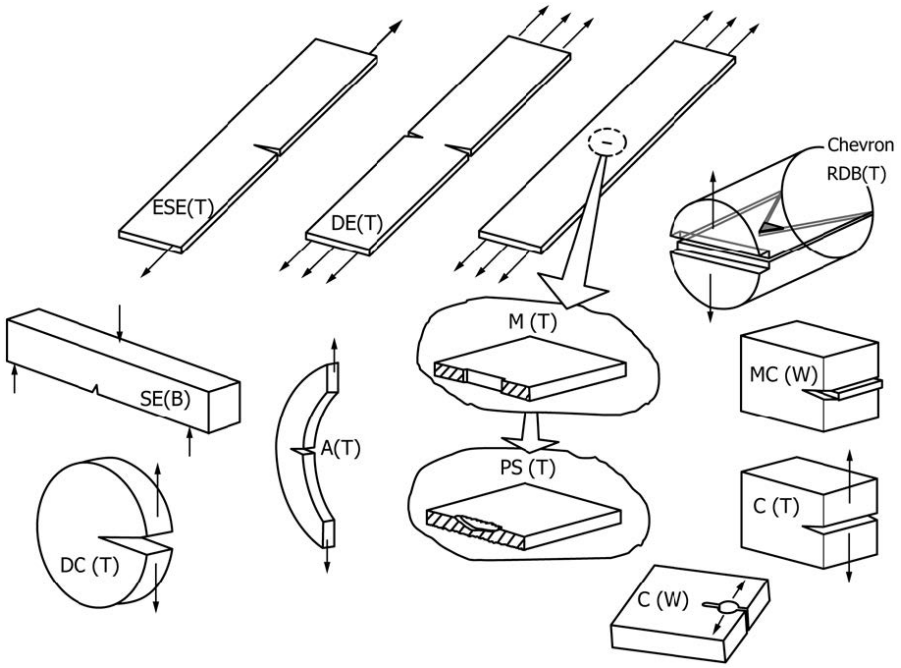

Figure 1.4: Specimen geometries (From ASTM-1823[10])

ESE(T): Eccentrically-loaded Single Edge notched (Tension)
DE(T): Double Edge notched (Tension)
M(T): Middle notched (Tension)
PS(T): Part-Through Surface notched (Tension)
Chevron RDB(T): Round Double Beam with Chevron notch (Tension)
SE (B): Single Edge (B)
A(T): Arc (Tension)
DC(T): Disk-Shaped Compact (Tension)
C(T): Compact (Tension)
C(W): Compact (Wedged)
MC(W): Modified Compact (Wedged)

For instance in the testing method used for the determination of the fracture toughness in as described by the J-integral method and the CTOD[9] method, the recommended specimen are:

- Single Edge Bend specimen, SE(B)
- Compact Tensile specimen, C(T)

- Disk-Shaped Compact specimen, DC(T)

Whereas a standard describing the methods typically used to determine the FCGR[12] recommended specimen are:

- Compact Tensile specimen, C(T)
- Middle-Tension specimen, M(T)
- Eccentrically-Loaded Single Edge Crack Tension specimen, ESE(T)

1.4.3. Methods for measurement

Measurement of the fracture toughness can be achieved using a number of measurements. In general the fracture toughness is measured by the load and extension of the crack, both for quasi static methods and dynamic methods. In the case of the critical fracture toughness measurement as described in LEFM, only the initial crack length and load is required. Whereas in the case of the fatigue crack growth rate or the J-test a measurements of the progression of the crack is required. In the case of the J-test the load-line displacement is also required in order to compute the plastic energy under the influence of the increasing load as the crack progresses.

The load is typically measured using a load cell, yet the progression of the crack can be measured using different methods. The most commonly used method to measure the progression of the crack are the potential difference method (EPDM) and the compliance method, which are both supported in standards[9][11].

The EPDM method measures the progression of the crack based on the electric potential difference between the measurement points on either side of he crack with a current applied to the specimen between these two points (as illustrated in Figure 1.5 for the C(T) specimen). As the crack progresses the resistance of the specimen increases due to the reduction of the surface where the current can be conducted, resulting in an increase of the potential difference.

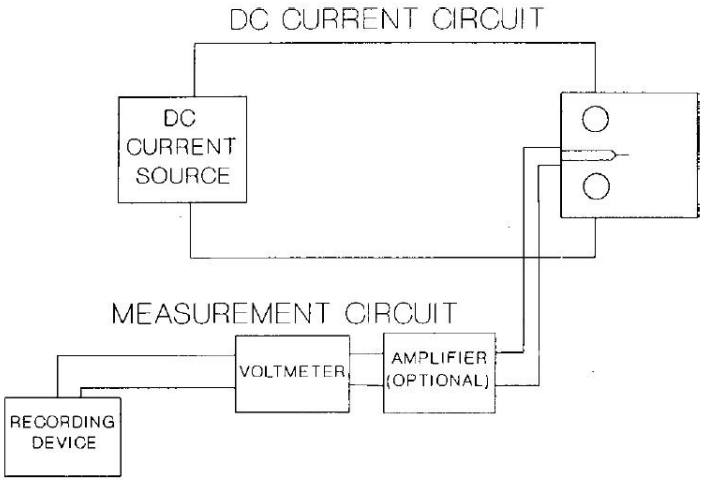

Figure 1.5: Electric potential difference method set-up with DC current source on a C(T) specimen[12]

The compliance method can be used to determine the length of the crack by the change of the compliance (or stiffness) of the specimen. This change of stiffness is measured with a partial unloading and loading cycle, where the load and displacement are then used to compute the compliance at a point in the measurement, as illustrated in Figure 1.6 by the partial unloading present in the force displacement curve. Depending on the specimen selected the compliance method can be implemented with relative ease, especially for specimen where the load-line displacement and the crack opening displacement are the same such as for instance the C(T) specimen. In the case of a J-test with a C(T) specimen this would imply that only 2 sensors are required: a load sensor and a sensor to measure the crack opening displacement, allowing for a relatively simple design.

Aside from the previously discussed methods there are a few other available methods. One of these other methods is the acoustic method, which infers the progression by recording the acoustic emissions that occur as the crack progresses. The acoustic method though promising is still mostly experimental and not yet very suited for implementation with standardized test methods, and this is the case with most other methods available.

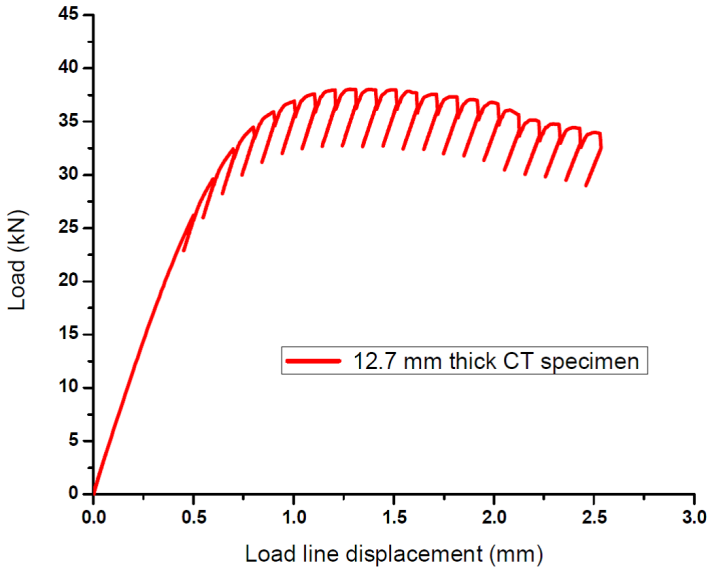

Figure 1.6: partial unloading compliance method[12]

1.4.4. Pre-crack

The initiation of the crack (or pre-cracking) is realised using Fatigue Crack Growth Rate(FCGR); using cyclic loading to "grow" initial crack. This initial crack is then used as a point of origin for various type fracture toughness tests. Generally two different schemes can be used for the initiation of a crack: a force controlled, and a displacement controlled scheme, also known as K-increasing and K-decreasing respectively.

With a force controlled crack initiation the Stress intensity factor or K increases as the crack progresses(see Figure 1.1). A force controlled scheme where a constant alternating force is applied to the specimen is suitable for the initial growth of a crack, yet as the crack progresses the stress intensity factor at the crack tip increases and rapid growth might occur if left unmonitored. With a displacement controlled initiation the K at the crack tip decreases as the crack progresses, the stiffness of the specimen is reduced from the initial situation. The force and resulting K reduces as the crack "grows" under the influence of the constant (varying relative) displacement of the load line. This allows for a controlled crack growth with a relatively straight crack front[9], with relatively little initial plasticity at the crack tip. In practice a combination of the two method is used, a K-increasing method for the rapid initiation of the crack, and a K-decreasing method for a controlled crack growth[13].

1.4.5. Cryogenics

As briefly discussed in order to reach the low temperature for certain applications a cryogenic coolant is required. There are a wide range of coolants available and the working principle is typically making use of the boiling point of a liquefied gas[13], see Table 1.1 for commonly used coolants and boiling points. The boiling point for these coolants differ, at atmospheric pressure the boiling point of liquid nitrogen is approximately 77 K[8][13], where the boiling point of liquid helium is at approximately 4 K (for He4 [8][13]) again at atmospheric pressure. In order to reach lower temperatures than the boiling points a coolant can be supercooled. Lowering the temperature can be achieved by using either a requiring a second coolant with a lower boiling point, or by lowering the pressure (see Figure 1.7). Using a vacuum pump the boiling temperature of liquid helium can for instance be lowered close to absolute zero (Helium 3 [8][13]). In certain application the coolant temperature is lowered both to ensure sufficient cooling and in the case of liquid helium to achieve a super-fluid state (He4[25]). In this state near frictionless flow can be achieved allowing the coolant for instance to permeate through magnetic coils resulting in a larger cooling surface and higher cooling capacity (due to the increased flow).

Table 1.1: Properties of cryogenic liquids [14]

	Oxygen	Nitrogen	Hydrogen	Helium-4	Air	Argon
Normal boiling point (K)	90.18	77.35	20.27	4.224	78.9	87.28
Density (kg/m^3)	1141.0	808.9	70.78	124.96	874.0	1403.0
Heat of vaporization (kJ/kg)	212.9	198.2	445.6	20.73	205.1	161.6
Specific heat (kJ/(Kg·K))	1.70	2.04	9.78	4.56	1.97	1.14
Viscosity (kg/(m·s) $\times 10^{-6}$)	188.0	157.9	13.06	3.57	167.0	252.1
Thermal conductivity (mW/(m·K))	151.4	139.6	118.5	27.2	141.0	123.2
Critical temperature (K)	154.58	126.20	32.98	5.201	133.3	150.7
Critical pressure (MPa)	5.04	3.40	1.29	0.227	3.90	4.87
Temperature at triple point (K)	54.35	63.15	13.80			83.8
Pressure at triple point (MPa)	0.151	12.53	7.042			68.6

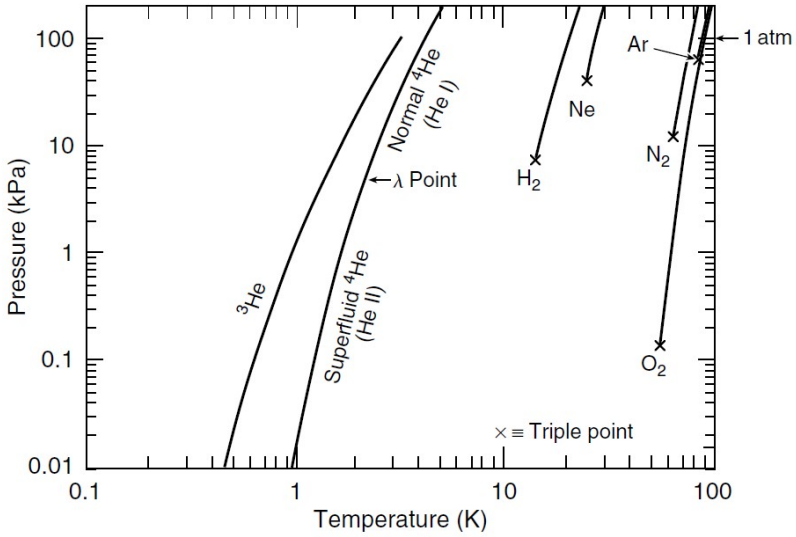

Figure 1.7: Boiling temperatures of commonly used cryogenic coolants [13]

Low temperatures can be achieved by using the boiling point of these coolants, but this also poses a challenge. As more heat is dissipated into the coolant the boiling will become more violent and thermal conductivity at the interface is reduced (as illustrated in Figure 1.8), which in turn can results in large increases in temperature due to low thermal capacity of materials close to absolute zero. Ideally the boiling is to be limited to the convective boiling. yet due to the low thermal flux at this regime nucleate boiling is expected to be nearly unavoidable. Fully developed film boiling should be avoided as specimen temperature can be inferred to be significantly higher than the desired testing temperature (with a delta T that can be over 10 degrees higher) as well as potential source of noise in the measurements.

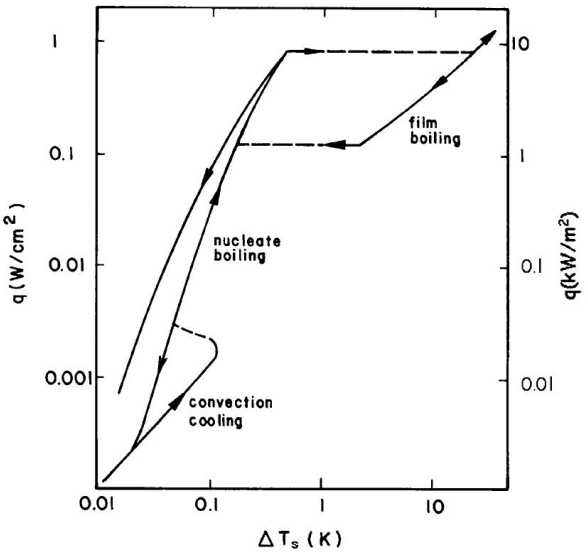

Figure 1.8: Typical heat transfer relationship for pool boiling liquid [25]

2

Design

This chapter contains an overview of the design process of the specimen and tooling based on the recommendation from various standards. Taking into account the design space, strength requirements, required measurements and testing conditions. As the most onerous test loads can typically be expected for the quasi static testing methods this was used as the initial starting point for the design, yet while still attempting to allow the design to be suitable for other tests such as FCGR test. The test load is estimated based on available test results from literature and a design for the specimen and tooling is proposed based on the expected loading and validity requirements.

2.1. Boundary

As mentioned in the introduction the sub-system is to be designed to function within the current cryogenic tensile test set-up. The current system is comprised of a cryostat (Figure 2.2) which is mounted in a tensile test machine as shown in Figure 2.1.

The total design space can be considered limited to the inside diameter of the dewar (Figure 2.3) up to the baffle plates (Ø173x440 mm). With additional limitations posed by the internal support structure (Figure 2.4). Any components designed would need to fit between the columns of the structure where the available space is 51.3 mm. Additionally the bounding cylinder of any assembly inside the columns should be limited to the diagonal of 85 mm (as seen for the tooling for the tensile test in Figure 2.3).

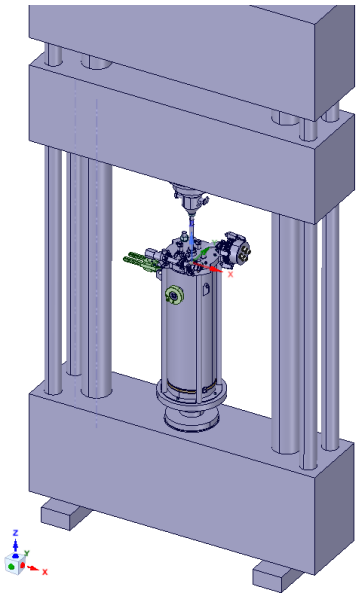

Figure 2.1: Cryostat in tensile test bench

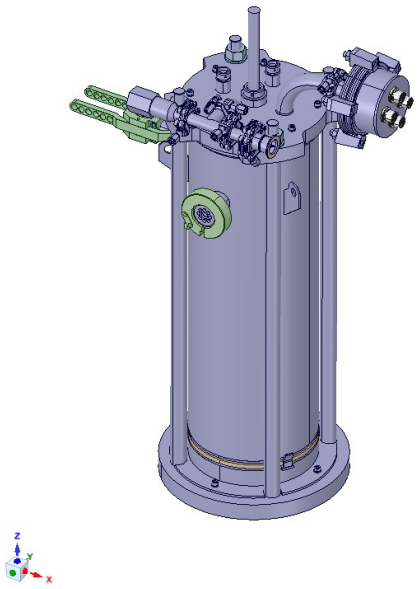

Figure 2.2: Cryostat with external support frame

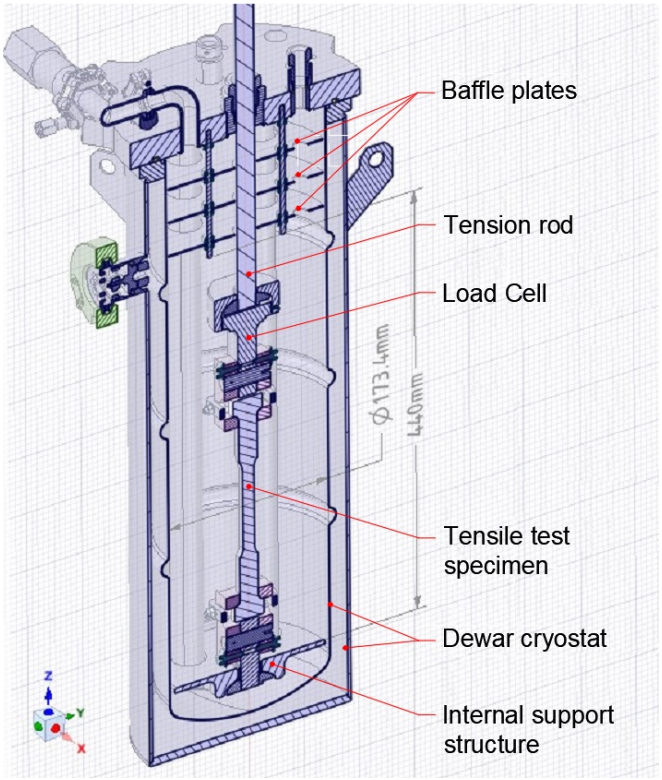

Figure 2.3: Cross section of the cryostat with tensile specimen

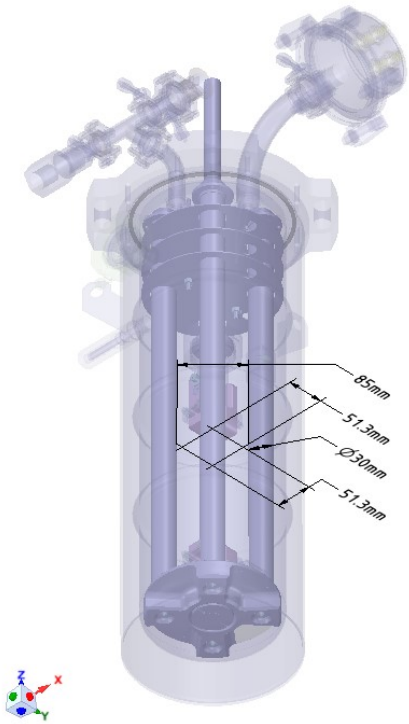

Figure 2.4: Internal support structure

2.2. Specimen and tooling

2.2.1. Specimen

There are a number of different specimen geometries suggested in standards, with consideration to: the testing method, loading conditions and material properties (as briefly discussed in subsection 2.2.1). Of these specimen the compact tensile specimen (C(T)) can be used for a number of tests, with the added benefit that it can be easily implemented in the current test bench. This specimen is relatively compact and allows for a direct measurement of the load-line displacement (as opposed to the indirect measurement on for instance the Side Edge Bend specimen SE(B)). The C(T) specimen can be applied for a range of tests (subsection 1.4.1), such as FCGR and allowing for measurement of the fracture toughness both for LEFM and EPFM.

The compact geometry of the specimen also limits the coolant required for the initial cooling of the specimen (due to the relatively low mass). Where the compact size of the specimen should allow for the design of a set-up inside the limited design space (section 2.1).

The typical geometry of a C(T) specimen are given all in relation to a characteristic dimension "W", as illustrated in Figure 2.5. Where the basic geometry is defined for two different relative pin diameters in relation to W. The characteristic dimension "W" is dependent on the materials to be tested; a minimum thickness is required to obtain a thickness independent characterisation of the fracture toughness. The basic geometry of a C(T) sample are given by the characteristic dimension "W" and the thickness "B", where the thickness "B" is typically $W/2$ or satisfies the condition $2 \leq W/B \leq 4$[9]. The size of the specimen is determined in subsection 2.2.2, by designing the specimen based on some of the relatively tougher materials with high yield the size requirements are met for a range of materials.

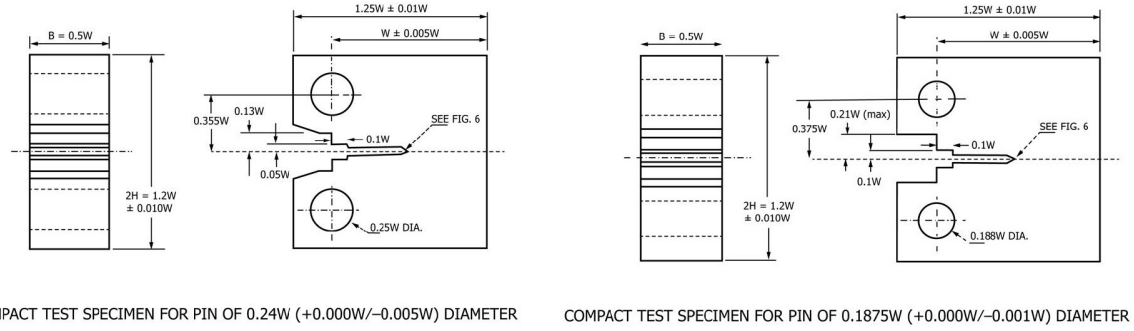

Figure 2.5: Specimen geometries in relation to relative pin diameter[9]

Testing clevis The geometry for the testing clevis with tolerances are given in the standard (see Figure 2.1) in relation to the characteristic dimension "W" of the sample, as shown in Figure 2.5. The tension testing clevis is a general piece of tooling which can be used to apply tension to the specimen. The clevis can be used for a pinned tension specimens, such as the Arc Tension AC(T), The Disc shaped Compact tension DC(T) or in this case the Compact Tension C(T) specimen (specimen and others as shown in 1.4.2). For these specimen tension is applied in a tests such as a FCGR test (cyclic) or a Stress intensity test (steadily increasing load). The design of the testing clevis for the existing set-up is discussed in more detail in subsection 2.4.2.

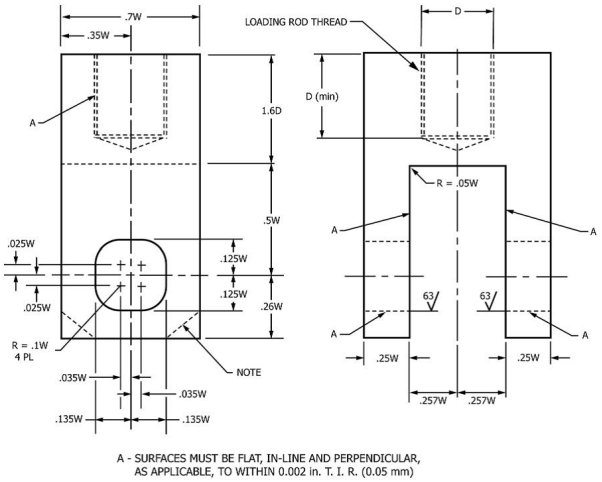

Figure 2.6: Tension testing clevis[9]

2.2.2. Geometry

The geometry of both the specimen and the tooling are defined in relation to a parameter W. This parameter can be can be chosen within a range as long as certain requirements are met, such as the required thickness of the sample and the ligament length. In subsection 2.2.1 the thickness of the specimen is defined as $0.5W$, yet in the standard a relation between the thickness (B) and size (W) is specified as $2W \geq B \geq 4W$. With an additional requirement on the thickness such to ensure a thickness independent measurement of the fracture toughness as specified in section A.9[9]:

The thickness of the specimen (B see Figure 2.5) and the initial ligament length b_0 need to fulfil the relation shown in Equation 2.1. The initial ligament length is related to the size (W) of the sample and the length of the pre-crack (a_0); $b_0 = W - a_0$. This requirement can be related to the size of the plastic area in relation to the ligament, where the plastic area is required to be significantly smaller than the length of the ligament. In general this should be valid for any specimen with sufficient thickness, where $B \geq W/2$ with the length of the pre-crack $a_0 = 0.45W$. In the case of larger pre-cracks closer to the upper limit of $0.45 \leq a_0 \leq 0.70$, this only holds if $B \geq W/3.33$ (where $b_0 = 0.3W$).

As for the thickness of the specimen an estimate of the toughness (J_Q) and yield stress (σ_y) are required, or the validity of the test is to be verified for an assumed thickness using the test results. With the valid-

ity requirement specified by the standard to ensure a plane-strain toughness measurement of the fracture toughness (see also subsection 1.4.1).

$$B, b_0 \geq 10\ {}^{J_Q}/_{\sigma_y} \tag{2.1}$$

For the purposes of the design, material groups which have shown to have excellent material properties at cryogenic temperatures in literature are used with conservative margins to provide an estimate for the thickness. These materials (generally metals with an FCC crystal structure) are relatively tough materials, with a high yield stress at cryogenic temperatures while still maintaining ductile behaviour (as opposed to the typical brittleness one might expect at these temperatures). A small selection of these materials such as Austenitic steel 316 (FCC) and Titanium grade 5 (BCC) and their respective properties are listed in Appendix G.

For these materials the yield stress is higher at lower temperatures than that specified at room temperature. The actual material properties are depending on a number of factors such as: heat treatment, variation in alloy and fabrication methods. The materials used for the initial design are shown to range between 500-1200 MPa (as illustrated in for instance Sas et al. [23]), with the J_Q toughness ranging between 200-420 N/mm[20].

Using these material values in combination with 2.1 an estimate on the required thickness for a specimen can be calculated:

$$B \geq 10 \times {}^{420}/_{500} \tag{2.2}$$

The minimum required thickness for the specimen is 8.4 mm. To allow for side grooves the thickness of the specimen is chosen as 10 mm.

2.3. Load estimate

The expected test load is estimated from documented tests, in the paper from Nyalis et al. [20] a load-displacement graph is provided for an C(T) specimen with W = 36mm and B = 4mm. The highest load documented is approximately 8 kN, using this the maximum load for a sample with a thickness of 10 mm is estimated.

For convenience the parameter W is chosen the same, which is in the upper bounds of the allowable specimen size with $W/2 \leq B \leq W/4$ (subsection 2.2.1). Where in this case $B \approx W/3.6$, and as this satisfies $B \geq W/3.33$ (from subsection 2.2.2) this allows for the validity requirements as stated in Equation 2.1 to be met with regards to the remaining ligament (b_0) length for any pre-cracked specimen with $0.45 \leq a_0 \leq 0.70$ meeting the thickness requirement.

The stress intensity factor (SIF) in the specimen can be considered to be primarily attributed to the tensile and bending stress in the specimen, where the SIF at which failure occurs is material dependent. In general the effects at the crack tip are required to be relatively small; the behaviour of the remaining ligament is expected to be primarily elastic. As such the behaviour at the crack tip is considered negligible with respects to its elastic behaviour for samples with similar material properties and toughness. As such the simplification of the stress state in the specimen as shown in Figure 2.7 is used for the estimate of the load.

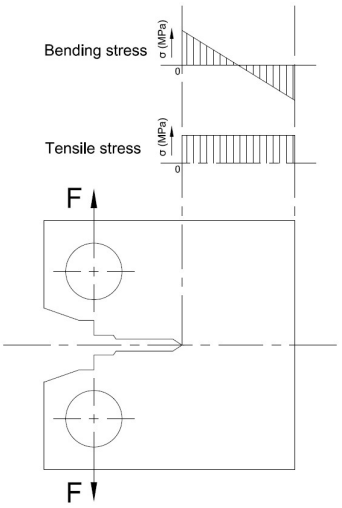

Figure 2.7: Stress in specimen

The stresses are shown in the area of the specimen along the remaining ligament b_0, and are for convenience considered constant along the thickness (B). The stresses in the specimen can be expressed in terms of: the load F, thickness B and ligament b_0. With the tensile stress σ_T and σ_B as shown in Equation 2.3 and 2.4 respectively. A linear relation can be discerned with regards to the thickness B with both the tensile and bending stresses. For the remaining ligament b_0 the contribution is somewhat more difficult to discern; with a linear relation with regards to the tensile and what can be considered a quadratic relation with the bending stress. Conservatively the relation is considered completely quadratic with regards to b_0.

$$\sigma_T = \frac{F}{B \cdot b_0} \tag{2.3}$$

$$\sigma_B = \frac{F \cdot (W + \frac{1}{2} b_0)}{\frac{1}{12} \cdot B \cdot b_0^3} \tag{2.4}$$

The crack size at which the J-test was performed was at $a \approxeq 0.5W$ (remaining ligament $0.5W$). For a specimen with a similar size pre-crack and assuming an linear relation between the load and the thickness of the specimen. An initial estimate of the load based on solely the thickness can be calculated as shown in Equation 2.5.

$$8\,\text{kN} \cdot {}^{10\,\text{mm}}/_{4\,\text{mm}} = 20\,\text{kN} \tag{2.5}$$

The minimum crack size at which at J-test is to be performed is at $a_0 = 0.45W$ (ligament $b - 0 = 0.55W$). With the assumed quadratic relation between the remaining ligament and the load, the resulting in a maximum load which is to be expected is 24 kN (as calculated in Equation 2.4).

$${}^{(0.55}/_{0.5)^2} \cdot 20\,\text{kN} = 24.2\,\text{kN} \tag{2.6}$$

2.4. Design considerations

2.4.1. Initial design calculations

For the specimen (Figure 2.5) an initial calculation of tooling is performed by calculating the stresses in the pin. The pin itself is a given for any chosen specimen size W, where in this case $W = 36\,\text{mm}$ as discussed in section 2.3. There are 2 different specimen geometries proposed in the standard, with a relative pin of $0.188W$ and $0.24W$. The tooling as shown in 2.6 can be modified as needed, provided that it does not affect the measurement[9]. As such the stresses in the pin are considered in this design step.

The stresses in the pin are calculated using for a pin length of 30 mm with the load distribution shown in the plots in Figure 2.9 and 2.10. Using symmetry the loading is calculated for only half of the pin length, with the symmetry plane at $x = 15\,\text{mm}$ (the centre of the specimen).

The loading of the pin is applied as a distributed load as shown in Figure 2.9 where the total force on the pin is 24.2 kN (Equation 2.6 from section 2.3).

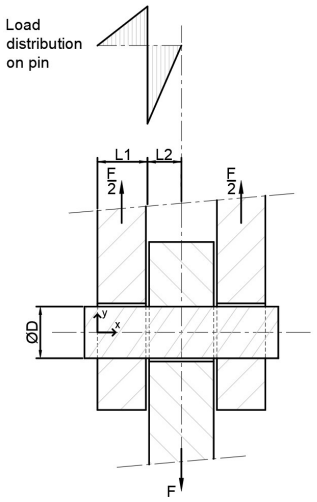

Figure 2.8: Pin calculation outline

- Load distribution:

$$LD_{(x)} = \begin{cases} c_1 \times x, & \text{for } [0 \leq x < L_1] \\ c_2 \times x + c_3, & \text{for } [L_1 \leq x \leq L_1 + L_2] \end{cases} \tag{2.7}$$

- With the shearing force given by integrating the load distribution along the length of the pin:

$$S_{(x)} = \int LD_{(x)}\, \mathrm{d}x \tag{2.8}$$

- Where the bending moment is given integrating the shearing force

$$M_{(x)} = \int S_{(x)}\, \mathrm{d}x \tag{2.9}$$

The resulting shearing force and bending moments are calculated from this distributed load using the symmetry condition at the centre and the boundary conditions imposed by the clevis and specimen. Where in this case 12.1 kN per pin side, which is the total shear force on the pin as shown to be the 12.1 kN at the transition from the clevis to the specimen (at $x = 10\,\text{mm}$). With the maximum bending moment of $6.05 \times 10^4\,\text{Nmm}$ at the symmetry plane of the pin (middle of the pin).

The stresses in each point of the pin can be calculated with Equation 2.10 through 2.13, where the evaluated results of Equation 2.12 & 2.13 are shown in Figure 2.10. The evaluation of the shear stress separate from the bending stress is valid considering that the maximum stresses occur at different heights in the pin. The maximum shear occurs at the neutral line, whereas the maximum bending occurs at the outer most height from the neutral line of the pin[**?**].

$$\tau_{(x),\text{mean}} = \frac{S_{(x)}}{\pi/4 D^2} \tag{2.10}$$

$$\tau_{(x),\text{max}} = 4/3 \cdot \tau_{(x),\text{mean}} \tag{2.11}$$

$$\sigma_{(x),\text{Maxeq.shear}} = \sqrt{3} \cdot \tau_{(x),\text{max}} \tag{2.12}$$

$$\sigma_{(x),\text{Maxbending}} = \frac{M_{(x)} \cdot D/2}{\pi/64 \cdot D^4} \tag{2.13}$$

The calculated stresses shown in Figure 2.10 are for the pin with a diameter of $0.24W$ or 8.6 mm, and are also listed in Table 2.1.

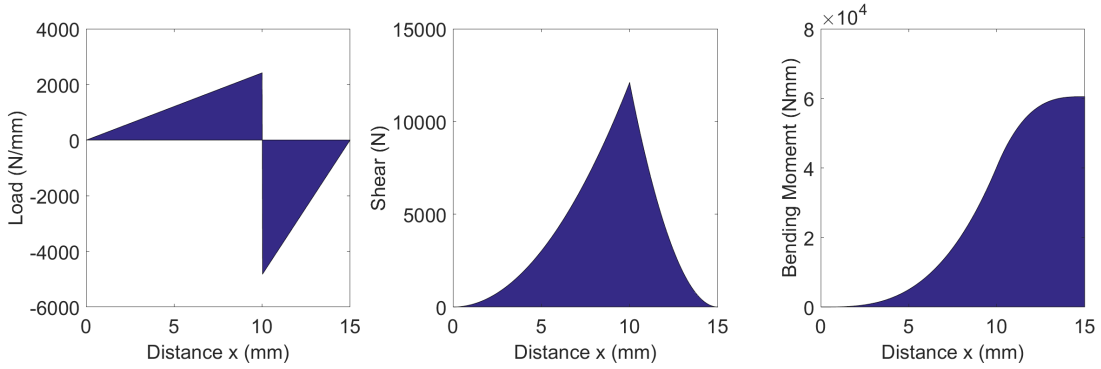

Figure 2.9: Loading conditions pin clevis-specimen

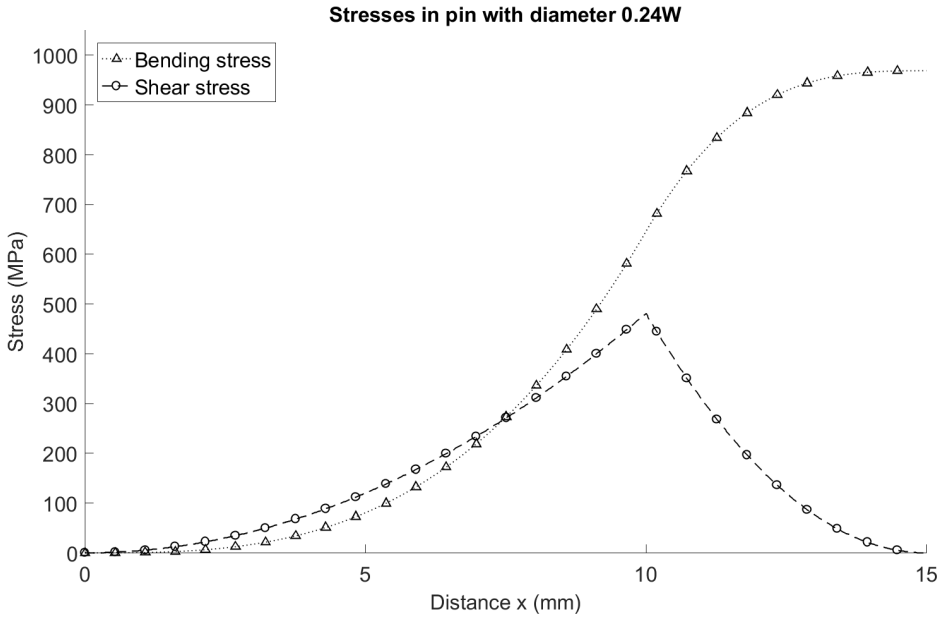

Figure 2.10: Stresses calculated in pin with diameter $0.24W$

The contact stresses between the pin and the tooling are also calculated, the contact is considered as a line contact as shown in Figure 2.11. For the calculation of the contact stresses the Young's modulus of the material

is required; the contact stresses are calculated for steel (200 GPa) and Titanium (114 GPa).

$$p_{max} = \sqrt{\frac{F}{2{,}86l} \cdot \frac{1}{D_1} \cdot \frac{2E_1 \cdot E_2}{E_1 + E_2}}$$

$$P_M = \frac{p_{max}}{1{,}27}$$

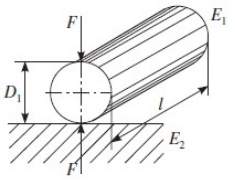

Figure 2.11: Contact stress[2]

Table 2.1: Calculated stresses

	0.188W Ø6.8 mm		**0.24W** Ø8.6 mm	
Bending stress (maximum occuring)	1987.8 MPa		968.6 MPa	
Shear stress (max. equivalent)	776.7 MPa		481.1 MPa	
Contact stress (mean contact stress)	**Steel** 2784.1 MPa	**Titanium** 2102.0 MPa	**Steel** 2459.6 MPa	**Titanium** 1864.7 MPa

The stresses (as listed in Table 2.1) in the pin and the contact stresses are relatively high when compared even to the yield stress of the maraging steel of 1900 MPa (yield stress at room temperature Appendix G). Where yielding due to bending can be expected to occur with the specimen of $0.188W$ in addition to the high contact stresses, this specimen geometry is considered as not suitable when high test loads are to be expected. The stresses the specimen with pin diameter $0.24W$ are also quite high, yet well below the yield stress of the maraging steel, but higher than the yield stress of stainless steel and titanium (at room temperature Appendix G).

The contact stresses occurring in the tooling and the bending and shear stresses in the pin even for the $0.24W$ pin can be considered quite high. In order to ensure a sufficient safety in the design a modified specimen using a larger pin diameter is proposed. A pin diameter has been calculated such that a significant margin is achieved in the design; resulting in a pin of Ø11 mm, with the stresses as shown in Table 2.2.

In order to accommodate for this larger pin the specimen is modified such that sufficient material is available for the distribution of the load as illustrated in Figure 2.12 (for the fabrication drawing refer to Appendix A). A comparative study is performed on the effect of this modification in relation to the 2 specimen proposed in the standard which is included in Appendix C, and is shown to have a minimal impact.

There is a small difference in the fracture toughness value calculated in the simulation between modified specimen and the standard specimen as proposed in the standard. The additional stiffness can be considered to introduce a small amount of error in the measurement of the material toughness. This small amount of error is considered a worthwhile trade-off for a more robust set-up, especially when considering that the increase of stiffness reduces another source of error. In particular the plastic deformation when estimating the crack size using the compliance method[26]. The high contact stresses in the specimen result in significant plastic deformation which change the expected behaviour of the specimen when partially unloading for the estimate of the stiffness.

Table 2.2: Calculated stresses modified diameter

	Ø11 mm	
Bending stress (maximum occuring)	459.2 MPa	
Shear stress (max. equivalent)	291.6 MPa	
Contact stress (mean contact stress)	**Steel** 1652.5 MPa	**Titanium** 1247.6 MPa

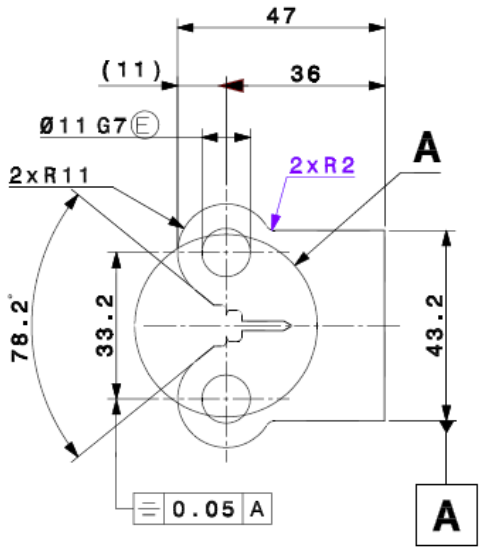

Figure 2.12: Modified specimen

2.4.2. Clevis

Alignment of the specimen with the tooling is taken under consideration. Misalignment can result erroneous measurement due to resulting from uneven loading of the sample. Two approaches have been considered, either a rigid system which can be adjusted to ensure alignment, or to design the system such that alignment is ensured by the load.

A number of design optimisation have been performed to ensure alignment of the loading structure inside the cryostat.

The clevis as proposed in the standard (see Figure 2.6) was used as a basis for the design, and modified to allow for it to be incorporated in the cryostat. The clevis was modified with an additional pinned connection that would allow for easy assembly onto the existing pin connection at the bottom plate of the internal support structure (Figure 2.3). The same pinned connection could be used with the load cell allowing for a symmetrical design, with little modifications to the internals of the cryostat. In the case that the existing load cell would not be used a simplified pinhole could easily be fashioned to fit on the connector at the tension rod. The pinned connections in the clevis were placed at a rotated angle of 90 deg; as shown in Figure 2.13. As the loading of the specimen is always under tension this should allow the tension to align the tooling with the specimen along the direction of the loading using the two rotational degrees of freedom.

In order to minimise the expenditure of the coolant during the initial cooling the mass of the clevis was minimized by reducing its volume. The design of the clevis was modified to be as compact while still being as stiff as possible resulting in the design as shown in Figure 2.13. The verification using finite elements of the final design clevis is included in this report in section 3.2.

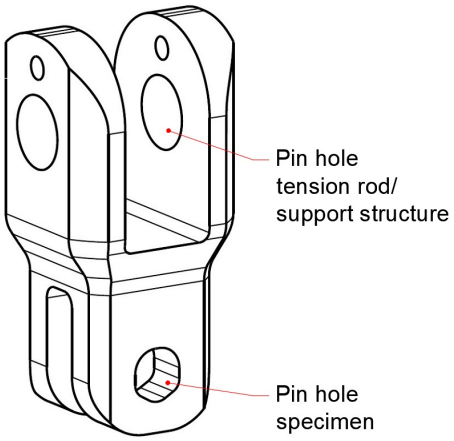

Figure 2.13: Modified Clevis

The alignment of the internal structure (Figure 2.4) has been validated for the tensile specimen test, and as such is deemed suitable for the fracture toughness tests. The typical design for the clevis contains a flat area at the pin connection as can be seen in Figure 2.6. With the clearance on the hole as shown in Figure 2.6, this flat area does allow for a sliding of the pin. This degree of freedom is somewhat undesirable, in addition this connection is shown to result in high contact stresses(subsection 2.4.1). In order to align te specimen with the clevis a contoured hole with slope angles of 30° is included at the bottom of the hole in the clevis. With the benefit of reducing the contact stresses as an additional point of contact is introduced. The shape of the hole and tolerances defined for the contoured hole ar shown in Figure 2.14, for the complete design drawing refer to Appendix A.

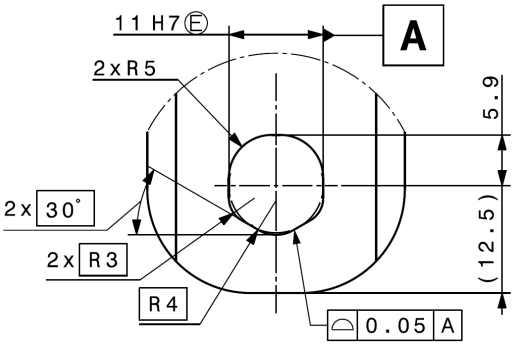

Figure 2.14: Contoured hole in clevis

The internal structure of the cryostat well aligned, and the alignment of the specimen is further assured with the connection at the clevis. Additionally the tooling was designed with pinned connections to allow for rotational degrees of freedom around two axis to allow for alignment by the loading of the assembly under tension. By introducing these degrees of freedom in combination with the tolerances the entire assembly should in principle cancel out any minor misalignments when loaded in tension.

2.4.3. Material selection

The material for the tooling specified in the standard is maraging steel, these steels have excellent material properties at room temperature (yield stress >1400 MPa) and good machinability. This type of steel does become brittle at cryogenic temperatures as indicated by the significant reduction in the elongation at break at 4 K as listed for example in G.3 (inherent to its BCC structure). The use of this material is still possible but poses design and manufacturing challenges; especially with the high contact stresses as shown in subsection 2.4.1. High contact stresses do not necessarily constitute failure, some plasticity underneath contact surface is acceptable, after which subsequent loading at the contact remains elastic. The brittleness of the maraging steel

at 4K however allows for very limited plastic deformation, and material failure can be expected at the contact area as a result; which in turn can be expected to result in critical failure of the clevis.The tooling can be considered to be used primarily for tests at low temperatures, hence maraging steel is not considered as a suitable material for fabrication of the tooling.

With the uncertainty in the design a material is selected which does retain some ductility even at these low temperatures. Of the materials readily available for the construction of the tooling meeting this requirement the selection was limited to austenitic stainless steels and titanium alloys. These materials retain ductility at low temperatures, and can be considered to have relatively high yield and tensile strength especially at cryogenic temperatures. The material however is needed to be applicable under a wide range of temperatures, from room temperature down to cryogenic temperatures.

Of the materials considered Titanium grade 5 meets the requirements, with good mechanical properties at room temperature and at cryogenic temperatures, while also retaining ductile behaviour at temperatures down to 4 K (engineering strain of approximately 18% at 4 K see Table 2.3 properties from [13]). This material does not have a FCC structure, yet due to its Hexagonal close-packed (HCP) structure it does retain some ductility. The mechanical behaviour of an HCP material is typically between that of an ductile FCC and the brittle BCC materials[22]. HCP materials such as Titanium are however less ductile at low temperatures than FCC materials due to the limited dislocation movement available at low temperature in the structure. As such the titanium alloy selected is not the best option for testing at extremely low temperatures, but it is a suitable material for low temperature conditions down to 4 K, and one that is suited for a wide range of temperatures up to room temperature.

Table 2.3: Mechanical properties Ti6Al4V

	ρ	ν	E	Yield stress Rp 0.2%	Ultimate tensile stress	Elongation	Fracture toughness
	(kg/m^3)		(GPa)	(MPa)	(MPa)	(%)	(MPa$\sqrt{\text{m}}$)
295 K	4540	0.342	114	830	1170	15	47
77 K		0.327	118	1300	1480	17	38
4.2 K*		0.311	119	1780	1860	18	38

*Yield stress, UTS, and elongation listed are at 29 K (-254 °C)

This material is somewhat more difficult to machine, yet this did not pose any significant impediment for the fabrication, with the only downside of it being somewhat more expensive. An additional benefit of using titanium is the relatively low thermal contraction (as shown in Figure G.2 in Appendix G). Minimizing the clearance required for testing at cryogenic temperatures, and allowing for easier design of specimen (for materials with higher thermal contraction). Thermal contraction effects would primarily only need to be considered with respect to the clearance between the pin and specimen.

2.5. Measurements

In order to obtain a measure on the fracture toughness two parameters need to be measured: the load and the extension of the crack (see subsection 1.4.1 and for a more detailed listing the literature review[17]). Where depending on the test performed some additional measurements such as the load-line displacement are also required.

Due to the enclosed environment of the cryostat, the low temperatures and the submersion in the coolant measuring inside the cryostat poses some challenges. These challenges can be mitigated and or accounted for by using suitable materials and/or correcting for temperature effects[13]. Though implementation inside the cryostat poses challenges it would allow for measurement closely on the specimen itself, minimizing potential sources of error such as friction.

Measuring outside of the cryostat is also possible to some extend, yet poses other challenges such as the friction of the tension rod with the seal at the top of the cryostat(Figure 2.3), which could vary (due to assembly and/or the presence of water). Making accounting for them difficult and additionally the elasticity of the load-line would need to be taken into account (which the varying friction would impede).

For the initial design it was opted for a simple set-up where the load applied to and the crack opening (also the load-line) displacement of the C(T) specimen are measured. These two measurements can be used for a range of testing methods, such as the quasi static J-test or the dynamic FCGR test(see subsection 1.4.2).

2.5.1. Displacement

The load-line opening displacement can be measured with relative ease using a clip gage extenso-meter. In Figure 2.15 a measurement set-up is shown from the ASTM E1820, with the gage attached to knife edges machined on the specimen. These knife edges can be either machined on the specimen or attached by other means. Upon examination of available solutions for the fabrication of a clip-gage such as strain gages suitable for cryogenic service, a complete solution suited for testing at cryogenic temperatures was found. A clip gage was ordered with working temperature range from -270 °C up to 100 °C, as shown in Figure 2.16, image from data-sheet (included in Appendix B).

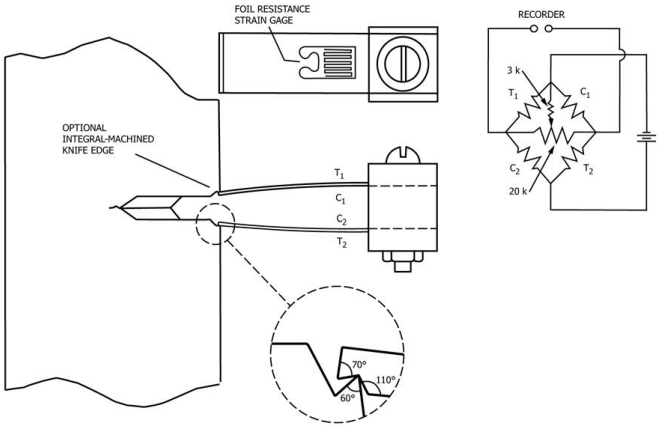

Figure 2.15: Measurement of the CTOD[9]

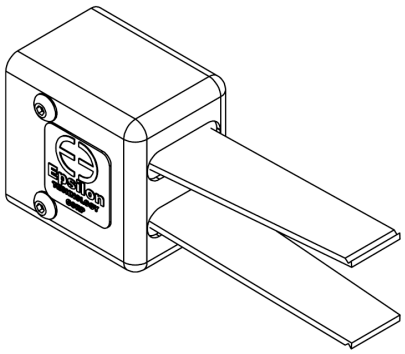

Figure 2.16: Clip gage

2.5.2. Load

The load applied to the specimen is could be measured either using the current load-cell, used for the tensile tests, or could be inferred using strain gages on the testing clevis. An investigation showed that in the current compact design of the clevis no suitable areas of uniform strain where present, hence not suited for the application of gages (refer to Figure E.12 in Appendix E).

It was decided to use the load-cell already in use for tensile tests. This was considered a viable option as any major sources of friction occur above this load-cel, with the additional benefit that the load-cel is validated and calibrated for use at low temperatures in conjunction with the tensile test machine.

2.5.3. Temperature

An additional parameter of interest is the temperature of the specimen. Cooling is achieved by immersing the specimen inside a cryogenic cooling liquid (e.g. liquid helium or nitrogen). After a suitable amount of time the specimen can be considered to have the same temperature as the boiling temperature of the coolant.

Specimen temperature is an important factor in the fracture mechanics test, and the temperature of the specimen should be maintained at the desired test temperature. Thermo-mechanical heating during testing could however increase temperature above the desired temperature of the tests[17][21]. The thermo-mechanical heating of materials is caused by the conversion of plastic work to heat, and is dependent on a large number of factors such: strain rates, the type of material, the structure, amount of energy stored in the lattice, defects and impurities. In general when testing a material the only parameter of these which can be affected during testing is the strain rate.

At the time of this work no resources where available to include a continuous reliable measurement of the temperature. In order to limit the effect of heating the test was performed by limiting the cross-head displacement speed, reducing the strain rates in the specimen, within the limit of the boiling off of the coolant (due to temperature losses of the cryostat and generated heat).

2.6. Design

Taking into account a number of design constraints such as; the loading, temperature and limited space, the following design was proposed and fabricated internally at the CERN workshop. In Figure 2.17 an assembly of the tooling is shown with: the testing clevis, specimen and clip gage. The system mounted in the internals of the cryostat is shown in Figure 2.18, with the load-cel at the upper clevis. for the drawings of the clevis, pins and the specimen refer to Appendix A.

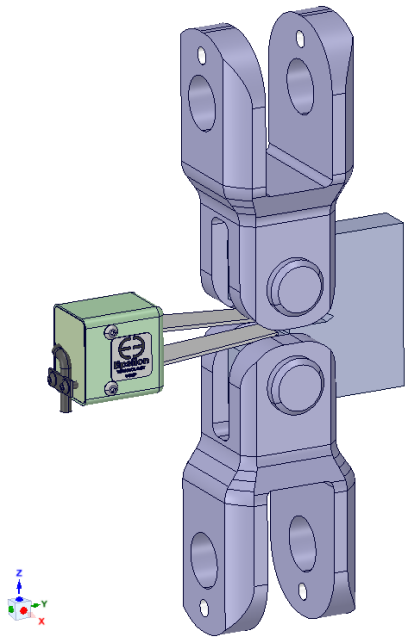

Figure 2.17: Assembled subsystem with specimen

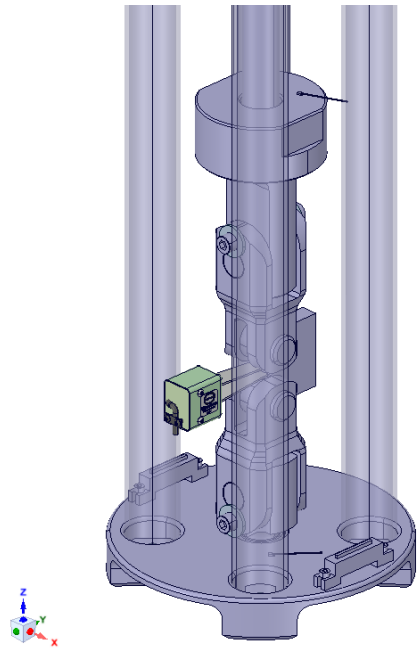

Figure 2.18: Assembled subsystem in cryostat

3

Design verification

This chapter contains a summary on the design verification: of modified specimen, the tooling and a verification of the cryostat for the various loading conditions. The internal structure was designed and verified for a test load of 100 kN by the engineering department prior to this work and is therefore omitted.

3.1. Modified specimen

As discussed in subsection 2.4.1 the contact stresses occurring can be considered quite high. A modified specimen is proposed using a larger pin diameter of 11 mm. This modified specimen can be considered to have an increase in stiffness near the hole of the pin and modified behaviour due to the larger pin diameter. This could in principle affect the stiffness near the crack[26] and subsequently the stress intensity factor at the crack tip. In order to asses the effect of this modification a comparison study is performed of this modified specimen in relation to the two standard geometries[9] for the upper and lower bounds of the initial crack length; of $0.45 \leq a/W \leq 0.7$.

3.1.1. Model and Mesh

A model is prepared for the 3 specimen geometries, with a crack of $0.45W$ and another set with $0.70W$. In Figure 3.1 the model is shown of the three specimen with crack size $0.45W$, for the specimens with $0.70W$ see Figure C.2 in Appendix C. The pins are also modelled inside the holes in with contact for the application of the loads similar to those during tests (omitted from view in Figure 3.1). The material defined for these models is a relatively mild steel with Young's modulus of 200 GPa and a yield stress of 250 MPa. The Young's modulus of the material is relatively constant for the steels and stainless steel alloys at room temperature and lower temperatures, 200 GPa ± 20 GPa (see Appendix 2). The yield stress used in the simulation is somewhat typical for a steel at room temperature. The yield stress is lower than the stainless steel materials tested at low temperatures, yet as this is a comparison study between the specimen geometries the lower yield stress does not have any impact on the validity of the comparison. This as all specimen are simulated using the same material.

For a finite element model a typical rule of thumb is the more points(nodes) the higher the accuracy of the simulation, as the deformation can be more accurately simulated. This can generally be achieved by two methods a H-refinement and a P-refinement, where an H-refinement is increasing the number nodes by increasing the amount of elements and P-refinement increasing the polynomial order of the basic functions of the element (adding nodes to the element). Increasing the number of elements or the element order comes at a cost i.e. computation time, making it impractical to use an extremely high number of elements. typically for a sufficiently meshed model the improvement of the model accuracy is only marginal when decreasing the mesh size(or increasing the amount of elements).

For this simulation a combination of the two methods is used, where the specimens are meshed with a global mesh size of 0.5 mm, with a refinement at the crack tip to an specified element size of 0.2 mm (local H-refinement). In order to more accurately capture the non-linear behaviour quadratic elements have been used. the quadratic element capture the deformation using quadratic basic functions, which in turn allow for an evaluation of a linear stress distribution in the elements (whereas stresses evaluated in a linear element can be considered constant for the entire element).

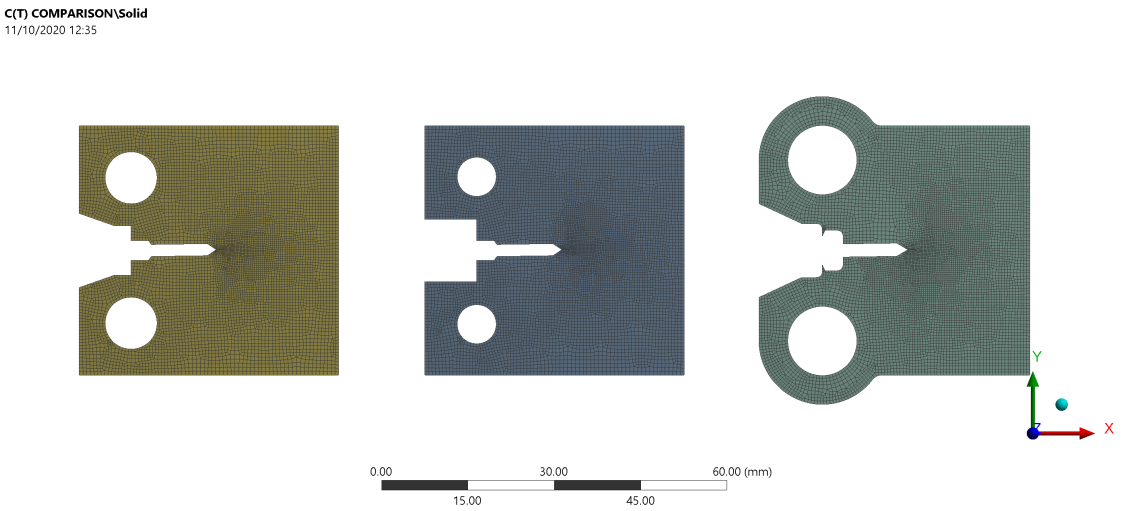

Figure 3.1: Model and mesh of all three specimen - initial crack length $0.45W$

3.1.2. Boundary conditions

The pins are constraint along the X-axis with the lower pin also along the Y-axis, and a few points in the model along the Z-axis to constraint rigid body movement. A frictional contact with coefficient 0.1 is defined at the interface between the pins and specimen, a typical value for steel to steel contact is between 0.1-0.3. Where for dynamic friction a value of 0.1 is a realistic assumption, the contact specimen is rotation over the pin surface as displacement increases. As an additional precaution weak springs have been included in the solver to ensure that the rigid body modes of the specimen is suppressed when there is very little friction present between the pin and specimen in the simulation (at the initial start of the simulation).

The loading on the models is applied at the upper pins, where a load of 8 kN is applied on the models with the crack $0.45W$, and a load of 3 kN on the models with crack $0.70W$.

3.1.3. Results

The stresses in the model have been compared near the crack tip with little to none noticeable difference, as shown for the specimen with crack $0.45W$ in Figure 3.2. As part of a more detailed investigation the stress intensity factor (SIF) (see Figure 3.3) and J-integral value (see Figure 3.4) are computed for the crack. For all computed contours and the combined plot for the specimen with initial crack of $0.45W$ and $0.70W$ refer to section C.2 in Appendix C. The largest difference in the computed fracture toughness values was for the specimens with initial crack length $0.45W$ (see Appendix C). The difference found in the SIF and J_{IC} between the modified specimen and the standard with a pin diameter of $0.24W$ was found to be in around 1.26%. very similar to the difference found between the two standard specimen with pin diameter of 0.24 and 0.188. The J-intergral values between the specimen are found to differ slightly more. With a difference of 2.5% between the modified and specimen with diameter of $0.24W$, against the around 2% between the two standard specimen with pin diameter of 0.24 and 0.188.

In general the difference can be considered marginal with only a deviation of at most 2.5%. As the fracture toughness value calculated for the modified specimen shows a similar variation as found between the specimen proposed in the standard this is even more so considered as an reasonable modification with little impact on the validity of the test (the $0.188W$ and $0.24W$ pinned specimen[9]). In general the expected measured fracture toughness value of the modified specimen can be expected to be slightly lower than those measured with the standard specimen, this is also considered an acceptable trade off as a lower reported value can be considered a conservative fracture toughness estimate.

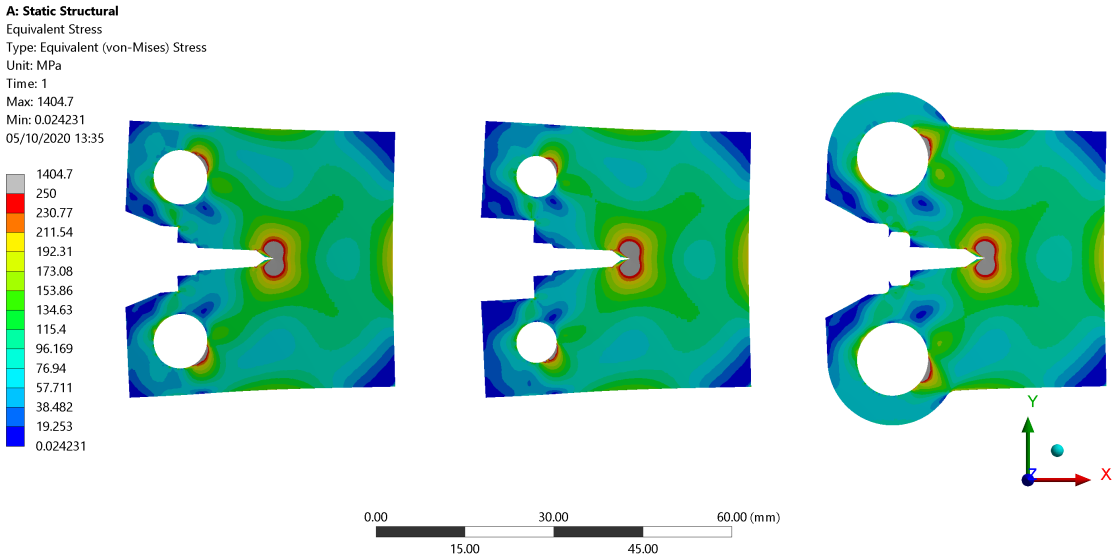

Figure 3.2: Total equivalent stress - Crack 0.45W

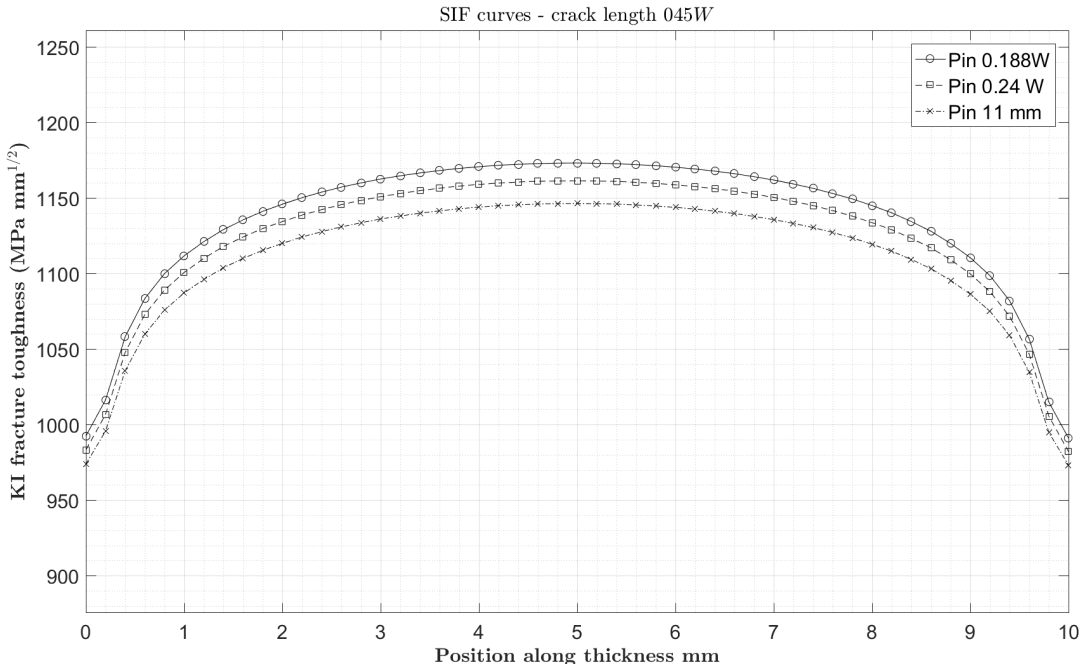

Figure 3.3: KI fracture results - Crack 0.45W

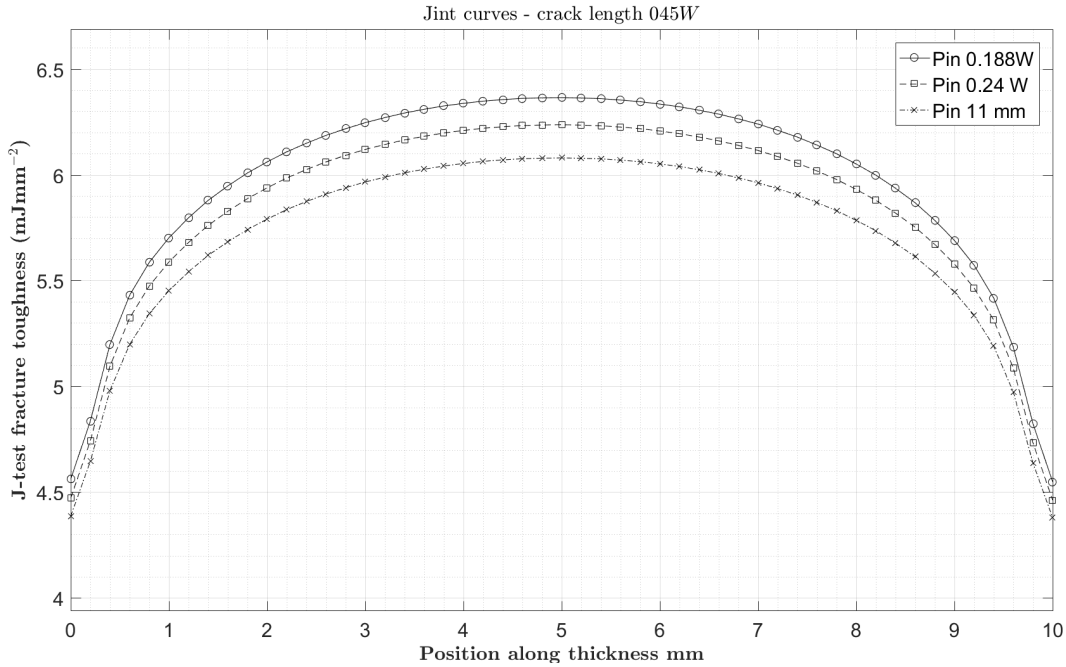

Figure 3.4: J-integral fracture results - Crack 0.45W

3.2. Design verification tooling

A number of design iteration were involved to reach the final design presented in 2.6. Taking into consideration the design space, required strength and also whilst trying to minimize the geometry as to limit the expenditure of the cooling liquid. As briefly discussed in subsection 2.4.3 the material selected for the tooling was the alloy titanium grade 5 (Ti6Al4V). This as the material was considered to meet the requirements, such as high yield stress and ductile behaviour even at low temperature.

The design iterations have been initially performed using analytical methods (such as briefly discussed in subsection 2.4.1) to calculate the stresses, and as the design progressed is was assessed using finite element method. The load used to calculate the stresses in the design was the estimated load of 24 kN. In this section a summary is presented for the verification of the final design, for the complete assessment refer to Appendix E.

3.2.1. Model

The specimen and loadcel with the pin conditions are included in the final model. Using symmetry conditions the model is reduced to the smallest representative size possible. With a division along the middle of the specimen and along the vertical symmetry plane of the specimen and clevis, the model is shown in Figure 3.5 (for more details refer to appendix E).

The material defined for all parts is the titanium alloy previously mentioned (with properties as listed in appendix G). Symmetry constraints have been applied to the respective planes, and friction less contacts are defined at the pin connections. The effect of friction on the stresses in the clevis are minimal, the frictionless contact is used to include the contact stresses in the simulation model. using a friction less contact also allow for easier comparison with the analytical method used in subsection 2.4.1. The load of 24 kN is applied at the connection interface from the loadcel to the UTS-machine.

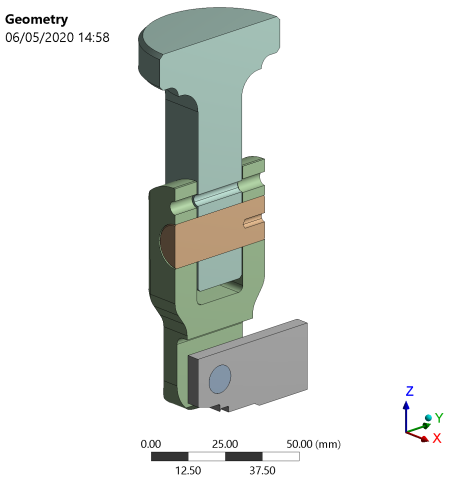

Figure 3.5: Simulation model

3.2.2. Results

The design is verified for the test load of 24 kN with the model described in 3.2.1. The stresses in the set-up, and the clevis in particular are evaluated, and aside from the contact stresses in the design and primarily the clevis are generally below 200 MPa (as can be seen in Figure 3.6). With the lowest yield stress of the material at 830 MPa (293 K Table G.2); this leaves a factor of safety of over 4. The contact stresses can be considered as the limiting factor in the design, this allows for easy analytical calculation of the allowable load under the different design conditions.

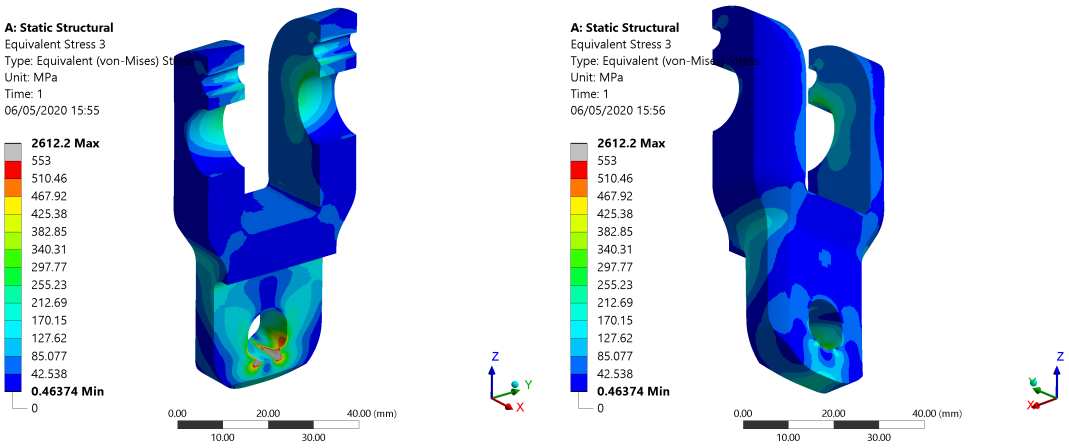

Figure 3.6: Total equivalent stress in clevis

A minor design deviation from the default described in the standard[9] is by slightly increasing the pin diameter to a better fit in the standard sample. For the design with $W = 36$ mm this results in a pin diameter of 9 mm, with a fitting tolerance taking into account different thermal contraction and operating fitting. Additionally a design is proposed with an even larger pin of 11 mm, showing little to no impact on the fracture toughness values (refer to appendix C). With this larger pin the contact stresses are reduced allowing for higher test loads, which for materials with increasing fracture toughness relative to current materials might be required.

The maximum allowable test load for these two diameters and the default pin of $0.1875W$ specimen is calculated using the analytic method used for the initial calculations. This ultimate test load is calculated with: bending and equivalent shear stress up to the yield stress and the contact stress up to 0.83 times the plastic yield criterion. (refer to appendix E).

The ultimate test loads shown in Table 3.1 do not contain any factors of safety, yet these are however computed for stresses up to the yield stress. It is recommended to abort any test where the load approaches this ultimate load, with a reasonable margin (to be left tot the operator).

Table 3.1: Ultimate Load

Ultimate test load	Ø8.6 mm	Ø9.0 mm	Ø11.0 mm
293 K	21 kN	24 kN	43 kN
70 K	32 kN	37 kN	67 kN
4 K	36 kN	42 kN	92 kN

3.3. Design verification cryostat vessel

This section presents a summary of the calculations performed in order to assess the structural strength of the cryogenic vessel. For the full design assessment of the cryostat designed to be integrated into a tensile test machine to allow performing tensile tests down to 4.2K refer to CERN document 1269348V1[18] (included in D). The vessel is verified in accordance with En 13445[4] and EN 13458[5] for the static loading expected for: normal operating, testing and exceptional conditions.

3.3.1. Simulation outline

The assembled cryostat can be considered to consist of three main structural component, as indicated in Figure 3.7. The verification is only with respect to the dewar, with the other components already verified by the engineering department prior to fabrication of the cryostat.
The dewar is verified using two different models: using an axis-symmetric model to verify the stresses, and a full 3D model to verify the dewar with respect to buckling (see Figure 3.8). For the axis-symmetric model only a cross-section surface in the positive X-Y plane is required; allowing for a detailed simulation at limited computational costs (model partially shown in Figure 3.9). Where in this model the of the bolts and pre-tension are emulated using a pre-tensioned spring with equivalent stiffness.

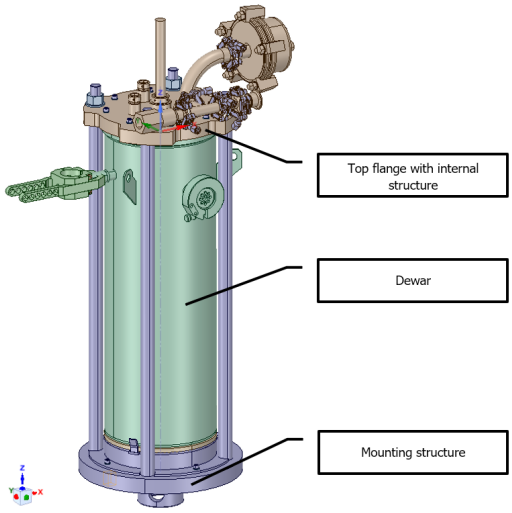

Figure 3.7: Dewar vessel with mounting structure

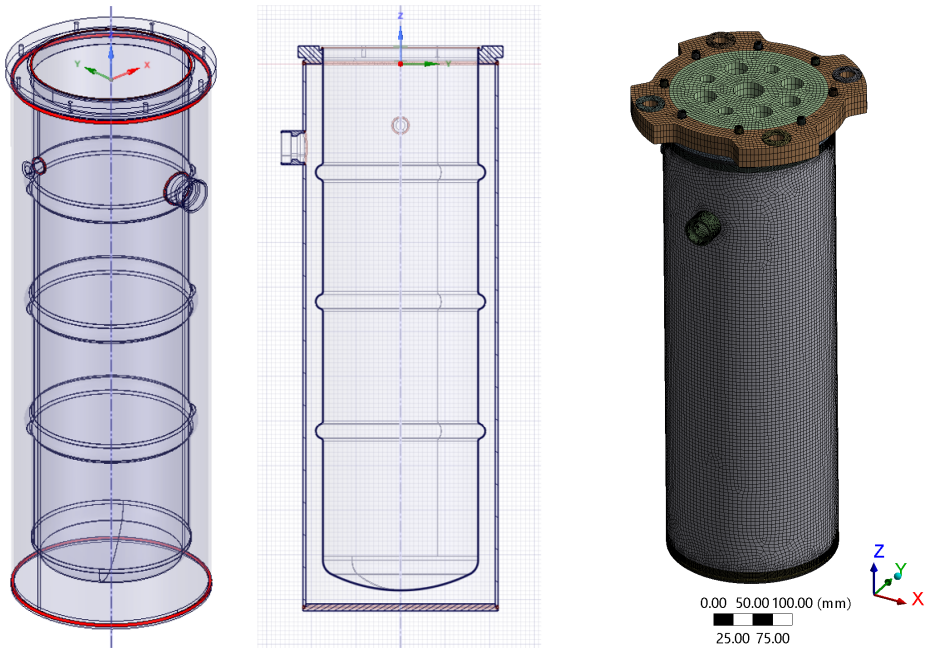

Figure 3.8: 3D model dewar

Thermal loading from the cooling and the convection on the outside of the vessel are included in the simulation, With applicable pressure applied in the 2 compartments for the different design conditions. The chamber between the internal and external chamber is used as a vacuum insulation chamber. The pressure used in the simulation is full vacuum a pressure of 0 bar(a) (-0.1 MPa). The internal pressure is set at the relief pressure of 1.5 bar(g) and the full vacuum (0 bar(a)) which is applied prior to testing.

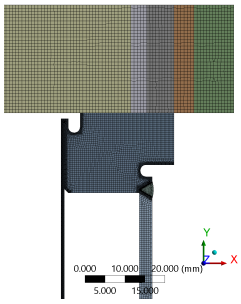

Figure 3.9: Axis-symmetric model - detail

3.3.2. Results

The primary stresses in the dewar are evaluated using the axis-symmetric model with the stress results shown in Figure 3.10. In this stress result three areas of interest are investigated, and in the area designated 2 the highest primary stresses were found. The stress distribution across the thickness is shown in Figure 3.11, and the primary membrane stress (115 MPa) is found to be below the allowable stress.

The primary membrane+bending stresses are also evaluated and are found to be slightly above the allowable. With a value of 235 MPa the stresses exceed the allowable of 225 MPa with a less than 5%. Strictly speaking this is not acceptable, yet as the pressure of 1.5 bar(g) used in the simulation as normal operating it is in closer to a accidental load case (or the test case), for which a higher allowable stress is applicable. Under normal operating conditions the internal pressure is approximately atmospheric, where the 1.5 bar(g) would only occur if the pressure release valve is triggered.

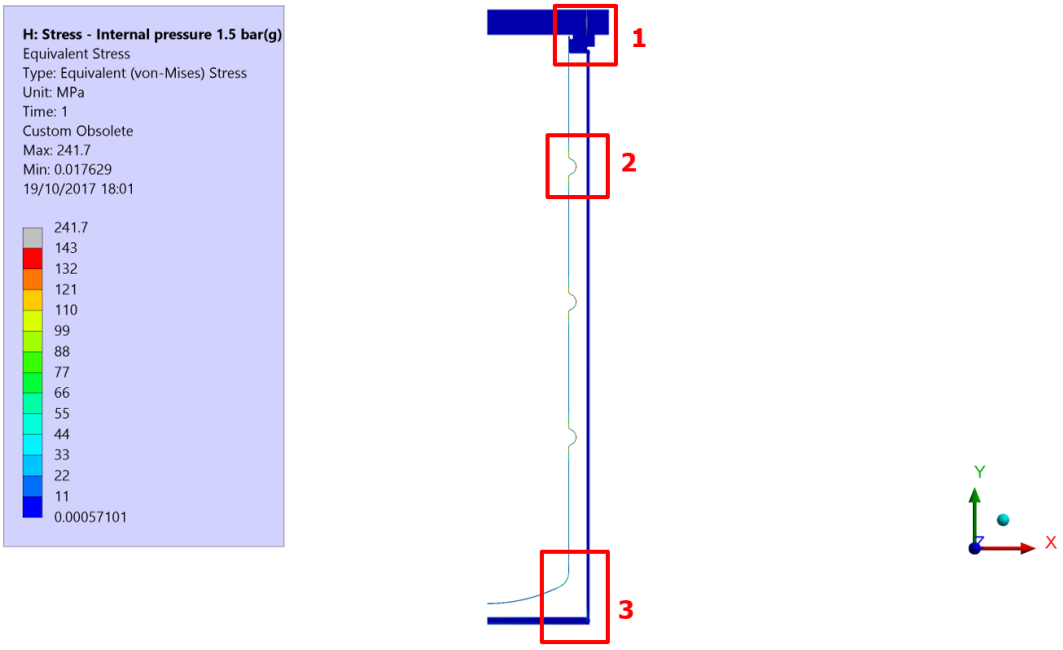

Figure 3.10: Axis-symmetric model - Primary stress results

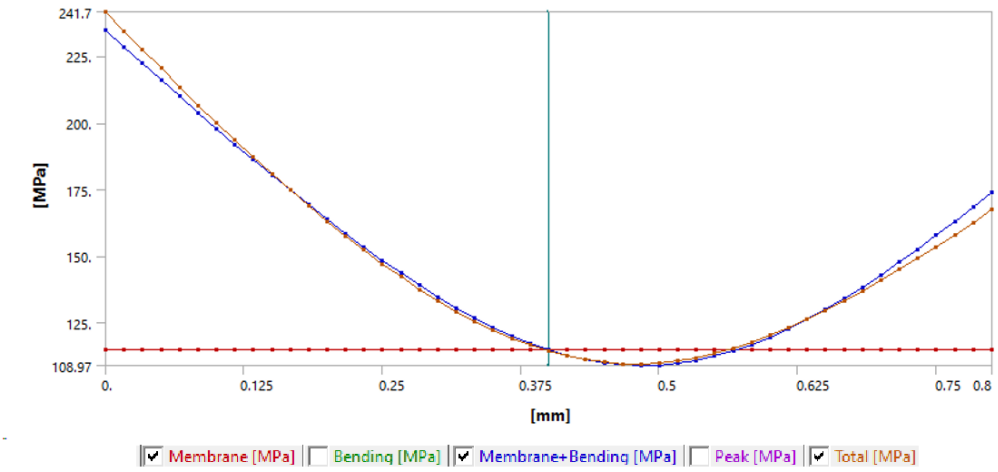

Figure 3.11: Axis-symmetric model - Primary stress - Detail 2

The weld joining the inner vessel to the top flange in area 1 (Figure 3.10 and Figure 3.10) also show high secondary stresses. Due to the manner in which the vessel is joined this can almost be characterised as a circular crack. The stress intensity factor at this weld is computed in the axis-symmetric model and verified in a small section from the 3D model using sub-modelling(Figure 3.12).

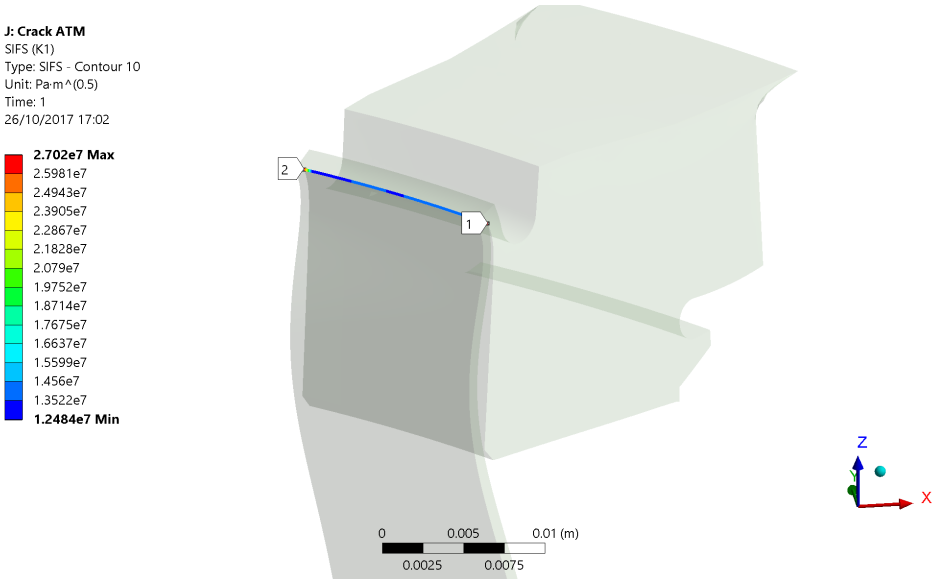

Figure 3.12: Sub-model - SIF KI - Detail 1

The SIF in the weld is relatively low with a value around $K_I \approx 12\,\text{MPa}\sqrt{\text{m}}$ (Figure 3.12), with the SIF reaching up to $K_I \approx 27\,\text{MPa}\sqrt{\text{m}}$ at the boundary conditions. Immediate failure is not to be expected as it is much lower that the K_{IC} of the materials from which the vessel is constructed (typically $K_I \geq 150\,\text{MPa}\sqrt{\text{m}}$ Table G.1). The weld can be considered to be somewhat susceptible to failure from fatigue, yet with a relatively low growth rate of 1.2×10^{-6}mm/cycle for the $K_I \approx 12\,\text{MPa}\sqrt{\text{m}}$ allowing for a high number of cycles.

3.4. Conclusion

The design tooling is verified for the expected loading form section 2.3, and the maximum load computed for the tooling is typically much higher than that of the expected load. This maximum load is computed with an analytical method which where found to be more conservative than the results from the finite element simulation. This analytical method took into account the bending and shear stress in the specimen and the contact stresses. For loads up to the loads specified in Table 3.1 no gross plastic deformation is expected, in addition the contact stresses are expected to remain below the plastic flow criterion.

It can be concluded that the presented analysis validates the design of the dewar of the cryostat for tensile tests (and therefore also for KIC an J-tests) at cryogenic temperatures. The design is validated for the loading scenarios required by the standard used for the validation[4], and as discussed in section 7 of the design verification report report[18] (also included in Appendix D), and is shown to meet the requirements as listed in subsection 3.3.2(and chapter 10 and 11[18] see Appendix D). Both the primary and secondary stresses are considered to be acceptable under te conditions specified in the EN13445 and EN 13458.

4

Tests

In order to verify the design of the tooling and sensors with the current set-up an in situ test is performed using 4 specimen; 2 fabricated in stainless steel 316 L and 2 in titanium grade 5. In order to allow for a more robust test set-up the modified specimen design as proposed in subsection 2.4.1.

4.1. Specimen preparation

The specimen are fabricated with the geometry and tolerances according to the drawing as shown in Figure 4.1 (full page size included in Appendix A).

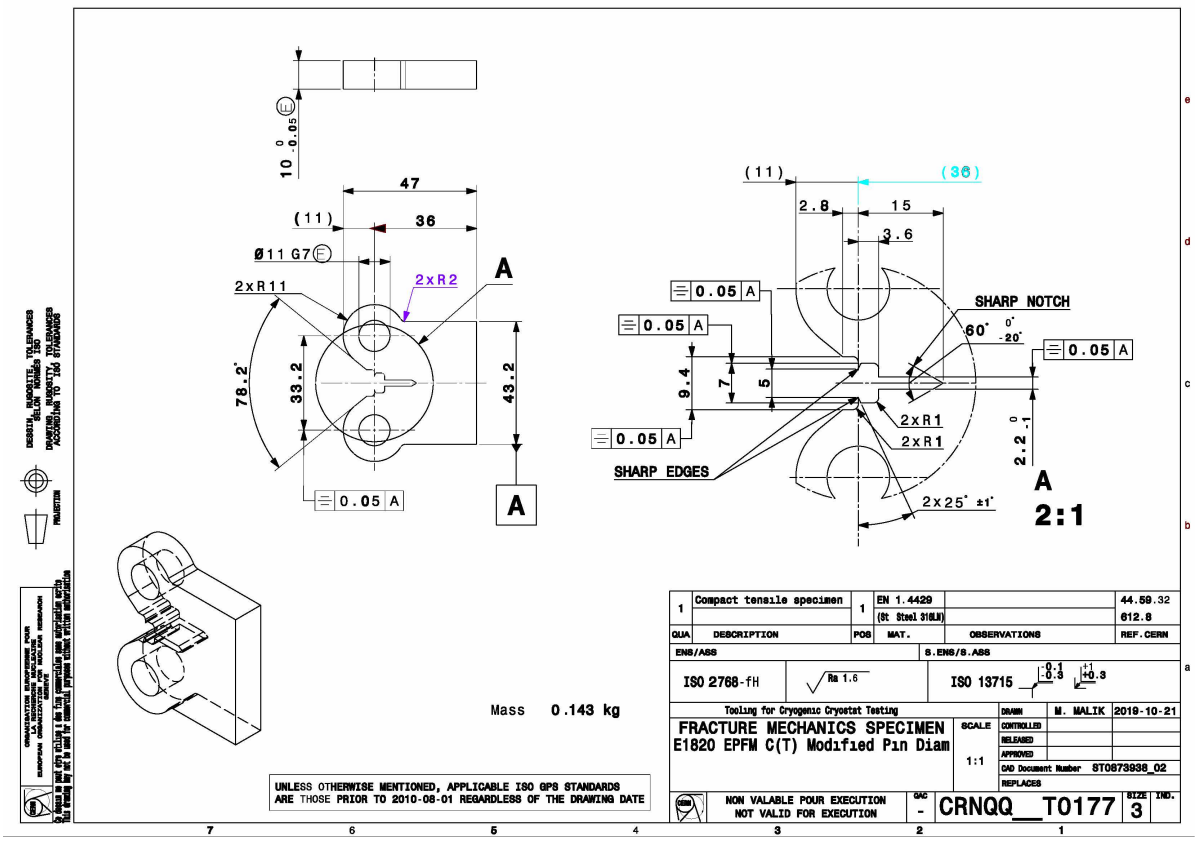

Figure 4.1: Fabrication drawing of the modified specimen

The specimen as shown in Figure 4.1 was fabricated with an unintended deviation of the starter notch (see Figure 4.2), instead of a depth of 15 mm a depth of 11.4 mm was machined (a result from parametrization error). Though strictly speaking this is not in accordance with the testing standard it is of little consequence for these initial tests. The initial tests are used to verify the set-up and verify the sensor output at low temperatures, and to investigate whether the required data for a fracture toughness test can be captured using the set-up. Though the test results are not strictly valid in accordance with a testing standard a crack should still progress from the pre-crack, and with sufficient sensor data a quatification of the fracture toughness should still be possible. Incidentally a higher test load can also be expected during the test, yet the design with the modified specimen is designed with sufficient margin to accommodate this higher load (see Table 3.1).

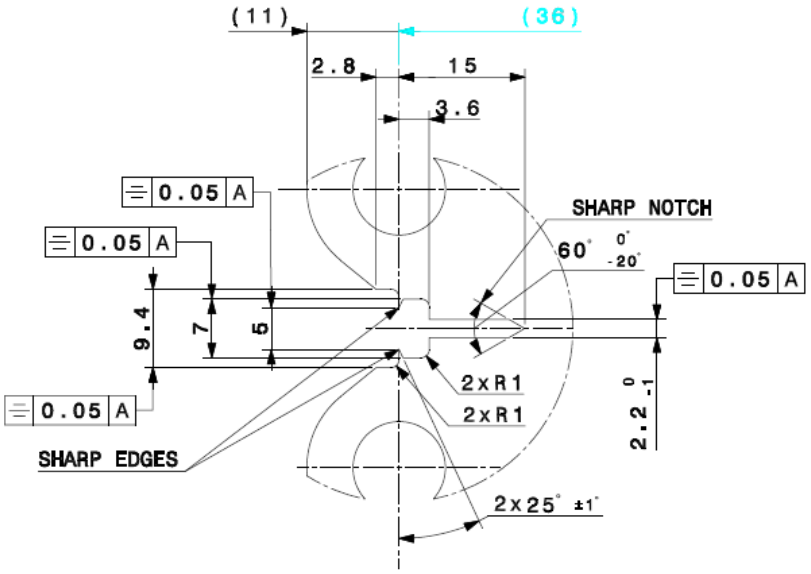

Figure 4.2: Detail specimen - desired starter notch

Initially it was attempted to correct by increasing the pre-crack depth of the specimen, though this appeared difficult to realize. The specimen where pre-cracked at an external facility in accordance with the ASTM E-1820, with the resulting pre-cracks as listed in Table 4.1, with the images on which the measurement where perfomed as shown in Appendix H. The initial crack depth is measured on both sides of the specimen from the pre-notch(at 11.4 mm from the load-line), with the initial averaged depth for each specimen listed in Table 4.1.

The pre-crack in each of specimen are uneven, indicative of a possible misalignment during pre-cracking (uneven depths listed for each side in Table 4.1). As it was performed externally no data was available to verify this. Additionally the specimen titled Ti6Al4V-2 is shown to contain a relatively large pre-crack with even some visible plastic deformation as the crack progressed, as can be seen in Figure H.13 and H.14. With a possible explanation being that the sample was pre-cracked using a force controlled scheme(see subsection 1.4.4), which was either not monitored sufficiently and/or the amplitude of the force was set too high.

Table 4.1: Depth pre-crack specimen

specimen	L	R	a_0 (avg. L&R)	a_0/W
316LN-1	1690 µm	1190 µm	12.84 mm	0.36
316LN-2	1450 µm	550 µm	12.4 mm	0.34
Ti6Al4V-1	4180 µm	1820 µm	14.40 mm	0.40
Ti6Al4V-2	11600 µm	10700 µm	22.55 mm	0.63

4.2. Outline

The measurements on the specimen is performed using the clip-gage as described in subsection 2.5.1 with the load measurement using the load-cell as mentioned in subsection 2.5.2. The test is controlled however with a program using the sensors on the test bench and visual feedback from the internal sensors.

In order to verify the initial set-up a room temperature test is performed using the cryostat, whilst omitting the dewar for easy of access and visual monitoring. This allowing for an test which is effectively similar as the set-up used for a cryogenic test, without the limitation of an enclosed environment around the specimen. For this initial verification of the sensors and set-up the specimen Ti6Al4V-2 was used (see Table 4.1 and appendix H).

After the initial verification using the room temperature test the other three specimen where tested at 4 K using the complete test set-up cooled with liquid helium. As these material are shown to contain significant plastic behaviour even at 4 K a non linear fracture mechanics testing program was defined for the tests.

4.2.1. Testing program

As the two materials selected for the specimen can be considered relatively ductile these specimen are tested using the methods described in the ASTM E1820 [9] for a J-test. The test bench was programmed with the loading of the specimen using 2 different schemes:

1. loaded up using a force controlled scheme using an initial estimate for the specimen
2. followed by a displacement controlled scheme to allow for a more controlled crack growth in the specimen.

The estimation of the crack size is performed using the compliance method with a force controlled unloading and loading. this compliance method is programmed at regular intervals in the displacement controlled scheme; using a unloading and loading with a fixed amplitude to determine the compliance of the specimen. In order to ensure that no data of interest was lost in the initial loading this was also implemented during the last portion of the loading sequence (as shown in **??**). Both the displacement and the load controlled schemes were programmed at a low cross-head speed, within the limit of the boiling off of the cooling liquid of approximately 30 minutes (in order to limit strain rates and allow for the capture of sufficient data points).

4.3. Results

4.3.1. Sensor read-out and processing

The four specimen listed in Table 4.1 are tested and the data is captured from the sensors on the specimen. In Figure 4.3 the captured data is shown of the specimen designated 316LN-2, with thick marks at one in every 300 data points. For each of the test an Load Line Displacement (LLD) curve is constructed from the captured data, one such LLD is shown in Figure 4.4. From these LLD curves a value of the fracture toughness is calculated, for the calculation methods used refer to subsection 4.3.2 & 4.3.3 for the the titanium and stainless steel specimen respectively. Without processing the data the initial results from the test seem promising, where the sensor data can be used to construct a similar J-R curve as found in for J-test at low temperature in literature[20].

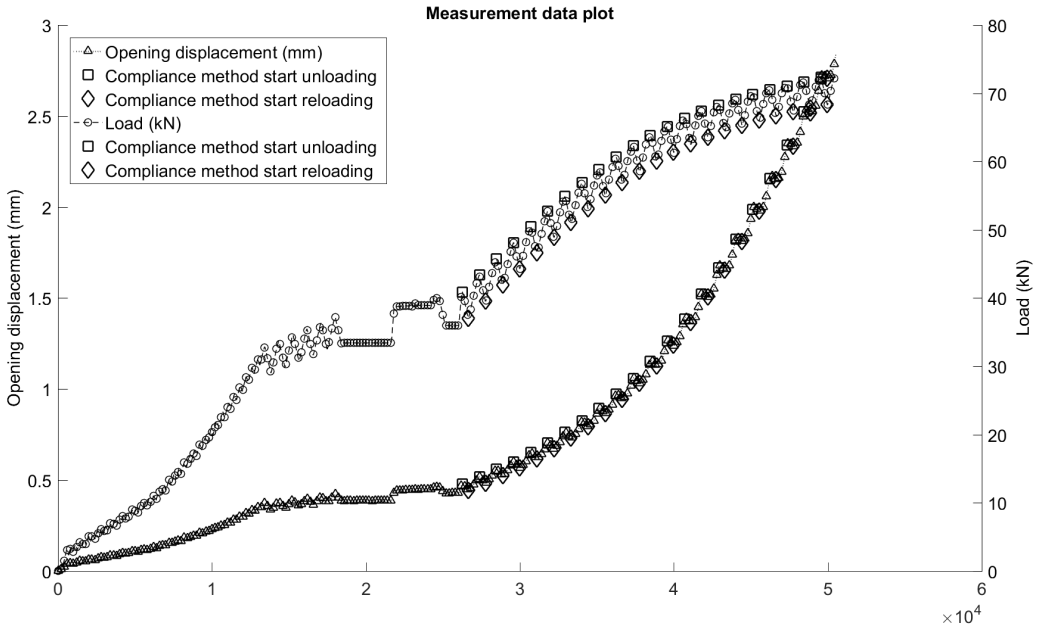

Figure 4.3: Measurement data on specimen 316LN-2

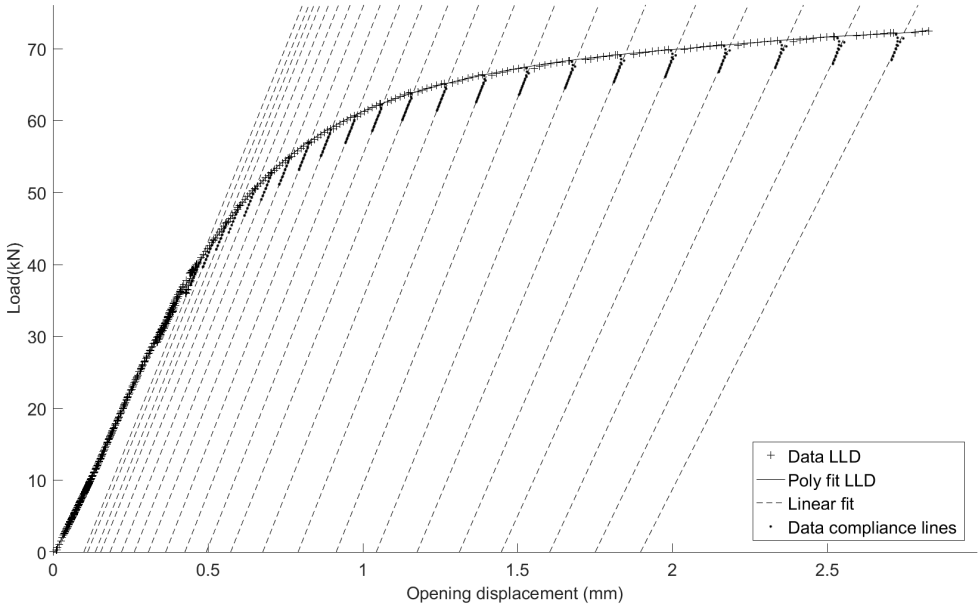

Figure 4.4: LLD specimen 316LN-2 with compliance lines indicated

4.3.2. Titanium specimen

The tests on the titanium specimen did not allow for a valid J-test as it did not meet the requirements[9], were both specimen showed relatively brittle behaviour (see Figure 4.5 & 4.6). Instead a LEFM approach[11] was used to obtain a value of the fracture toughness(see appendix F.2 & F.1). With the room temperature test on specimen Ti6Al4V-2 it is shown that the compliance method allows for an estimate of the crack size (refer to appendix F.1). Using the 0.95 secant lines the load P_Q is determined and using this load the fracture toughness is determined (listed in Table 4.2).

Table 4.2: Fracture toughness results

specimen	Testing temperature	Initial crack length a_0	Max. measured load	Fracture toughness
Ti6Al4V-1	4 K	14.4 mm	10.38 kN	36.9 MPa$\sqrt{\text{m}}$ [1]
Ti6Al4V-2	293 K	22.5 mm	8.42 kN	67.3 MPa$\sqrt{\text{m}}$ [2]

[1] Data allows for a fracture toughness value in terms of K_{IC}, yet strictly speaking the specimen did not meet all the requirements set forth by the standard

[2] Toughness value K_Q

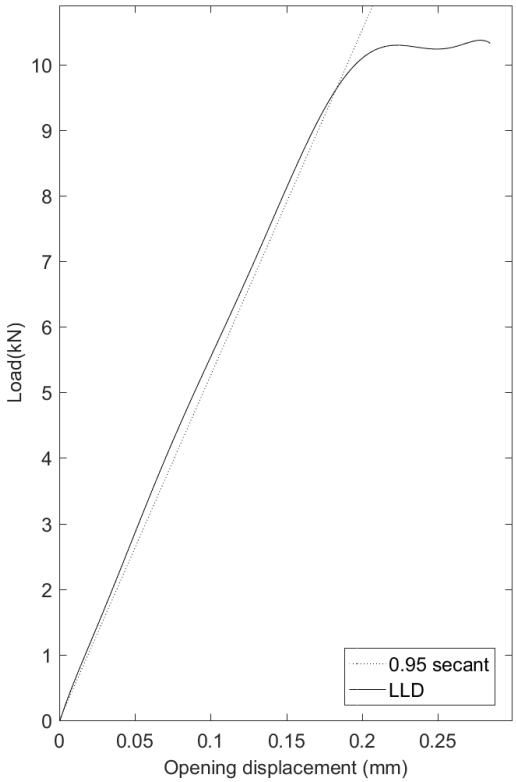

Figure 4.5: Ti6Al4V-1 - Test at 4K

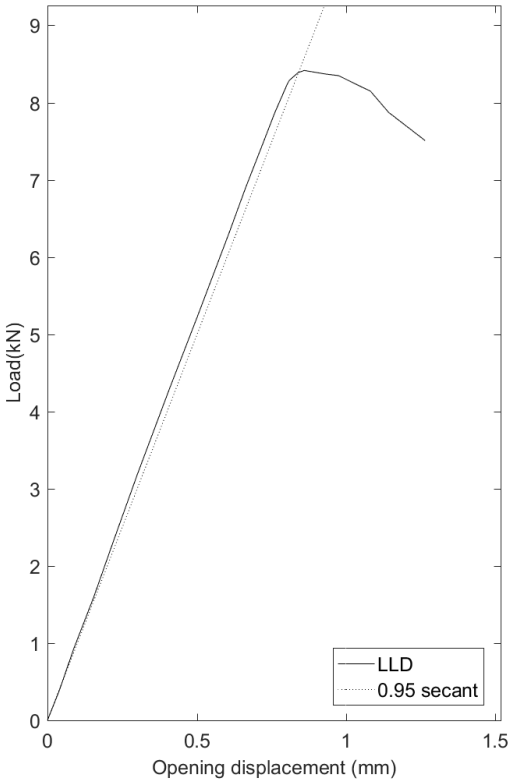

Figure 4.6: Ti6Al4V-2 - Room temperature test

Ti6Al4V-1 In the data from this test there are only 2 valid points for the compliance measurement (see Figure F.9 in Appendix F), and the test also shows relatively brittle behaviour, as such the LEFM method is used to determine the fracture toughness of this specimen.

The load at the intersection between the 0.95 secant line and LLD curve is the load P_Q as illustrated in Figure 4.5, which is used to determine the fracture toughness K_Q. Where the test is a valid test result if the relation shown in Equation 4.1(from section 9.1.3[11]) with the maximum load (P_{max}) is met.

$$P_{max}/P_Q \leq 1.10 \tag{4.1}$$

In this case P_Q = 9.63 kN and P_{max} = 10.83 kN, resulting in P_{max}/P_Q = 1.08; which meets the validity requirement. Using the load P_Q and the method outlined in the standard for a C(T) specimen the fracture toughness K_Q is calculated; $K_Q = 36.9\,\text{MPa}\sqrt{\text{m}}$.

Using this computed fracture toughness the second validity requirement (Equation 4.2) is used to determine if the value $K_Q = K_{IC}$. Using the material properties at 4 K from Table G.2 and b_0 = 21.6 mm, yields 1.075 mm ≤ 21.6 mm, so in this case we can consider $K_{IC} = 36.9\,\text{MPa}\sqrt{\text{m}}$.

$$2.5 * (K_Q/\sigma_{YS})^2 \leq b_0 \tag{4.2}$$

The computed K_{IC} is less than the specified toughness for the material of $K_{IC} = 38\,\text{MPa}\sqrt{\text{m}}$(Table G.2), yet considering uneven pre-crack (section 4.1) and material uncertainty this discrepancy seems negligible.

Ti6Al4V-2 In this specimen the pre-crack crack was relatively large at approximately 11 mm, with the starter notch at 11.4 mm, the total crack initial length was 22.4 mm. With the specimen size W at 36 mm this initial crack was at a ratio of 0.62 of the specimen, with the requirements stating a crack length of between 0.45 and 0.7 W this can still be considered acceptable by the standard however the crack is relatively large.

The load at the intersection between the 0.95 secant line and LLD curve is the load P_Q as illustrated in Figure 4.6, which used to determine the fracture toughness K_Q. Where the test is a valid test result if the relation shown in Equation 4.1 with the maximum load (P_{max}) is met. In this case P_Q = 8.394kN and P_{max} = 8.416kN, resulting in P_{max}/P_Q = 1.0024; acceptable. Using the load P_Q and the method outlined in the standard for a C(T) specimen the fracture toughness K_Q is calculated; $K_Q = 67.3\,\text{MPa}\sqrt{\text{m}}$.

This computed fracture toughness is used for the second validity requirement as shown in Equation 4.2[11] to determine if this value $K_Q = K_{IC}$. Inputting the material properties at room temperature from Table G.2 and b_0 = 13.45mm yields 16.41mm ≤ 13.45mm; the test specimen does not meet the requirements for a valid LEFM test.

The test does not meet the requirements for a valid LEFM toughness measurement (see section 1.4), where the requirement on the initial remaining ligament is not met[11]. The test yielded only a fracture toughness value in terms of $K_Q = 67.3\,\text{MPa}\sqrt{\text{m}}$. This value is higher than the minimum specified toughness for this material at room temperature $K_{IC} = 47\text{MPa}\sqrt{\text{m}}$ (Table G.2). In this case the large pre-crack made the test invalid for a K_{IC} characterisation of the toughness, yet the test method itself is shown to provide suitable data for a LEFM test.

4.3.3. Stainless steel specimen

The two specimen fabricated in the material 316LN are both tested at 4 K, and display significant plastic behaviour to be considered suitable for a J-test. This can be seen in the Load line displacement graphs shown in Figure 4.7 and 4.8 with significant increase in displacements with a relatively small increase of the load. The data of the stainless steel specimen are processed in the following paragraphs, te results of which are listed in Table 4.3. The first test though showing plastic deformation yielded insufficient data to determine the EPFM toughness, fortunately the second specimen did with an adjustment to the testing program; which consisted primarily of an increase in the compliance range.

Table 4.3: Fracture toughness results

specimen	Testing temperature	Initial crack length a_0	Max. measured load	Fracture toughness
316LN-1	4 K	12.84 mm	80 kN [3]	NA
316LN-2	4 K	12.4 mm	75 kN [1]	469.3 MPa$\sqrt{\text{m}}$ [4]

316LN-1 Of the two specimen this specimen did not allow for an estimate of the crack size at the compliance points. The amplitude of the unloading cycle was shown to be insufficiently large to allow for an estimate of the compliance (see Figure 4.7), and subsequently did not allow for an estimate of the crack size required for a construction of a J resistance curve (JR curve). (for the test results and processing refer to section F.3)

[3] Extrapolated value

[4] Toughness value from J-test, K_{JQ}

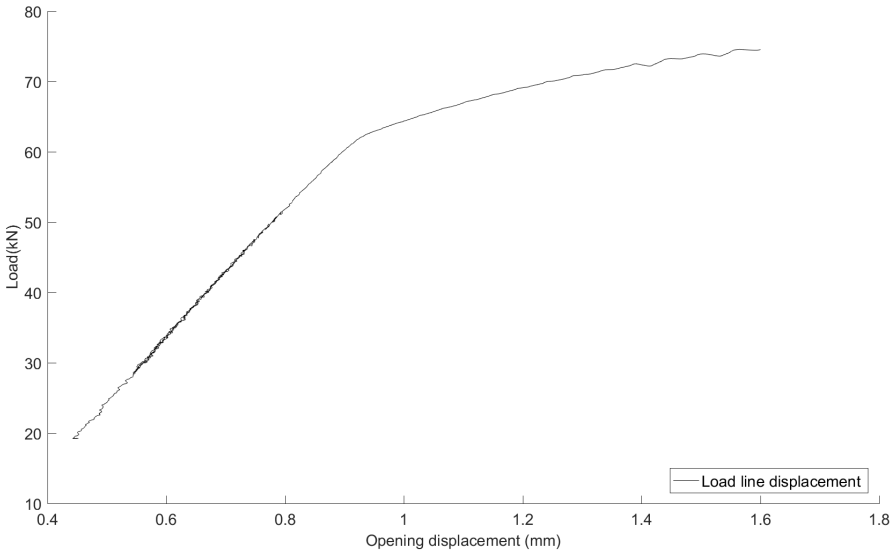

Figure 4.7: LLD specimen 316LN-1

316LN-2 The second specimen 316LN-2 was tested with a higher amplitude on the unloading cycle and did allow for an estimation of the compliance at each of the points. In Figure 4.8 the LLD curve is shown with the fit to the compliance points allowing for the estimate of te crack size, and a fit is shown on the LLD curve used to calculated the energy involved in the extension of the crack.

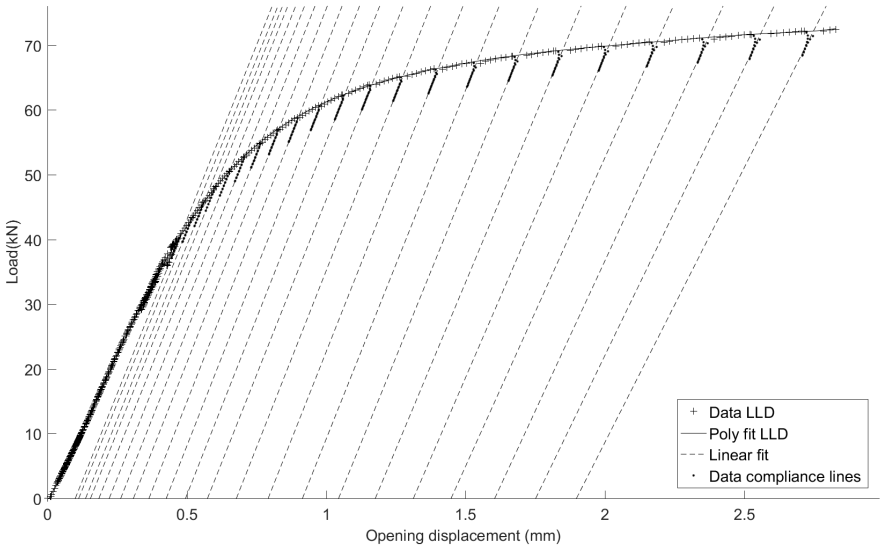

Figure 4.8: LLD specimen 316LN-2

Using the extracted data from the LLD the JR curve is constructed, and a value for the fracture toughness is determined. For this specimen the value of the toughness was calculated at $J_Q = 1014.8\,\mathrm{kJ/m^2}$. For a more in detail description of the interpretation and the processing of the data refer to section F.4. From this value the fracture toughness equivalent is calculate for this specimen at $K_{JQ} = 469.27\,\mathrm{MPa}\sqrt{\mathrm{m}}$.
The design of the specimen took into account the validity requirements 2.2.2, for J_Q as a size independent value of the fracture toughness; J_{IC}. With the validity requirement:

$$B, b_0 \geq 10\ J_Q/\sigma_y \tag{4.3}$$

For this specimen $b_0 = 23.6$ mm, and $B = 10$ mm; thickness of the specimen is governing for the validity of the test for $J_{IC=J_Q}$. Using the value for J_Q, the thickness B and the yield stress of the material in Equation 4.4 results in:

$$10 \times 10^{-3}\,\mathrm{m} \geq 10\,\frac{1014.8\,\mathrm{kJ/m^2}}{1000\,\mathrm{MPa}} \tag{4.4}$$

Evaluating Equation 4.4 the validity requirement is not met, yet considering the fact that the minimum required yield stress for the material is used in this evaluation it would likely pass this requirement if the actual yield stress of the specimen was used.

$$10 \times 10^{-3}\,\mathrm{m} \ngeq 10.15 \times 10^{-3}\,\mathrm{m} \tag{4.5}$$

The test did not meet the requirements to consider the J_Q as a thickness independent value of the fracture toughness:

$$J_Q \neq J_{IC}$$

This in part due to the high value of J_Q, and the fact that the minimum required yield stress was used in the validation of the specimen size, hence only an approximate value is shown in **??**.

As the validity requirement is not met the calculated J_Q can not be considered as a thickness independent value. The J_Q is used to compute the equivalent LEFM fracture toughness value K_{JQ} with the use of Equation 4.6. Evaluating the equation yields $K_{JQ} = 469.27\,\mathrm{MPa}\sqrt{\mathrm{m}}$.

$$K_{JQ} = \sqrt{J_Q \times \frac{E}{1-\nu^2}} \tag{4.6}$$

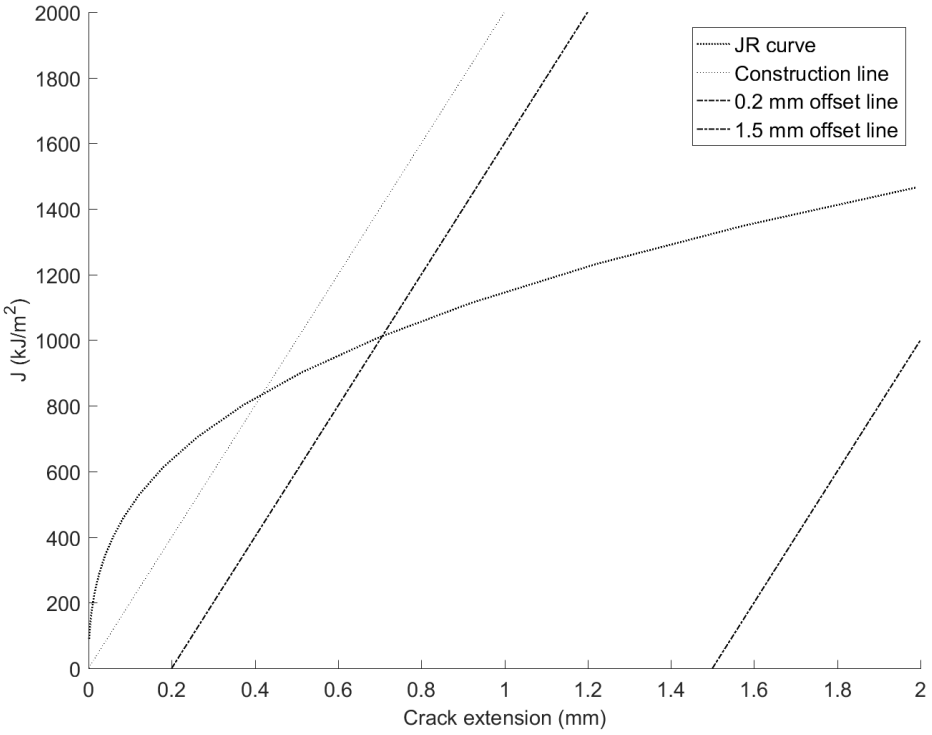

Figure 4.9: J-R curve specimen 316LN-2

5

Conclusion

The set-up is designed with the intend of allowing for the measurement of the fracture toughness as a thickness independent value. A suitable specimen thickness was estimated using available material properties of material groups under consideration for design at cryogenic temperatures (subsection 2.2.2).

The design taking into account the geometric requirements is subsequently verified for an design load; for the estimated load of 24.2 kN at 4K (section 2.3). For this design load it is shown that significant stresses occur at the pin connection of the specimen. It is recommended to use the specimen with a the larger pin diameter of $0.24W$ when testing materials which are expected to have a high fracture toughness. Additionally a modified design of the C(T) specimen is proposed to account for these high stresses (refer to subsection 2.4.1 and for the drawing see Appendix A). Based on the required measurements for a fracture toughness test sensors where selected and implemented in the design of the test set-up, while considering the temperature requirements.

The final design of the set-up is verified in more detail and a maximum load is determined for the three specimen with different pin diameters in relation to the testing temperature (see Figure 3.7). Turing each of the test once the measured load approached the calculated maximum load the test was aborted.

Additionally a detailed verification of the dewar of the cryostat is performed in order to verify the design for the pressures and temperatures which can be expected during testing. The dewar was verified in accordance with relevant pressure vessel standards [4][5], and was shown to meet the requirements listed therein (section 3.3).

In general it is shown that the set-up allows for the generation of data that allows for a characterization of the fracture toughness in accordance applicable standards at cryogenic temperatures(as discussed in section 4.3). The data generated can be processed in a structured manner and the result can be interpreted to obtain a value for the fracture toughness.

Table 5.1: Fracture toughness results

specimen	Testing temperature	Initial crack length a_0	Max. measured load	Fracture toughness
316LN-1	4 K	12.84 mm	80 kN [1]	NA
316LN-2	4 K	12.4 mm	75 kN [1]	469.3 MPa$\sqrt{\text{m}}$ [2]
Ti6Al4V-1	4 K	14.4 mm	10.38 kN	36.9 MPa$\sqrt{\text{m}}$ [3]
Ti6Al4V-2	293 K	22.5 mm	8.42 kN	67.3 MPa$\sqrt{\text{m}}$ [4]

[1] Extrapolated value
[2] Toughness value from J-test, K_{JQ}
[3] Data allows for a fracture toughness value in terms of K_{IC}, yet strictly speaking the specimen did not meet all the requirements set forth by the standard
[4] Toughness value K_{Q}

5.1. Recommendations

Validation The set-up has been used to test the fracture toughness of the modified specimen for two types of materials. The set-up is shown to provide useful data for both LEFM and EPFM, yet these first test did not meet the validity requirements set out by the used testing standards.

Though it is shown using numerical methods that the modified specimen should provide a similar fracture toughness as the default specimen set forth in standards it is not supported by experimental data. For future work it is recommended to validate the modified specimen using experiments by comparison to the default specimen (square shaped) for a selected range of materials, where especially tougher materials should be considered as the modified specimen is particularly useful when high test loads can be expected.

As a result of time constraints a comprehensive validation of the test set-up with regards to the sensor calibration and alignment was not possible. Care is taken in the design to ensure proper alignment with regards to the load, yet this is yet to be validated by measurements in the set-up. the The clip gage is calibrated within a margin of error, yet a more comprehensive calibration of the clip gage is recommended to reduce error in measurement (especially important for reliable results with regards to the compliance measurements).

Control using sensors on the specimen Test bench used though practical and allowing for a testing regime for both LEFM and EPFM is limiting. The software on the test bench is limited in the sense that it does not allow for sensor input from the sensors placed on the specimen. Allowing for control with feedback from the sensors has the following benefits: less influence from the friction between the sealing rings on the loading rod, and easier programming of the test regime (friction and elasticity of the loading assembly is no longer included in the measurements for the control).

Cyclic loading The current test-bench is not equipped with the capability for cyclic loading, the rate of loading is not suitable for a FCGR test or for pre-cracking of the specimen. The lack of a machine for cyclic loading was one of the challenges in this project as it required the aid of an external facility for a crucial part of the sample preparation.

For future work the procurement of in house capability for cyclic loading is highly recommended. Either by supplementing the current test bench with hardware (actuators) that will allow for tests with cyclic loads or the procurement of a test bench specifically designed for it.

This additional capability would be highly beneficial as it would allow for additional fracture toughness tests and preparation of the specimen. In the case the test set-up allows for both dynamic as well as dynamic testing, possibly even in sequence, meaning that a single specimen could be used for both FCGR test and a J-test for instance.

Additional measurements Additional measurement capabilities would be nice to have such as: coolant liquid level gages, EPDM and measurement of acoustic emissions.

Currently the set-up is filled with coolant and the maximum level is inferred from the filling duration, sensor feedback and icing on the return line. Once the coolant level reaches the baffle plates of the cryostat boiling effects creates significant noise, additionally significant icing can be detected on the return line. At first this icing is primarily water vapour, if sufficient cooling occurs in the return line the air itself could potentially condense (oxygen and nitrogen), leading to a possibly hazardous situation (especially so as liquid oxygen is highly flammable). Measurement of the liquid level allows for sufficient control of the specimen temperature, less expenditure of coolant and less sensor noise at the onset of the test.

Electric potential difference method will allow for in-situ measurement of the crack length, this would allow for a more continuous measurement of the crack length without the necessity to interrupt the test for the compliance measurements for the inference of the crack progression. EPDM does pose some challenges which will require some research prior to implementation, the influence of the cooling of the specimen and wires would need to be known or mitigated. Additionally some materials could become superconducting at these low temperatures, effectively meaning that there is no resistance to be measured, this however can be circumvented by using an adhesive film on which the EPDM measurement is performed. For Reliable crack length measurement additional work will be required and potentially also correlation tests.

Another promising method for fracture toughness measurements is by acoustic emissions. At the time this work was performed no testing standards were found readily available for the measurement of the fracture toughness using acoustic emissions, yet as the techniques are further developed this is could be an interesting additional measurement capability for the current set-up.

Bibliography

[1] *Technical note D-7532*. NASA, 1973.

[2] *Polytechnisch zakboek*. Reed bussines information, 2004.

[3] Cryocomp. Software, 2011. v 5.0.

[4] EN 13445. Unfired pressure vessels. 2016.

[5] EN 13458. Cryogenic vessels. static vacuum insulated vessels. 2002.

[6] Ted L Anderson and TL Anderson. *Fracture mechanics: fundamentals and applications*. CRC press, 2005.

[7] CERN. Technical spec. 1000, 1.4429, aisi 316ln. *Materials Technical Specification GS-IS & EN-MME*, N° 1000 ed. 5, 2013.

[8] Antony Julian Croft. *Cryogenic laboratory equipment*. Springer Science & Business Media, 2013.

[9] ASTM E1820. Standard test method for measurement of fracture toughness. 2015.

[10] ASTM E1823. Standard terminology relating to fatigue and fracture testing. 2013.

[11] ASTM E399. Standard test method for linear-elastic plane-strain fracture toughness kic of metallic materials. (01), 2012.

[12] ASTM E647-13a. Standard test method for measurement of fatigue crack growth rates. 2013.

[13] Jack Ekin. *Experimental techniques for low-temperature measurements: cryostat design, material properties and superconductor critical-current testing*. Oxford university press, 2006.

[14] Thomas M. Flynn. *CRYOGENIC ENGINEERING: Revised and Expanded, Second Edition*. Marcel Dekker, second edition edition, 2005.

[15] M. Janssen, J. Zuidema, and R.J.H. Wanhill. *Fracture Mechanics*. VSSD, second edition, 2006.

[16] S. Langeslag. *Procedure for the use of liquid helium during tensile and compression tests on the UTS 200*. CERN. Internal document.

[17] N. Malik. Development of a universal cryogenic test facility - literature review. Master's thesis, TU Delft, 2017.

[18] R. Betemps (Robin.Betemps@cern.ch) N. Malik (naseem.malik@cern.ch), L. Alberty (L.Alberty@cern.ch). Calculation report strength analysis static cryogenic vessel 4.2k he cryostat for tensile tests. Technical report, CERN, 2017.

[19] A Nyilas, K Nikbin, A Portone, C Sborchia, U Balachandran, and Melinda Adams. Tensile, fracture, fatigue life, and fatigue crack growth rate behavior of structural materials for the iter magnets: the european contribution. In *AIP Conference Proceedings*, volume 711, pages 176–183. AIP, 2004.

[20] Arman Nyilas, K-P Weiss, Stefano Sgobba, Maud Scheubel, and Paul Libeyre. Fatigue crack growth rate and fracture toughness of iter central solenoid jacket materials at 7 k. In *AIP Conference Proceedings*, volume 1435, pages 47–54. AIP, 2012.

[21] T Ogata, T Yuri, Y Ono, U Balachandran, Kathleen Amm, Lance Cooley, K Ted Hartwig, Michael Osofsky, Sastry Pamidi, Richard Reed, et al. Review of specimen heating in mechanical tests at cryogenic temperatures. In *AIP Conference Proceedings*, volume 1574, pages 86–91. AIP, 2014.

[22] Richard P. Reed and Alan F. Clark. *Materials at low temperatures*. American Society for Metals, 1983.

[23] J Sas, KP Weiss, and A Jung. The mechanical and material properties of 316ln austenitic stainless steel for the fusion application in cryogenic temperatures. In *IOP Conference Series: Materials Science and Engineering*, volume 102, page 012003. IOP Publishing, 2015.

[24] CF Shih. Relationships between the j-integral and the crack opening displacement for stationary and extending cracks. *Journal of the Mechanics and Physics of Solids*, 29(4):305–326, 1981.

[25] Steven W Van Sciver. *Helium cryogenics*. Springer Science & Business Media, 2012.

[26] Voss. The use of the partial unloading compliance method for the determination of j-r curves and jic. *American society for testing and materials*, pages 117–130, 1985.

[27] M Wilson. Superconducting materials for magnets. *CERN EUROPEAN ORGANIZATION FOR NUCLEAR RESEARCH-REPORTS-CERN*, pages 47–70, 1996.

Appendices

A

Drawing tooling and specimen

A.1. Specimen

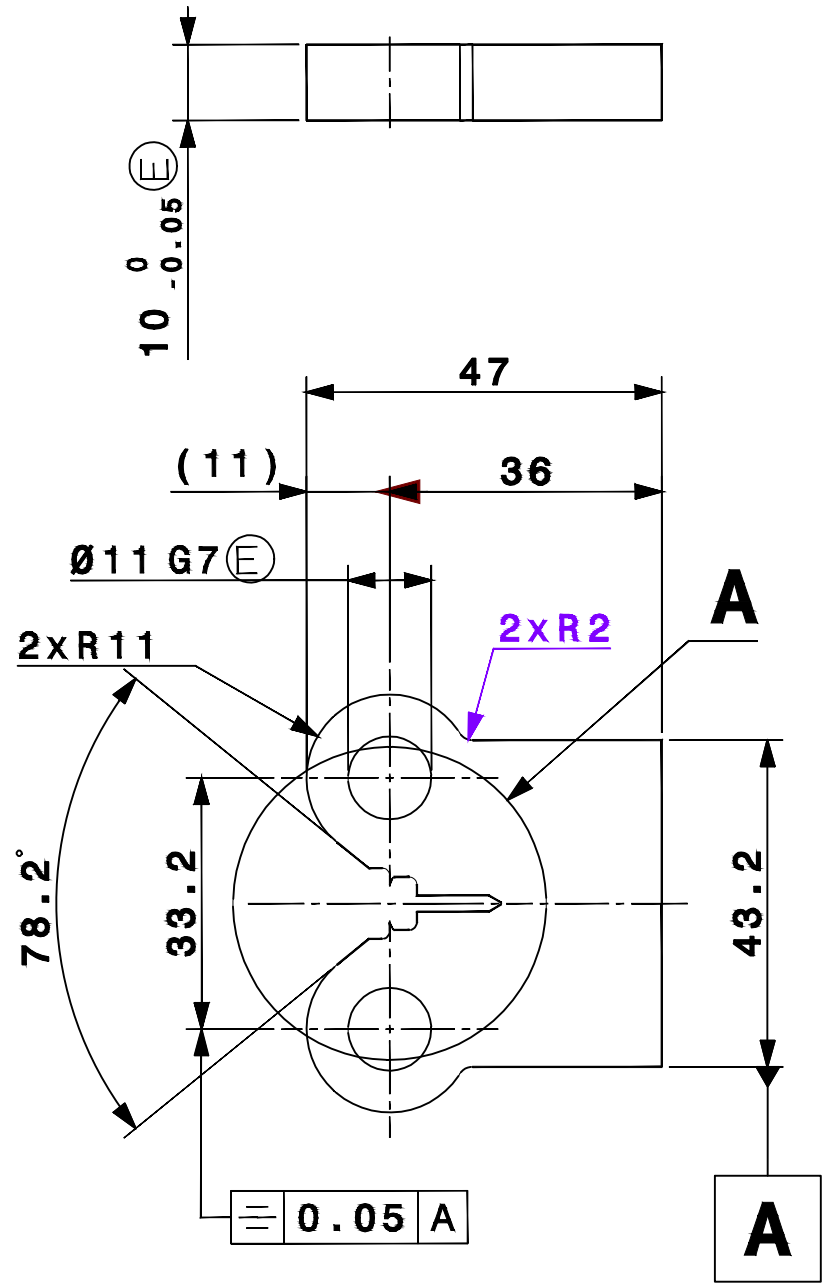

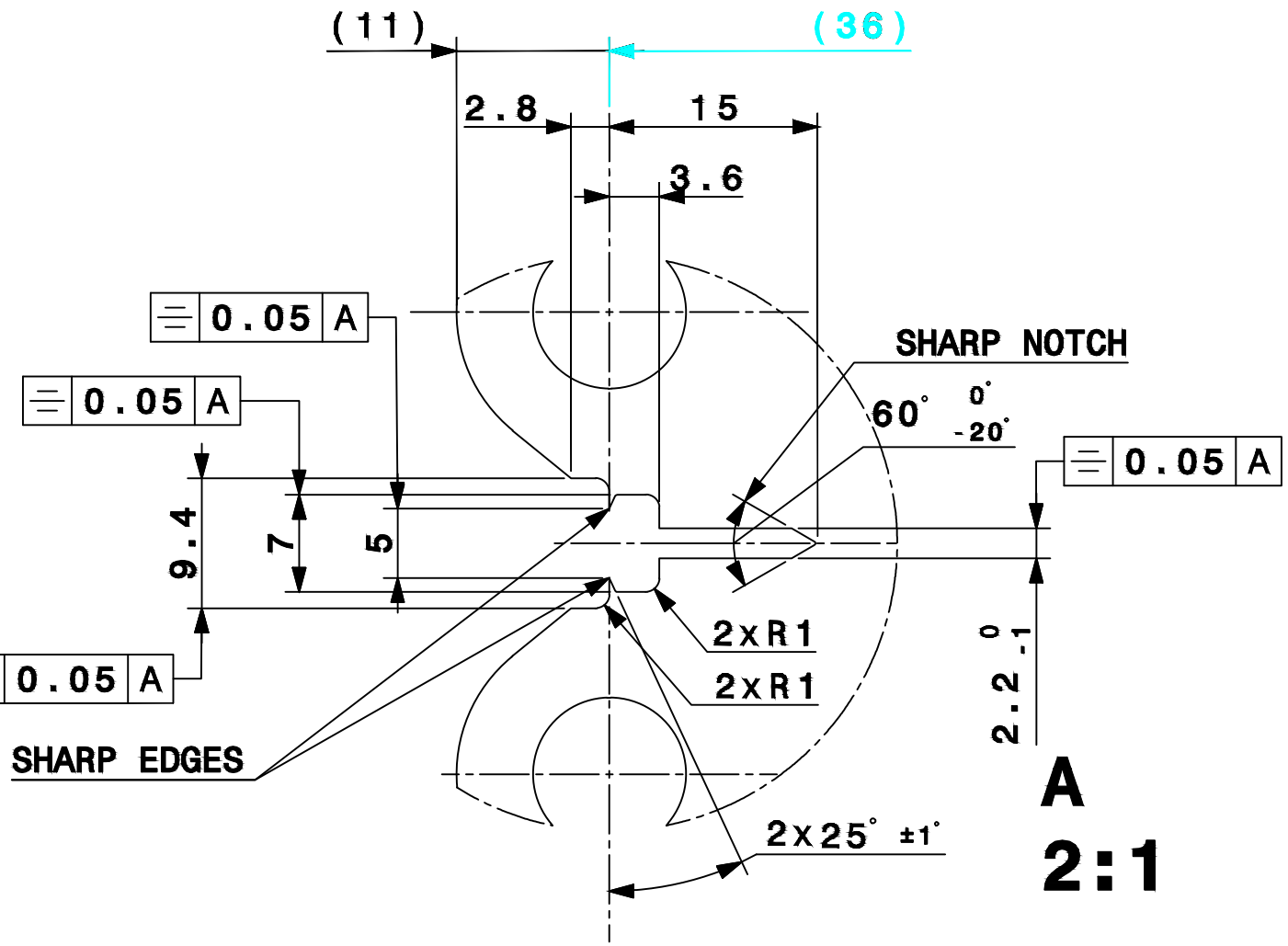

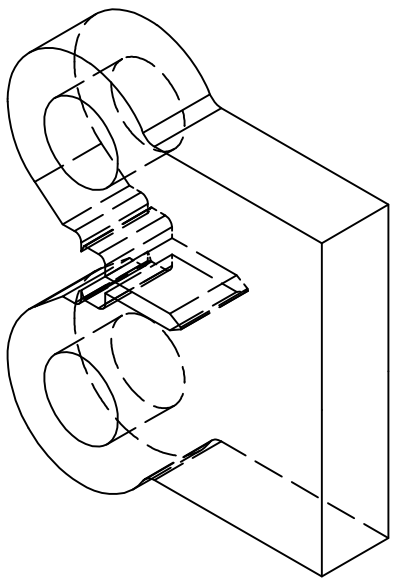

Mass 0.143 kg

UNLESS OTHERWISE MENTIONED, APPLICABLE ISO GPS STANDARDS
ARE THOSE PRIOR TO 2010-08-01 REGARDLESS OF THE DRAWING DATE

1	Compact tensile specimen	1	EN 1.4429 (St Steel 316LN)		44.59.32 612.8
QUA	DESCRIPTION	POS	MAT.	OBSERVATIONS	REF.CERN
ENS/ASS		S.ENS/S.ASS			
ISO 2768-fH	Ra 1.6	ISO 13715 -0.1 -0.3 +1 +0.3			

Tooling for Cryogenic Cryostat Testing		DRAWN	M. MALIK 2019-10-21
FRACTURE MECHANICS SPECIMEN E1820 EPFM C(T) Modified Pin Diam	SCALE 1:1	CONTROLLED	
		RELEASED	
		APPROVED	
		CAD Document Number	ST0873938_02
		REPLACES	

CERN	NON VALABLE POUR EXECUTION NOT VALID FOR EXECUTION	QAC -	CRNQQ__T0177	SIZE 3	IND.

DESSIN RUGOSITE, TOLERANCES SELON NORMES ISO
DRAWING ROUGHNESS, TOLERANCES ACCORDING TO ISO STANDARDS

PROJECTION

ORGANISATION EUROPEENNE POUR LA RECHERCHE NUCLEAIRE
EUROPEAN ORGANIZATION FOR NUCLEAR RESEARCH
GENEVE

7 6 5 4 3 2 1

e d c b a

DESSIN RUGOSITE TOLERANCES SELON NORMES ISO
DRAWING RUGOSITY TOLERANCES ACCORDING TO ISO STANDARDS

PROJECTION

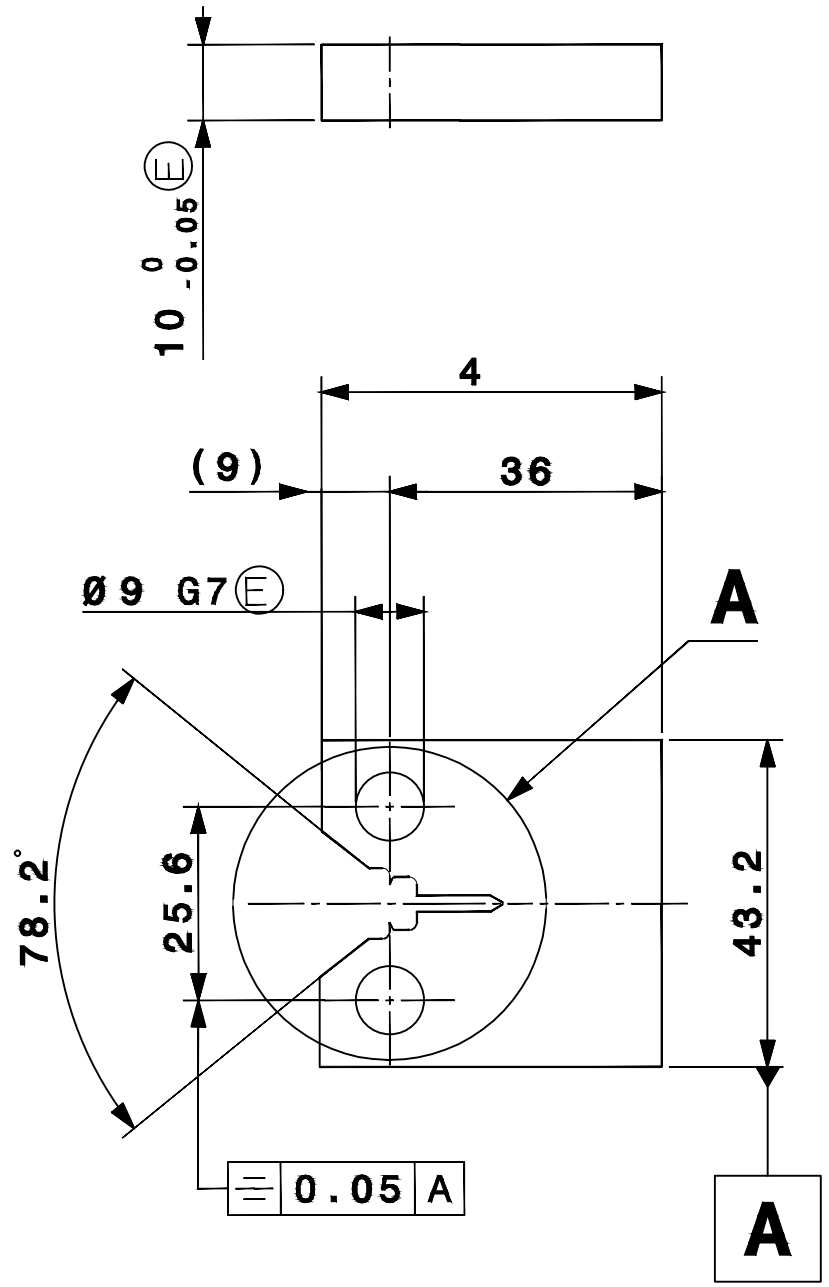

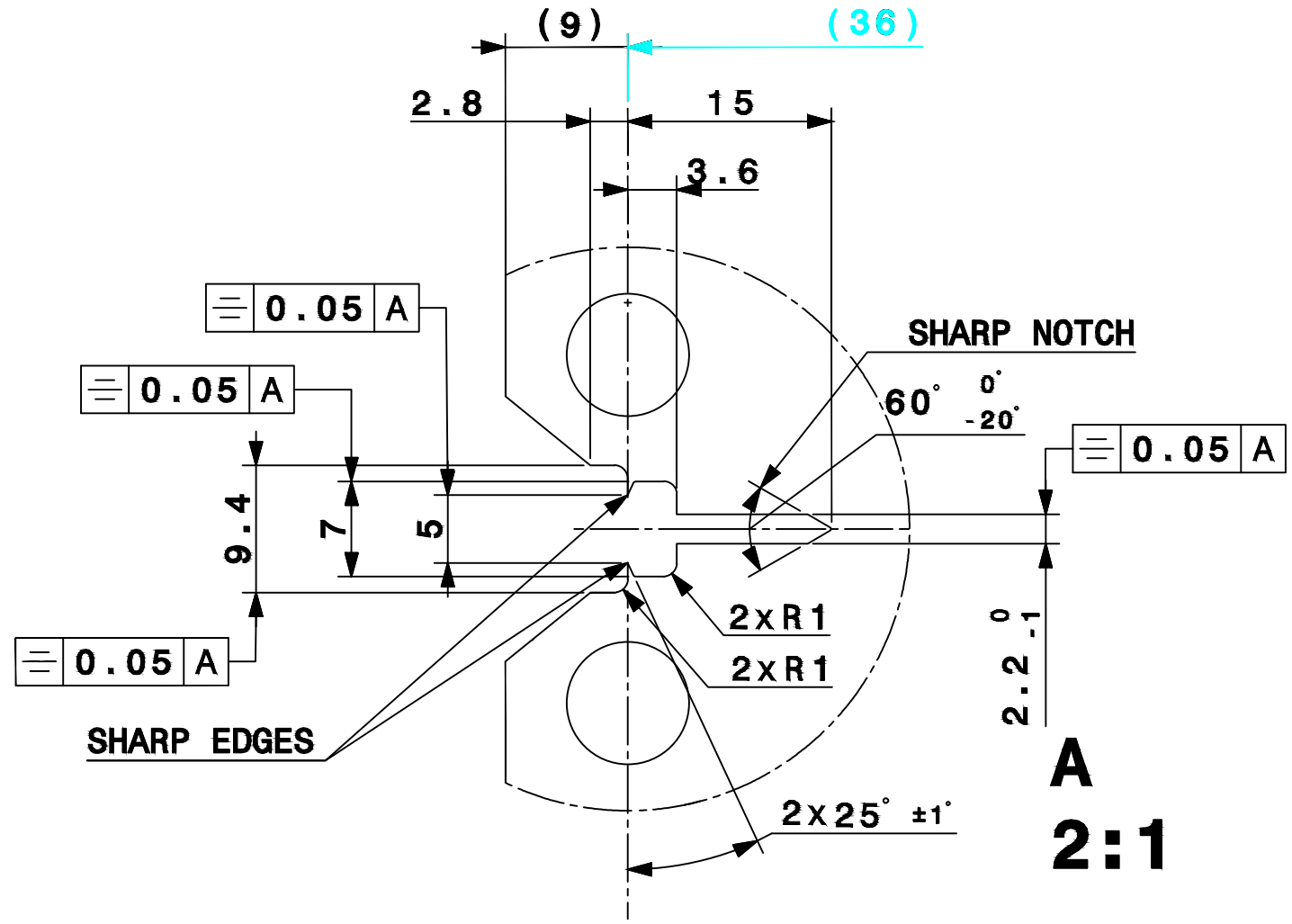

Mass 0.139 kg

UNLESS OTHERWISE MENTIONED, APPLICABLE ISO GPS STANDARDS
ARE THOSE PRIOR TO 2010-08-01 REGARDLESS OF THE DRAWING DATE

1	Compact tensile specimen	1	EN 1.4429 (St Steel 316LN)		
QUA	DESCRIPTION	POS	MAT.	OBSERVATIONS	REF.CERN
ENS/ASS		S.ENS/S.ASS			
ISO 2768-fH	Ra 1.6	ISO 13715 -0.1 -0.3 +1 +0.3			

Tooling for Cryogenic Cryostat Testing

FRACTURE MECHANICS SPECIMEN E1820 EPFM C(T) 0.24 W Pin

SCALE 1:1

DRAWN	M. MALIK	2019-10-21
CONTROLLED		
RELEASED		
APPROVED		
CAD Document Number		
REPLACES		

NON VALABLE POUR EXECUTION
NOT VALID FOR EXECUTION

QAC -

CRNQQ__T0178

SIZE 3

IND.

7 6 5 4 3 2 1

e d c b a

A.2. Tooling

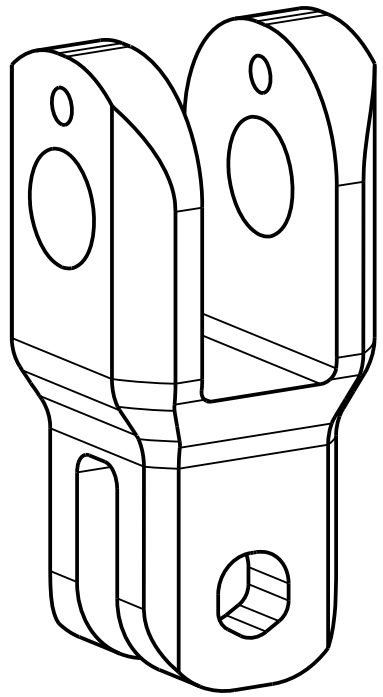

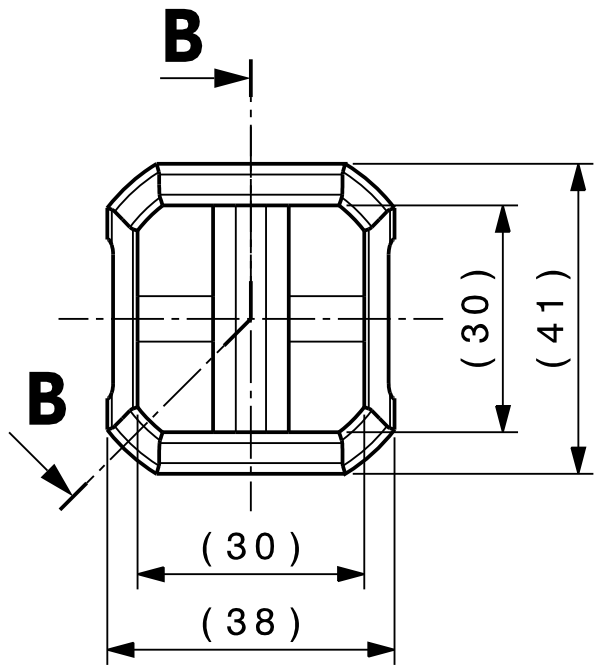

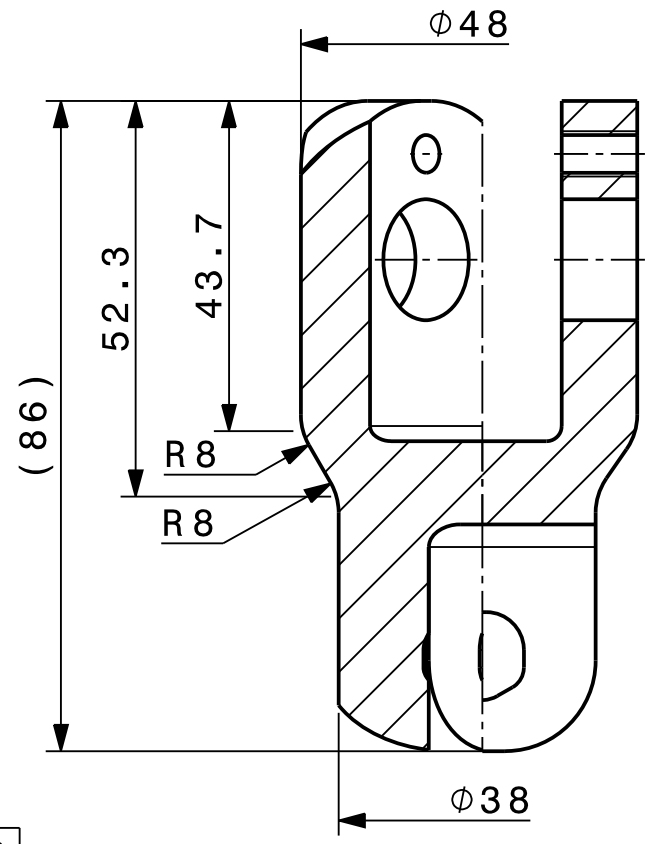

B-B

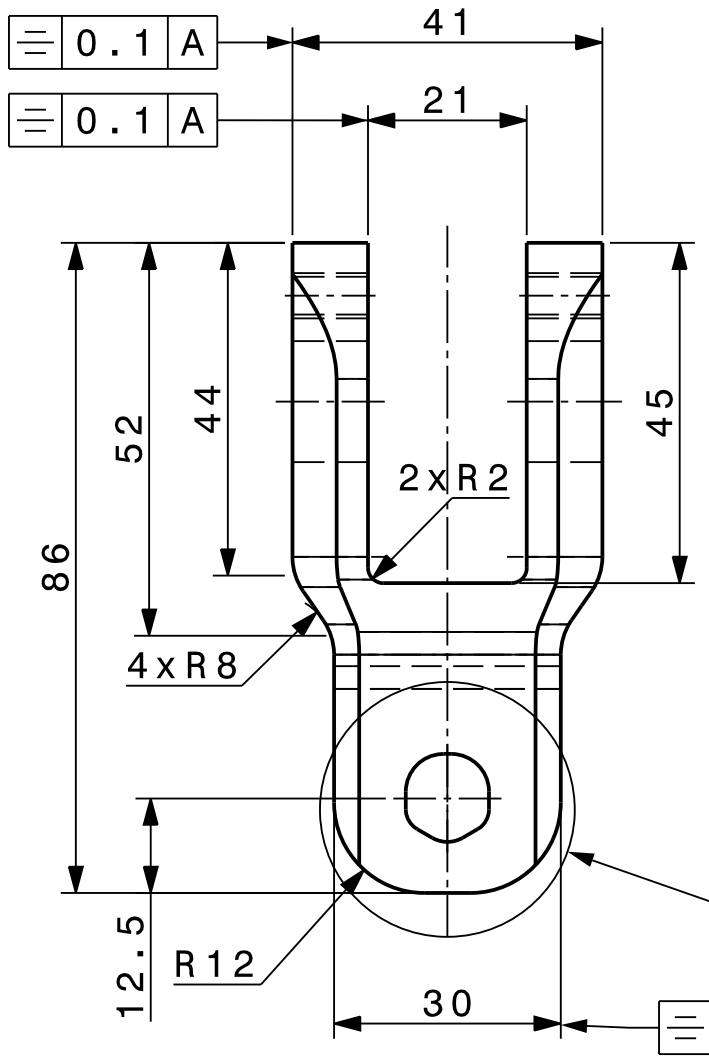

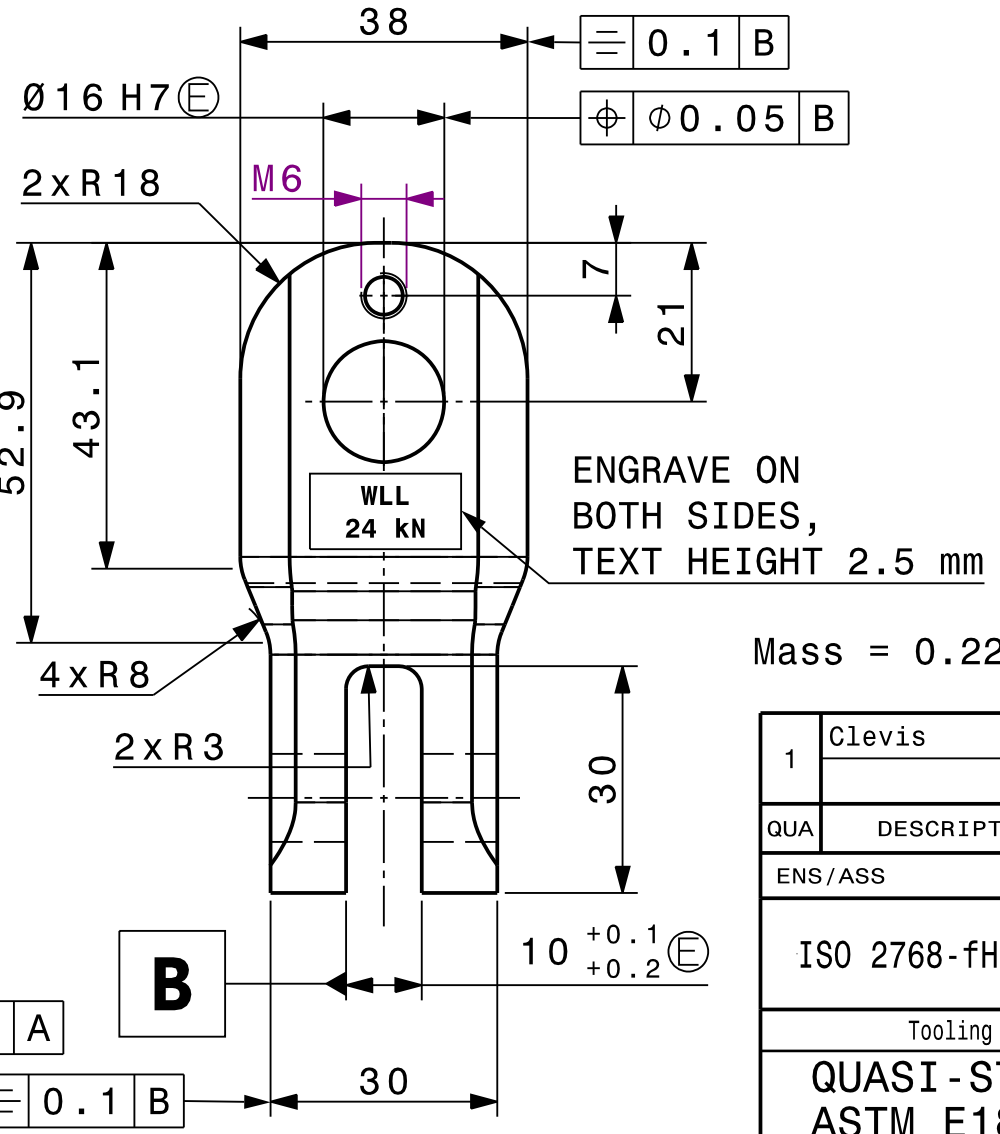

ENGRAVE ON
BOTH SIDES,
TEXT HEIGHT 2.5 mm

Mass = 0.224 kg

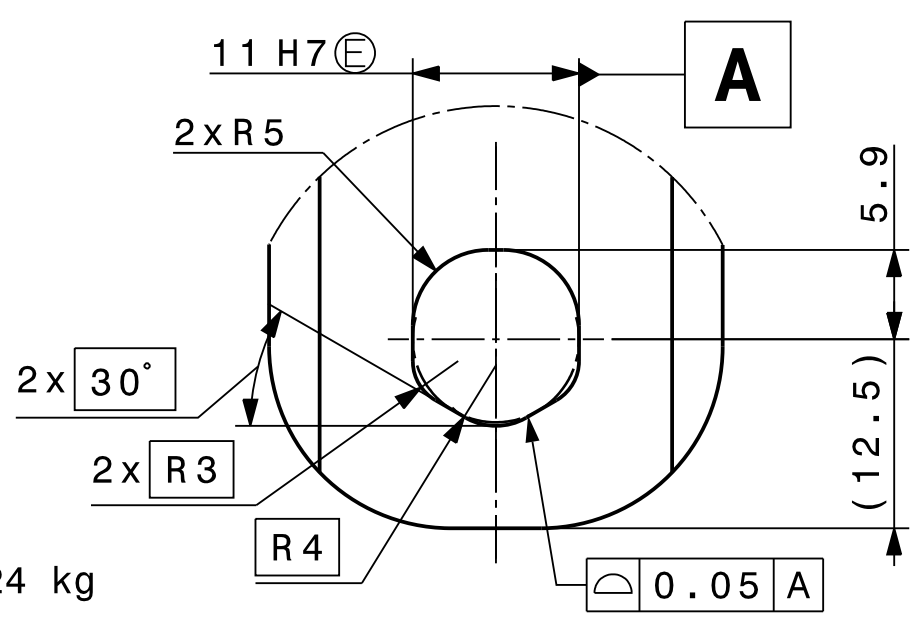

C
2:1

1	Clevis	1	Titanium Ti-6Al-4V annealed		44.05.10 050.7
QUA	DESCRIPTION	POS	MAT.	OBSERVATIONS	REF.CERN
ENS/ASS		S.ENS/S.ASS			

ISO 2768-fH | Ra 1.6 | ISO 13715 -0.3 -0.5 +1 +0.5

Tooling for Cryogenic Cryostat Testing

QUASI-STATIC EPFM TOOLING
ASTM E1820 Ti6Al4V Clevis

SCALE 1:1

DRAWN	M. MALIK	2017-08-09
CONTROLLED		
RELEASED		
APPROVED		
CAD Document Number	ST0873402_02	
REPLACES		

NON VALABLE POUR EXECUTION
NOT VALID FOR EXECUTION

QAC -

CRNQQ__T0174

SIZE 3 | IND.

UNLESS OTHERWISE MENTIONED, APPLICABLE ISO GPS STANDARDS
ARE THOSE PRIOR TO 2010-08-01 REGARDLESS OF THE DRAWING DATE

DESSIN, RUGOSITE, TOLERANCES SELON NORMES ISO
DRAWING, RUGOSITY, TOLERANCES ACCORDING TO ISO STANDARDS

PROJECTION

7 6 5 4 3 2 1

e d c b a

DESSIN, RUGOSITE, TOLERANCES SELON NORMES ISO
DRAWING, RUGOSITY, TOLERANCES ACCORDING TO ISO STANDARDS

PROJECTION

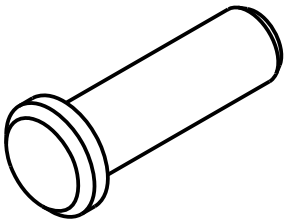

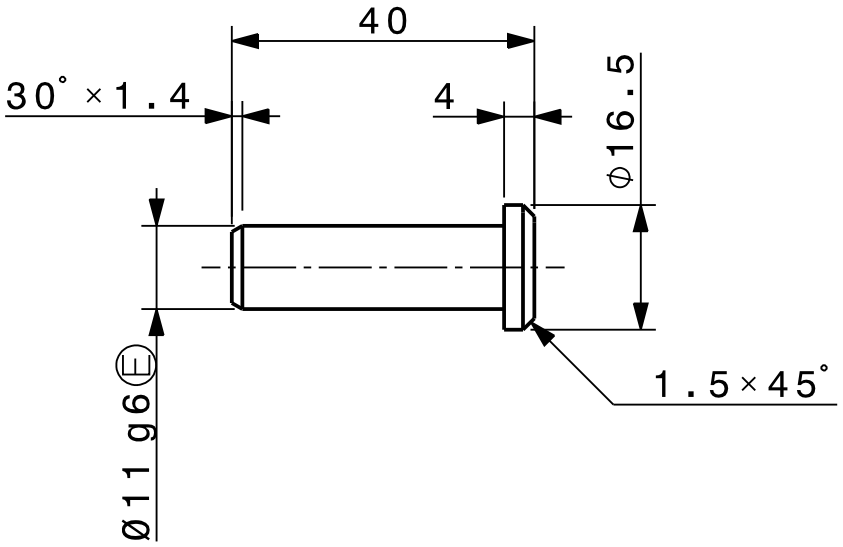

Mass = 0.019 kg

UNLESS OTHERWISE MENTIONED, APPLICABLE ISO GPS STANDARDS ARE THOSE PRIOR TO 2010-08-01 REGARDLESS OF THE DRAWING DATE

QUA	DESCRIPTION	POS	MAT.	OBSERVATIONS	REF.CERN
1	Pin	1	Titanium Ti-6Al-4V annealed		44.05.10 020.3

ENS/ASS | S.ENS/S.ASS

ISO 2768-fH | Ra 1.6 | ISO 13715 -0.1 -0.3 +0.5 +0.3

Tooling for Cryogenic Cryostat Testing

QUASI-STATIC EPFM TOOLING
E1820 Pin clevis-specimen

DRAWN	M. MALIK	2017-08-09
CONTROLLED		
RELEASED		
APPROVED		
CAD Document Number	ST0874222_02	
REPLACES		

SCALE 1:1

NON VALABLE POUR EXECUTION
NOT VALID FOR EXECUTION

QAC -

CRNQQ__T0173

SIZE 4 | IND.

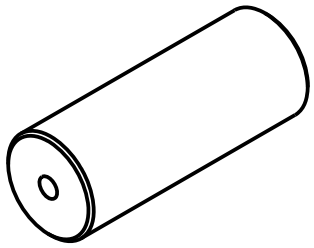

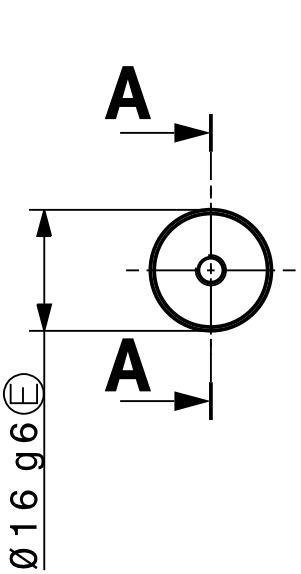

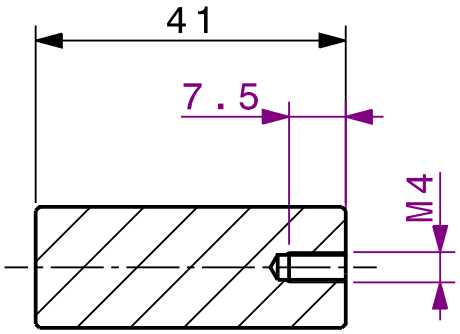

A-A

Mass = 0.036 kg

UNLESS OTHERWISE MENTIONED, APPLICABLE ISO GPS STANDARDS
ARE THOSE PRIOR TO 2010-08-01 REGARDLESS OF THE DRAWING DATE

DESSIN, RUGOSITE, TOLERANCES SELON NORMES ISO
DRAWING, RUGOSITY, TOLERANCES ACCORDING TO ISO STANDARDS

PROJECTION

1	Fixing pin clevis	1	Titanium Ti-6Al-4V annealed		44.05.10 020.3
QUA	DESCRIPTION	POS	MAT.	OBSERVATIONS	REF.CERN

ENS/ASS ST0874544 S.ENS/S.ASS ST0874488

ISO 2768-fH | Ra 1.6 | ISO 13715 +0.5 -0.05 -0.3

Tooling for Cryogenic Cryostat Testing

QUASI-STATIC EPFM TOOLING AXE DIA 16 POUR CLEVIS

SCALE 1:1

DRAWN	M. MALIK	2017-08-10
CONTROLLED		
RELEASED		
APPROVED		
CAD Document Number	ST0874492_02	
REPLACES		

NON VALABLE POUR EXECUTION
NOT VALID FOR EXECUTION

QAC -

CRNQQ__T0175

SIZE 4

IND.

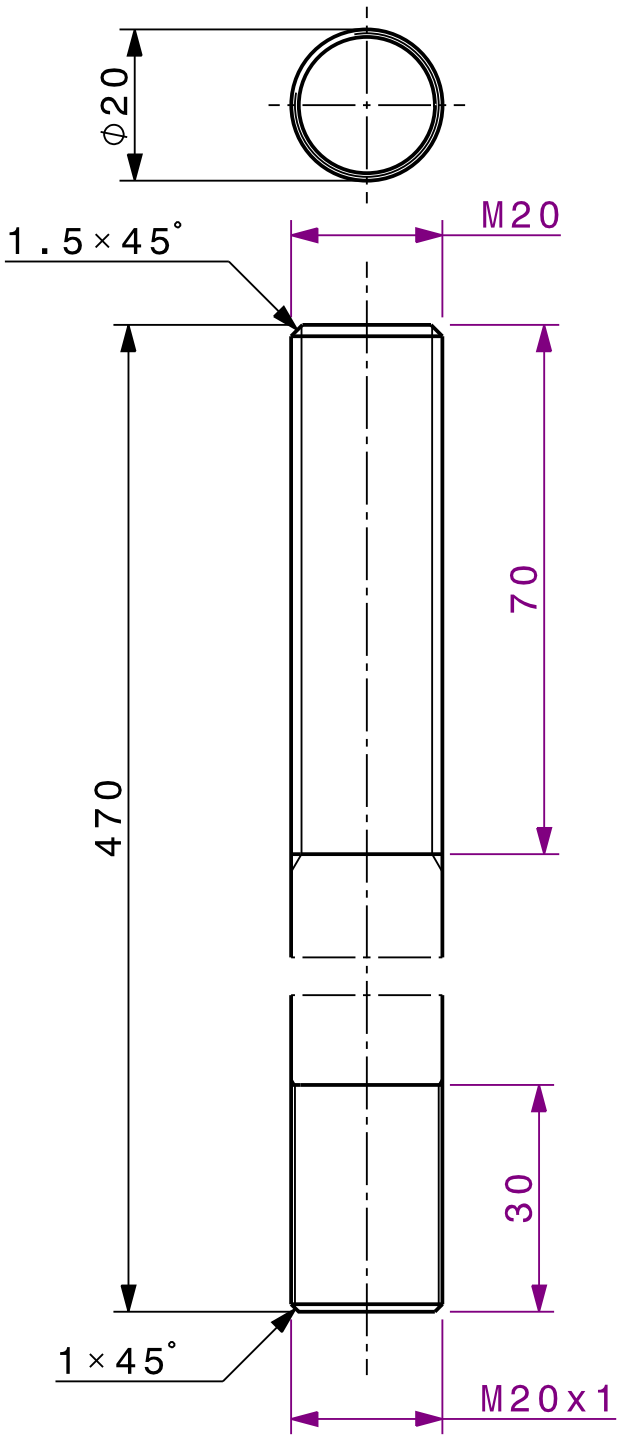

DESSIN, RUGOSITE, TOLERANCES SELON NORMES ISO
DRAWING, RUGOSITY, TOLERANCES ACCORDING TO ISO STANDARDS

PROJECTION

Mass = 0.654 kg

UNLESS OTHERWISE MENTIONED, APPLICABLE ISO GPS STANDARDS ARE THOSE PRIOR TO 2010-08-01 REGARDLESS OF THE DRAWING DATE

1	Tension rod for FM tests	1	Titanium Ti-6Al-4V annealed		44.05.10 020.3
QUA	DESCRIPTION	POS	MAT.	OBSERVATIONS	REF.CERN

ENS/ASS | S.ENS/S.ASS

ISO 2768-fH | Ra 3.2 | ISO 13715 -0.3 -0.5 +0.3

Tooling for Cryogenic Cryostat Testing

QUASI-STATIC EPFM TOOLING
Tension rod - Fracture toughness

SCALE 1:1

DRAWN	M. MALIK	2017-08-10
CONTROLLED		
RELEASED		
APPROVED		
CAD Document Number	ST0874544_02	
REPLACES		

NON VALABLE POUR EXECUTION
NOT VALID FOR EXECUTION

QAC -

CRNQQ__T0176

SIZE 4 | IND.

B

Datasheet clip gage

MODEL 3541 CLIP-ON GAGE

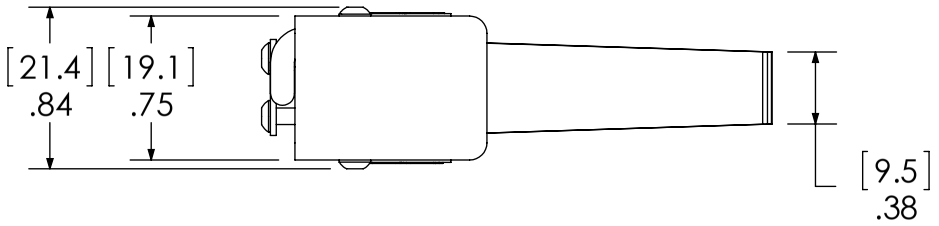

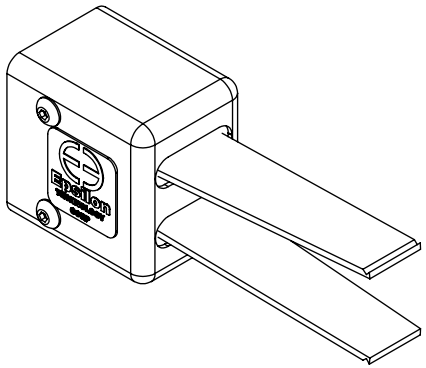

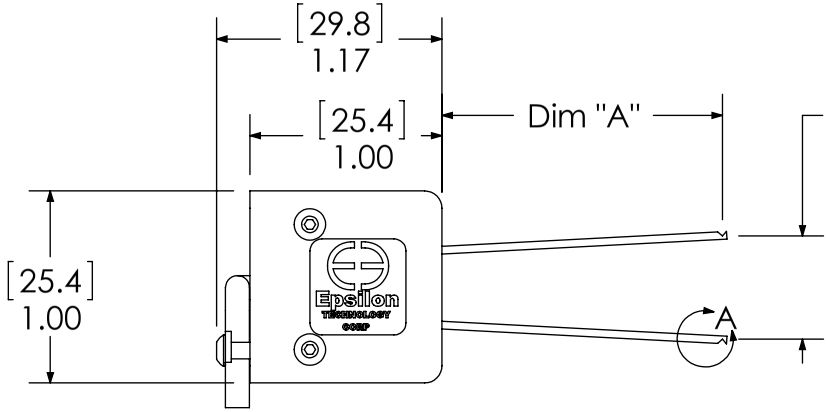

Shown "At Rest" Position,
when attached to the specimen
arms are at gage length

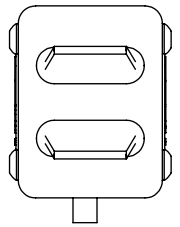

Model Number	Dim "A"	Rated Travel
3541-xxxx-100T	1.11 [28.2]	+0.100" / -0.050"
3541-xxxx-100T-E399	1.48 [37.6]	+0.100" / -0.050"
3541-xxxx-150T	1.48 [37.6]	+0.150" / -0.050"
3541-xxxx-150T-E399	1.97 [50.0]	+0.150" / -0.050"
3541-xxxx-200T	1.48 [37.6]	+0.200" / -0.050"
3541-xxxx-250T	1.97 [50.0]	+0.250" / -0.050"
3541-xxxx-500T	3.09 [78.5]	+0.500" / -0.100"
3541-xxxx-025M	1.11 [28.2]	+2.5mm / -1.0mm
3541-xxxx-025M-E399	1.48 [37.6]	+2.5mm / -1.0mm
3541-xxxx-040M	1.48 [37.6]	+4.0mm / -1.0mm
3541-xxxx-040M-E399	1.97 [50.0]	+4.0mm / -1.0mm
3541-xxxx-070M	1.97 [50.0]	+7.0mm / -1.0mm
3541-xxxx-100M	2.47 [62.7]	+10.0mm / -1.0mm
3541-xxxx-120M	3.09 [78.5]	+12.0mm / -2.0mm

CLIP-ON ARM GROOVE DETAIL

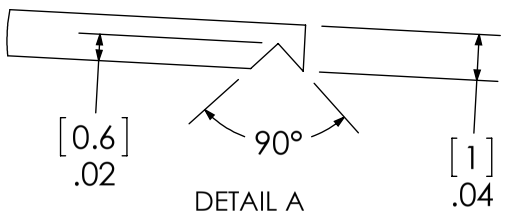

DETAIL A
SCALE 6 : 1

Epsilon Technology Corp.
Jackson, WY, USA

3541-xxxx-xxxx Clip-On Gage, Outline

[mm]
inch

DWG. NO.	REV.
3541-xxxx-xxxx-OTLN	C

SIZE	SCALE	DATE	SHEET
A	1:1	5/21/2013	1 OF 1

3541, Bolt-On Knife Edge

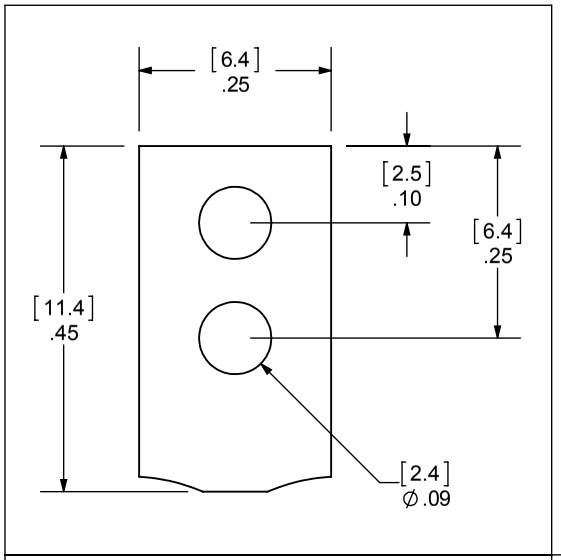

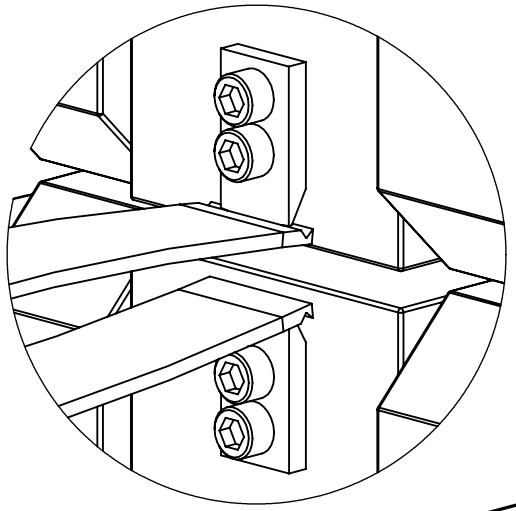

DETAIL A
SCALE 2 : 1

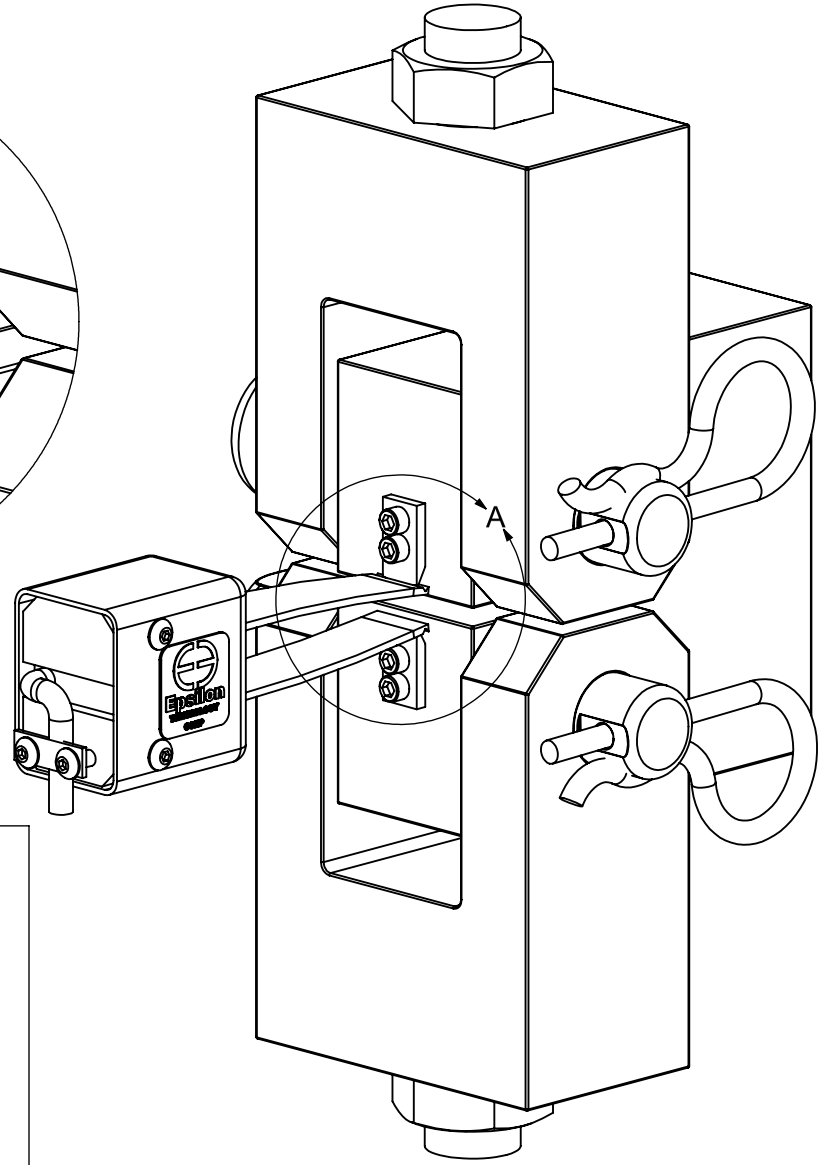

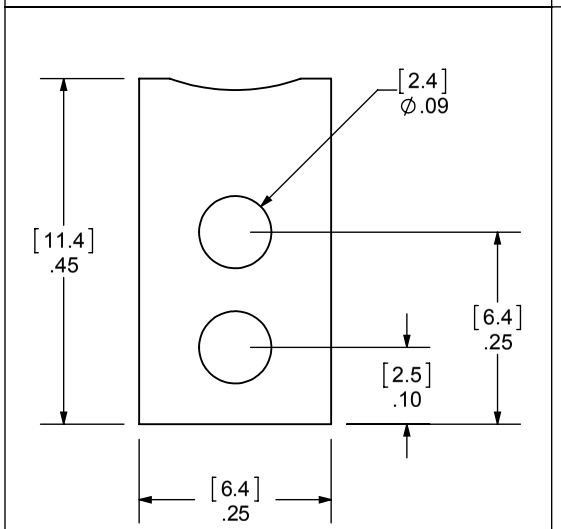

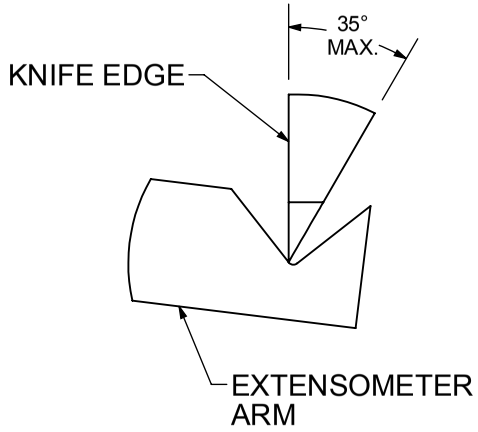

KNIFE EDGE DETAIL

Epsilon Technology Corp.
Jackson, WY, USA

3541, Bolt-On Knife Edge Outline

[mm]
inch

DWG. NO.	REV.
OTLN-3541-KE	A

SIZE	SCALE	DATE	SHEET
A	4:1	4/24/2013	1 OF 1

Epsilon technology corp
Extensometers for materials testing

3975 S. Hwy 89
Jackson, WY 83001
(307) 733-8360
(307) 733-8375 (Fax)
www.epsilontech.com

Quotation

Quote Number:	23955
Date:	06/23/2017
Valid Until:	09/23/2017
Prepared by:	Kenneth Blount
	kblount@epsilontech.com

Contact Info

Naseem Malik
CERN

muhammad.naseem.malik@cern.ch

-

Shipping Provider:	UPS Express (prepay and add)
Lead Time:	2-3 weeks (until shipment)
Payment Terms:	Net 30 with receipt of a purchase order

Products:

Quantity	Part Number:	Product	Unit Price	Ext. Price
1	3541-005M-040M-LT	COD Gage 5.0 mm compressed gauge length +4.0 mm/-1.0 mm measuring range -270 °C to 100 °C (-454 °F to 210 °F) temperature range This unit meets the accuracy requirement of ASTM E1820 Bare leads	$1,715.00	$1,715.00
		Total:		$1,715.00

INCOTERMS 2010 - EXW, Ex Works (Jackson, Wyoming)

Epsilon technology corp

Digitally signed by Kenneth Blount
DN: cn=Kenneth Blount gn=Kenneth Blount c=United States
l=US o=Epsilon Technology Corp. e=kblount@epsilontech.com
Reason: I am the author of this document
Location: Jackson, WY
Date: 2017-06-23 15:52-06:00

C

Modified specimen

As discussed in subsection 2.4.1 the contact stresses occurring in the tooling and the bending and shear stresses in the pin can be considered quite high; close to the yield stress of the material. In order to ensure a sufficient safety in the design a modified specimen using a larger pindiameter is proposed, where the effect of the modification is compared with the standard specimen geometry according to the ASTM E-1820.

A pin diameter has been calculated such that a significant margin is achieved in the design; the diameter of the pin is considered sufficient at Ø11 mm. In order to accommodate for this larger pin the specimen is modified such that sufficient material is available for the distribution of the load. (refer to appendix A).

This modified specimen can be considered to have an increase in stiffness near the hole of the pin. This could in principle affect the stress intensity factor at the crack tip, especially for cracks in the lower bounds of $0.45 \leq a/W \leq 0.7$. In order to asses the effect of this modification a comparison study is performed of the 2 standard geometries[9] in relation to the modified specimen for the lower and uppper bounds of the initial crack length.

C.1. Model and Mesh

A finite element model is prepared with all three different specimen geometries for 2 different crack geometries; a relative crack length of 0.45W and 0.70W, the lower and upper limit for a valid J-test. quadratic elements with a mesh of 0.5 mm is defined for the entire specimen, with further refinement down to a size of 0.2 mm at the crack tip. The pin is also modelled for the application of the boundary conditions; obscured from view in Figure C.1.

C.1.1. Material

The material properties defined for the material are those of a general steel. This as the material is considered of little influence in this comparison study. The J-test fracture toughness is a measure where plasticity is of importance; the development of a plastic zone at the crack tip. In order to be able to compare the effect with regards to the J-test, plastic behaviour is included in the simulation. The yield stress of the material is defined at a relatively low yield stress in order to allow for the largest gradient in stiffness.

Table C.1: Material properties

Young's modulus:	200.0	GPa
Poisson ratio	0.3	
Yield stress	250.0	MPa

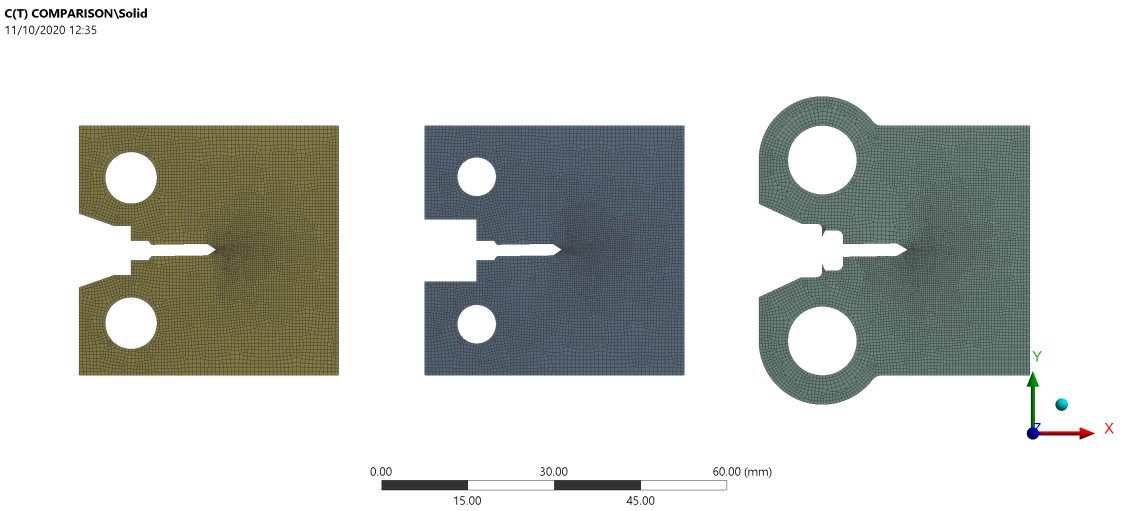

Figure C.1: Model and mesh of all three specimen - Crack $0.45W$

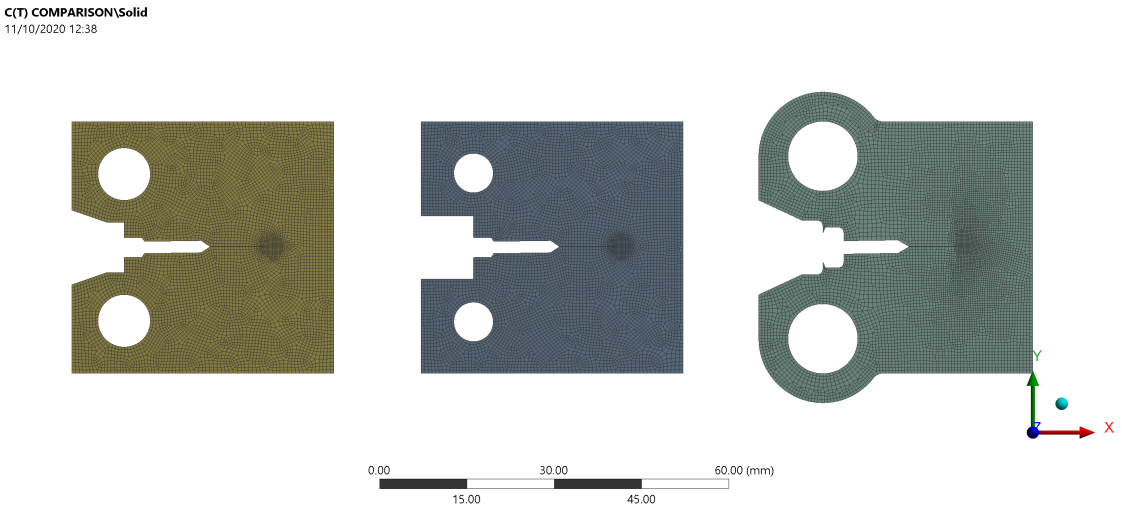

Figure C.2: Model and mesh of all three specimen - Crack $0.70W$

C.1.2. Boundary conditions

The pins are also included in the model, contact between the pin and specimen is defined as a frictional contact, with a coefficient of 0.1. The lower pins are constrained in along the X and Y-axis of the model, with a load of 8 kN defined on the upper pins along the Y-axis, As shown in Figure C.3. With one side of the pins and a corner of the specimen also constrained along the Z-axis. Weak springs have been added in the solver settings to ensure a fully constrained model.

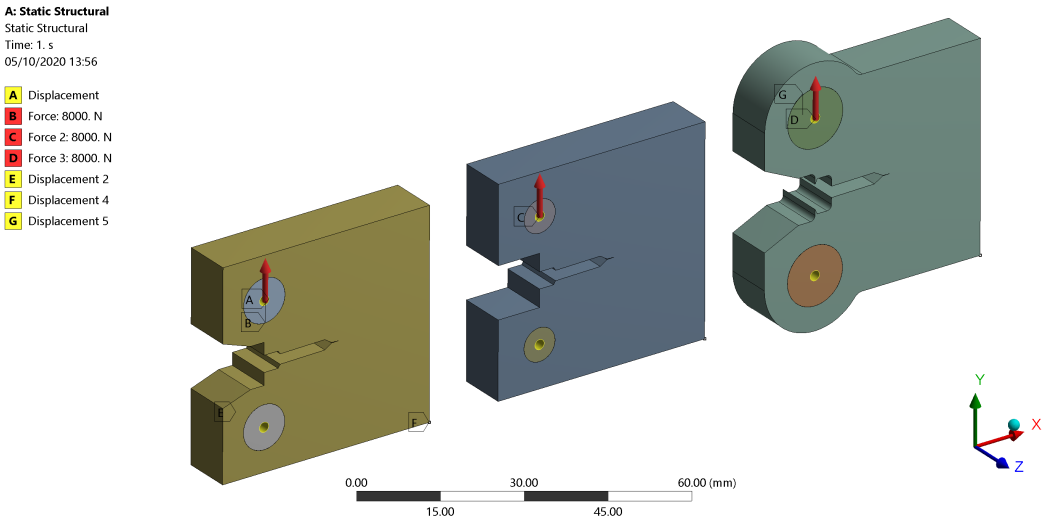

Figure C.3: Boundary conditions - Crack 0.70W

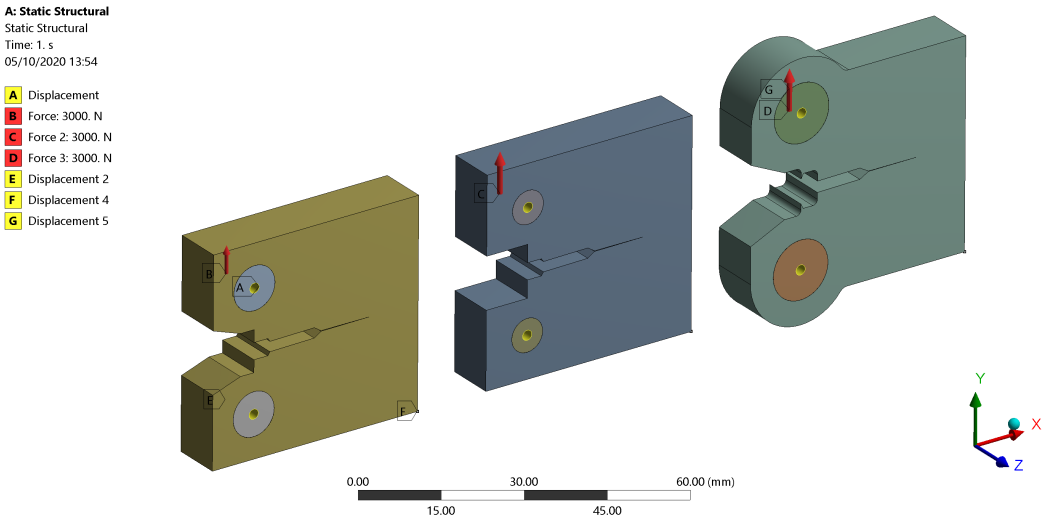

Figure C.4: Boundary conditions - Crack 0.70W

C.2. Results

C.2.1. Specimen crack length 0.45W

In the figures C.5 through C.7; the deformation, equivalent stress and equivalent strain are shown for the specimen with crack length 0.45W. Hardly any difference in these results could be inferred at the crack tip, with similar stresses, and plastic region size. A more in depth comparison of these specimen is preformed based on the numerically computed fracture characterization, both KI and J-integral. In figure C.9 through C.10 the computed KI curves are shown, showing a converged result for the computed curves.

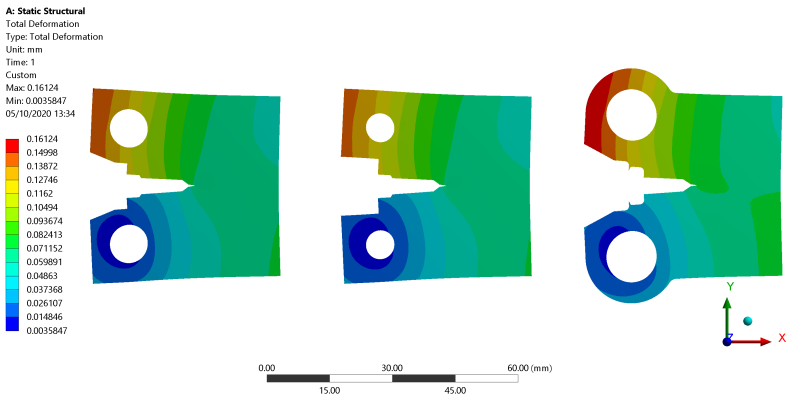

Figure C.5: Total deformation - Crack 0.45W

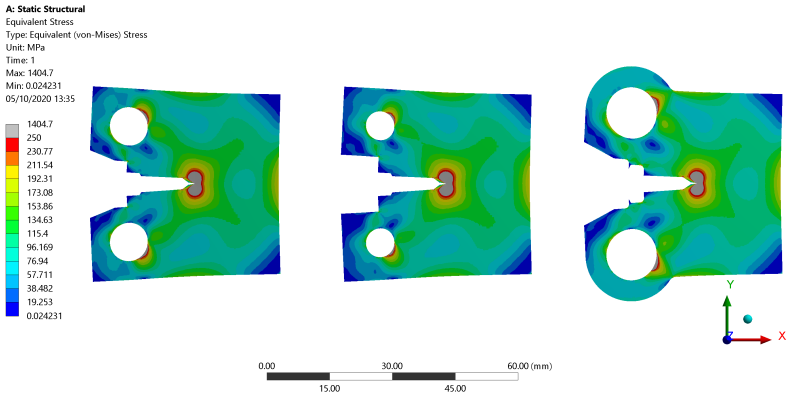

Figure C.6: Total equivalent stress - Crack 0.45W

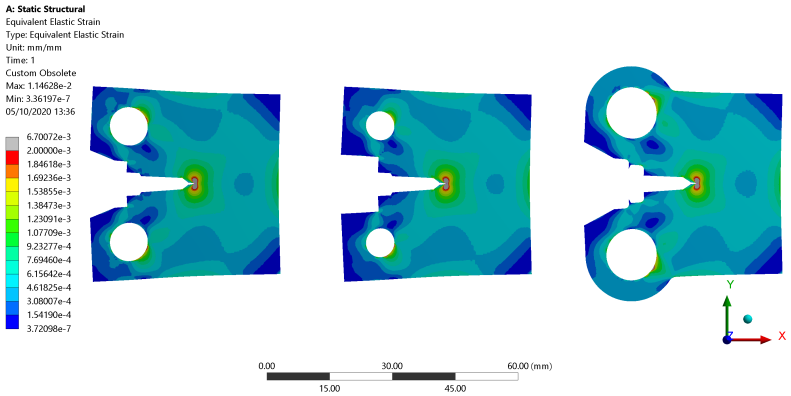

Figure C.7: Total equivalent strain - Crack 0.45W

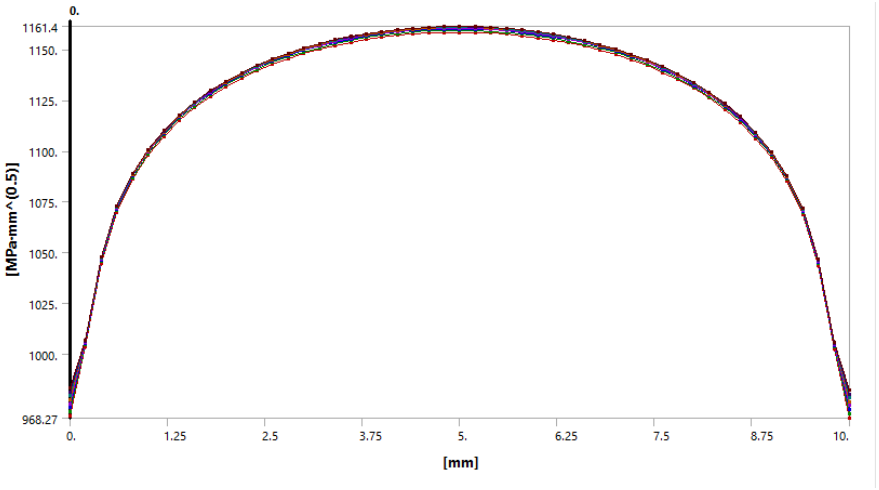

Figure C.8: SIFS curves specimen $0.24W$ - Crack $0.45W$

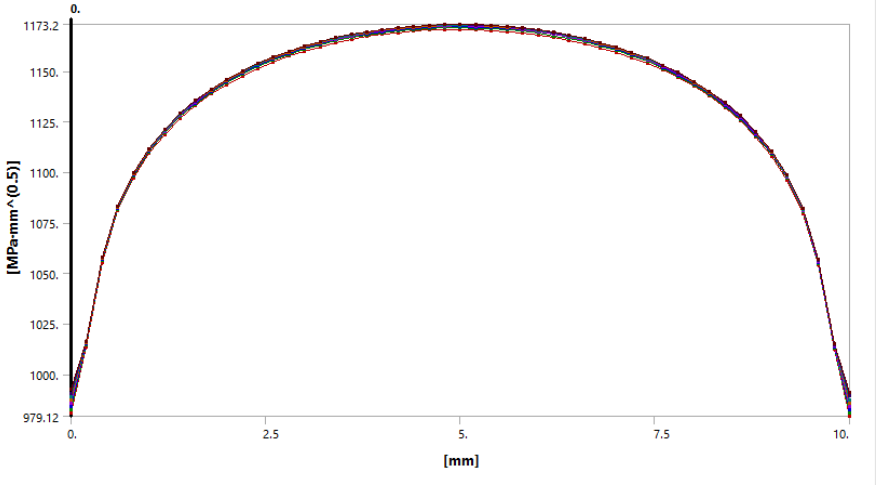

Figure C.9: SIFS curves specimen $0.188W$ - Crack $0.45W$

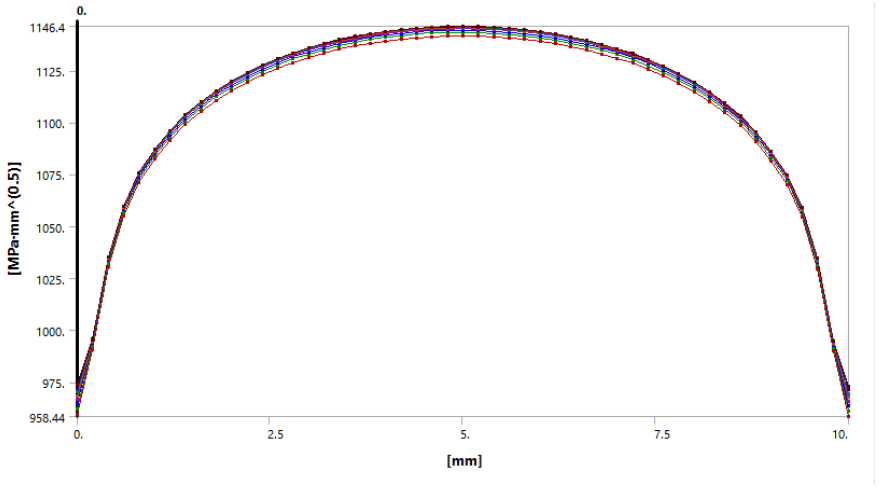

Figure C.10: SIFS curves specimen pin 11 mm - Crack $0.45W$

C.2.2. Specimen crack length 0.45W

In the figures **??** through **??**; the deformation, equivalent stress and equivalent strain are shown for the specimen with crack length 0.70W. Again no discernible difference between the specimen, both KI and J-integral are evaluated for all three specimen. In figure **??** through **??** the computed KI curves are shown, showing convergence of the results.

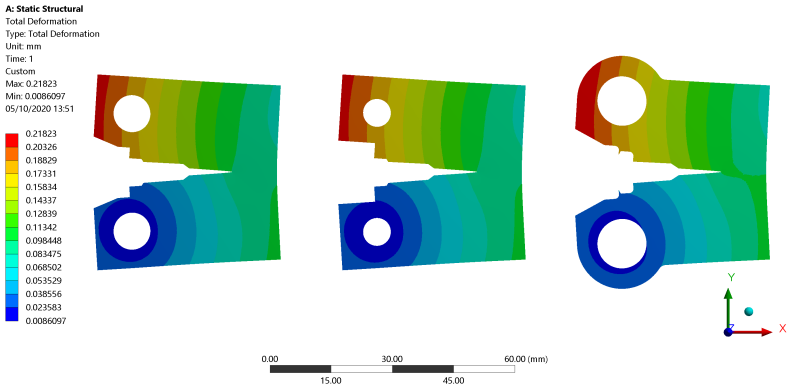

Figure C.11: Total deformation - Crack 0.70W

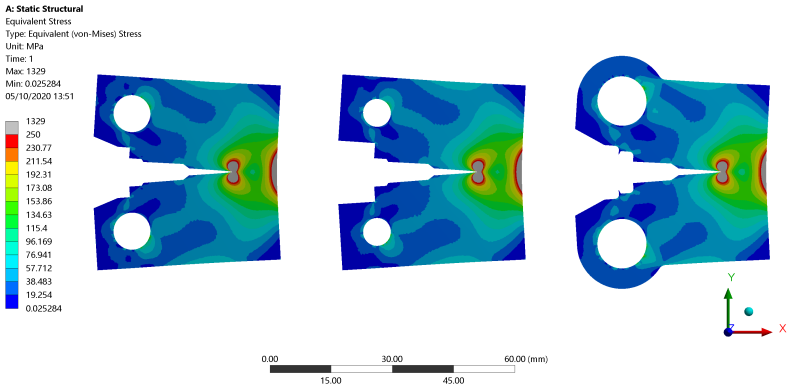

Figure C.12: Total equivalent stress - Crack 0.70W

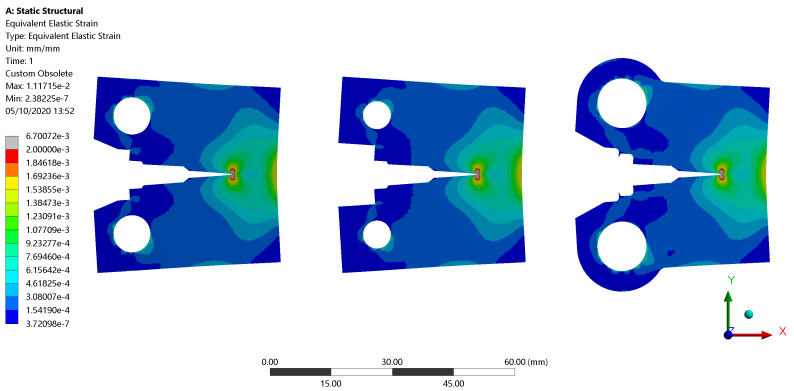

Figure C.13: Total equivalent strain - Crack 0.70W

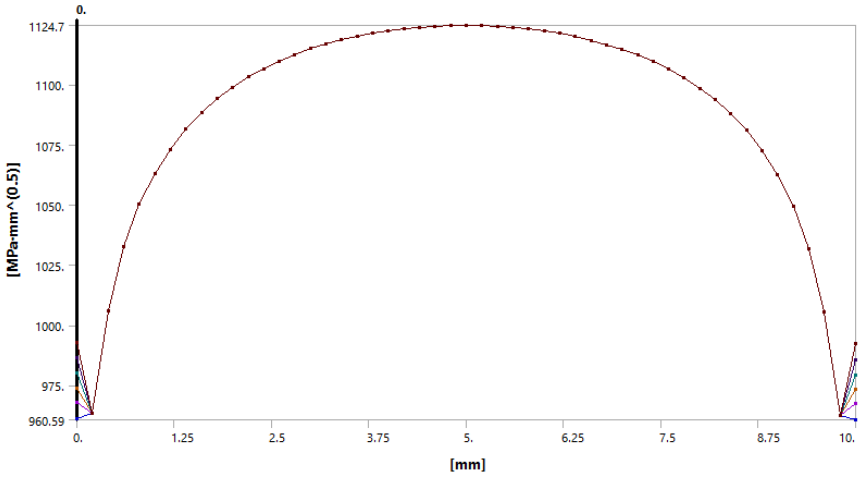

Figure C.14: SIFS curves specimen $0.24W$ - Crack $0.70W$

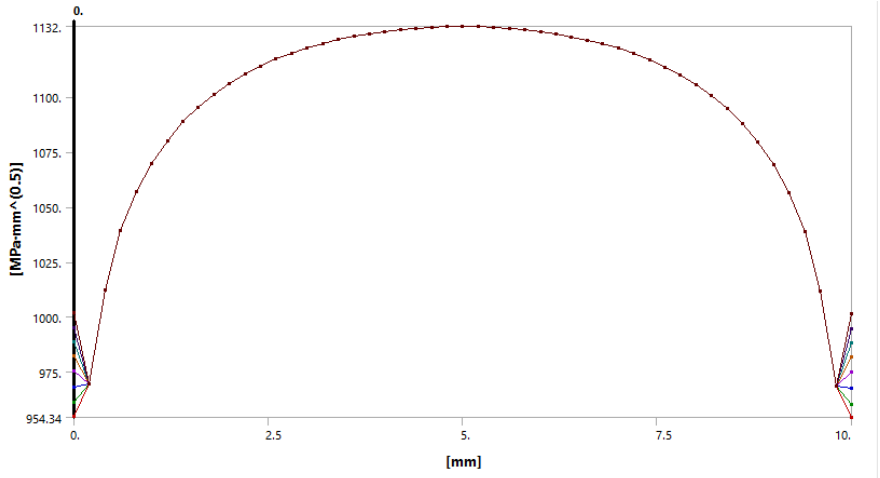

Figure C.15: SIFS curves specimen $0.188W$ - Crack $0.70W$

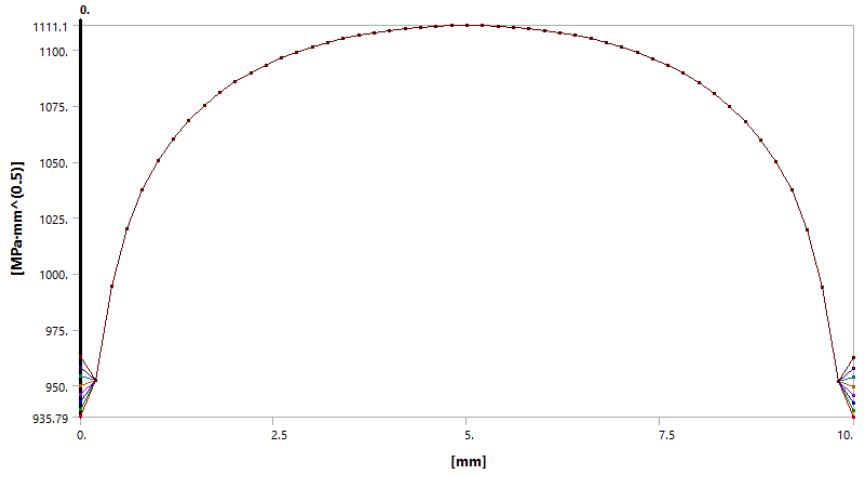

Figure C.16: SIFS curves specimen pin 11 mm - Crack $0.70W$

C.3. Conclusion

The resulting KI stress intensity factors and the J-integral computed for the three samples are compared for the converged curves as shown in Figure C.17 through Figure C.20. The change in stiffness at the pin can be considered negligible when comparing the specimen, with at most a difference in value of 1.31% for crack $0.45W$, where this influence decreases as the crack progresses to $0.70W$ to around 1.26%. In part this difference in result can be contributed by the change of the diameter of rotation at the connection. This is illustrated when comparing the standard specimen geometries from the standard with pin $0.188W$ and $0.24W$; showing an difference in computed value of also about 1%.

As The difference between the specimen can be considered as negligible, similar as that found between the two proposed geometries in the standard. The use of the modified specimen can be considered to comply with the ASTM E-1820, and is considered to allow for the similar processing of the results as described in the standard.

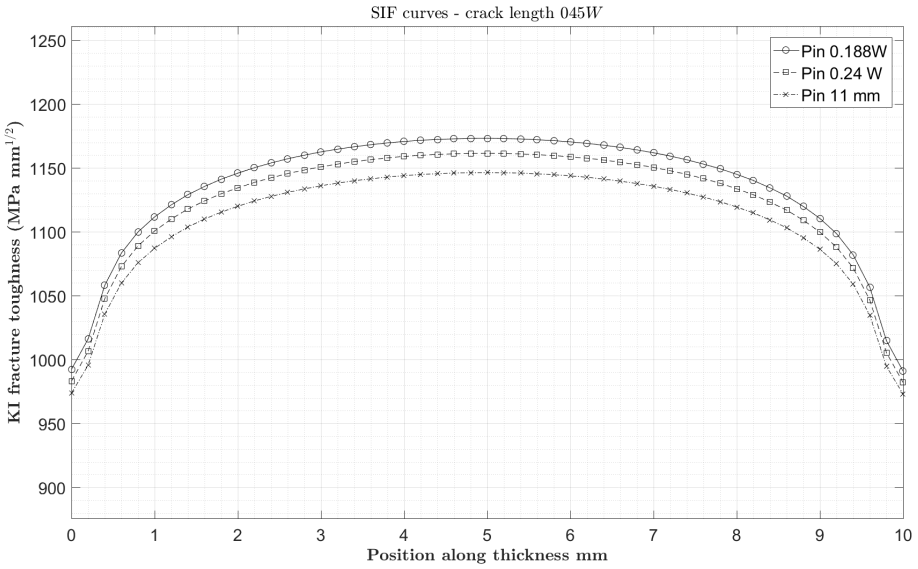

Figure C.17: KI fracture results - Crack $0.45W$

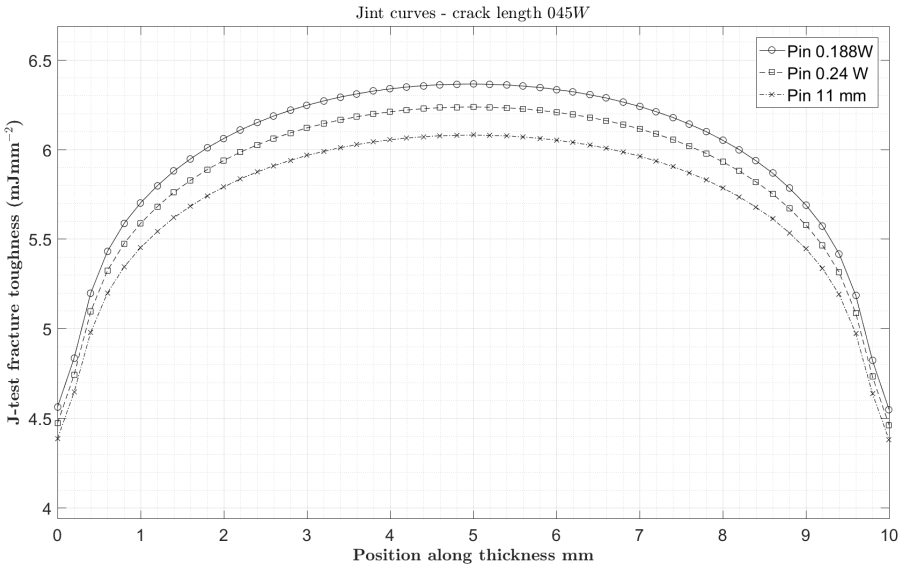

Figure C.18: J-integral fracture results - Crack $0.45W$

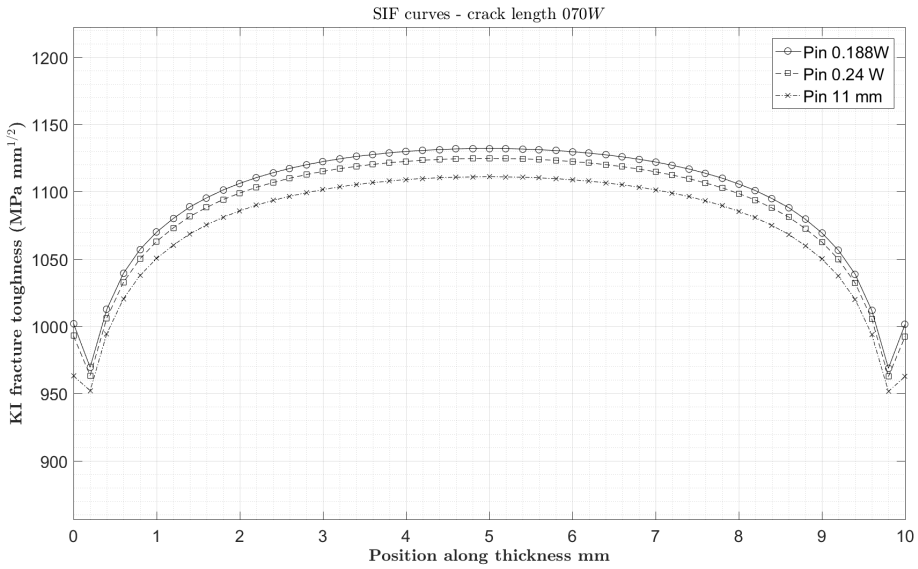

Figure C.19: KI fracture results - Crack 0.70W

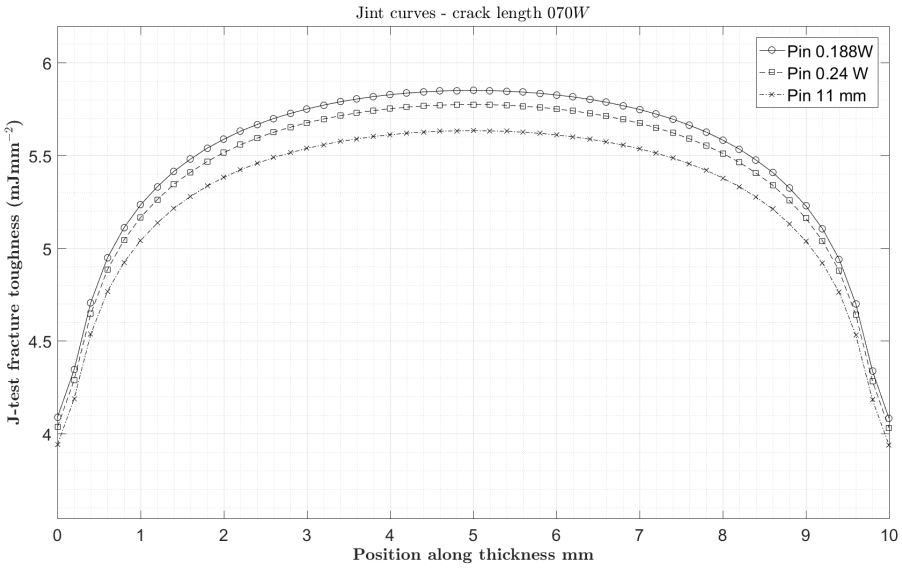

Figure C.20: J-integral fracture results - Crack 0.70W

D

Design verification cryostat

Static verification cryogenic vessel, 4.2K He Cryostat for Tensile Tests (included PDF document, CERN document no. 1269348V.2 [18]).

CERN
CH1211 Geneva 23
Switzerland

EDMS NO.	REV.	VALIDITY
1269348	**1.0**	**PRELIM**

REFERENCE
1269348V.2

EN Engineering Department

Date : 2017-09-14

CALCULATION REPORT

STRENGTH ANALYSIS

Static cryogenic vessel

4.2K He Cryostat for Tensile Tests

EN/MME

DOCUMENT PREPARED BY:	DOCUMENT CHECKED BY:	DOCUMENT APPROVED BY:
N. MALIK naseem.malik@cern.ch L. ALBERTY (L.Alberty@cern.ch) R. BETEMPS (Robin.Betemps@cern.ch) EN/MME		

HISTORY OF CHANGES

REV. NO.	DATE	PAGES	DESCRIPTIONS OF THE CHANGES
0.1	2013-02-13	20	First draft for engineering check
0.2	2014-12-08	20	Released without modifications
1.0	2017-08-15	44	Update of model and load cases

TABLE OF CONTENTS

1. Scope

This document presents the results of the calculations performed in order to assess the structural strength of the cryogenic vessel of a cryostat designed to be integrated into a system which will allow performing tensile tests at 4.2K. The equipment concerned by the present analysis was designed and built inside the EN/MME group and aims supporting the activities of EN/MME-MM.

2. Drawings

The functional system is defined by the following drawings:

- CRNQQ__T0061 – Assembly Dewar
- CRNQQ__T0060 – Safety Valve
- CRNQQ__T0059 – Assembly External Chamber
- CRNQQ__T0058 – Top Flange Dewar
- CRNQQ__T0057 – Assembly Thin Wall Tube Dewar
- CRNQQ__T0064 – Assembly Cryostat Installation

3. Standards

This document incorporates provisions from the following standards:

- EN 13445 – Unfired pressure vessels [1];
- EN 13458 – Cryogenic vessels – Static vacuum insulated vessels [2];

4. Technical description

Table 1 – Technical description

-Technical description-		Geometry preview:
Geometry:		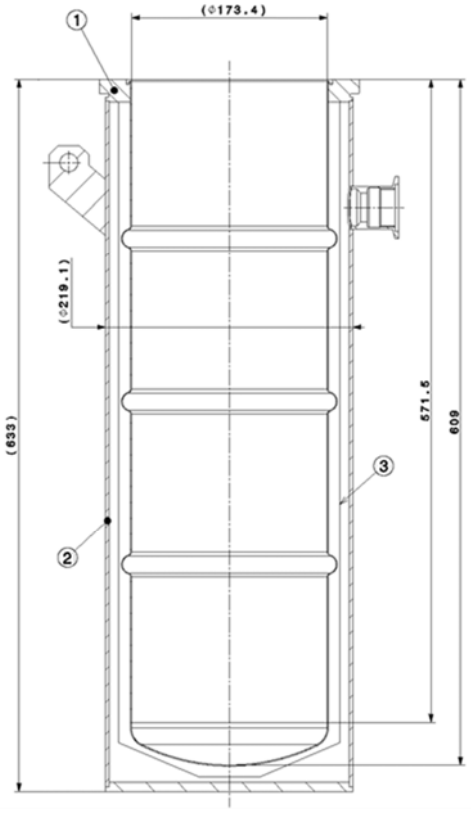
Envelope dimensions	Ø220x635 mm	
Internal volume (He)	~14.4 L	
Weight	~18 kg	
General:		
Maximum allowed pressure, PS	1.5 bar(g)	
Test pressure, P_T	3.6 bar(g)	
Maximum allowable temperature, TS_{max}	50 °C	
Minimum allowable temperature, TS_{min}	-270 °C	
Fluid	He, Group 2 fluid - 97/23/EC	
Risk category to PED 97/23/EC	Article 3 paragraph 3 (sound engineering practices)	

Figure 1 - Dewar

1. Thin wall tube Dewar Internal
2. Thin wall tube Dewar External
3. Multilayer isolation 30 layers

5. Verification

This chapter contains the outline of the verification: the requirements listed in the code and the corresponding acceptance criteria. The

5.1 General requirements

As per EN13458 the static cryogenic vessel (dewar) shall safely withstand the mechanical loads, thermal loads and the chemical effects encountered during pressure test and normal operation.

The chemical effects can be neglected and no corrosion allowance or inspection openings are required. This because of the nature of the cryogenic liquid, the vacuum between the inner and outer jacket and the materials used in the construction. [2]

5.1.1 Mechanical loads

The static cryogenic vessel shall resist the mechanical loads mentioned without such deformation which could affect safety and which could lead to leakage.

The mechanical loads which are to be considered are loads under normal operating conditions and the loads exerted on the vessel during test conditions. The loads during normal operating conditions, are those resulting from the maximum allowable pressure set by the relieve device.

PS = 1.5 bar(g)

The loads exerted on the dewar during the test conditions, are those resulting from the test pressure:

PT = 1,43 (PS +1) (+1 to account for the external vacuum)

The following loads are considered to act in combination, as required by [2]:

- the pressure exerted by the liquid when filled to capacity;
- loads produced by the thermal movement of the inner vessel, outer jacket and interspace piping;
- full vacuum in the outer jacket

5.1.2 Thermal conditions

The following thermal conditions shall be taken into account [3]:

a) for the inner vessel and its associated equipment the full range of temperature expected;

b) for the outer jacket and equipment thereof:

- the lowest scheduled ambient temperature;
- a maximum working temperature of 50 °C.

5.2 Verification method

The dewar is verified for the loads as outlined in section 5.1 set forth by [2], using the acceptance criteria from EN13445-3 "Annex C (Normative) – Design by analysis" [1]. Where the allowable stress "f" as mentioned in [1] is determined in accordance with [2], and which are listed for the respective materials in Table 3. The acceptance criteria for the different stress categories are outlined in Table C-3 [1]; included in this report as Figure 2.

The geometry of the vessel requires that it is modelled and simulated using multiple elements across the thickness (solid elements). The stress results from these analysis however show the total equivalent stress, and therefore the evaluation of the membrane stress is not possible using a global stress representation. The total stresses will be verified for the allowable stress for the membrane stresses and any area where the stresses exceed the allowable will be examined in more detail.

The thermal stresses are to be considered as secondary stresses hence two different analyses are required: an analysis to verify primary stresses resulting from the pressures (internal pressure and external vacuum), and an analysis to verify the secondary and peak stresses.

Table C-3 — Illustration of assessment criteria

	Stress Categories				
	Primary stress			Secondary membrane + bending stress	Peak stress
	General membrane stress	Local membrane stress	Bending stress		
Description (For practical examples, see Table C-2)	Primary mean stress calculated across the wall thickness without taking into account discontinuities and stress concentrations. Caused only by mechanical loads.	Primary mean stress calculated across the wall thickness taking into account large discontinuities, but not stress concentrations. Caused only by mechanical loads.	Primary stress component proportional to the distance from the centroid of the solid wall section. Does not include discontinuities and stress concentrations. Caused only by mechanical loads	Self-equilibrating stress necessary to satisfy the continuity of the structure. Occurs at large discontinuities, but does not include stress concentrations. Can be caused by both mechanical loads and thermal effects.	a) Addition to primary or secondary stress because of stress concentration. b) Certain thermal stresses which may cause fatigue, but not distortion.
Symbol	P_m	P_L [1]	P_b	Q ($= Q_m + Q_b$)	F
assessment againts static loading	$(\sigma_{eq})_{P_m} \le f$ (eq. C.7.2-1) [2]; $(\sigma_{eq})_{P_L} \le 1{,}5f$ (eq. C.7.2-2); $(\sigma_{eq})_P \le 1{,}5\,f$ (eq. C.7.2-3) [2]; $(\Delta\sigma_{eq})_{P+Q} \le 3\,f$ (eq. C.7.3-1) [3] [7]; ——— = design loads, - - - - - = operating loads				
fatigue assessment (only if required)	Assessment [4] based on : [5] [7] $(\Delta\sigma_{eq})_{P+Q}$ or max $(\Delta\sigma_i)$ or $(\Delta\sigma_{eq})_{P+Q+F}$ [6] [7]				

[1] $P_L = P_m$ does not occur at the point in question.

[2] In assessment criteria given in Equations (C.7.2-1) to (C.7.2-3), the value of the nominal design stress f shall be that relevant for the loading condition under consideration (normal operation, exceptional operation, proof test), as defined in clause 6.

[3] If $(\Delta\sigma_{eq})_{P+Q}$ is greater than $3f$, see C.7.6

[4] Fatigue assessment shall consider all the applied cycles of various types, each of them being characterised by their own relevant stress range (see footnotes 5 and 6), mean temperature and mean stress (if relevant). Clause 18 (detailed fatigue assessment) should normally be used.

[5] The primary + secondary stress range (named "structural stress range" in Clause 18 on detailed fatigue assessment) applies to assessment of welded joints. In that case, either the equivalent stress range $(\Delta\sigma_{eq})_{P+Q}$ or the principal stress ranges $(\Delta\sigma_i)$ may be used.

[6] The primary + secondary + peak stress range, named "total (notch) stress range" in clause 18 on detailed fatigue assessment, applies to assessment of unwelded parts.

[7] It should be observed that, depending on the model used, the computer programs usually give directly the primary + secondary stresses ($P + Q$) or the primary + secondary + peak stresses ($P + Q + F$).

Figure 2 - Acceptance criteria from EN13445-3 [1]

6. Materials

The mechanical properties of the selected materials are summarized in Table 2 and Table 3. The thermal properties used in the simulation are included in ANNEX B; where the thermal conductance and expansion curves are constructed using data extracted from [4].

Table 2 – Reference physical properties at room temperature

Physical properties at room temperature		
Material: Austenitic Stainless Steel Specifications: EN 10088-1 Annex A [5] EN 13155-3 Annex O [3]		
Poisson's ratio	Elastic modulus	Density
	(GPa)	kg/m^3
0.3	200	8000

Table 3 – Reference material properties at room temperature

Component (Position on drawing)	**Material**	**Shape**	**Minimum mechanical properties at room temperature**		
			$R_{p1.0}$	Max. allowable stress [2]	
				Normal conditions	Test/exceptional conditions
Inner vessel					
Pos. 1 CRNQQ__T0057	EN 10028 1.4429 (AISI 316LN)	Forged blank	320 MPa	213 MPa	305 MPa
Pos. 2 CRNQQ__T0057	EN 10216-5 1.4435 EN 10216-7 1.4435 (AISI 316L)	Tube	225 MPa	150 MPa	214 MPa
Pos. 3 CRNQQ__T0057	EN 10028-7 1.4435 (AISI 316L)	Sheet t= 0.8 mm	270 MPa	180 MPa	257 MPa
Outer Jacket					
Pos. 1 CRNQQ__T0059	EN 10088 1.4306 (AISI 304L)	Tube	215 MPa	143 MPa	205 MPa
Pos. 2 CRNQQ__T0059	EN 10088 1.4306 (AISI 304L)	Sheet t= 8 mm			
Pos. 4 CRNQQ__T0059	EN 10088 1.4306 (AISI 304L)	Blank			

7. Model

The assembled cryostat can be considered to consist of three main structural components, as indicated in Figure 3. The verification in this report is only with respect to the dewar, where the top flange with internals and support structure are included in the boundary conditions.

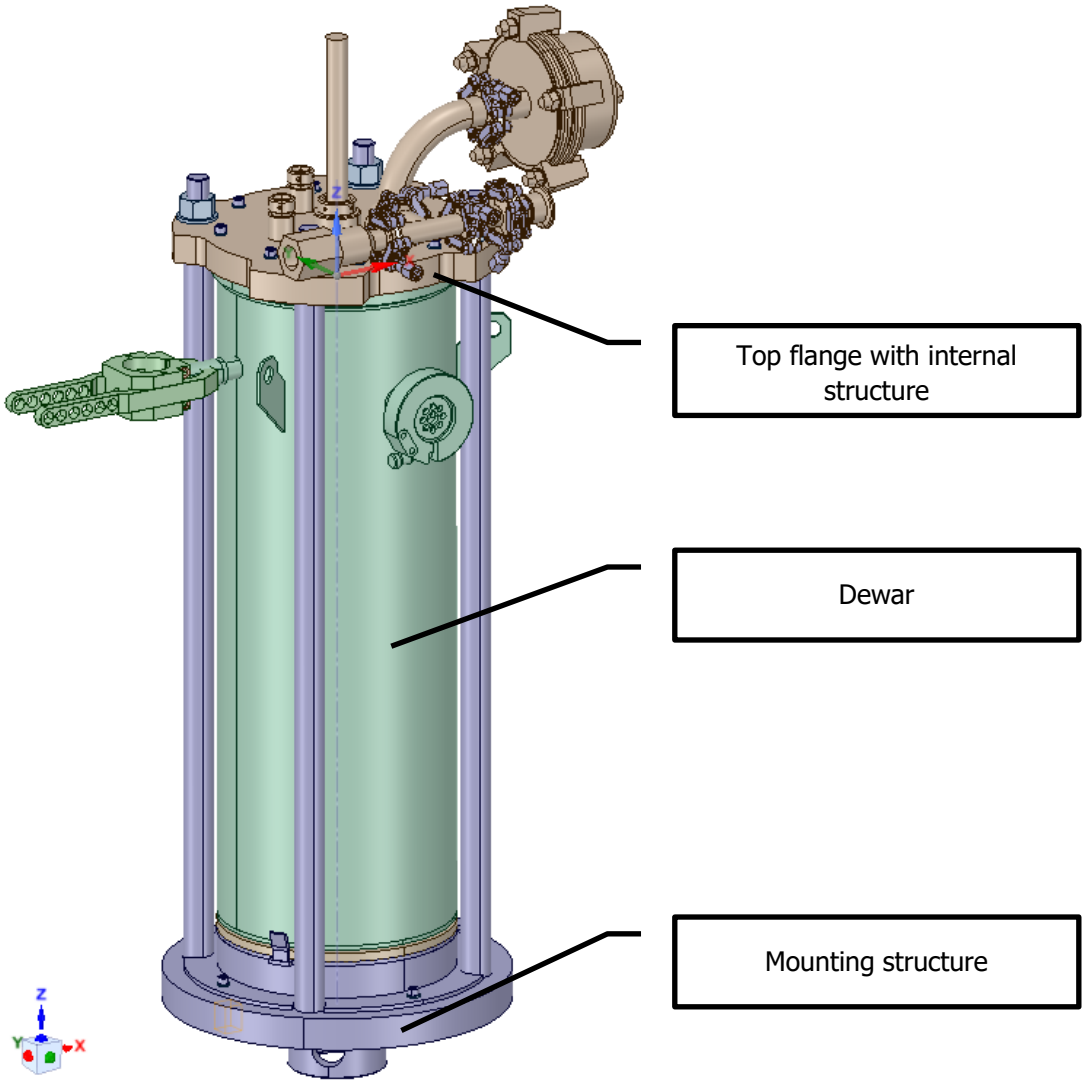

Figure 3 - Cryostat complete

7.1 Geometry

The dewar is modelled according to drawings (CRNQQ__T0057, CRNQQ__T0059 and CRNQQ__T0061), consisting of the internal and external chamber. The welds are included in the model as a fully bonded model would result in unrealistic representation; the welds which are of significance with regards to the strength and stiffness and are highlighted in Figure 4. As the internal thin wall vessel however contains a full-pen weld it is therefore however modelled with full bonded contact. Of the attachments only a small portion is included in the model, this is a valid simplification as only a small portion reinforce the openings in the shell.

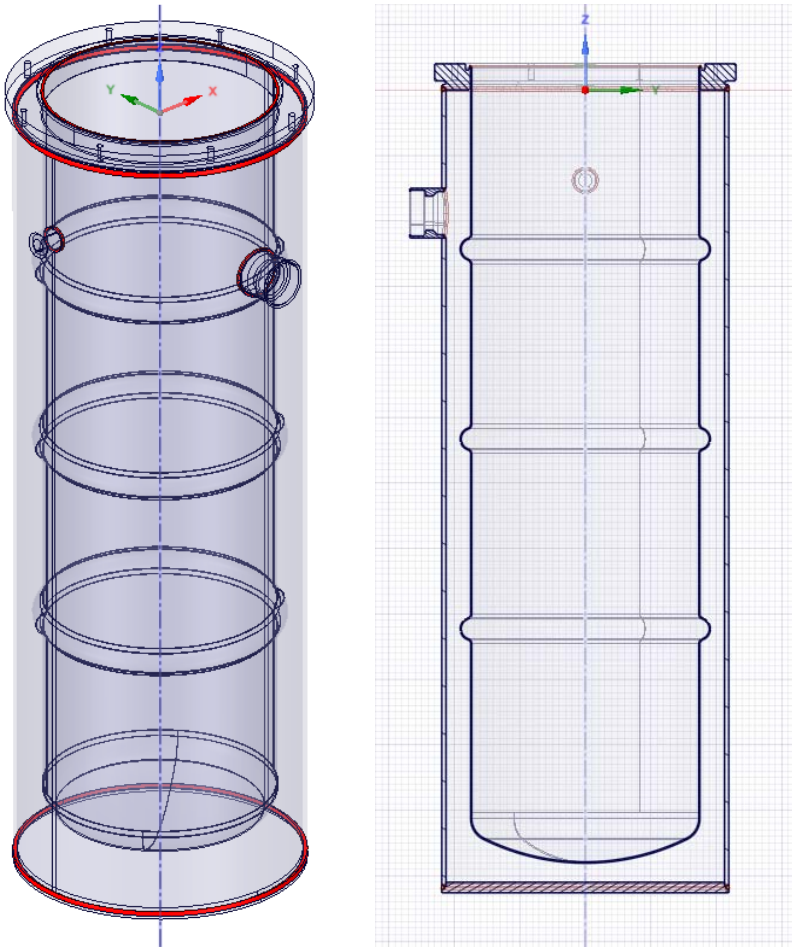

Figure 4 - Dewar with welds

The dewar is verified using two different models i.e. using an axisymmetric model to verify the stresses and a full 3D model to verify the dewar with respect to buckling. For the axisymmetric model only a cross-section surface in the positive X-Y plane is modelled, where the bolted connection is modelled as a small bonded section between the flange and the hub of the dewar (illustrated by the different section in the top flange in Figure 5).

7.2 Axisymmetric model

7.2.1 Elements

Table 4 – Finite elements formulation

Designation	Description	DOF	Observations
SOLID273	2D – 8 Node Axisymmetric elelemnt with quadratic displacement behaviour	UX, UY, UZ	Quadrilate elements

7.2.2 Mesh size

The axisymmetric model is computationally cheap and hence allows for a fine mesh. The top flange is meshed with an element size of 0.8 mm, the hub of the dewar with a mesh of 0.5 mm, where the model is refined up to a mesh size of 0.1 mm at the welds and other areas of interest.

7.2.3 Meshed model

Of the entire model only a small portion is shown in Figure 5 in order to allow for individual elements and the respective sizes to be discerned.

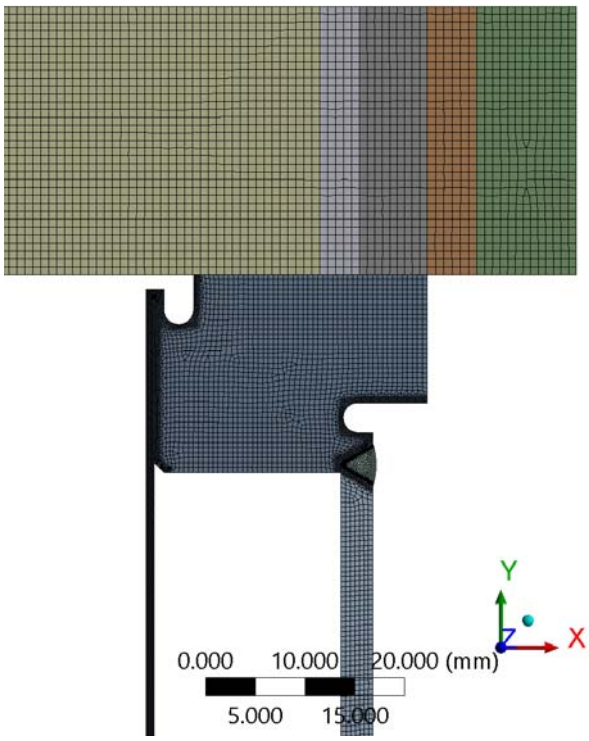

Figure 5 – Meshed model

7.3 Full 3D model

7.3.1 Elements

Table 5 – Finite elements formulation

Designation	Description	DOF	Observations
SOLID186	3D – 20 Node Homogenous structural solid with quadratic displacement behaviour	UX, UY, UZ	Hexahedral structural solid assigned automatically for hexahedrons-dominant meshing methods.
SOLID187	3D – 10 Node Structural with quadratic displacement behaviour	UX, UY, UZ	Tetrahedral structural solid recommended for complex geometries. Assigned automatically by ANSYS Workbench.
SOLSH190	3D – 8 Node Structural with linear displacement behaviour	UX, UY, UZ	Hexahedral structural element, which offer similar computational benefits of a shell element for thins section, but with hexagonal elements. Each node has three translational degrees of freedom, where linear interpolation is used to determine the behavior of the element and the orientation of the normal of the midplane of the element
SOLID185	3D –8 Node Homogenous structural solid with linear displacement behaviour	UX, UY, UZ	Hexahedral structural solid assigned automatically for hexahedrons-dominant meshing methods.

7.3.2 Mesh size

Thin sections

The thin-walled sections are modelled using the solid shell-elements (SOLSH190 as described in Table 5) with three elements across the thickness band a surface mesh of 5 mm.

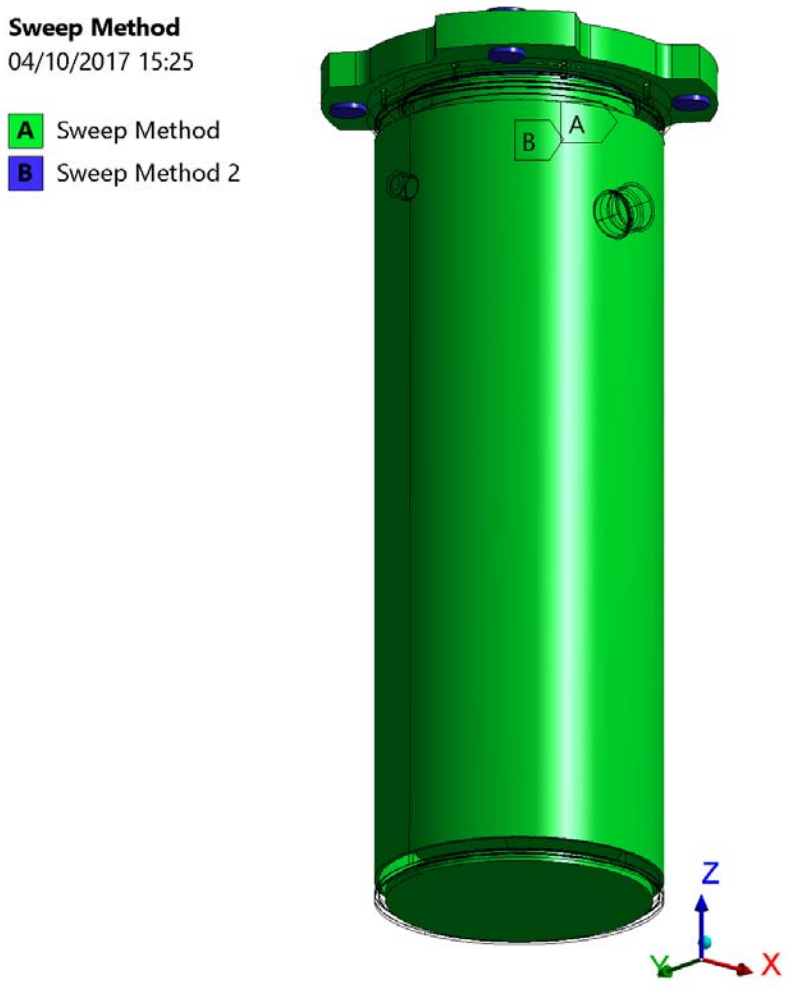

Figure 6 - Solid-shell meshed bodies

Solid parts

Parts which are either relatively thick or contain features which impact the quality of a solid-shell mesh are meshed using a HEX-dominant mesh containing a combination of the SOL186 and SOL187 elements (refer to Table 5). The parts meshed using these elements are the nozzles, top flange, bottom plate and welds, as highlighted in Figure 7.

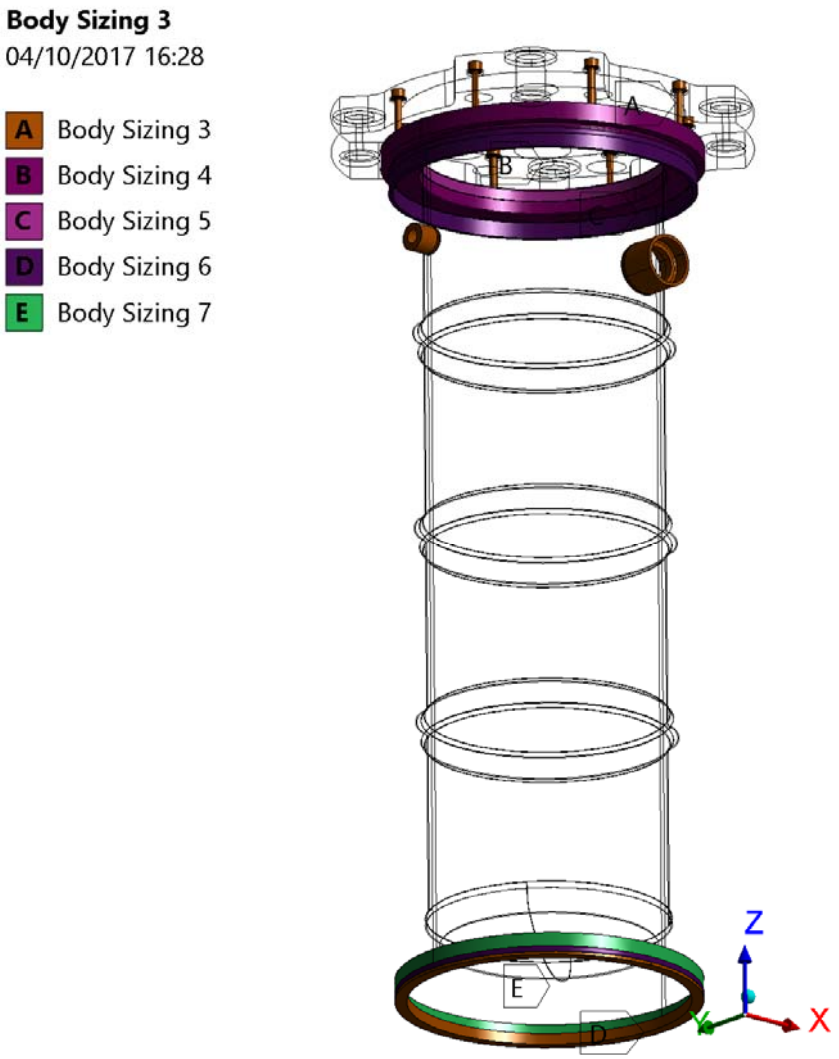

Figure 7 - Parts meshed with solid elements

The welds are meshed with a sweep mesh with at least three elements across the thickness and a surface mesh of 1.5 mm, which generates primarily hexahedral elements with some wedge elements. The top flange of the dewar and bottom are meshed with an element size of 5 mm respectively. The small nozzle reinforcements in the shell are meshed using an hex-dominant method with a mesh size of 1.5 mm.

7.3.3 Meshed model

Figure 8 – Meshed model

8. Boundary conditions and load cases

8.1 Load cases

The loading scenarios considered relevant for the present study are summarized in Table 6. The related failure modes and resulting limit states are summarized in Table 7.The dewar is verified for the primary stresses for the load cases listed and for the secondary stresses for the load cases listed combined with the thermal loads (as discussed in section 5.1).

Table 6 – Relevant load cases

Reference	**Type** [1]	**Description**	**Differential pressure, ΔP**
Inner vessel			
IV-LC1	Normal	Operation at PS	2.5 bar
IV-LC2[1]	Testing	Leak testing	-1.0 bar
IV-LC3[2]	Exceptional	Failure vacuum	-1.0 bar
Outer jacket			
OJ-LC1	Normal	Operation/vacuum	-1.0 bar
OJ-LC2	Testing	Leak testing (before top weld)	-1.0 bar
OJ-LC2	Exceptional	He leak into vacuum chamber	0.5 bar

Table 7 – Failure modes and related load cases

Failure mode	**Constitutive law**	**Related load cases**	**Resulting limit state[3]**
GPD (Gross Plastic Deformation)	Stress analysis: Linear-elastic Linear-plastic with Von Mises yield criterion and associated flow rule.	IV-LC1 IV-LC2 OJ-LC1	Ultimate limit
Buckling	Buckling: Linear-elastic	IV-LC2 OJ-LC1	

[1] For the verification of the stresses IV-LC1 is considered as governing; a linear-static stress analysis is used, hence higher pressure results in higher stresses.

[2] This case can be considered as less onerous than IV-LC2; the differential pressure is higher, and the allowable stress is the same for both cases.

[3] Failure modes induce limit states, which can be either classified as ultimate or as serviceability limit states. Ultimate limit states are related to structural failure that may endanger the safety of people. Serviceability limit states define a structural condition beyond which the service criteria specified for the equipment are no longer met. [1]

8.2 Loads

The loads are applied in a similar manner for both models; the axisymmetric model and the full 3D model.

8.2.1 Pressure

Full vacuum (between inner and outer jacket)	**Internal Pressure**
The chamber between the internal and external chamber is used as a vacuum insolation chamber. The pressure used in the simulation is full vacuum a pressure of 0 bar(a) (-0.1 MPa).	The internal pressure is applied on the surfaces as indicated in Figure 10; the relief pressure of 1.5 bar(g) and the full vacuum (0 bar(a))

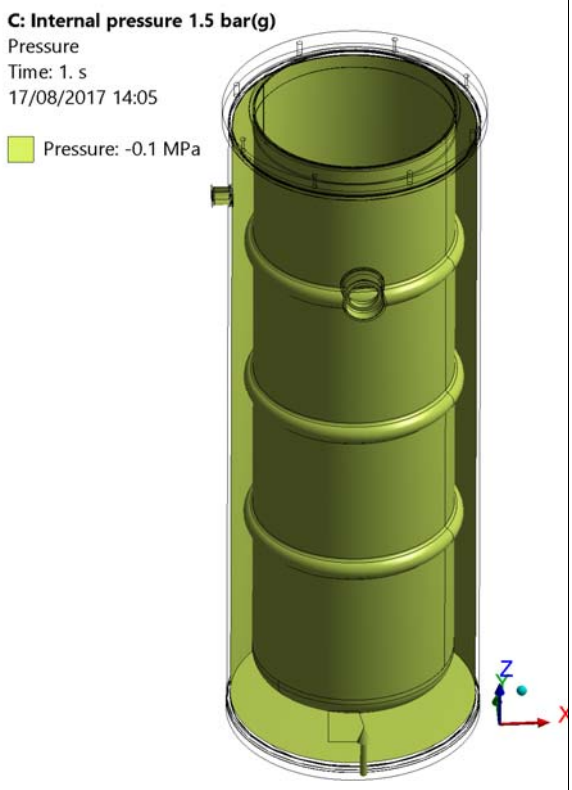

Figure 9 - Full vacuum in jacket

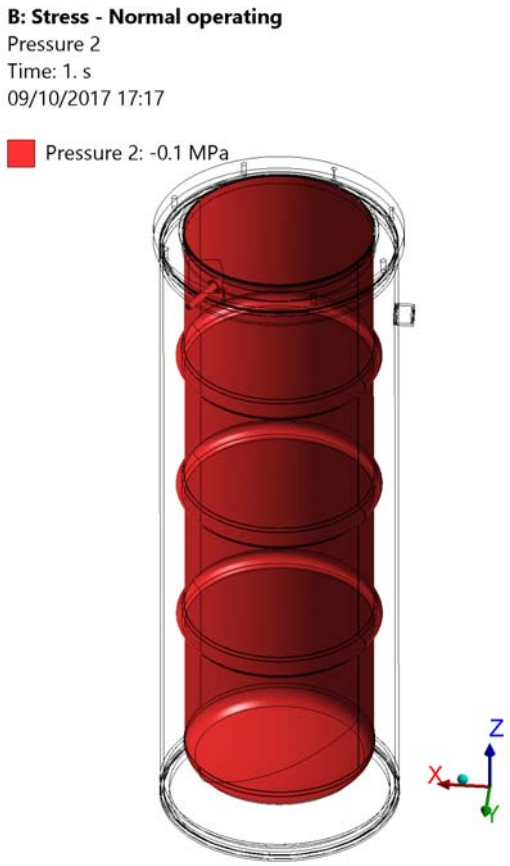

Figure 10 - Internal pressure

The maximum net effective pressure for the operational case is 2.5 bar(g), 1.5 bar(g) inside the dewar and full vacuum (-1bar(g)) in the chamber between the external and internal wall.

8.2.2 Dead-load

The self-weight of the dewar is included in the simulation using the standard earth gravity of 9.81 m/s² (Figure 11). The weight of the liquid helium in normal operating conditions is included in the simulations using an hydrostatic pressure with density 124 kg/m³. As shown in Figure 12 the hydrostatic pressure for the vessel full of liquid is negligible in comparison to the full vacuum between the inner and outer wall and the internal relief pressure of 1.5 bar(g).

Standard earth gravity	Resulting hydrostatic load

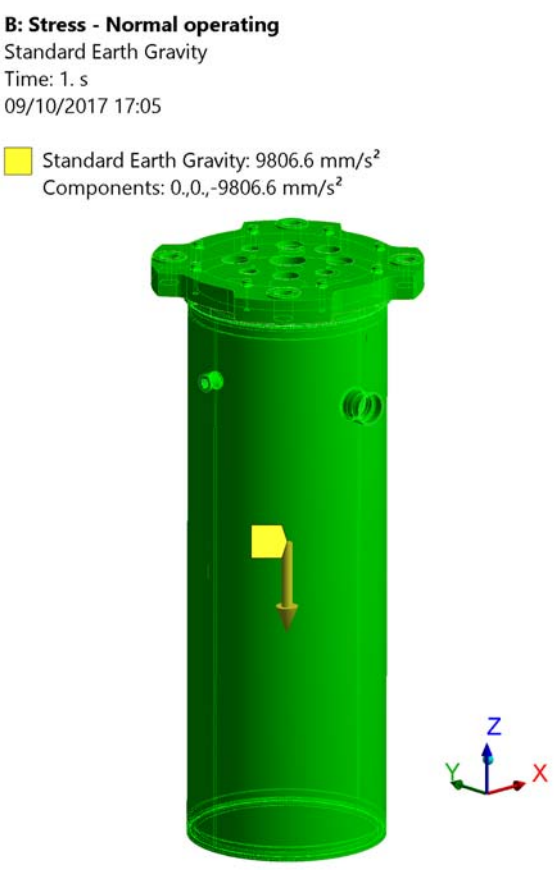

Figure 11 - Gravity

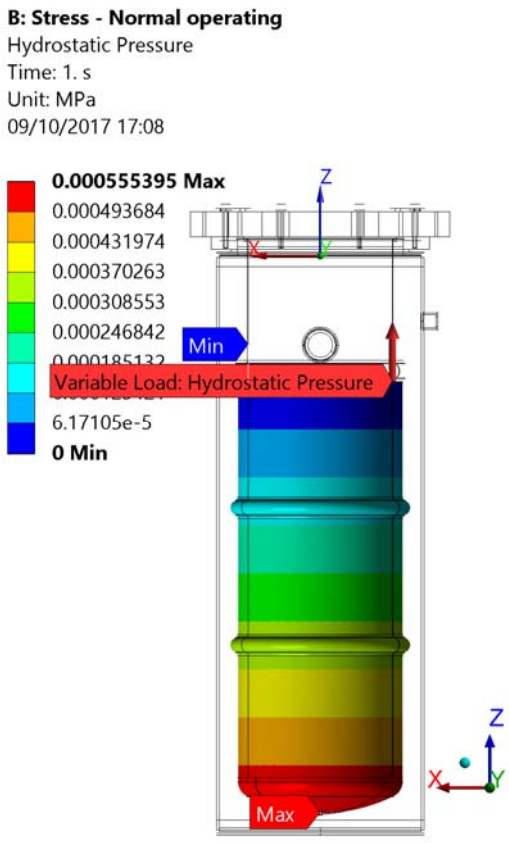

Figure 12 – Hydro static pressure

For the verification of the external jacket of the dewar the self-weight (gravity) is suppressed; as the weight acts contrary to the internal vaccum.

8.2.3 Thermal

For the thermal loads 2 cases are considered, both of which are simulated with a steady state thermal analysis:

1. The initial condition where liquid helium is first introduced into the vessel (temperature of 4.2 K at the bottom of the vessel as depicted in Figure 15), with the assumption that the cooling is gradual due to vapor cooling and relatively low flow rates, such that a steady state thermal simulation is adequate.
2. the vessel filled to max liquid level at 4.2 K (Figure 16), with the assumption that the return gas has a temperature of 15 K (realistic yet somewhat conservative based experience during normal operating).

The first case is used to verify the effect of the thermal gradient spanning almost the full length of the internal wall. A steady state thermal analysis is considered sufficient as even though the liquid helium is introduced the filling rate is considered to be significantly low. Hence the temperature is considered as quasi-static; due to the initial vapour cooling as the liquid flow is initiated and the relatively high thermal conductance of the wall

The thermal convection on the inside and outside of the vessel are calculated for the different mediums using the model of free convection along a vertical cylinder [6]. Where for both convection surfaces a temperature-dependency is included in the simulation, with regards to the surface temperature. The thermal convection curve used for the external surface (free convection in air) is shown in Figure 13, and the convection curve used in the application of the helium vapor cooling in Figure 14. Aside from the free convection in ambient air radiation is also included in the simulations on the outer surfaces, assuming an ambient temperature of 23 °C (295 K).

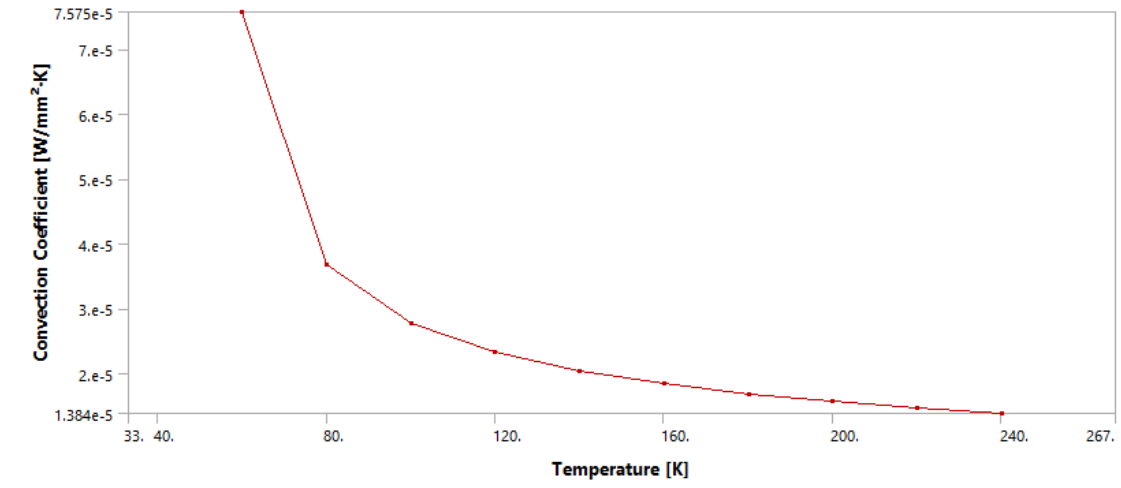

Figure 13 - Free convection – Ambient air

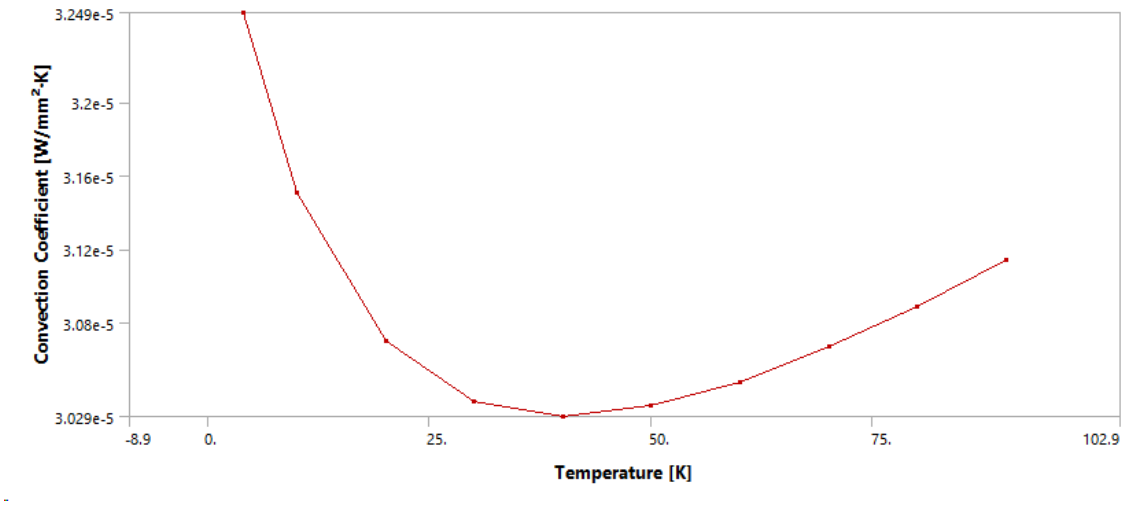

Figure 14 - Convection - Helium vapor cooling

Initial filling conditions	Vessel full of liquid
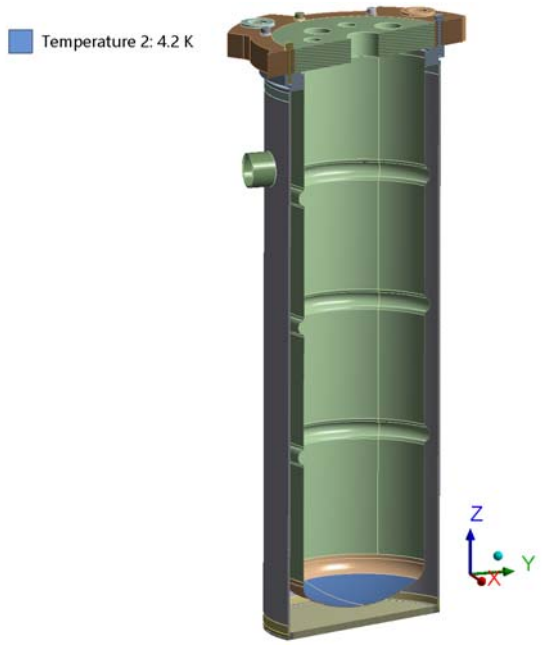	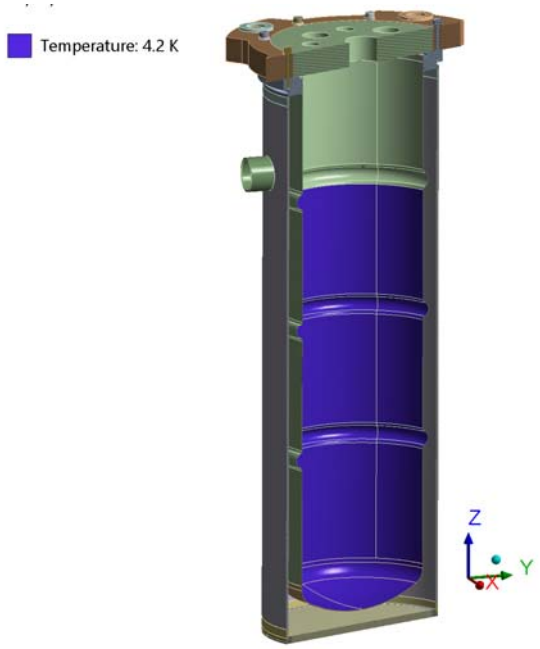
Figure 15 - Thermal - Initial	Figure 16 - Thermal - normal operating

Both models shown in Figure 15 and Figure 16 are in actuality full 3D models of the dewar, a section plane is used to allow for a more clear image of the load application.

8.3 Contraints

The top flange of is fixated to the threaded rods of the "Mounting and preloading structure" (Figure 3). Though the structure is pre-compressed (pre-load of ~60 kN total) there is considered to be limited stiffness in the radial direction. Hence the dewar is constraint in the vertical direction and the tangential direction (suppressing the rigid body motion); a cylindrical coordinate system is used for the definition of the constraints.

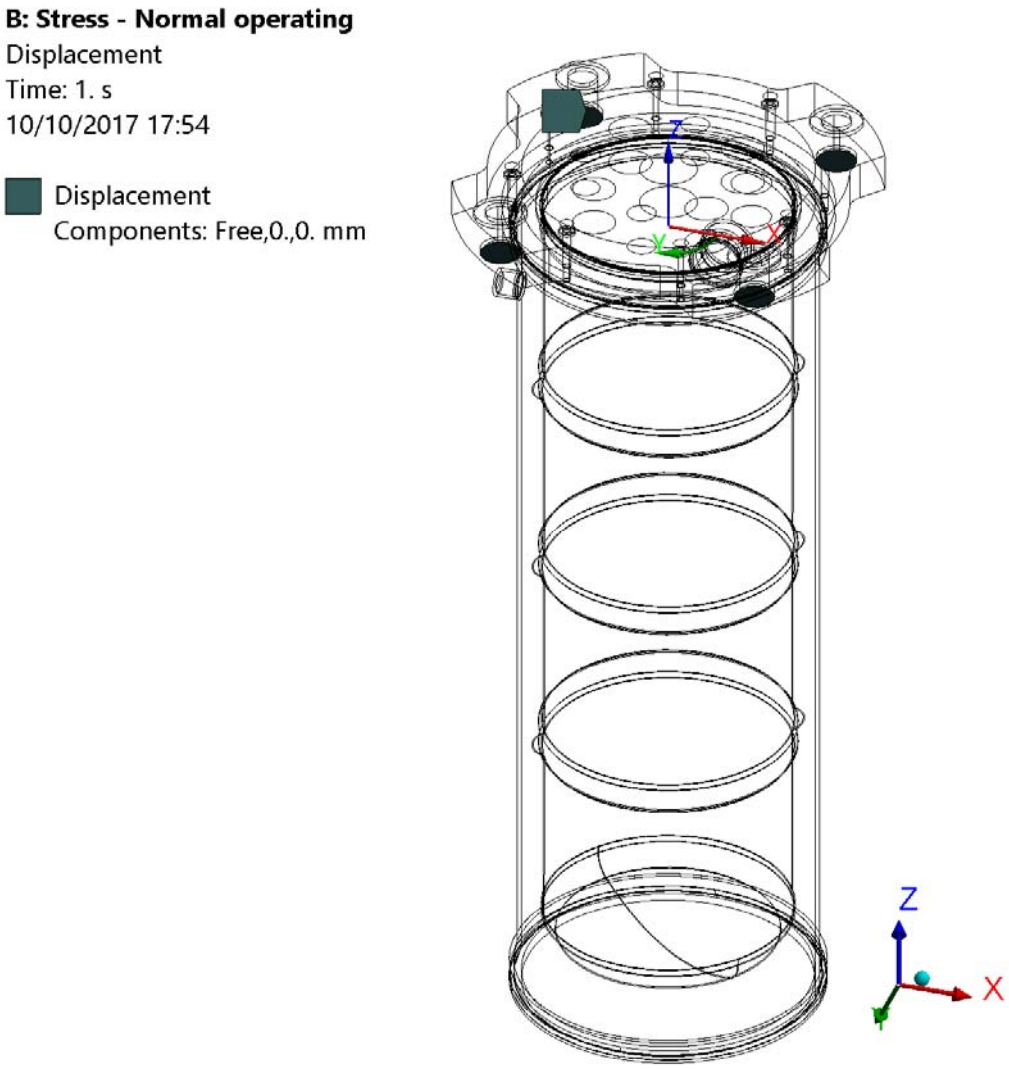

Figure 17 – Constraints

8.3.1 Contacts

The body to body contacts where applicable are all bonded, all welded contacts and the threaded contact bolt-dewar. All other surfaces where surface to surface contact occurs are modelled as frictionless contacts. The dewar is suspended from the top flange using 8 bolts M6, these bolts are considered to be pretensioned at 2 kN.

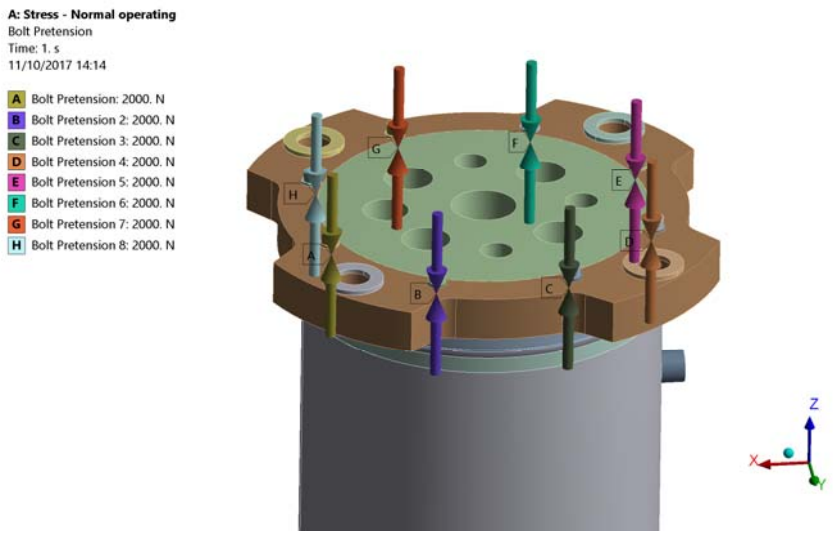

Figure 18 - Bolt pretension

Where the stiffness and the pre-tension of the bolts are emulated using a spring in the axisymmetric model (Figure 19); stiffness 86.4 kN/mm with 16 kN pretension (all 8 bolts combined, with M6: D_S=4.9mm and L_{EFF}=35 mm).

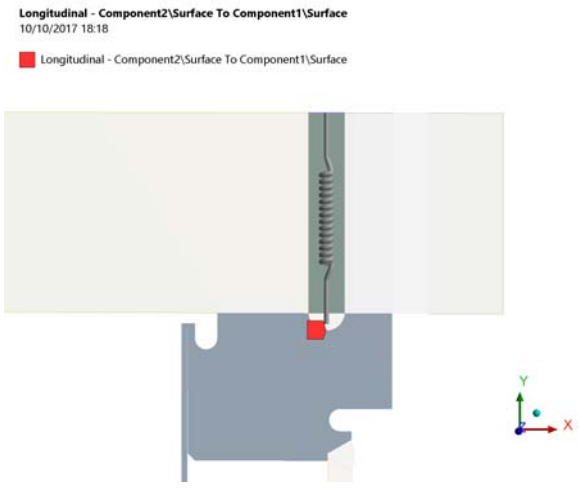

Figure 19 - Representation bolts in axisymmetric model

Any high-stress occurring in this area in the stress results can be ignored, the bolt stresses are verified using an analytical verification in section 9.1 and are also shown to be acceptable in the full 3D model as shown in section 11.1.

9. Pre-study: analytical calculations

Analytical calculations were performed on a pre-study phase aiming to check the structural strength of selected components. The results of such calculations are presented in ANNEX A – Pre-study: analytical calculations.

9.1 Verification bolts M6

The bolts M6 are grade A4 (stainless steel), where the effective diameter of the bolts is 4.9 mm.

Effective cross section	A_S	= 20.1 mm^2
Bolt pretension	F_{PL}	= 2 kN
Bolt stress	σ	= 100 MPa

The resulting stresses from the pressure are orders of magnitude smaller than those from the pretension (as shown in section 11.1), hence the bolt stresses are acceptable.

10. Results Axisymmetric model

The results from the simulation with regards to the resulting stresses and critical buckling load multiplier are evaluated presented in this chapter with the allowable stresses for each result. For the description of the load cases refer Table 6, and for the application of the various loads to section 8.2.

10.1 LC1

10.1.1 Primary stresses

The primary stresses of the inner (IV-LC1) and outer jacket (OV-LC1) are verified for the allowable stress listed in Table 3. Conservatively the global allowable stress is based on the lowest allowable at specified (at room temperature); where the lowest allowable for the primary stresses specified is 143 MPa. Where the stresses of any component examined in more detail the respective allowable stress is used.

As mentioned in section 5.2 the verification of the membrane stresses themselves is not possible due to the modelling requirements imposed by the geometry. As such the stresses shown are the total stresses, and the stresses are evaluated at sections of interest where the allowable stresses are exceeded.

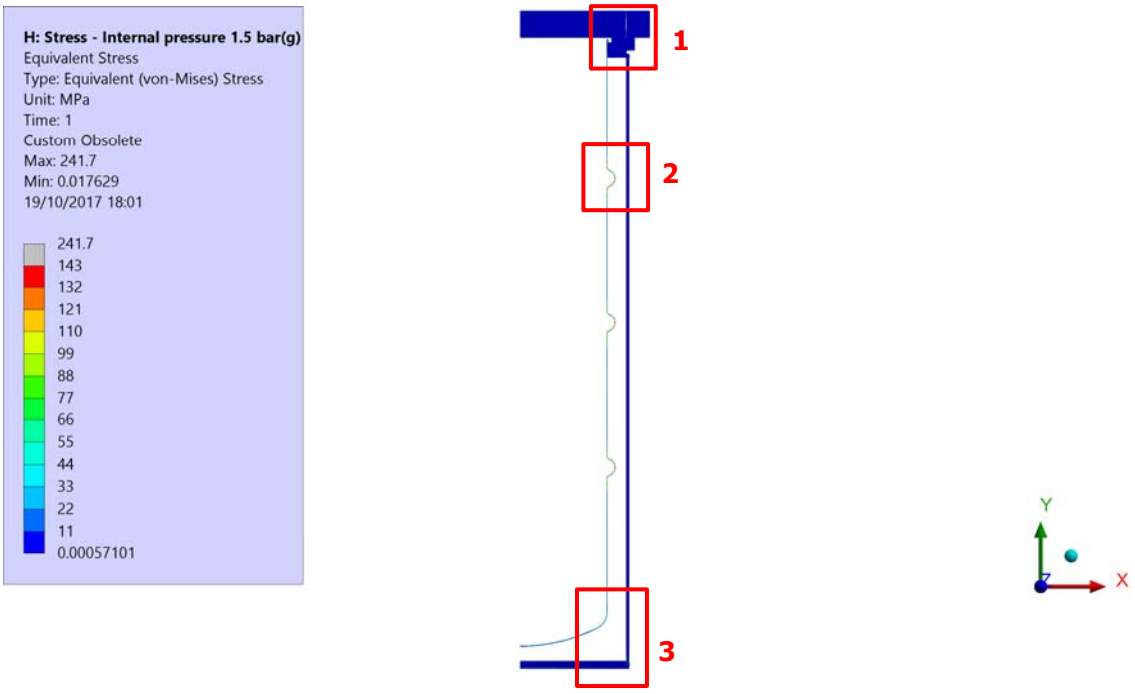

Figure 20 - LC1 - Primairy stress

As shown in Figure 20 the stress in the outer jacket of the vessel are below the allowable, with perhaps only very small areas with some minor stress concentrations. The stresses in the inner jacket of the vessel are however not that easily discerned to be allowable. There are three areas of interest where the stresses in the inner and outer and jacket are evaluated in more detail, as highlighted in Figure 20.

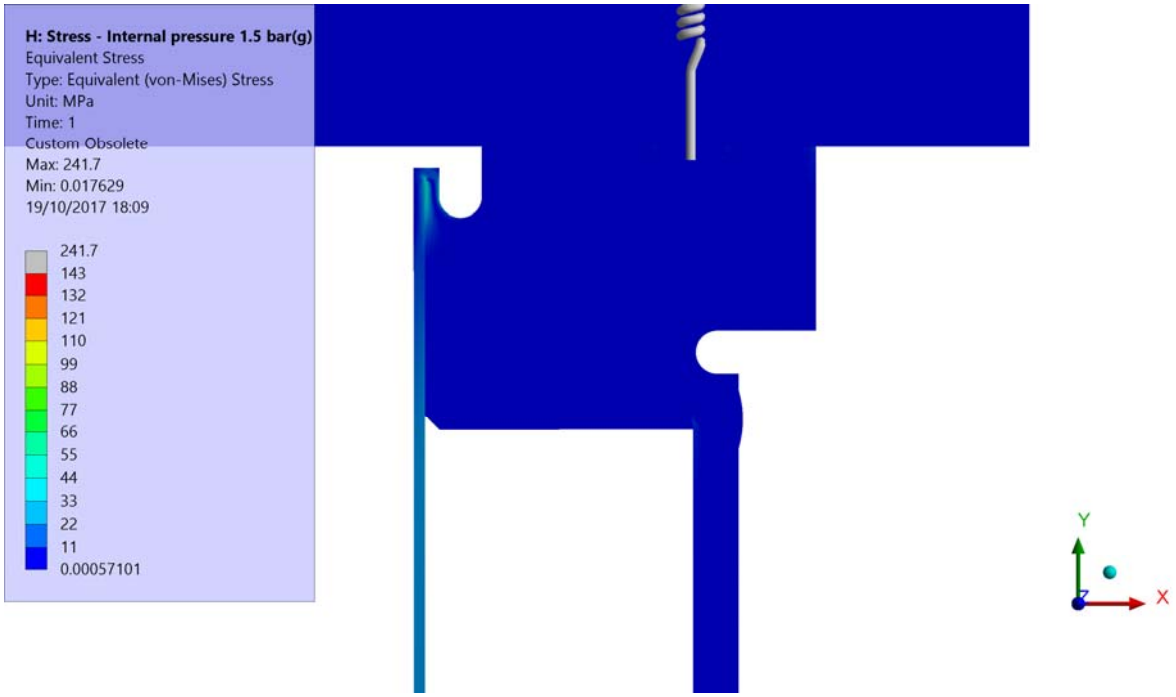

Figure 21 - LC1 - Primary stress - detail 1

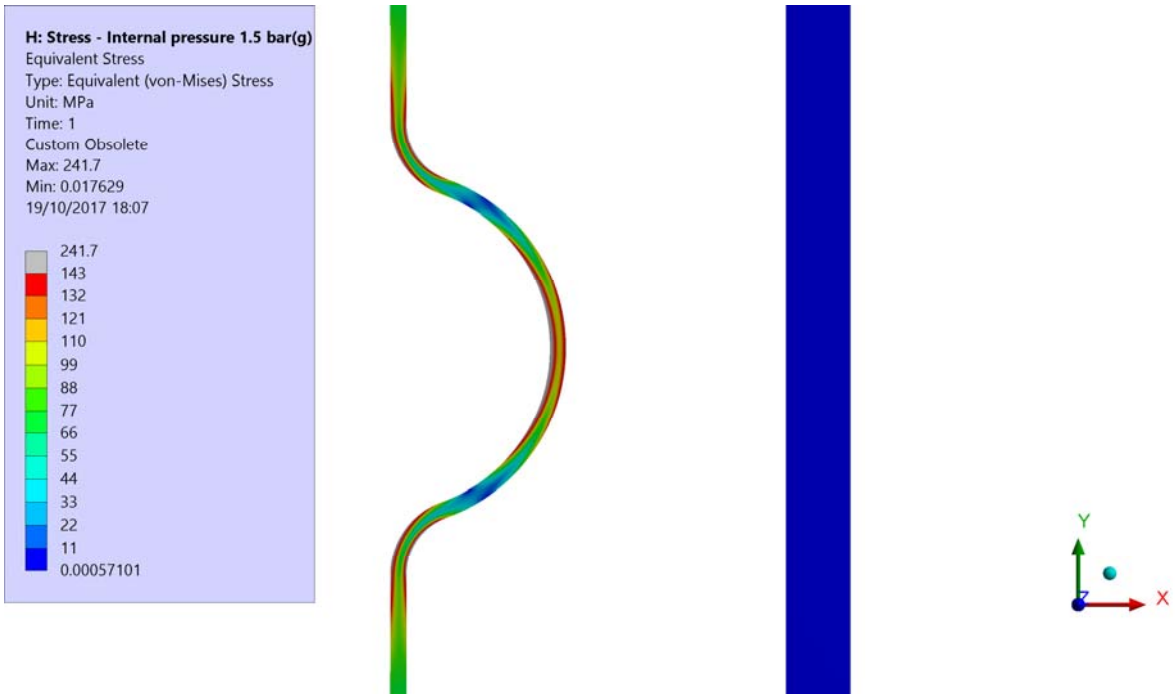

Figure 22 - LC1 - Primary stress - detail 2

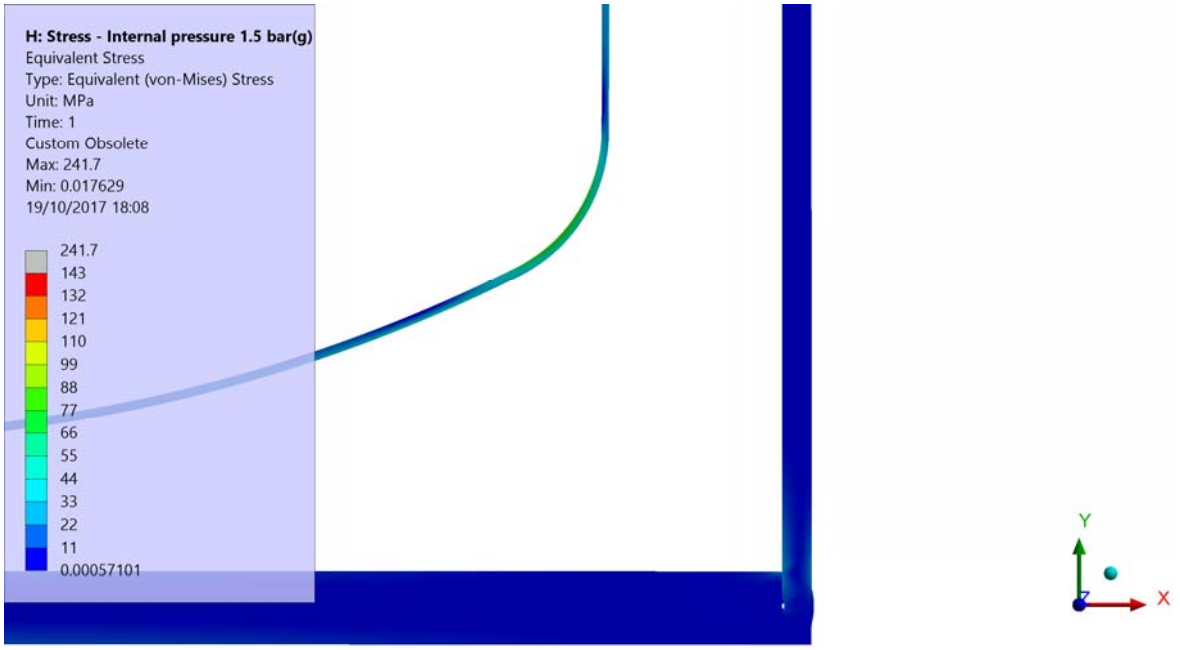

Figure 23 - LC1 - Primary stress - detail 3

The combined stresses exceed the allowable stress for primary membrane stresses only in the in the inner jacket at the reinforcements of the inner jacket (Figure 22). The stresses at the welds are all below the allowable for primary membrane stress hand are hence acceptable, as can be seen in Figure 21 and Figure 23.

The stresses in the reinforcement are for a large part bending stresses, as can be seen in Figure 22, which vary significantly across the thickness. The stresses are examined in more detail by examining the different stress components across the thickness where the highest stresses are calculated in the model.

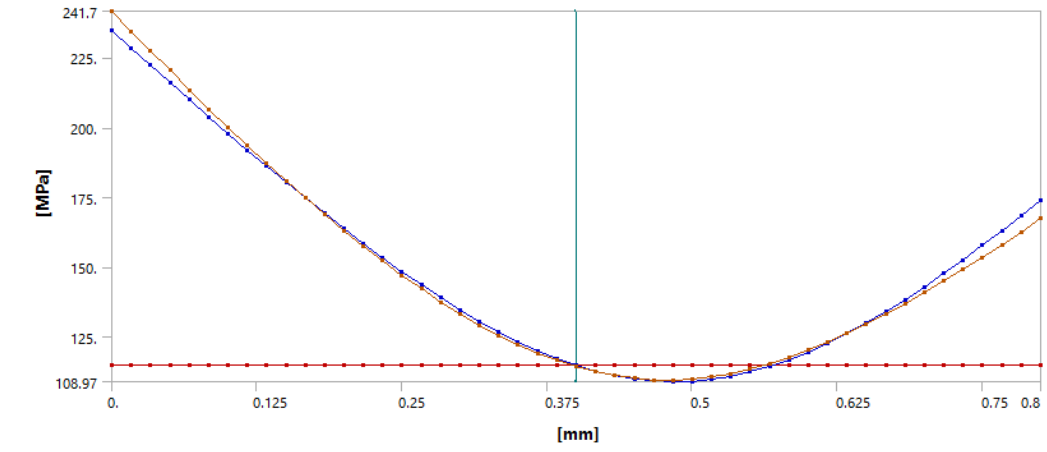

Figure 24 - LC1 - Primary stress - detail 2 - Examination stresses

The membrane stresses are shown to be acceptable in Figure 24, with a membrane stress of 115 MPa (below the allowable of 143 MPa). The maximum primary bending

stress is 235 MPa, this slightly exceeds the allowable of 225 MPa for the internal tube (Table 3). Though the stresses are above the allowable they exceed the allowable with less than 5%. Additionally, it should be noted that though strictly speaking this case should be evaluated as a normal operating condition it in actuality is an ultimate limit state. This small transgression of the allowable stress is therefore considered acceptable; the primary stresses are deemed acceptable.

10.1.2 Secondary stresses

For the secondary and peak stress evaluation the thermal effects are to be considered in the assessment. The thermal loads are included in an additional simulation using the loads and application thereof as described in subsection 8.2.3. Of the two cases presented the case with the vessel full of liquid is the only case considered for the secondary stresses. The thermal case describing the initial filling, do not result in stresses that differentiate significantly from the primary stress case. The thermal case with the dewar full of liquid (normal operating condition) does however result in significantly higher stresses.

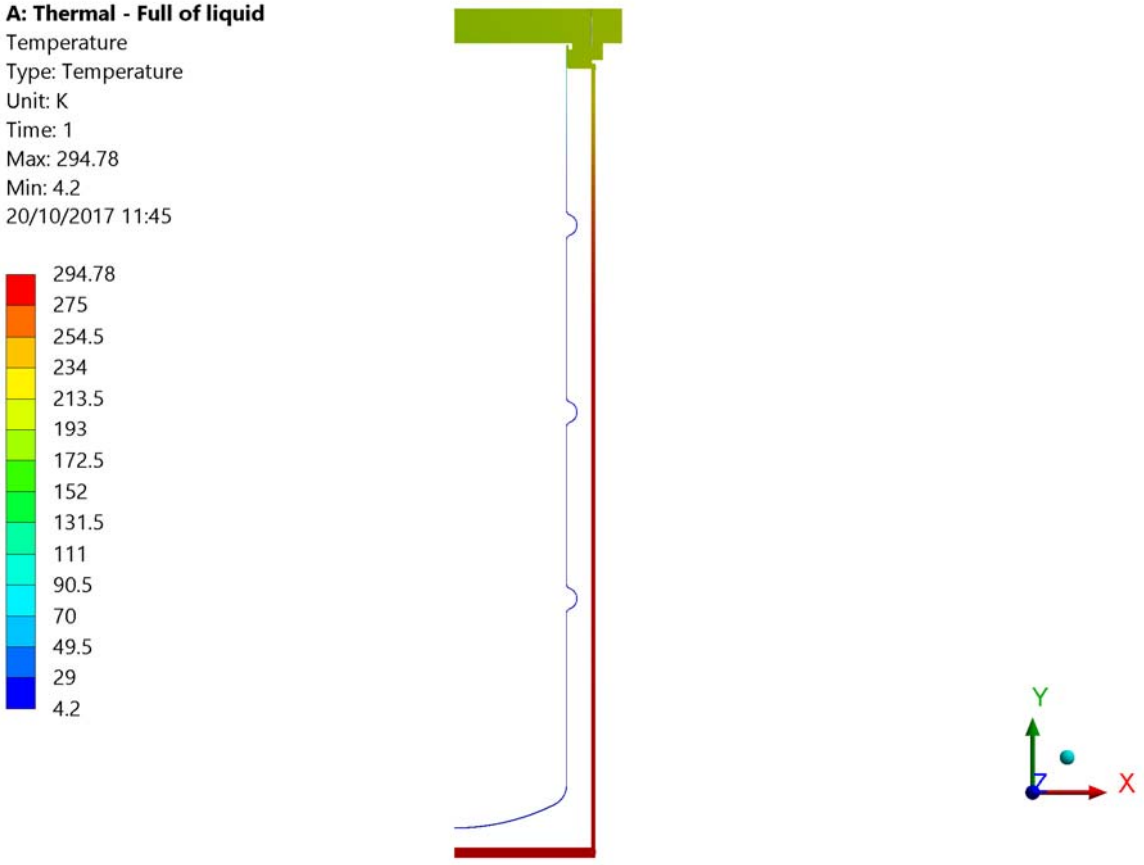

Figure 25 - Temperature distribution

The allowable stress for secondary stresses (P+Q) is 3*f* [1] (with *f* = 143 MPa); the allowable stress is 429 MPa.

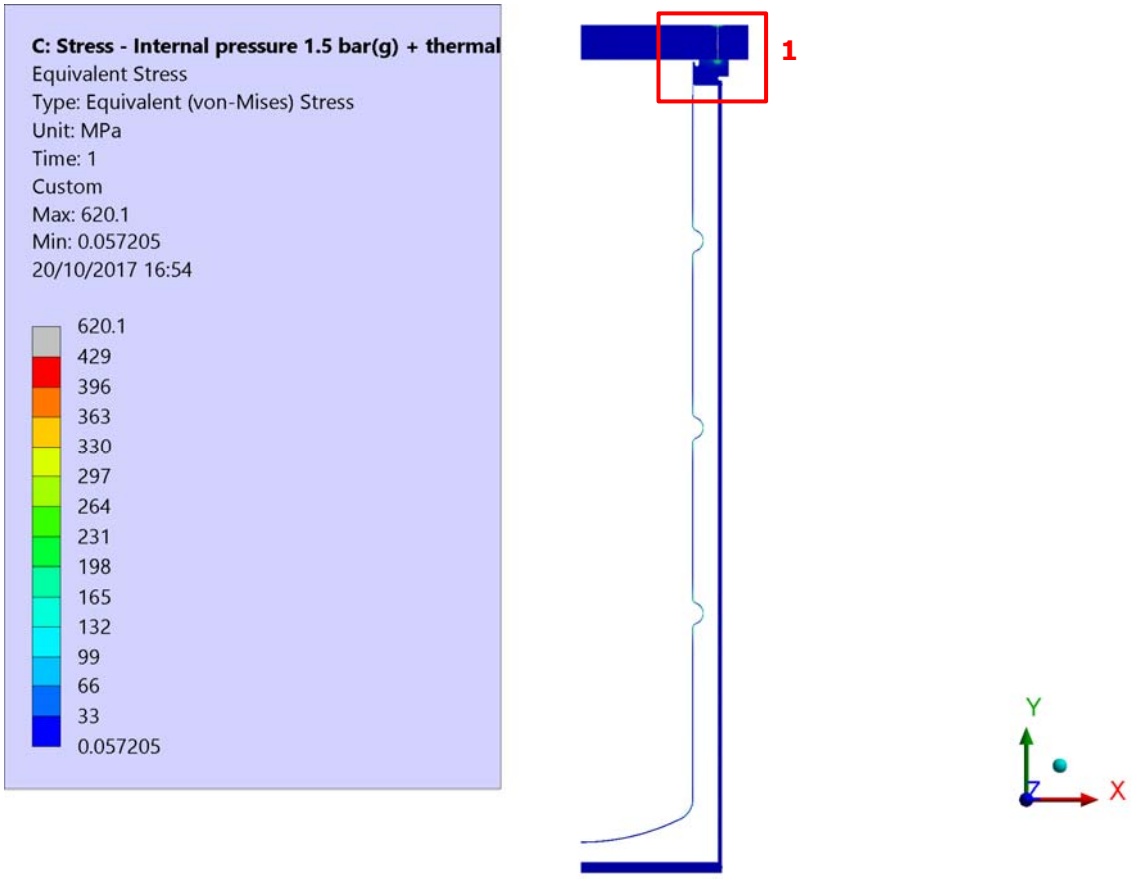

Figure 26 – LC1 - Secondary stresses

All of the secondary stresses are below the allowable except for a small overstressed region induced by boundary conditions, the maximum value in Figure 26. s these are therefore of no concern the secondary stresses are acceptable.

In spite of the stress results showing no overstressed areas there is one area of concern, which is the weld at the top flange. The detail as highlighted in Figure 26 is shown in Figure 27 with a scaling of the displacements with a factor of 20 in order to illustrate the area of interest. Due to a combination of the thermal contraction and the loads acting on the dewar the weld essentially is a crack loaded with a mixed mode crack opening (i.e. mode I and mode II). The stresses at the crack tip are relatively low, with a local maximum of approximately of 120 MPa (as indicated in Figure 28 with the mesh size also indicated). It should be noted however that the stresses in the corner would only increase with a finer mesh (linear stress singularity). This particular detail and the impact on the design is examined in more detail using the full 3D-model in section 11.1.

The secondary stresses are acceptable with the note that the weld of the inner jacket to the flange should be examined in more detail.

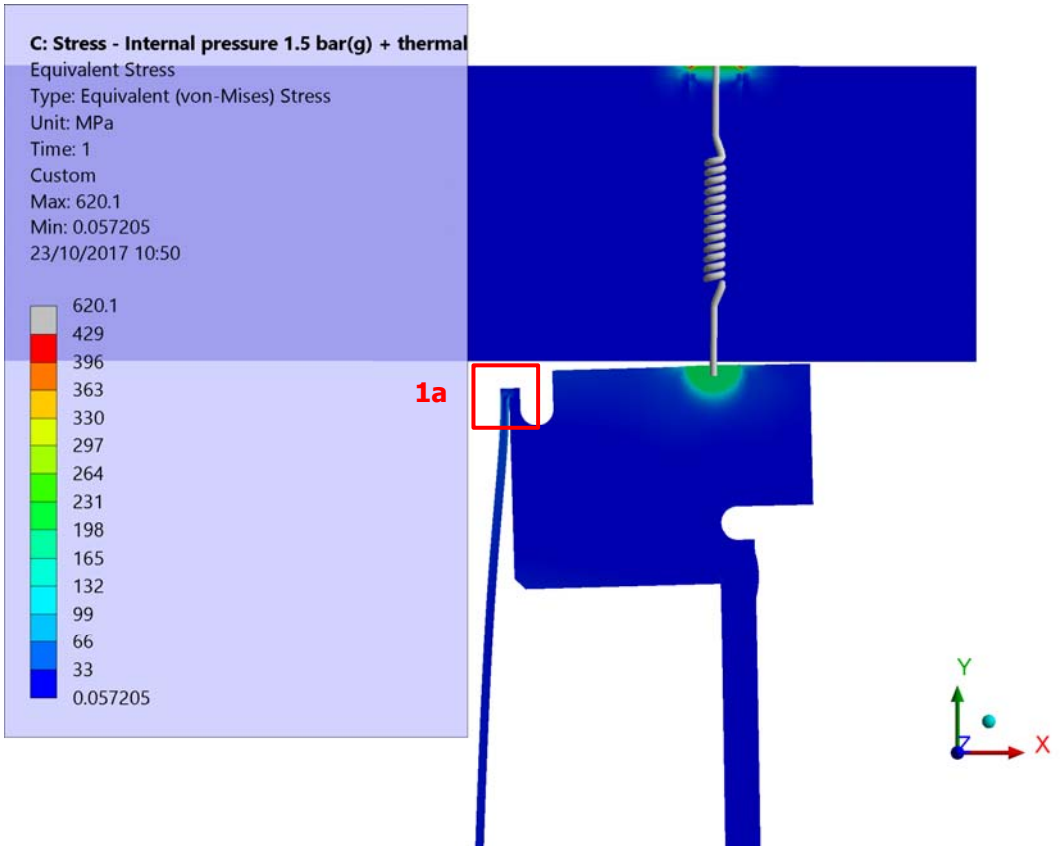

Figure 27 - LC1 - Secondary stress - Detail 1

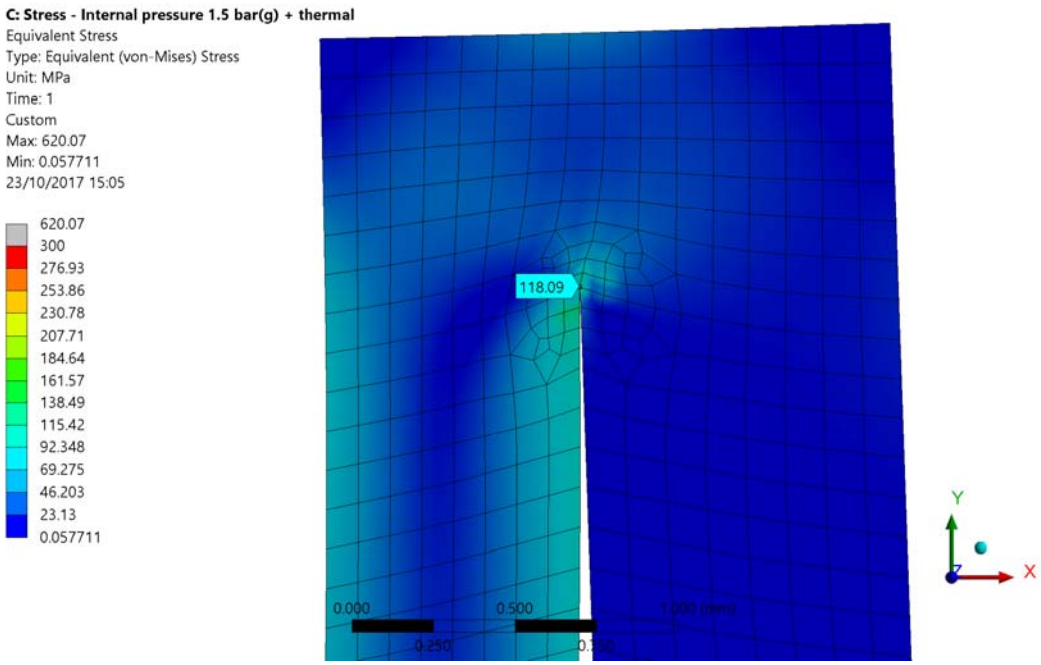

Figure 28 - LC1 - Secondary stress – Detail 1a

10.2 LC2 / LC3

10.2.1 Primary stresses

The primary stresses of the inner (IV-LC2 / IV-LC4) and outer jacket (OV-LC1 / OV-LC2) are verified for the allowable stress listed in Table 3. Conservatively the allowable stress is based on the lowest allowable at specified (at room temperature); where the lowest allowable for the primary stresses specified is 143 MPa.

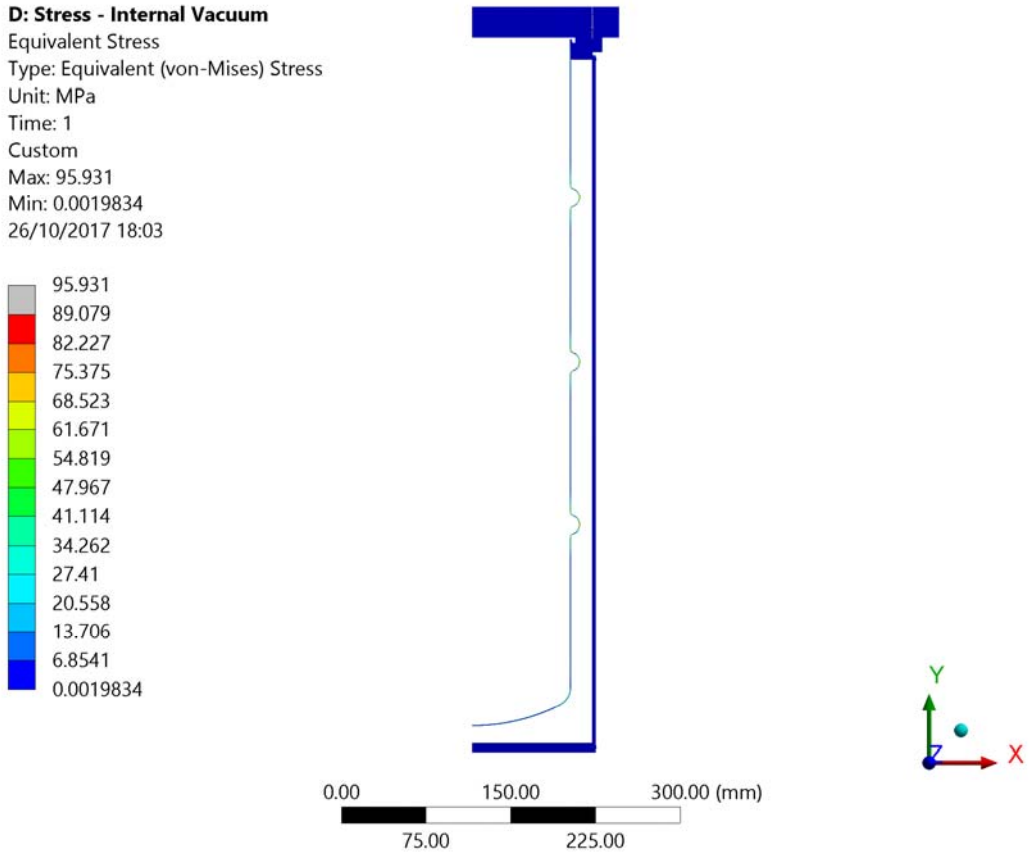

Figure 29 – LC2/LC3 - Primairy stress

As shown in Figure 29 all stresses are below the allowable of 143 MPa (with a max. value of 95 MPa); LC1 is governing for the stress evaluation.

11. Results 3D model

The full 3D model is used to verify the results from the 2D axisymmetric model as well as asses the (buckling) stability of the dewar for the load cases listed in section 8.1.

11.1 Verification stresses 3D model

11.1.1 Primary stresses

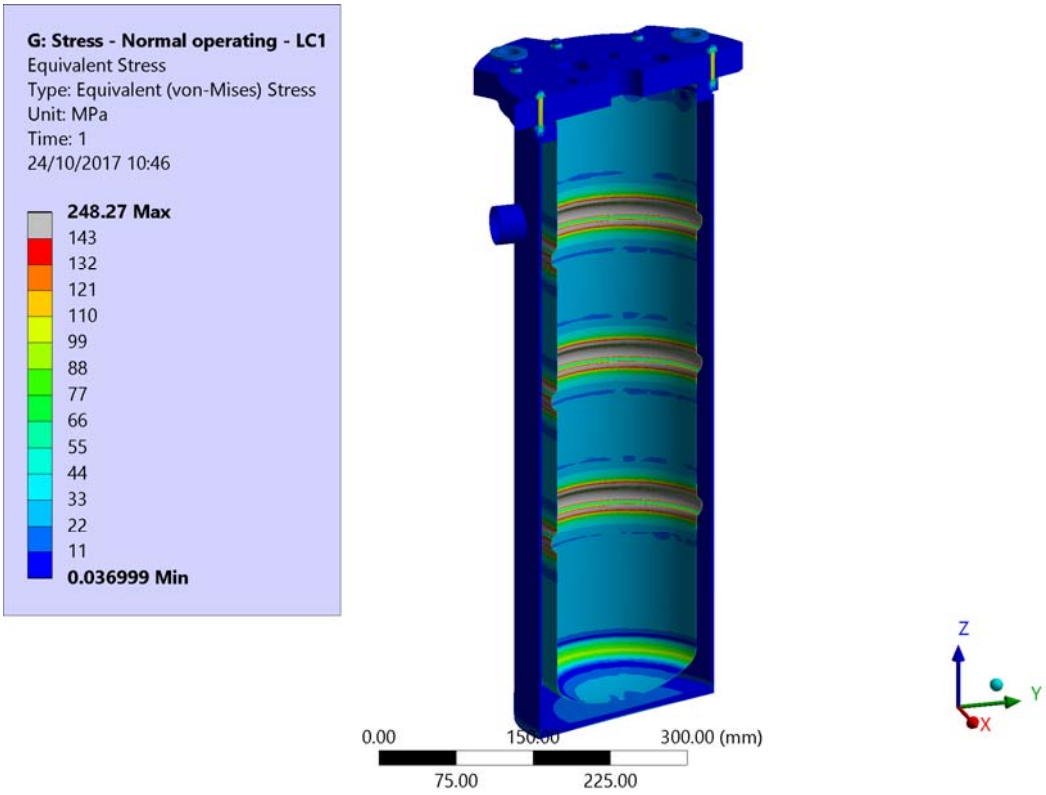

Figure 30 - LC1 - Primary stress – 3D model

The stresses in the dewar calculated with in the full 3D model (Figure 30) are similar to those of the 2D axisymmetric model (Figure 20 through Figure 23). There is a small error of approximately 2.5%, yet this to be expected considering the inherent numerical and truncation errors present in a finite element analysis and the different geometries (and thus elements) used to model the dewar. The verification of the stresses as performed in section 10.1 making use of the 2D model can therefore be considered as sufficiently accurate.

11.1.2 Bolt stresses

The bolts M6 are verified using analytical methods in section 9.1, where the bolt stresses resulting from the pre-tensioning alone are considered, with a stress 100 MPa. The pre-tensioning is included in the simulation and the stresses in the bolts are shown to be predominantly caused by this load, with an average bolt stress of approximately 108 MPa, with a maximum of 120 MPa induced by bending and boundary conditions (Figure 31).

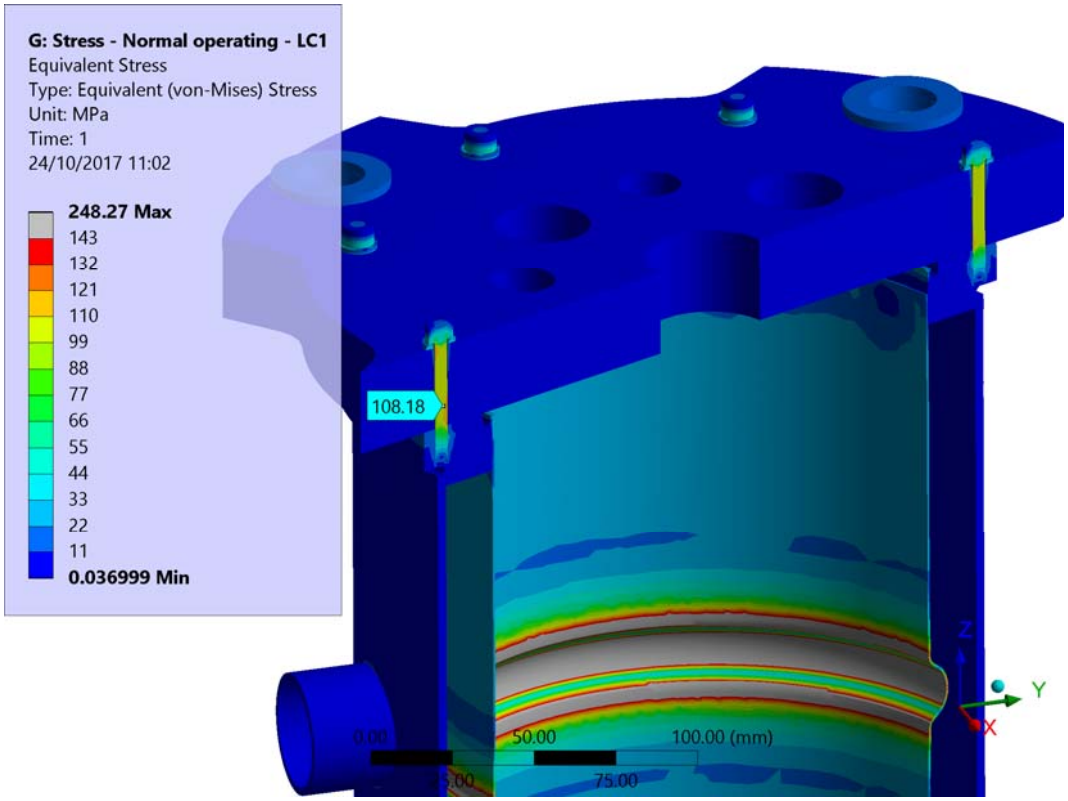

Figure 31 - LC1 - Primary stress - Bolt stresses

11.2 Buckling stability

The full 3D model is used to assess the stability of the dewar for the loads and load cases listed in chapter 8. The full model is required for this assessment as any reduced model has the potential to supress buckling modes. The load cases for which the dewar is verified with regards to stability are essentially two cases LC1 with full vacuum between the internal and external jacket (normal operating) and LC2 with a full vacuum in the inner jacket (failure and test case).

11.2.1 LC1

The buckling multiplier is computed using the stress result computed for LC1 (as shown in section 10.1), using a linear elastic bifurcation buckling analysis. The first positive buckling load multiplier is computed at 52.3, as shown in Figure 32 with its associated buckling mode. This buckling multiplier is considered sufficient to ensure stability for the loading. The EN13445-3 unfortunately doesn't specify any recommended multiplier, yet in most literature a minimum required multiplier of 2.5-3 is recommended. For example, the required load multiplier calculated using the rules from the ASME VIII div 2 (equivalent standard) is 2.7 for the external jacket.

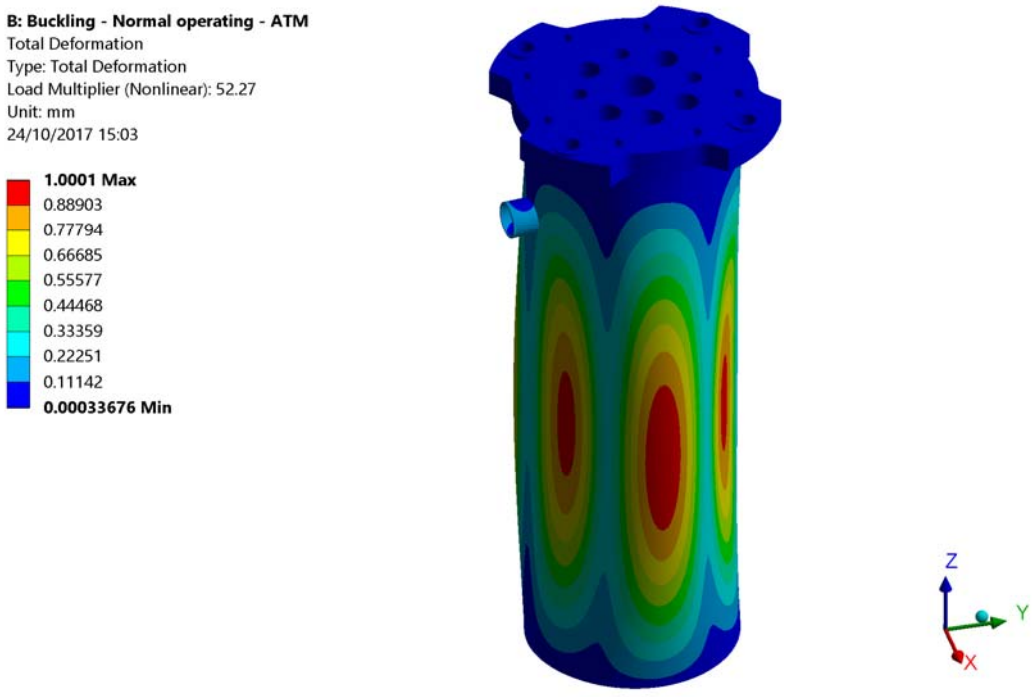

Figure 32 - LC1 - Buckling stability

11.2.2 LC2

The buckling multiplier is computed for LC2, the first positive buckling load multiplier is computed at 6.4, as shown using a section view of the dewar in Figure 33 with its associated buckling mode. The calculated load multiplier is considered acceptable as it is higher than a commonly recommended multiplier of 3, and it should be noted that this concerns a test and failure case.

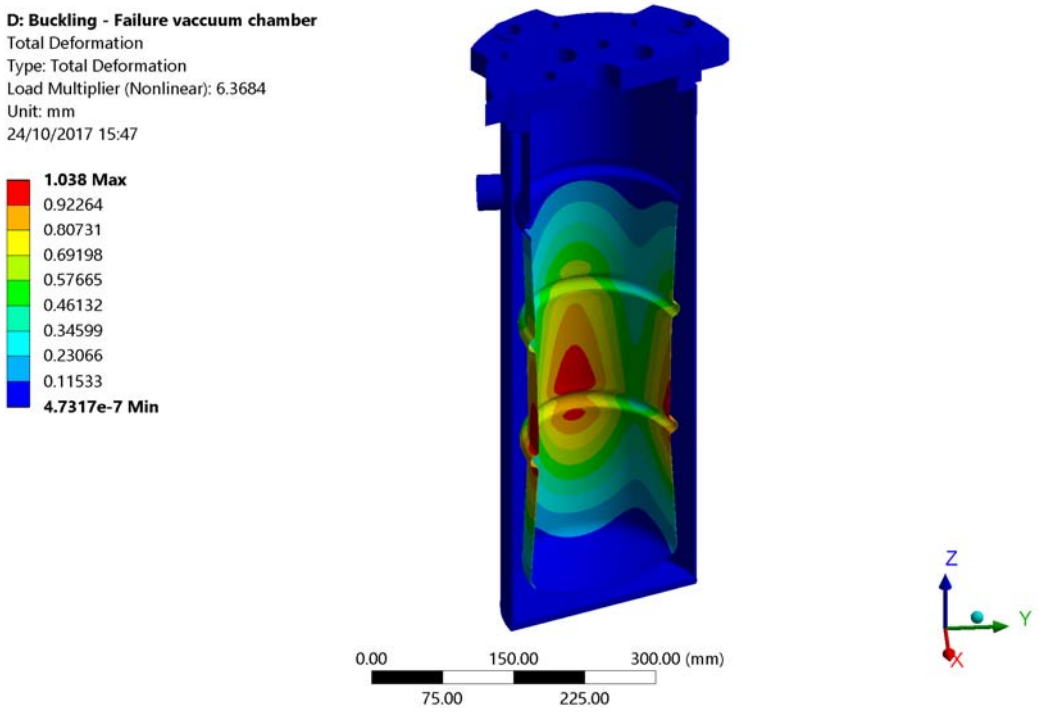

Figure 33 – LC2 - Buckling stability

11.3 Fracture analysis weld

The weld between the inner and outer jacket as highlighted in subsection 10.1.2 is evaluated using a fracture toughness approach. The stress intensity factors at the weld are determined and validated using the know fracture toughness of the material. For this case the internal pressure of 1.5 bar(g) is not applied to the model as it counteracts the opening; this will result in the most significant stress intensity factors. It should also be noted that during normal operating the dewar is typically atmospheric pressure. A small section of the dewar is used to evaluate the stress intensity factor at the weld as shown in Figure 34, where the stress intensity factors converge to K_I = 12 MPa√m (Figure 35) and K_{II} = 2 MPa√m (Figure 36).

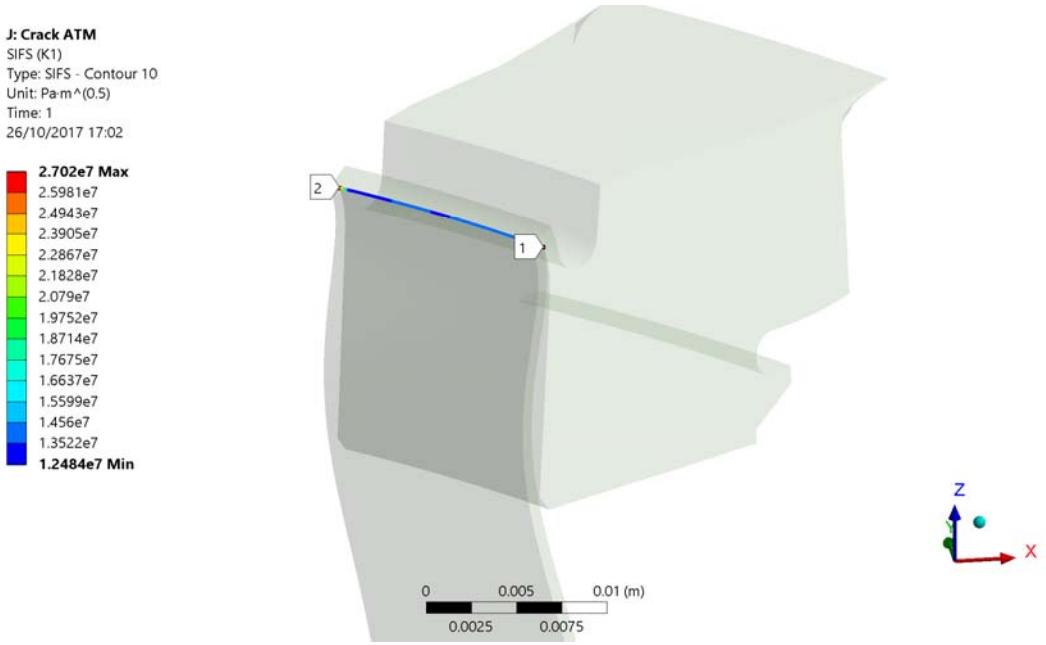

Figure 34 - Fracture

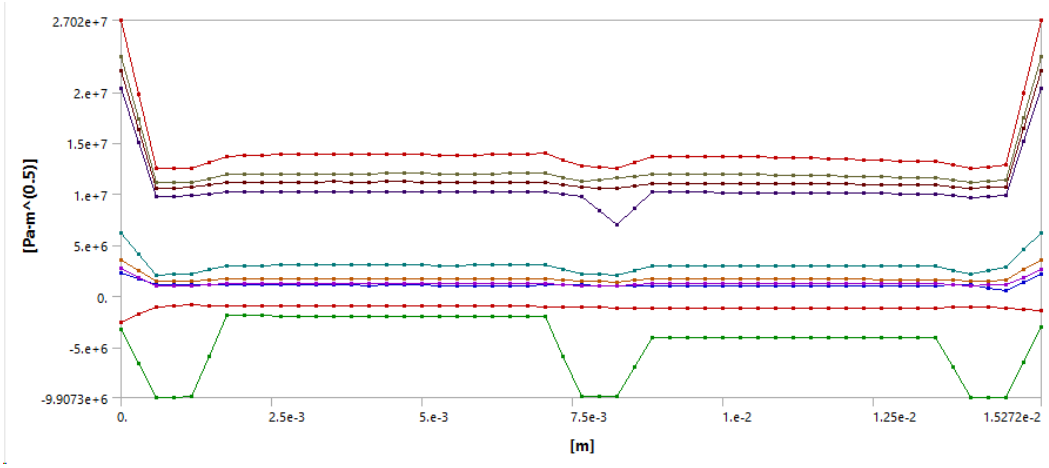

Figure 35 - K_I

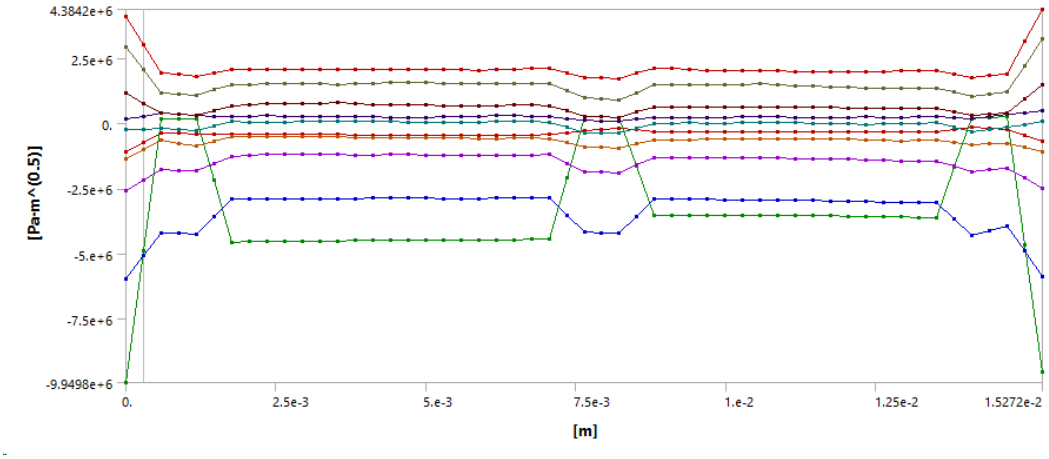

Figure 36 - K_{II}

The mode I stress intensity factor is not of concern with regards to imminent failure, yet it is susceptible to fatigue crack growth. The modelled geometry is an idealised case with a continuous smooth edge, whereas in reality this geometry can be considered to closer to that of a pattern of semi-elliptical cracks. The actual geometry should be therefore considered as less favourable than the modelled geometry. Fortunately, the calculated stress intensity factor for the ideal case will result in a relative slow initial crack growth, with for 316LN at 4 K and ΔK = 12 MPa$\sqrt{m}$ the da/dN is approximately 1.2×10^{-6} mm/cycle.

The mode II stress intensity is of little concern it is significantly low that it does not impact the design (also negligible in comparison to K_I). In the simulation a frictionless contact was used to define the contact at the crack; where friction would transfer some of the applicable load further reducing this stress intensity.

The weld is susceptible from failure due to fatigue crack growth, regular inspection of the vacuum between the inner and outer jacket of the dewar can be used to assess the integrity of the weld (assuming leak before burst). Catastrophic failure of this weld is not expected and it should be noted that the consequence of failure is only operational. Failure of this weld would not result in a containment breach and should be noticeable during operation due to leakage of helium into the vacuum chamber.

12. Conclusions

It can be concluded that the presented analysis validates the design of the cryogenic vessel of the test cryostat for tensile tests at cryogenic temperatures. The strength to the loading scenarios identified over section 7 is confirmed by the results from the finite elements analyses presented in chapter 10 and 11. The primary stresses are shown to be acceptable and similarly the secondary stresses. The thermal conditions imposed on the structure however are shown to result in a type of loading of the weld which could be described as a mode I and II crack opening; where mode I is predominant. The weld is shown to be susceptible to failure from fatigue, yet for a relatively high number of cycles.

Such analyses were performed following the specific guidelines given by the relevant European standards for pressure equipment [1], [2].

13. References

[1] *EN 13445:2002 - Unfired pressure vessels.*

[2] *EN 13458:2002 - Cryogenic Vessels - Static Insulated Vessels.*

[3] *EN 13155:2003 - Cranes - Safety: non-fixed load lifting attachments.*

[4] Cryocomp, "Version 5.1," Eckels Engineering Inc. , 2011.

[5] *EN 10088:2005 - Stainless steels.*

[6] A. Mills, Bsic heat and mass transfer, Essex: Pearson education limited, 2014.

ANNEX A

- Pre-study: analytical calculations –

Buckling of cylindrical sectors under external pressure

According to EN13458-2:

4.3.6.2.4 Elastic buckling

Calculations are performed using the following formula:

$$p_e = \frac{E}{S_k}\left\{\frac{20}{\left(n^2-1\right)\cdot\left[1+\left(n/Z\right)^2\right]^2}\cdot\frac{s-c}{D_a}+\frac{80}{12\cdot\left(1-v^2\right)}\cdot\left[n^2-1+\frac{2n^2-1-v}{1+\left(n/Z\right)^2}\right]\cdot\left[\frac{s-c}{D_a}\right]^3\right\} \quad (3)$$

where $Z = 0{,}5\pi D_a/l_b$ and n is an integer equal to or greater than 2 and greater than Z, so determined that the value for p_e is a minimum. n denotes the number of lobes produced by the buckling process which can occur at the circumference in the event of failure. The number of lobes can be estimated using the following approximation equation :

$$n = 1{,}63\cdot\sqrt[4]{\frac{D_a^{\,3}}{l_b^2\left(s-c\right)}} \quad (4)$$

Code:

```
EE=193000;
Sk=1.0;
Da=175;
ss=0.8;
v=0.3;
lbk=145;
cc=0

"EN 13458-2 Version Anglaise"

"Z"
Z=0.5*3.14*Da/lbk
"nn - INSERT N!"
nn=1.63((Da^3)/(lbk^2*(ss-cc)))^0.25

n=6;
"Pe (bar)"
Pe=EE/Sk*((80*((ss-cc)/Da)^3)/(12*(1-v^2)))*(n^2-1+(2*n^2-1-v)/(1+(n/Z)^2))+(ss-cc)/Da*20/((n^2-1)*(1+(n/Z)^2)^2))

"Deformation plastique"
"fa - moins de 5?"
fa=Da/lbk//N

K=175;
Sp=1.6;
u=2;

"Pp (bar)"
Pp=20*K*(ss-cc)/(Sp*Da*(1+1.5*u*(1-0.2*fa)*(Da/(100*(ss-cc)))))

"EN 13458-2 Version Française"
"Pef (bar)"
Pef=EE/Sk*(20/((n^2-1)*(1+(n/Z)^2))*(ss-cc)/Da*80/(12*(1-v^2)))*(n^2-1+(2*n^2-1-v)/(1+(n/Z)^2))*((ss-cc)/Da)^3)
```

Results:

```
Out[607]= 0
Out[608]= EN 13458-2 Version Anglaise
Out[609]= Z
Out[610]= 1.89483
Out[611]= nn - INSERT N!
Out[612]= 6.88668
Out[614]= Pe (bar)
Out[615]= 9.74014
Out[616]= Deformation plastique
Out[617]= fa - moins de 5?
Out[618]= 1.2069
Out[622]= Pp (bar)
Out[623]= 1.67267
Out[624]= EN 13458-2 Version Française
Out[625]= Pef (bar)
Out[626]= 0.00132515
```

Geometry:

Diameter: 175mm;
Length: 145mm;
Thickness: 0.8mm;

Conclusion:

Critical pressure calculated from the standard (output 15): 9.7 bar

Linear buckling analysis:

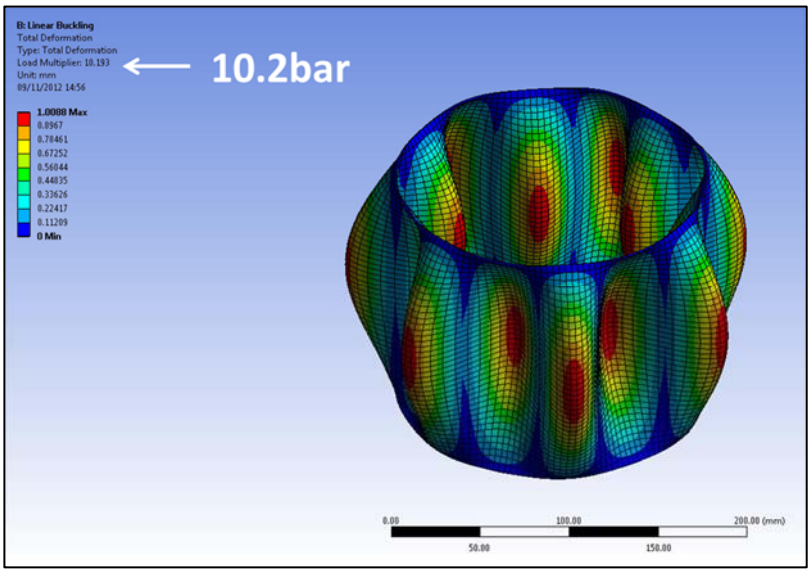

Non-linear buckling analysis:

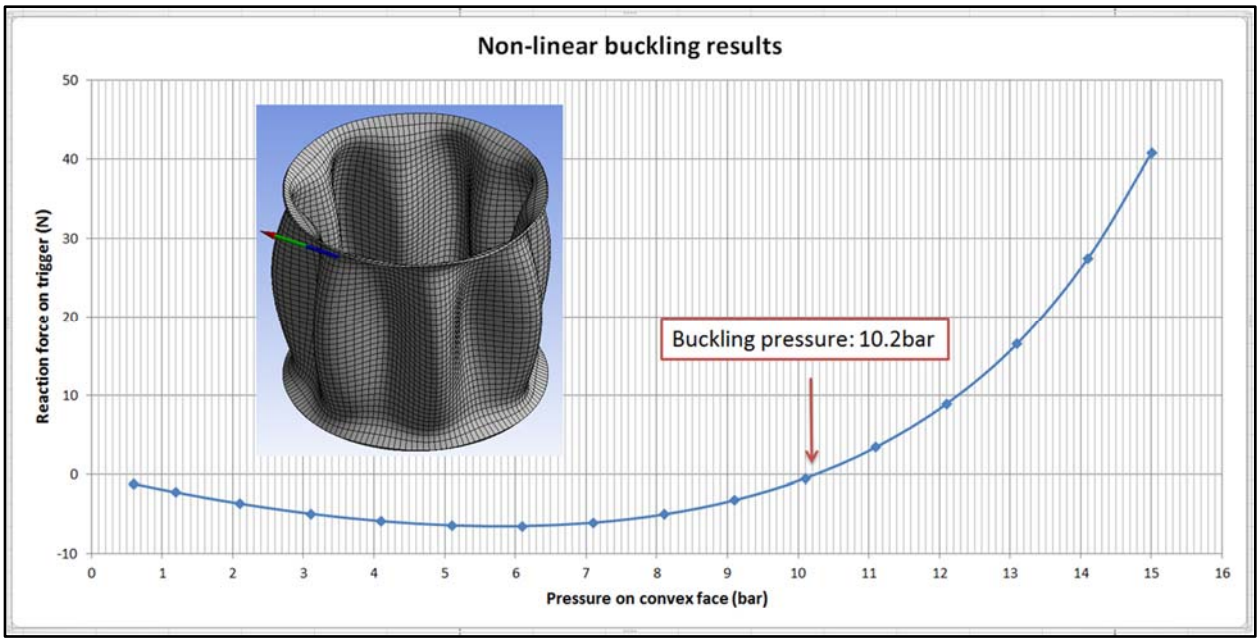

ANNEX B

- Thermal properties -

The curves as shown in Figure 37 through Figure 40, the thermal conductivity and expansion of 304 and 316 stainless steels are constructed from the exported data from CryoComp [4].

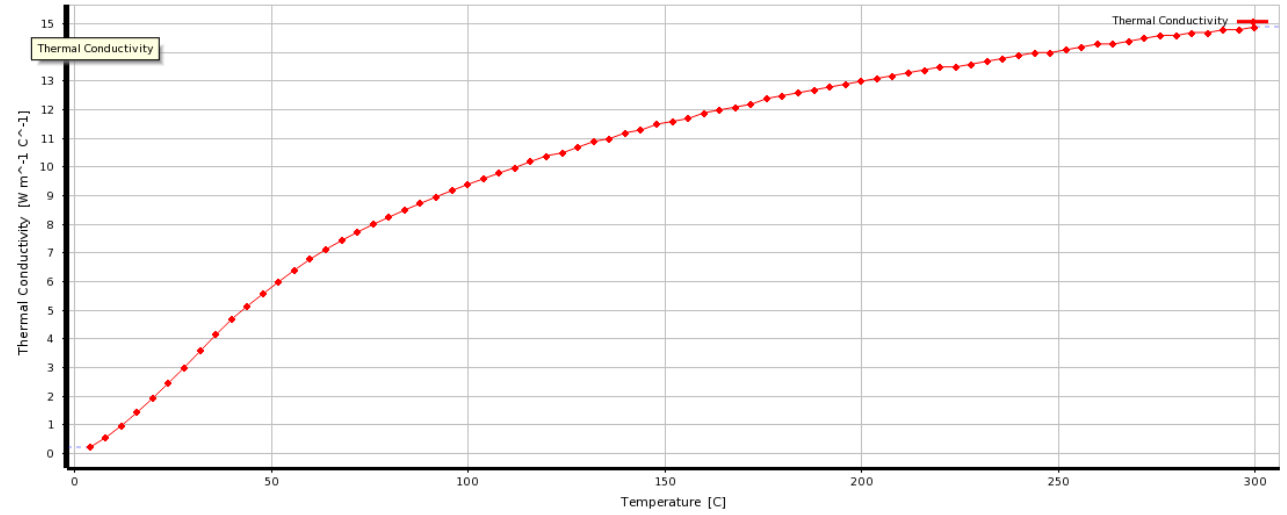

Figure 37 – Thermal conductivity 304

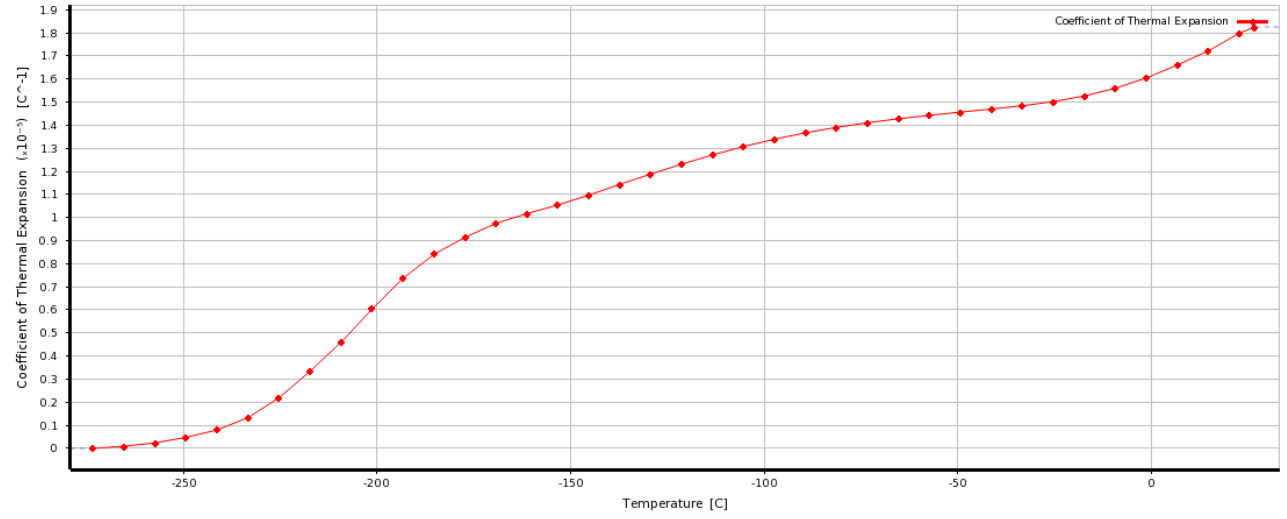

Figure 38 – Coefficient of thermal expansion 304

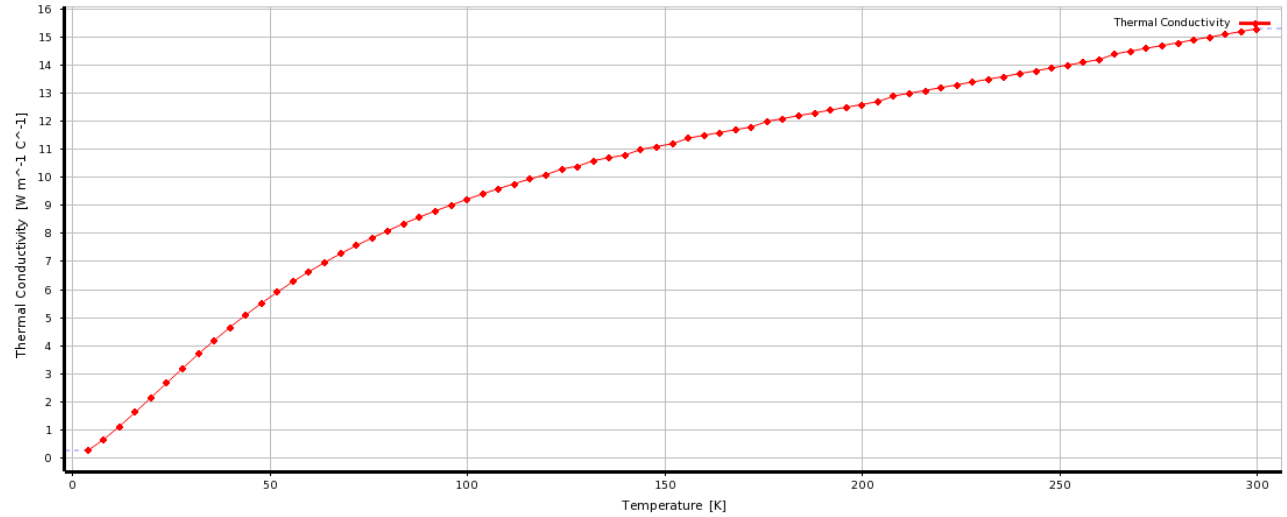

Figure 39 - Thermal conductivity 316

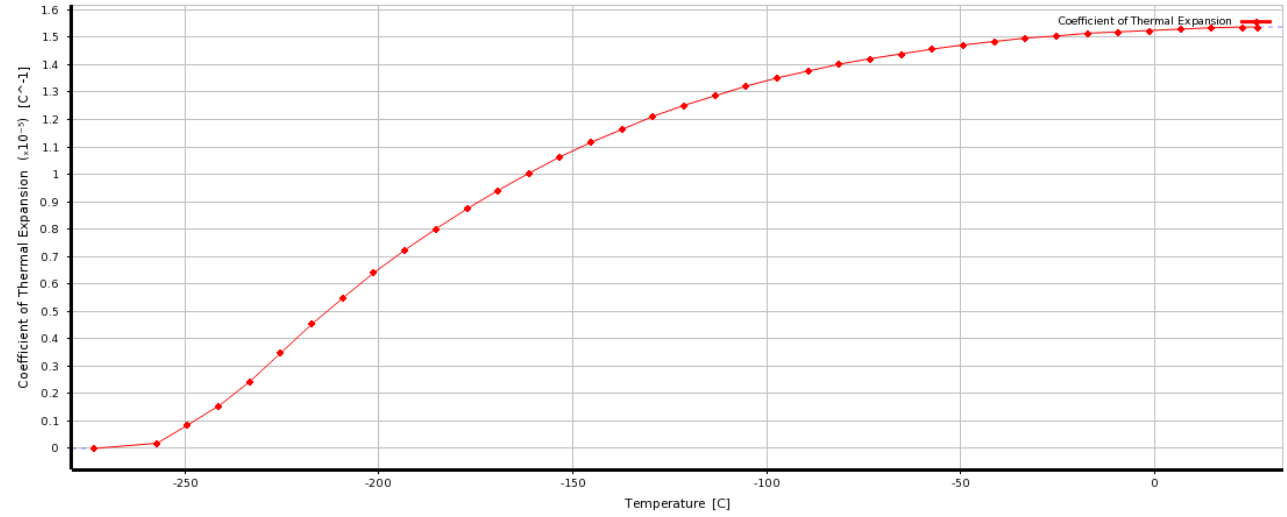

Figure 40 - Coefficient of thermal expansion 316

E

Design verification tooling

A number of design iterations have been performed in order to optimise the design, taking into consideration operating conditions and fabrication restrictions. A more comprehensive design verification is included in this appendix for the final design iteration.

E.1. Model and mesh

A reduced model is used to allow for a an high detail finite element simulation while reducing computation time. The model is reduced to the smallest representative size possible, with the resulting model as shown in Figure E.1 and with the symmetry conditions as shown in Figure E.3.

Strictly speaking the actual situation is not symmetrical, yet as a similar pin connection to that at the loadcel is present at the bottom half its considered as sufficiently representative. A fine mesh of 1 mm is

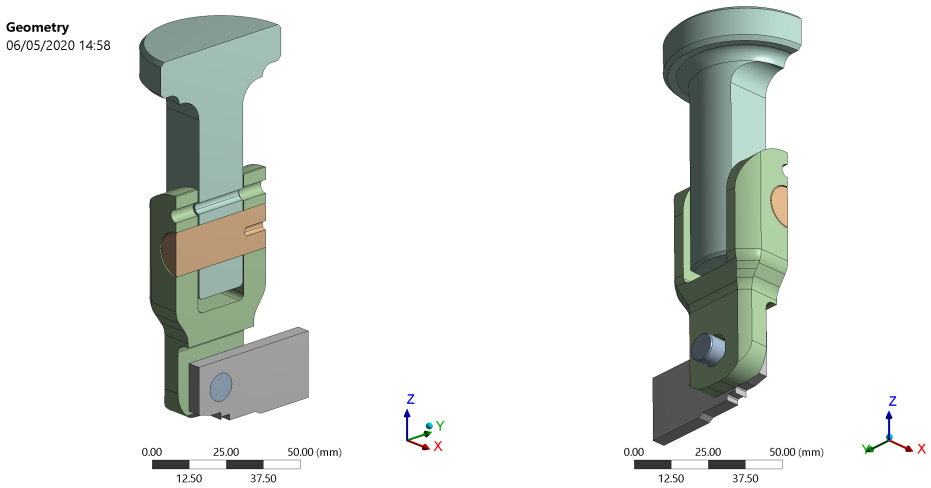

Figure E.1: Simulation model

defined for all bodies, with further refinement to 0.5 mm at the contact between the pin and the clevis (as illustrated in Figure E.2).

E.2. Boundary conditions

Symmetry conditions are applied to the model with some additional constraints to prevent rigid body movement (Figure E.3). Frictionless contacts are defined at the pins connections with a frictional constraint between the pin and the sliding faces on the clevis with a coefficient of 0.1 (Figure E.4). The load is applied at the interface from the load-cel to the UTS; as symmetry is used a load of 12 kN is applied as shown in Figure E.5.

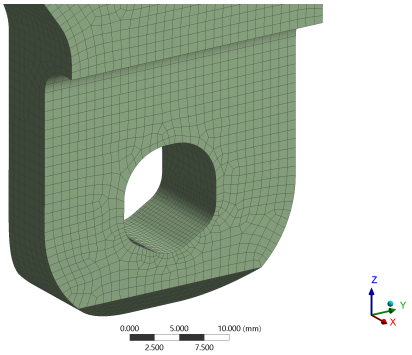

Figure E.2: Detail of the mesh

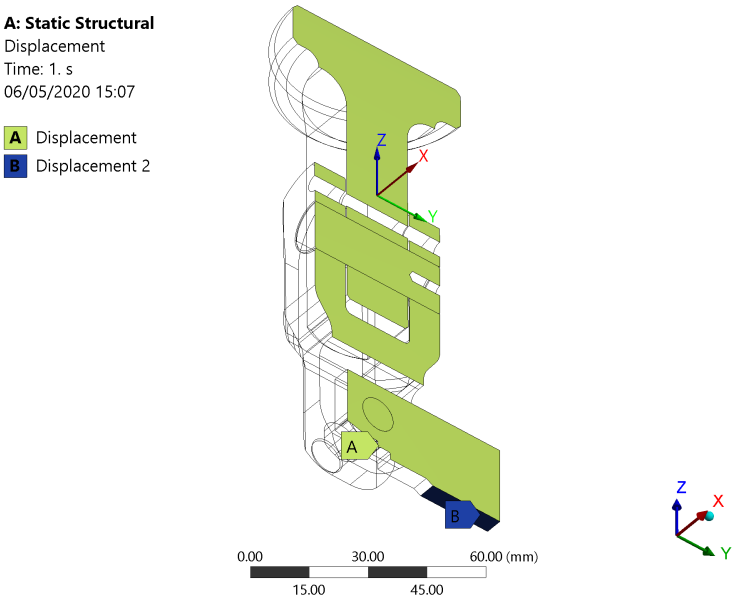

Figure E.3: Symmetry conditions

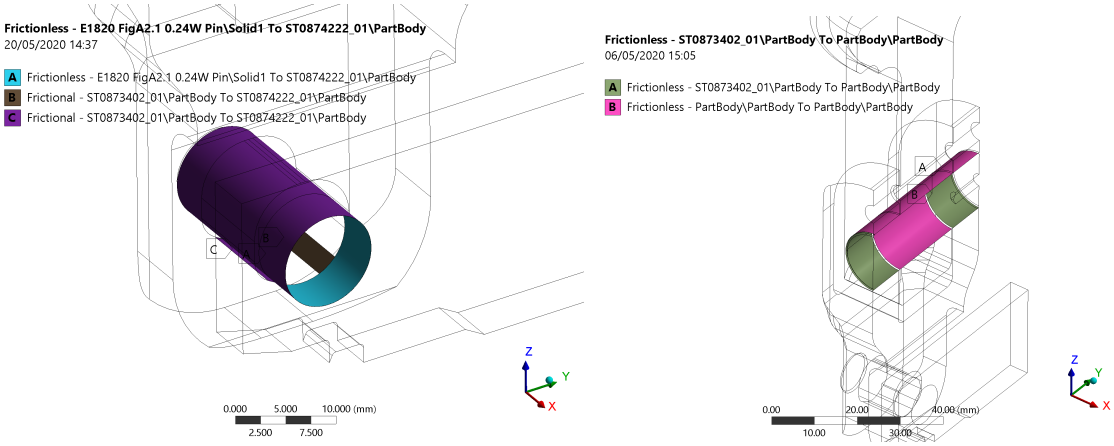

Figure E.4: Contacts

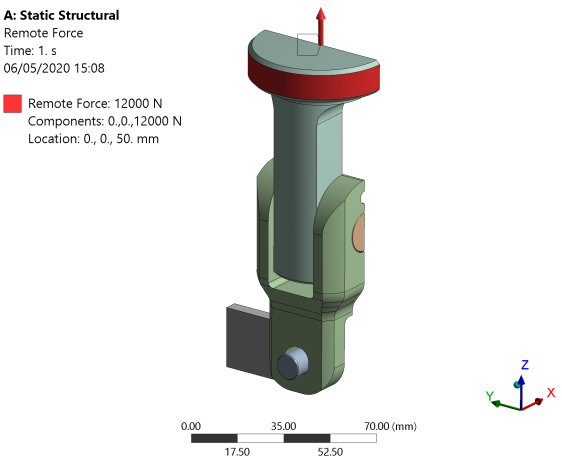

Figure E.5: Load application

E.3. Results

E.3.1. Deformation

In Figure E.6 the total deformation of the model is displayed. These are shown with an exaggeration factor of 10, showing small displacement; i.e rigid body movement properly suppressed.

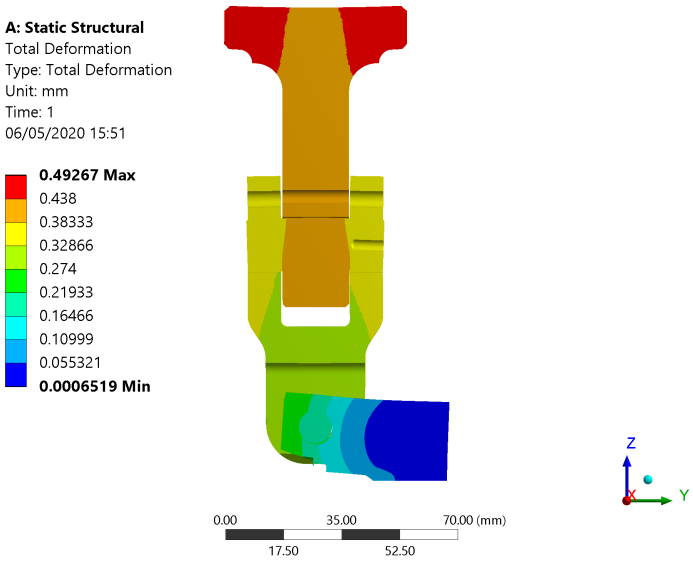

Figure E.6: total deformation

The shown deformation is for the load of 24 kN, the required test load estimated. Due to the nature of the model the expected load-line displacement (opening) at the knife edges can be considered at least twice that of the simulation of 0.194 mm (0.4 mm); where crack growth is not considered in this simulation.

E.3.2. Stresses

The stresses are displayed on a linear scale for the the clevis of 553 MPa; the yield stress of 830 MPa at room temperature Table G.2 with at least a factor of safety of 1.5. At cryogenic temperatures the yield stress of the material is typically much higher hence this is considered as conservative.

The stresses in the clevis are limited to approximately 200 MPa (Figure E.8), with the exception being the contact area; as shown in Figure E.9. The stresses at the contact are relatively high with a peak stress up to 2612 MPa, these high contact stresses where expected and are veried using the analytical method used for the initial calculations (Table 2.1).

The stresses in the pin as shown in Figure E.10 are less than those calculated (Table 2.1). These lower stresses can in part be attributed to the larger diameter of the pin in the final design, and also the more honerous contact assumption in the analytical method.

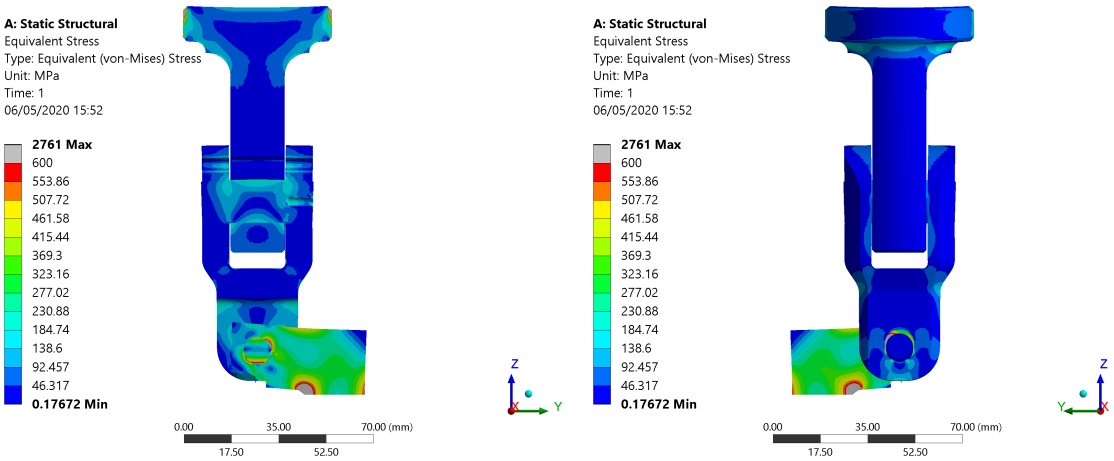

Figure E.7: Total equivalent stress (Von Mises)

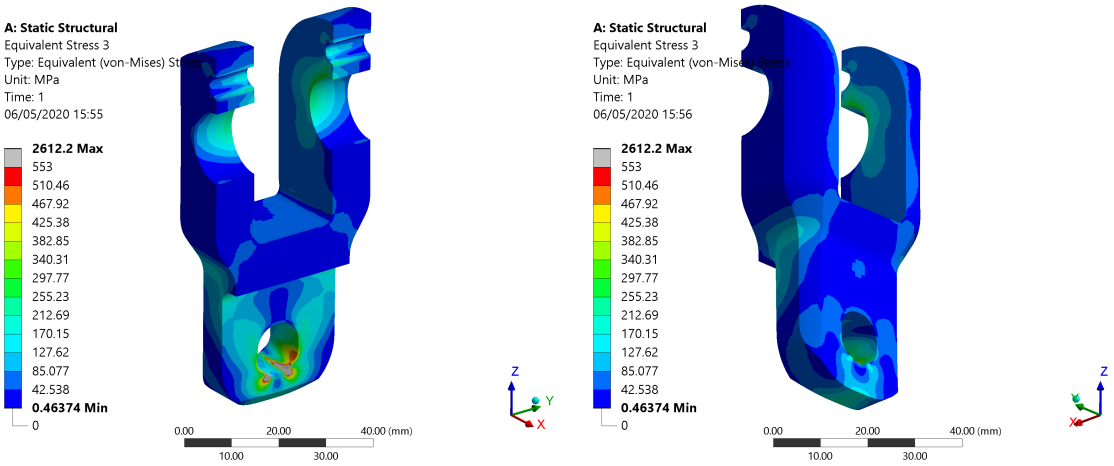

Figure E.8: Total equivalent stress in clevis

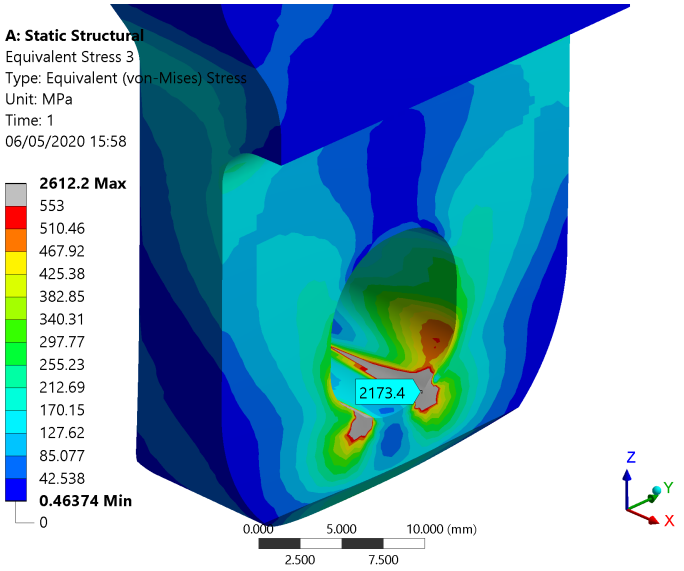

Figure E.9: Detail stresses clevis at contact area

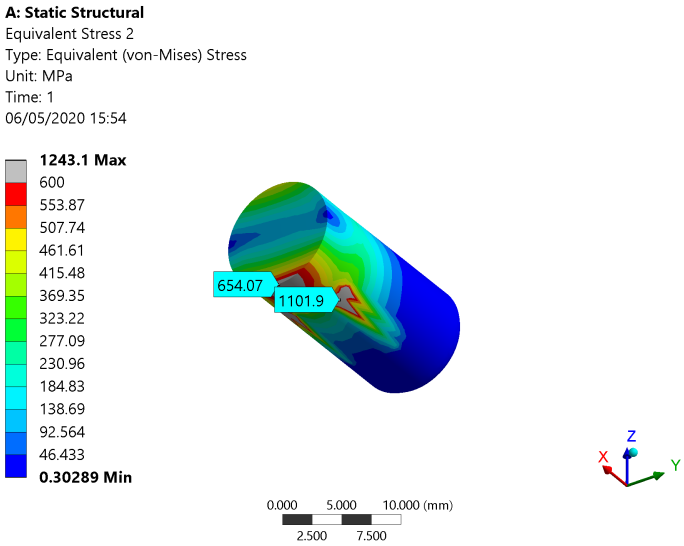

Figure E.10: Detail stresses in the pin

E.3.3. Strains

As part of an investigation on whether the clevis could be used to measure the load, the strains in the clevis are evaluated. There is a small area above the pin hole that might be suitable for the application of strain gages. Tough possible it became apparent upon further examination due to the small area and in-homogeneous strains application and calibration of the strain gages would prove to be difficult.

The load-cell used for tensile test in the current set-up was however also suitable for implementation, and as the current load-cell calibrated and could be implemented with ease it was decided to maintain this load-cell for expedience.

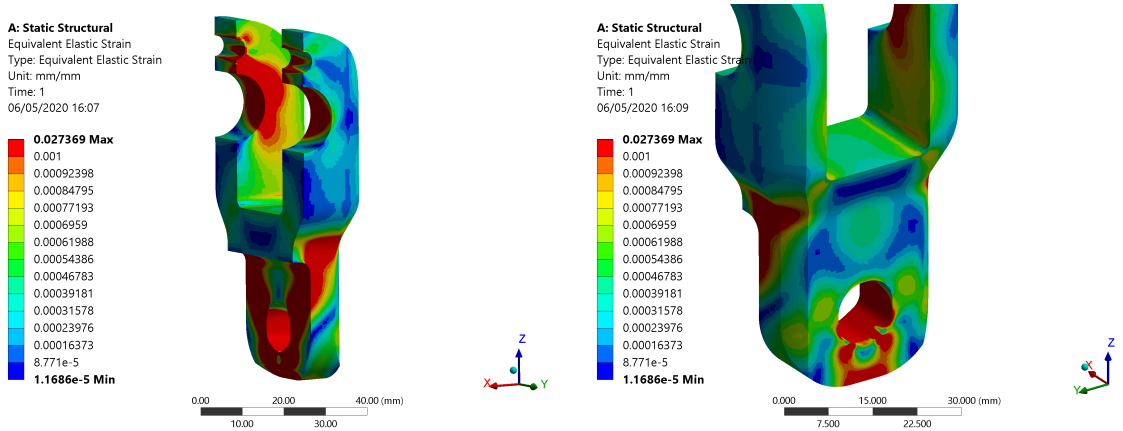

Figure E.11: Strains in clevis

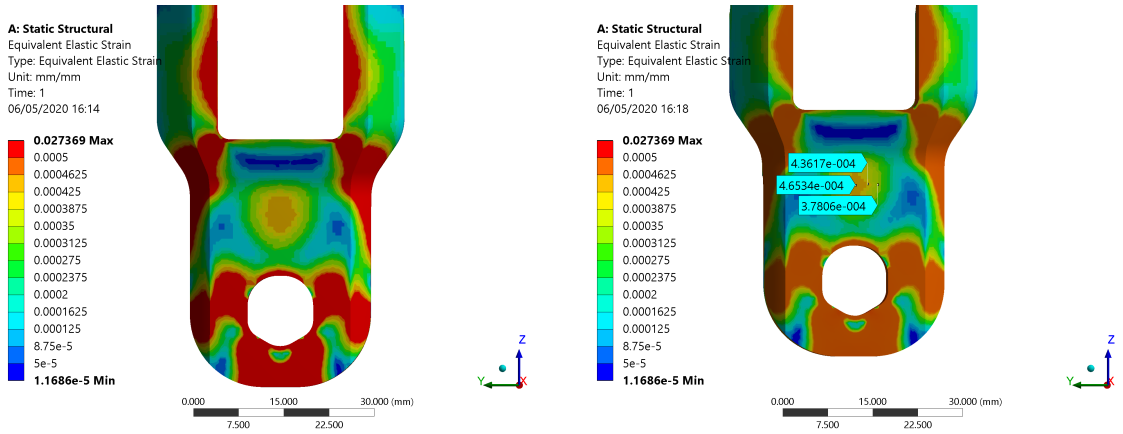

Figure E.12: Strains in clevis - Detail

E.4. Summary and conclusion

The stresses aside from the contact stresses in the design and primarily the clevis are generally below 200 MPa. With the lowest yield stress of the material at 830 MPa (Table G.2); this leaves a factor of safety of over 4. The contact stresses are the limiting factor in the design, this allows for easy analytical calculation of the allowable load under the different design conditions.

A minor design deviation from the default as described in the standard[9], is by slightly increasing the pin diameter to a better fit in the standard sample. For the design with W=36 this results in a pin diameter of 9 mm, with a fitting tolerance taking into account different thermal contraction and operating fitting.

Additionally in order to assure that the stresses in the design will remain primarily elastic and reducing contact stresses a design is proposed with an even larger pin of 11 mm. Showing little to no impact on the fracture toughness value (refer to appendix C). The maximum allowable load for these two diameters and the default pin of 8.4 mm is calculated using the analytic method used for the initial calculations (considered valid as the behaviour of the clevis is primarily linear elastic). As this concerns an ultimate test load a low factor of 1.2 is included in the calculation of the contact stress to account for the minor discrepancy found in the contact stresses between the simulation and the analytical method (Figure E.9 & Table 2.1).

With the allowable for the bending and equivalent shear stress at the yield stress of the material at the specified temperature (refer to appensix G.2). Where for the contact stress the allowable stress is set at the plastic flow contact stress; $2.8 \times \sigma_{YS}$.

The analytical method calculates the bending stress and shear stress without taking into account second order effects, and is found to be more onerous than finite element analysis. Using the analytical method limits the load to the bending stress, while the contact stress criteria is not met in any of the considered design scenarios.

Table E.1: Ultimate Load

Ultimate test load	**Ø8.6 mm**	**Ø9.0 mm**	**Ø11.0 mm**
293 K	21 kN	24 kN	43 kN
70 K	32 kN	37 kN	67 kN
4 K	36 kN	42 kN	92 kN

F

Test results

This appendix contains the output and processing of output from the tests of the 4 specimen, with the test performed as described in chapter 4. The program as described was used for each of the specimen, with either adjustments to account for the specimen or tweaks such as a larger loading and unloading force with the compliance method (allowing for a more accurate estimate of the compliance).

F.1. Room temperature test - Ti6Al4V-2

The was the first test and was performed at room temperature with the specimen designated Ti6Al4V-2. The program of as described in subsection 4.2.1 was used in this test with a modification on the loading and unloading of the compliance method. At each of compliance testing points in the program instead of a single cycle three cycles where performed. This allowing for three measurements of the stiffness, in an attempt to get a accurate reading and in order to verify the effect of this loading and unloading.

F.1.1. Measured data

As discussed in section 4.2 the entire system also used for cryogenic tests was used, with the only the dewar of the cryostat omitted to allow for visual feedback during the test. The data from the sensors on the specimen is captured and stored, in Figure F.1 the measurement data is shown with thick marks every 50 data point.

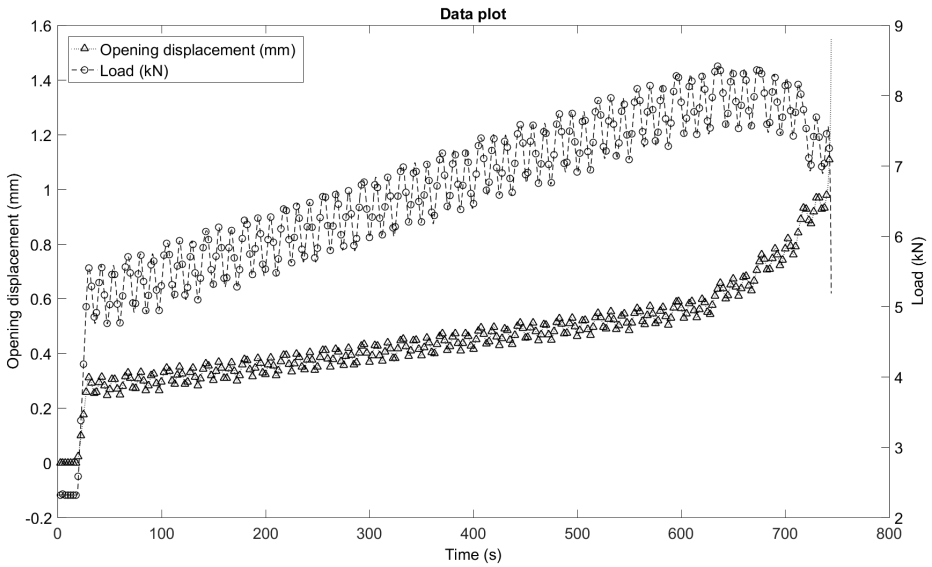

Figure F.1: Measurement data on specimen Ti6Al4V-2

F.1.2. Load-line displacement

The data from the measurement is used to construct a load-line displacement plot (LLD), where the opening displacement measured being the load-line displacement; the advantage of using a C(T) specimen. This LLD plot allows for the characterisation of the fracture toughness as described in the standard [9], the resulting graph is shown in Figure F.2.

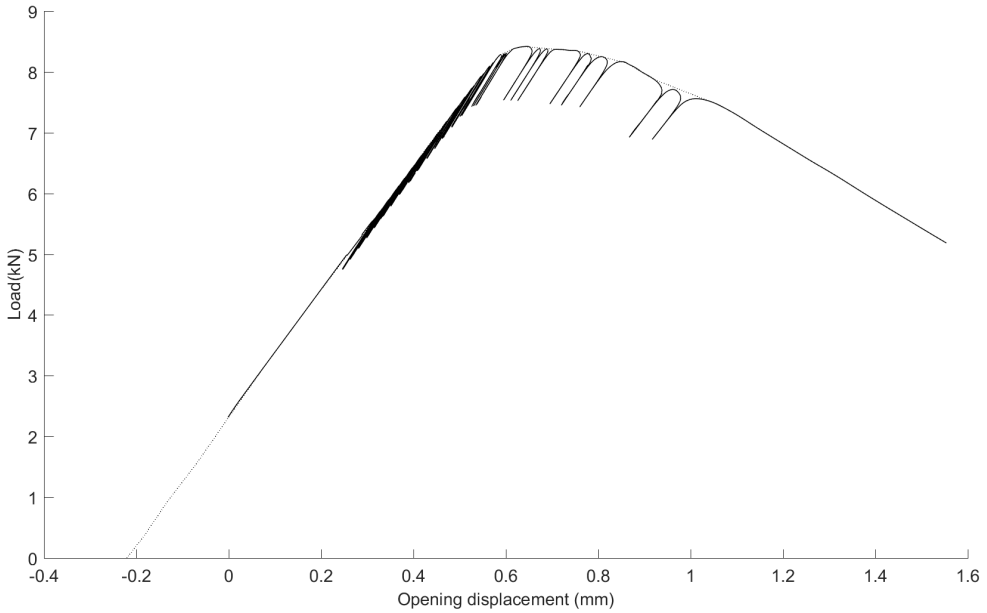

Figure F.2: LLD specimen Ti6Al4V-2

In the plot different regions of loading can be considered:

1. linear loading of the specimen from 0 to 0.5 mm opening. (linearly increasing load)
2. plasticity at the crack tip from approximately 0.4 to 0.65 mm opening displacement (non-linear increasing to an almost constant load)
3. plasticity and crack growth from approximately 0.66 to 1 mm opening displacement (a decreasing load; negative stiffness)
4. Failure of the specimen occurring for opening displacements greater than 1 mm

These regions can also be discerned in Figure F.1 to some extend, with predominately linear behaviour up to 600 sec, followed by non-linear behaviour from 600 up to 750 sec, after which failure of the specimen occurs.

The loading and unloading is shown to have a very limited effect in the linear loading region of the specimen. Though there is some effect, this becomes more apparent later in the test, as there is more plasticity at the crack tip, ratcheting can be observed. As the specimen is unloaded and subsequently loaded there is an increase in opening displacement; indicative of ratcheting, crack growth, or both. This effect becomes increasingly present and at later stages failure occurs during the second cycle of this repetition. This effect is undesirable and also defeats the purpose of the repeated cycle (as the crack propagates), and this was scrapped from the program.

F.1.3. Interpretation

In order to be able to construct a the J-R curve in accordance with the ASTM E-1820, two characteristics need to be determined from the measurement data. These are the energy involved with the progression of the crack and the compliance at each of the interpolation points. The data was processed extracting the compliance lines from the data, leaving the LLD curve. The measurement data with the extracted information is shown in Figure F.3, with in Figure F.4 only the extractec LLD curve and compliance lines. (both images with a correction to show 0 kN at a 0 mm opening displacement)

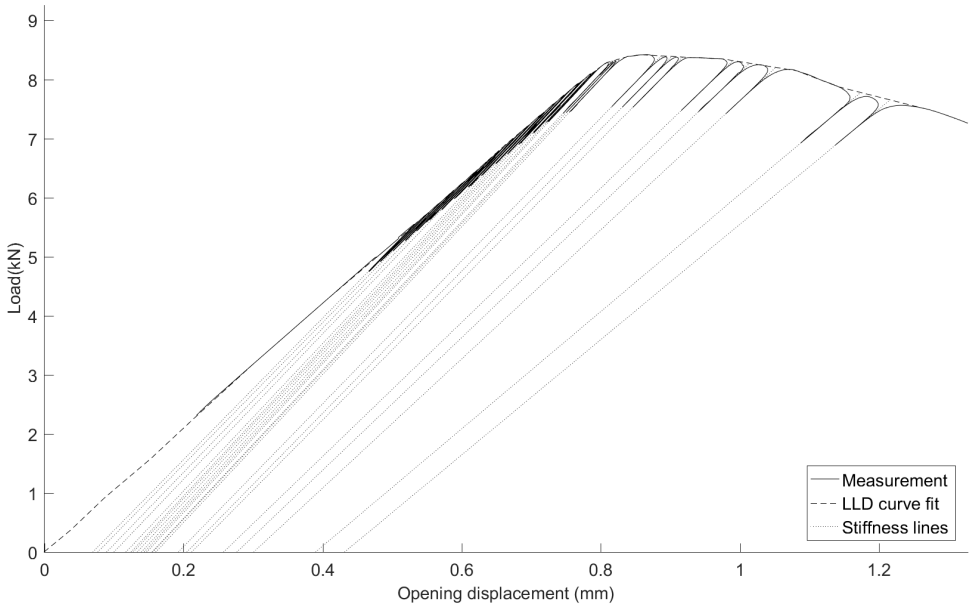

Figure F.3: Ti6Al4V-2 - LLD curve with extracted curves and lines

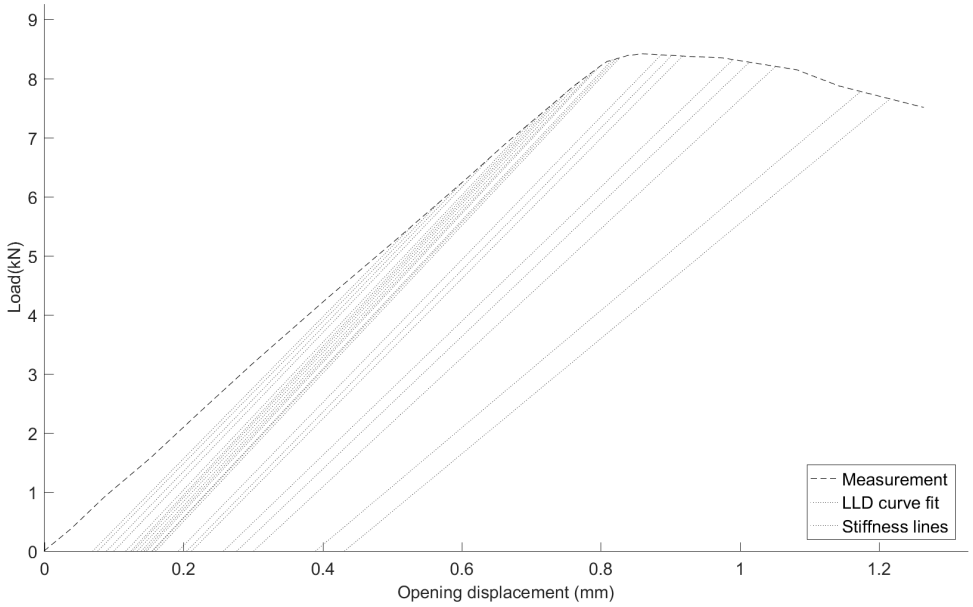

Figure F.4: Ti6Al4V-2 - Extracted information

Using the formulas provided in section A2.4[9] the crack size is estimated from the compliance lines which is shown in Figure F.5. There is a slight discrepancy between the original crack depth and initial depth according to the estimation, this can in part be attributed to the Young's modulus used in the calculation and the actual modulus. Another point of interest is the apparent negative crack growth, this can in fact be attributed to plastic hardening, due to the development of the plastic zone the compliance of the specimen decreases (as the stiffness increases).

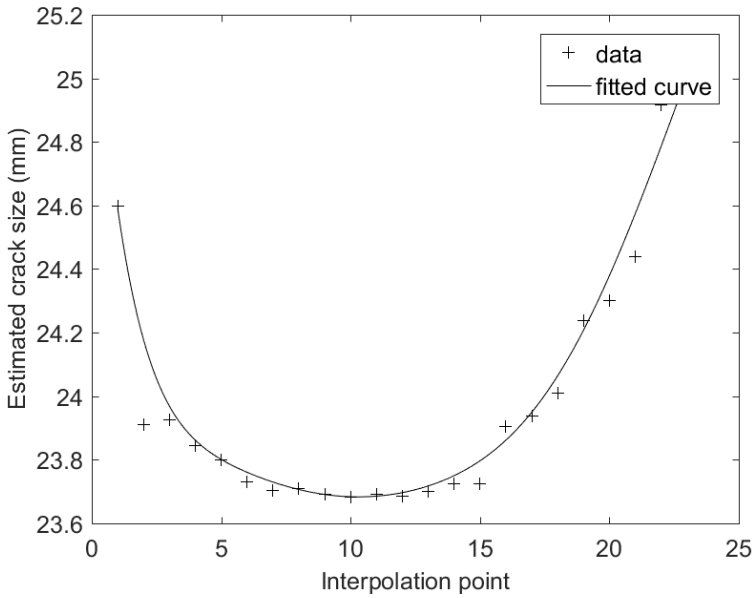

Figure F.5: Ti6Al4V-2 - Crack size estimate

Using integration the area under the LLD is computed for the test results as depicted in figure A1.2[9]. The area is computed between the LLD curve and the original loading slope up to an interpolation point. In order to allow for a more continuous representation the resulting A_{pl} (J) is plotted against the opening displacement as shown in Figure F.6.

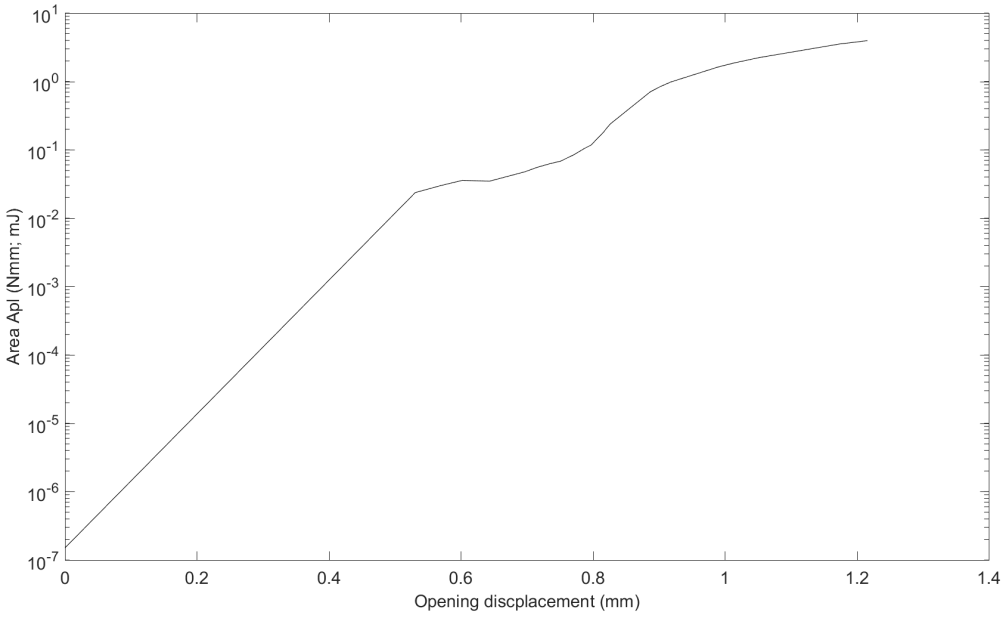

Figure F.6: Ti6Al4V-2 - Area Apl

The data set does not support a characterisation of the toughness according to the ASTM E1820. The fracture toughness can be characterized using the test method for Linear-Elastic Plane-Strain Fracture Toughness [11]. The position at which the measurement of the opening displacement is performed differs slightly, yet as this is used only indirectly in determining the toughness it is considered of little influence. The opening displacement is only used to construct a 0.95 secant line Figure F.7 to determine the load P_{Q}, as the relation

linear there should be little to no difference in the corresponding load.

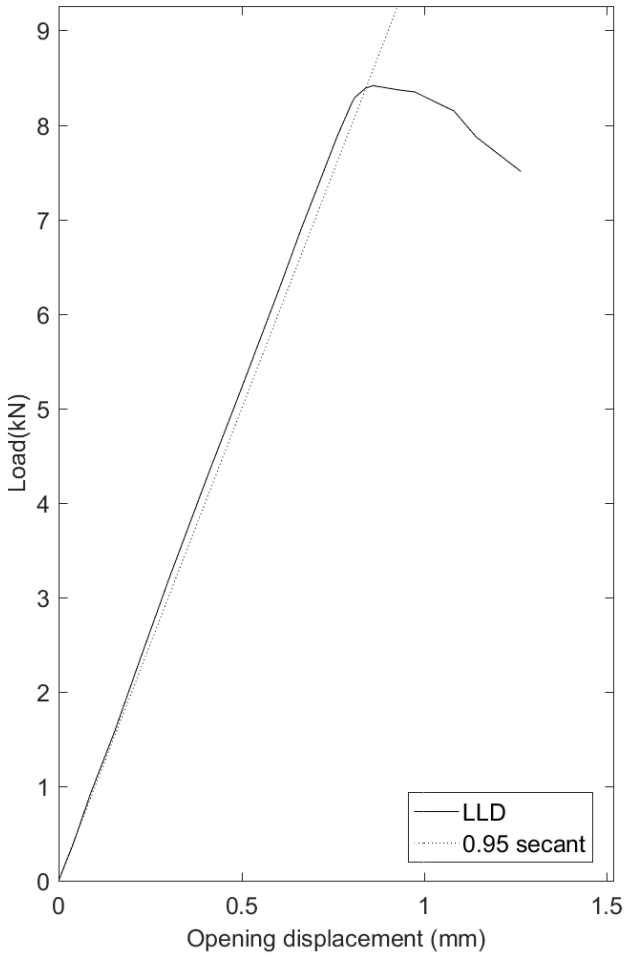

Figure F.7: Ti6Al4V-2 - 0.95 secant line

The load at the intersection between the 0.95 secant line and LLD curve is the load P_Q used to determine the fracture toughness K_Q. Where the test is a valid test result if the following relation with the maximum load (P_{max}) is met: $P_{max}/P_Q \leq 1.10$ section 9.1.3[11]. In this case $P_Q = 8.394$kN and $P_{max} = 8.416$kN, resulting in $P_{max}/P_Q = 1.0024$; acceptable. Using the load P_Q and the method outlined in the standard for a C(T) specimen the fracture toughness K_Q is calculated; $K_Q = 67.2\text{MPa}\sqrt{\text{m}}$. Using this computed fracture toughness the second validity requirement is used to determine if this value $K_Q = K_{IC}$. With the requirement being that $2.5 * (K_Q/\sigma_{YS})^2 \leq b_0$, using the material properties at room temperature from Table G.2 and $b_0 = 13.45$mm, yields 16.41mm ≤ 13.45mm, the test specimen does not meet the requirements for a valid LEFM test.

F.1.4. Conclusion

In this specimen the pre-crack crack was relatively large at approximately 11 mm, with the starter notch at 11.4 mm, the total crack initial length was 22.4 mm. With the specimen size W at 36 mm this initial crack was at a ratio of 0.62 of the specimen, with the requirements stating a crack length of between 0.45 and 0.7 W this can still be considered acceptable by the standard however the crack can be considered relatively large.

The fracture is not a typical brittle fracture, as discussed there is some plasticity, and crack growth can can be computed using the compliance of the specimen. The crack growth can be computed from the compliance of the specimen. The negative crack growth however for the initial interpolation points as shown in Figure F.5 is indicative of the fact that the size of the plastic zone in relation to the ligament b is relatively too big. The

results could be used for the construction, yet the data data set is not adequate to evaluate any toughness measures in accordance with the method[9].

Although this initial the test did not allow for a valid estimate of the fracture toughness of the specimen the data generated did provide a proof of concept. The data generated allows for the estimation of the crack size in using the compliance method and provided enough data for the construction of a LLD curve, which in turn could be for the determination of A_{pl} (used to calculate J).

The test however does meet the requirements for a valid LEFM toughness characterisation, where only the requirement on the initial remaining ligament is not met[11]. The test yielded only a valid fracture toughness K_Q = 25.5MPa$\sqrt{m}$. This value is higher than the minimum specified toughness for this material at K_{IC} = 47MPa$\sqrt{m}$ (Table G.2). In this case the large pre-crack made the test invalid for a K_{IC} characterisation of the toughness, yet the test method itself does provide suitable data for a valid LEFM test.

F.2. Cryogenic test - Ti6Al4V-1

This was the second test performed, in this test complete set-up was used and the specimen was cooled to approximately 4 K using liquid helium, for the cooling procedure see [16]. During the cooling the sensor noise increased as the sensors a were cooled, but stabilised relatively fast. As the coolant liquid level had risen to the level of the exhaust the noise signal suddenly increased once more clip gage signal. At this point the coolant flow was stopped and the test was resumed once the noise from this boiling subsided.

F.2.1. Measured data

For this specimen some modifications were made with regards to the testing program, the triple unloading was scrapped from the program, and the load for the first compliance measurement was increased. The captured data is shown in Figure F.8, where the delay shown on the time axis was in order to ensure that the noise from the cooling and boiling was as little as possible.

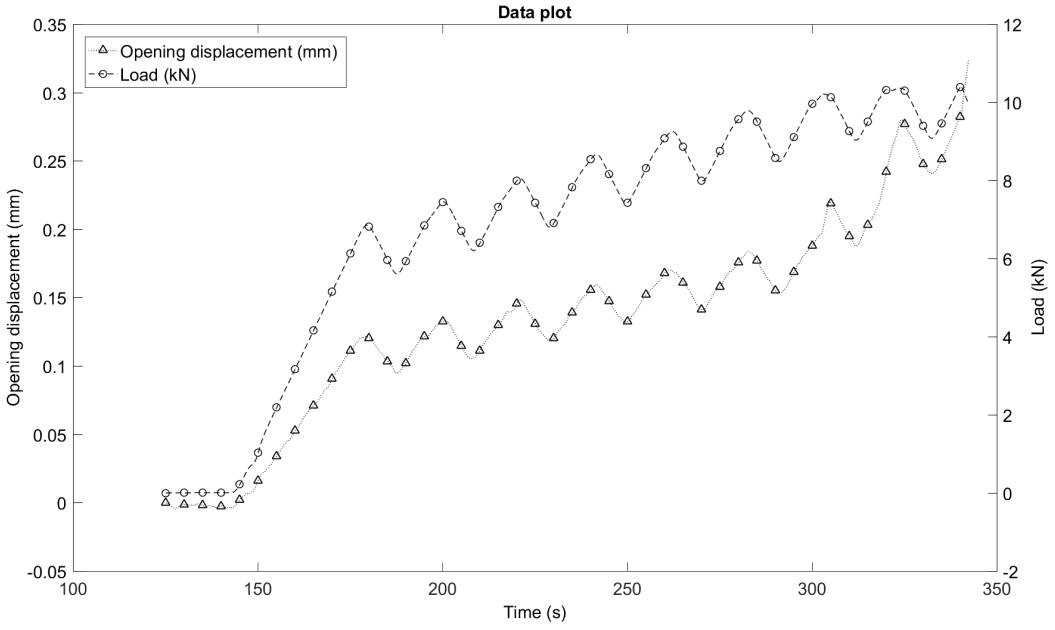

Figure F.8: Measurement data on specimen Ti6Al4V-1

F.2.2. Load-line displacement

The data from the measurement is used to construct a load-line displacement plot (LLD), where the opening displacement measured being the load-line displacement; the advantage of using a C(T) specimen. This LLD plot allows for the characterisation of the fracture toughness as described in the standard [9], the resulting graph is shown in Figure F.9. The data is processed and a least-squares fit is made on the data, for visibility of the fitted curves only one in every forty data points is shown in the right image in Figure F.9.

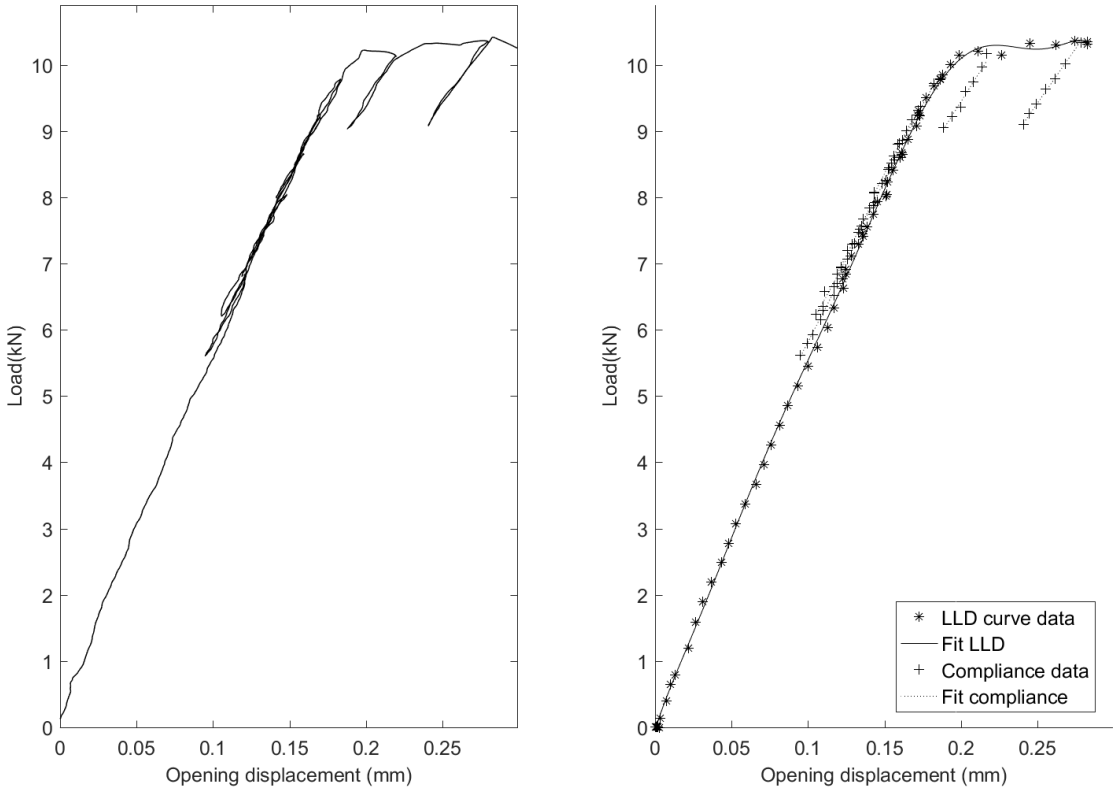

Figure F.9: LLD specimen Ti6Al4V-1 and data fit

In this specimen the fracture can be considered a brittle, especially when compared to the LLD of the room temperature test Figure F.2. In subsection F.1.3 its already shown that the data allows for the measurement of the compliance. Since in this test there are only 2 valid points for the compliance measurement, and the test also shows relatively brittle behaviour, only a LEFM method is used to determine the fracture toughness.

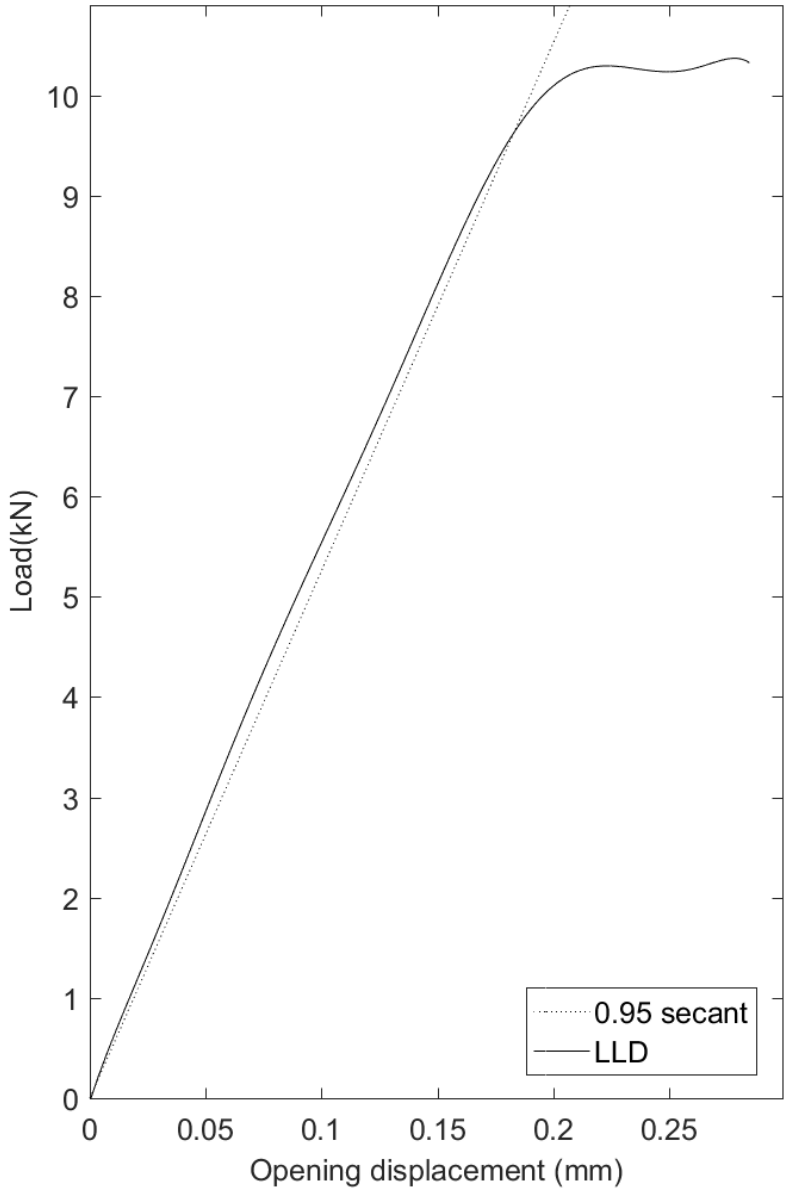

Figure F.10: Ti6Al4V-1 - 0.95 secant line

The test results are initially validated using the requirement on P_Q; the test is a valid test result if the following relation is met: $P_{max}/P_Q \leq 1.10$ (section 9.1.3[11]). In this case $P_Q = 9.63\,\text{kN}$ and $P_{max} = 10.38\,\text{kN}$, resulting in $P_{max}/P_Q = 1.08$; therefore acceptable. Using the load P_Q and the method outlined in the standard for a C(T) specimen the fracture toughness K_Q is calculated; $K_Q = 36.9\,\text{MPa}\sqrt{\text{m}}$. Using this computed fracture toughness the second validity requirement is used to determine if the value $K_Q = K_{IC}$. With the requirement $2.5 * (K_Q/\sigma_{YS})^2 \leq b_0$, using the material properties at 4 K from Table G.2 and $b_0 = 21.6\,\text{mm}$, yields $1.075\,\text{mm} \leq 21.6\,\text{mm}$, so in this case we can consider $K_{IC} = 36.9\,\text{MPa}\sqrt{\text{m}}$. The computed K_{IC} is less than the minimum specified for the material of $K_{IC} = 38\,\text{MPa}\sqrt{\text{m}}$(Table G.2), yet considering uneven pre-crack (section 4.1) and material uncertainty this discrepancy seems negligible.

F.2.3. Conclusion

This specimen showed significantly more brittle behaviour when compared to the roomtemperature test. The test results for this specimen does not allow for a valid J-test. The test result did however yield suitable data for a LEFM K_{IC} test, with the computed at $K_{IC} = 36.9\,\text{MPa}\sqrt{\text{m}}$.

F.3. Cryogenic test - 316LN-1

This was the first cryogenic test performed using a specimen fabricated in stainless steel 316LN. This material typically possesses excellent toughness even at low temperatures, and therefore should be suitable for a J-test.

F.3.1. Measured data

As expected the estimated maximum load section 2.3 based on previous samples was grossly exceeded, which in large part can be contributed to the small pre-crack. As the modified specimen was used the design however was able to cope with the higher load, allowing for loads up to 92 kN at 4 K. In the end however the test was aborted as the load increased to 80 kN, yet the initial data as seen in Figure F.11 seemed sufficient for a J-test, the gross non-linearuity towards the end of the test.

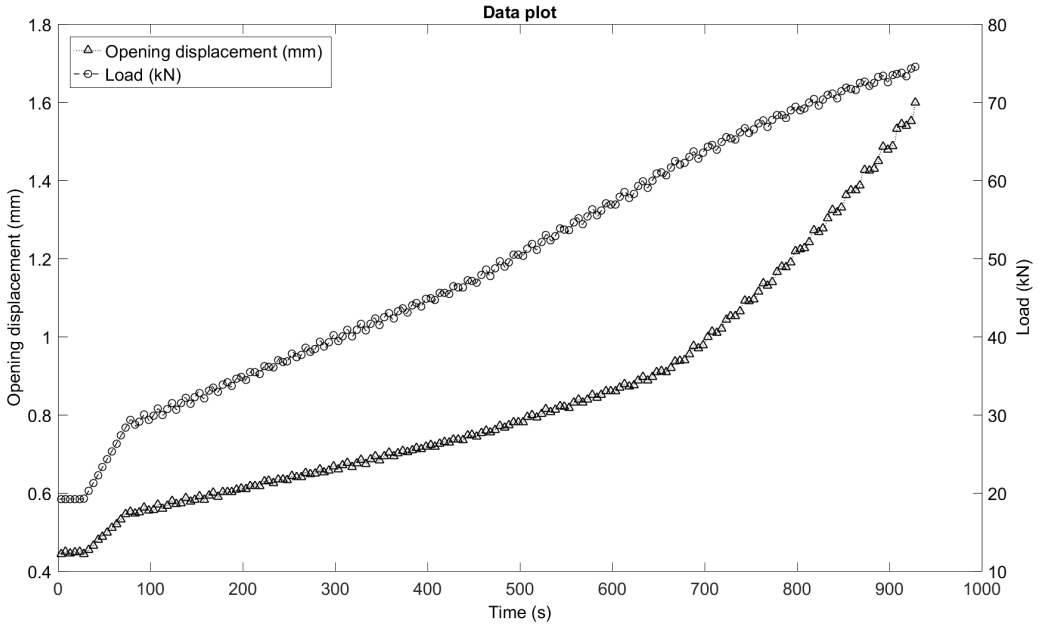

Figure F.11: Measurement data on specimen 316LN-1

F.3.2. Load-line displacement

As in previous sections (subsection F.2.2 & F.1.2) for the Ti6Al4V specimen, a load-line-displacement curve is constructed from the measurement data, shown in Figure F.12. The unloading cycle from for the complaince method is relatively small with regards to the magnitude of the load. initially this was considered of little importance as for the previous samples the magnitude of the unloading was sufficient to capture the compliance at each of the interpolation points. The compliance data from the measurement is filtered out and a fit on the LLOD data is performed, and all the interpolation points. Upon inspecting the LLD and computed stiffness at the interpolation points the magnitude of the unloading seemed too little in order to capture the stiffness accurately. The measured stiffness at each of the points is shown in Figure F.13, as can be seen even at the initial compliance measurements, and as these points are within the elastic region of the test it can be expected to be somewhat constant.As the compliance at each of the points is unreliable any J-test value found for this specimen would be unreliable, as the crack size at each of these points can not be accurately determined.

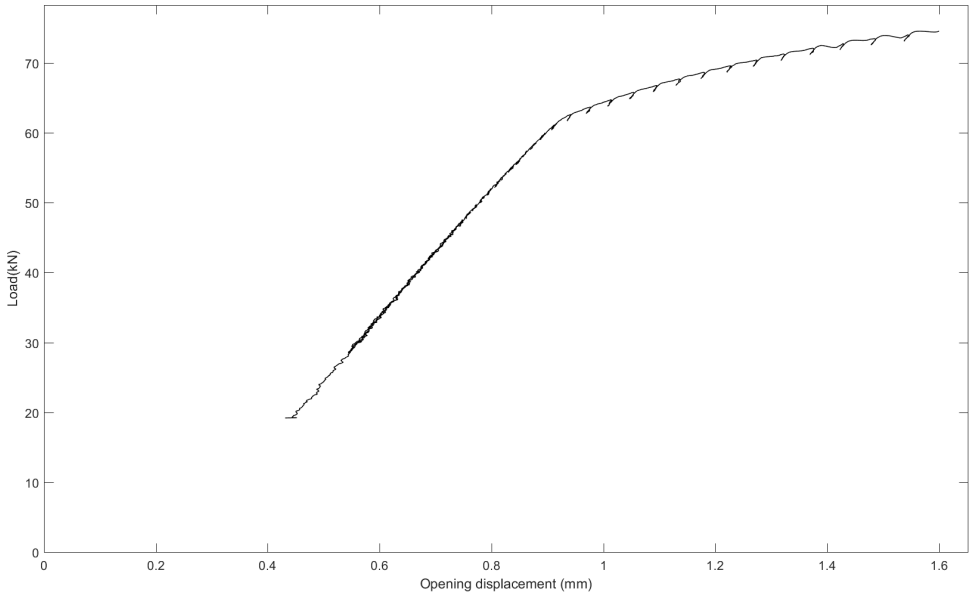

Figure F.12: LLD specimen 316LN-1

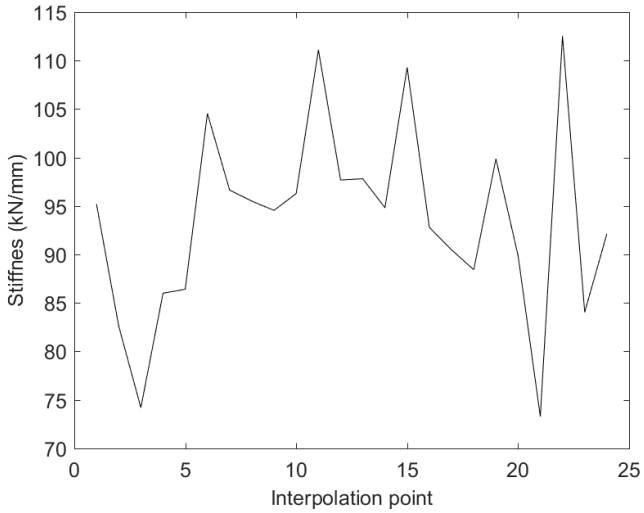

Figure F.13: Stiffness at interpolation points 316LN-1

F.3.3. Conclusion

This first test at 4 K with this material did not yield significant results, due to the limited unloading for the compliance method. The signal contained some noise, yet this should pose little prblem when extracting the relevant information, with sufficient unloading.

F.4. Cryogenic test - 316LN-2

This was the second cryogenic test performed using a specimen fabricated in stainless steel 316LN, and as was noted for the first sample the unloading for the compliance was increased (subsection F.3.3), and some other minor tweaks to the program.

F.4.1. Measured data

The specimen was tested using the program, the test bench however had a crash, hence the jump in the measurement capture around 16 minutes into the test (which was done with a different system). After a reboot of the test bench the test was resumed, and the subsequently aborted as the load reached over 70 kN, as shown in Figure F.14. The measurements shown in the figure are plotted with thick marks every 300 data points. In retrospect the test might have been continued till specimen failure as little increase in load was to be expected, and there was still some margin with respect to the maximum load of 92 kN (Table 3.1). However considering the amount of opening displacement measured the test was expected to yield sufficient data points for a JR curve.

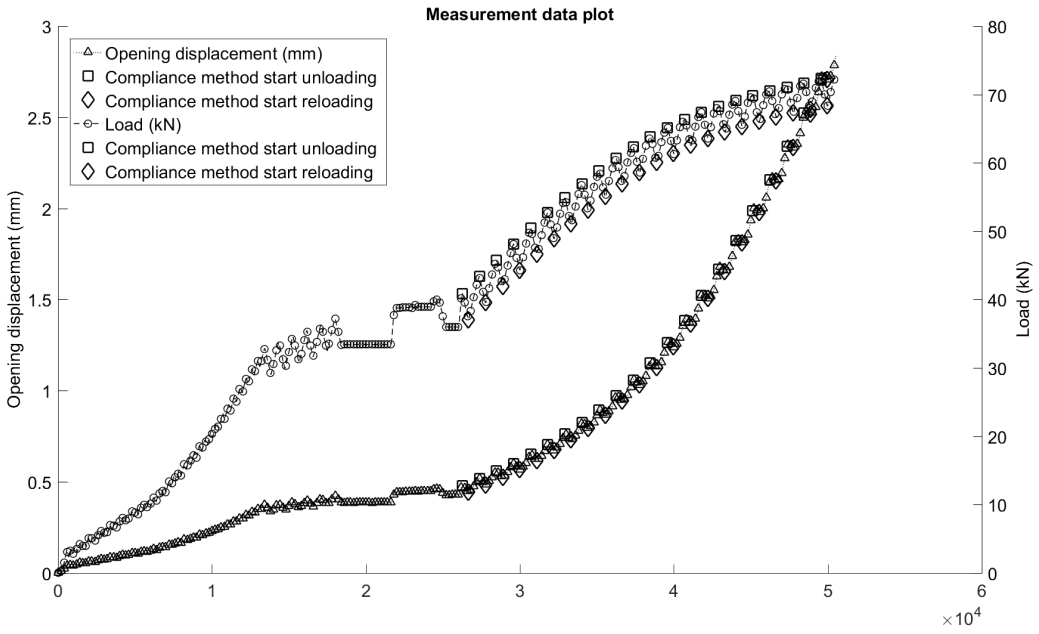

Figure F.14: Measurement data on specimen 316LN-2 with compliance interpolation points highlighted

F.4.2. Load-line displacement

The data load is once again set-out against the load line opening displacement and the resulting LLD is shown in Figure F.15. A minor correction was required to correct for the crash of the system, and aside from that than that the resulting LLD can be seen to be relatively unaffected. With the modification to the testing program the extraction of the compliance and LLD curve could be performed automatically with the fitted curves and lines shown in Figure F.15.

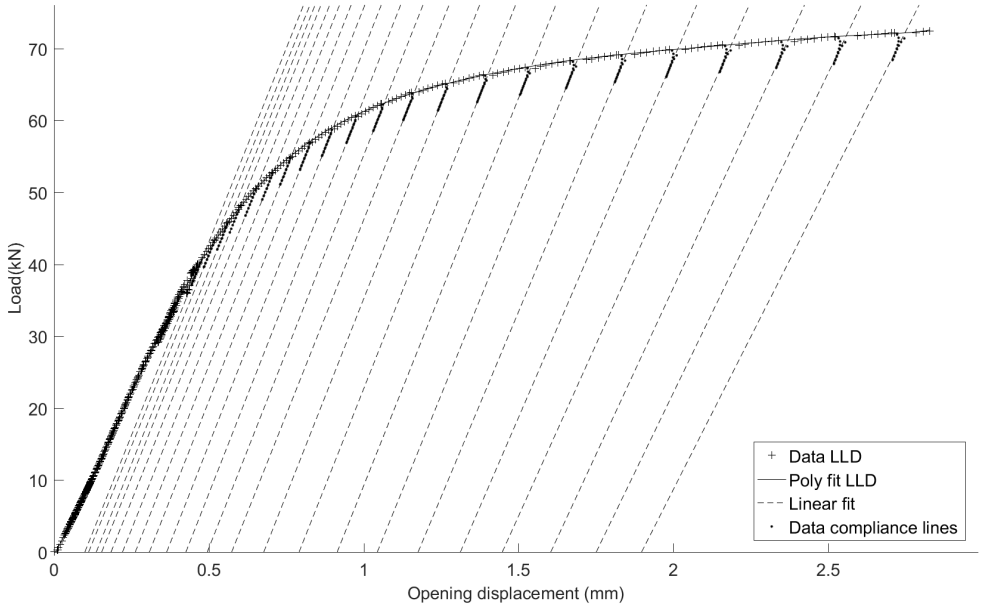

Figure F.15: LLD specimen 316LN-2 with stiffness interpolation lines

The compliance of the specimen processed in accordance with the standard[9], and an estimate of the crack size is calculated for each of the compliance points; the estimated crack size is shown in Figure F.16. The initial crack size a_0 is 12.4 mm, starter notch + pre-crack (averaged), and the estimated crack size at the start of the compliance measurement is approximately 12.8 mm. There is some minor negative crack growth at the beginning of the test, this is corrected using least squares fir as outlined in section A9.3.3.1[9], which the line titled adjusted crack size in Figure F.16.

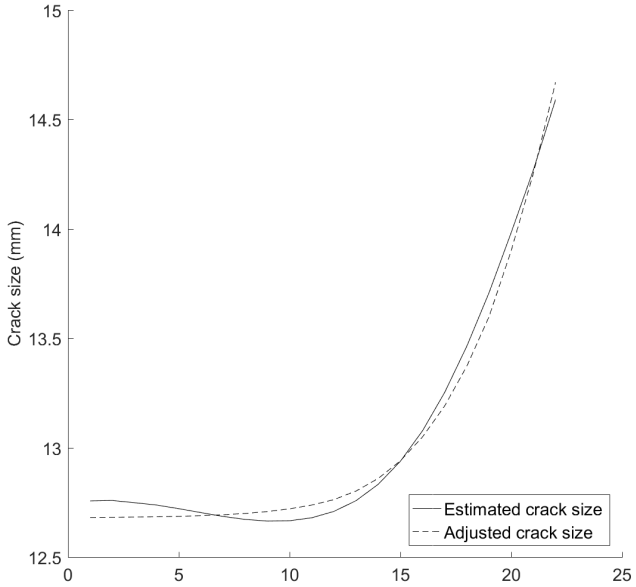

Figure F.16: Specimen 316LN-2 - Crack size estimate

The adjusted crack size is used in conjunction with the competed J values at each step to generate the J resistance curve shown in Figure F.17. The acceptable data for the estimation of J_Q is also shown in the figure,

wit hthe construction line and 0.2 mm crack extension offset line. The value of J_Q is computed for the fit to the acceptable data and the 0.2 mm offset line; $J_Q = 1014.8\,\text{kJ/m}^2$.

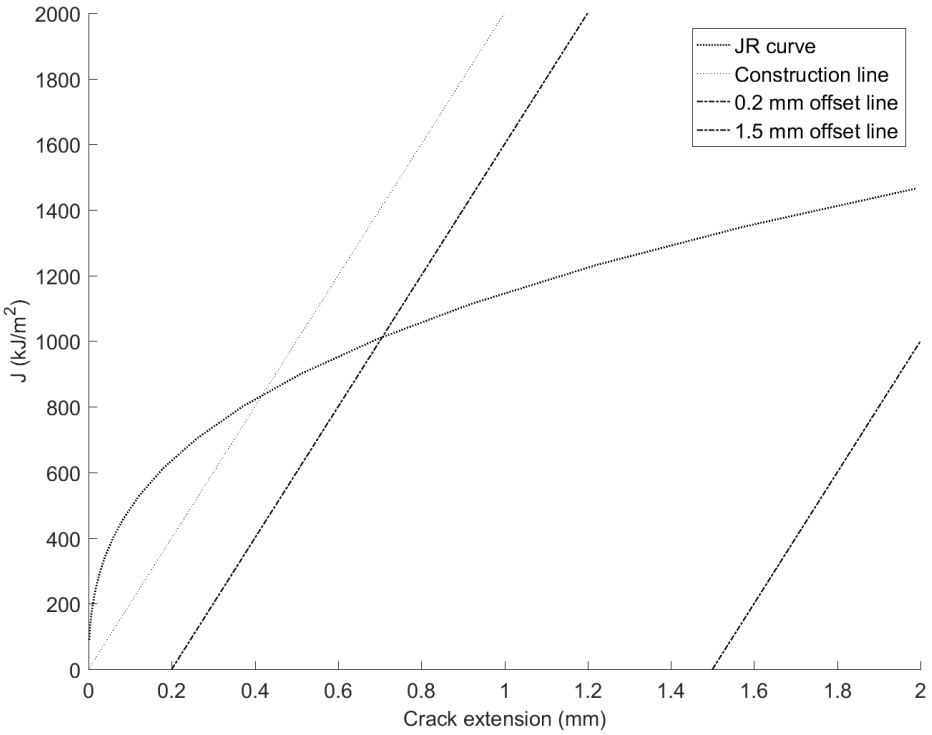

Figure F.17: J-R curve specimen 316LN-2

The design of the specimen took into account the validity requirements 2.2.2, for J_Q as a size independent value of the fracture toughness; J_{IC}. With the validity requirement:

$$B, b_0 \geq 10\ J_Q/\sigma_y \tag{F.1}$$

For this specimen $b_0 = 23.6$ mm, and $B = 10$ mm; thickness of the specimen is governing for the validity of the test for $J_{IC=J_Q}$. Using the value for J_Q, the thickness B and the yield stress of the material in Equation F.2 results in:

$$10 \times 10^{-3}\,\text{m} \geq 10\ \frac{1014.8\,\text{kJ/m}^2}{1000\,\text{MPa}} \tag{F.2}$$

Evaluating Equation F.2 the validity requirement is not met, yet considering the fact that the minimum required yield stress for the material is used in this evaluation it would likely pass this requirement if the actual yield stress of the specimen was used.

$$10 \times 10^{-3}\,\text{m} \ngeq 10.15 \times 10^{-3}\,\text{m} \tag{F.3}$$

As the validity requirement is not met the calculated J_Q can not be considered as a thickness independent value. The J_Q is used to compute the equivalent LEFM fracture toughness value K_{JQ}, where $K_{JQ} = \sqrt{J_Q \times \frac{E}{1-\nu^2}}$; evaluating the expression yields $K_{JQ} = 469.27\,\text{MPa}\sqrt{\text{m}}$.

F.4.3. Conclusion

The test set-up with a larger magnitude on the unloading cycle for the compliance method allowed for a measurement of the fracture toughness. The computed fracture toughness value is strictly speaking not comparable with the K_{JIC} listed in Table G.1 as the validity requirement is not met. Considering the low yield stress used in the evaluation of the validity it is considered reasonable to do so for the purposes of validating the test set-up.

For this specific material some fracture toughness results where found in literature, these values ranged greatly and in some the value might be considered not to be thickness independent. For this material a fracture toughness of around 275 MPa$\sqrt{\text{m}}$, was to be expected, the calculated toughness was $K_{\text{JQ}} = 469.27\,\text{MPa}\sqrt{\text{m}}$. Though there seems to be a large discrepancy with regards to the value from literature this value does not seem unreasonably large, especially not when compared to the $K_{\text{JIC}} = 430\,\text{MPa}\sqrt{\text{m}}$ 316 annealed at 4 K Table G.1.

G

Material Properties

Table G.1: Austenitic stainless steels

	ρ (kg/m^3)	ν	E (GPa)	Yield stress Rp 0.2% (MPa)	Ultimate tensile stress (MPa)	Elongation (%)	Fracture toughness (MPa$\sqrt{\text{m}}$)	Thermal conductivity (W m^{-1} K^{-1})	Thermal expansion ($\times 10^{-6}$ K^{-1})	Specific heat (J kg^{-1} K^{-1})	Specific resistance (nΩ m)
304 annealed [a, b, c]											
295 K	7860	0.290	200	227.5	586.1	60		14.8	15.8	468	717
77 K		0.278	214	393.7	1416.9	43		8.07	6.4	188	527
4.2 K		0.279	210	439.2	1685.8	48		0.227	0.1	1.88	490
310 annealed [a, b, c]											
295 K	7850	0.305	191	310.3	655.0	60	150	12.1	15.8	469	889
77 K		0.295	205	585.4	1095.9	54	220	6.48	6.9	189	724
4.2 K		0.292	207	796.3	1223.8	56	210	0.357	0.2	2.24	683
316 annealed [a, b]											
295 K	7970	0.294	195	240	600	59	350	15.2	15.8	487.0	772
77 K		0.283	209	570	1300	59	510	7.92	6.9	205.0	568
4.2 K		0.282	208	700	1600	52	430	0.273	0.2	1.95	540
316LN annealed											
295 K[d]	7990	0.305	195	510	720	35					
77 K		0.292	199	800	1000	30					
4.2 K [e, f]		0.288	199	1000	1500	28	140-275				

[a] Thermal and electrical properties at specified temperatures from CryoComp[3]

[b] Density, Young's modulus, fracture toughness; from Ekin[13] and references listed therein

[c] Mechanical properties: yield stress and elongation from Flynn [14]

[d] The values at room temperature are the minimum from specification N° 1000 - Ed. 5[7] for 316LN: the yield (Rp 0.2%), ultimate tensile stress (UTS) and the elongation.

[e] Mechanical properties at 4.2 K from approximate values from Sas et al. [23]

[f] Approximate values for the fracture toughness at 7 K from Nyilas et al. [19]

Table G.2: Titanium alloys

	ρ (kg/m^3)	ν	E (GPa)	Yield stress Rp 0.2% (MPa)	Ultimate tensile stress (MPa)	Elongation (%)	Fracture toughness (MPa$\sqrt{\text{m}}$)	Thermal conductivity (W m^{-1} K^{-1})	Thermal expansion ($\times 10^{-6}$ K^{-1})	Specific heat (J kg^{-1} K^{-1})	Specific resistance (nΩ m)
Ti6Al4V [g]											
295 K [h]	4540	0.342	114	830	1170	15	47	7.57	7.9	536	1700
77 K		0.327	118	1300	1480	17	38	3.37	3.39	217	1500
4.2 K [i]		0.311	119	1780	1860	18	38	0.403	0.1	0.066	0

Table G.3: Maraging steel

	ρ (kg/m^3)	ν	E (GPa)	Yield stress Rp 0.2% (MPa)	Ultimate tensile stress (MPa)	Elongation (%)	Fracture toughness (MPa$\sqrt{\text{m}}$)	Thermal conductivity (W m^{-1} K^{-1})	Thermal expansion ($\times 10^{-6}$ K^{-1})	Specific heat (J kg^{-1} K^{-1})	Specific resistance (nΩ m)
18%Ni (Type 300) [j]											
295 K	8000	0.314	189.6	1900	1980	15.5					
77 K		0.307	194.3	2340	2475	10.0					
4.2 K		0.312	196.4	2375	2685	0.922					

[g] Thermal and electrical properties at specified temperatures from CryoComp[3]
[h] Density, Young's modulus, fracture toughness; from Ekin[13] and references listed therein
[i] Yield stress, UTS, and elongation listed are at 29 K (-254 °C), the properties at 4 K are considered to be similar
[j] Mechanical properties from NASA-TN-D-7532[1]

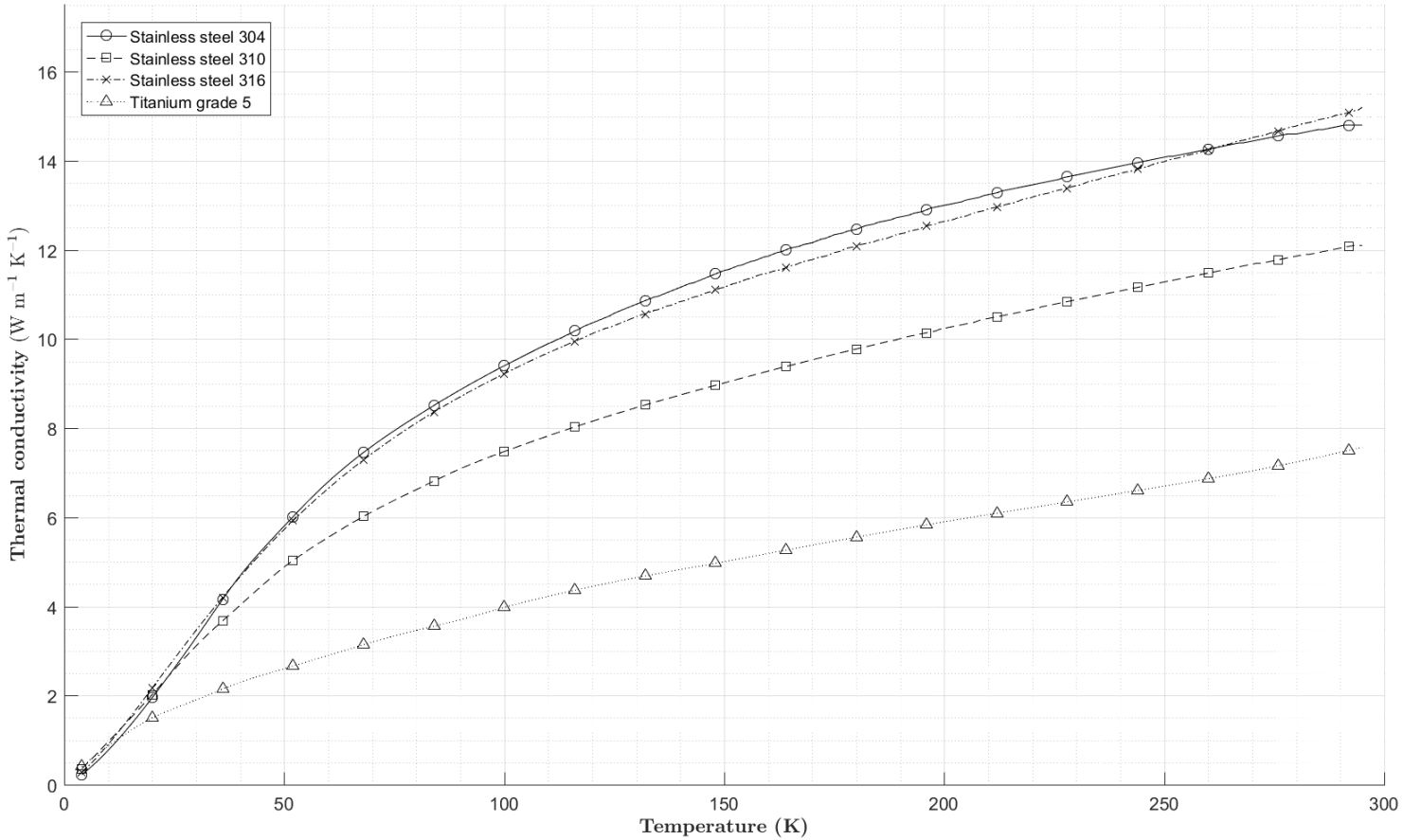

Figure G.1: Thermal conductivity

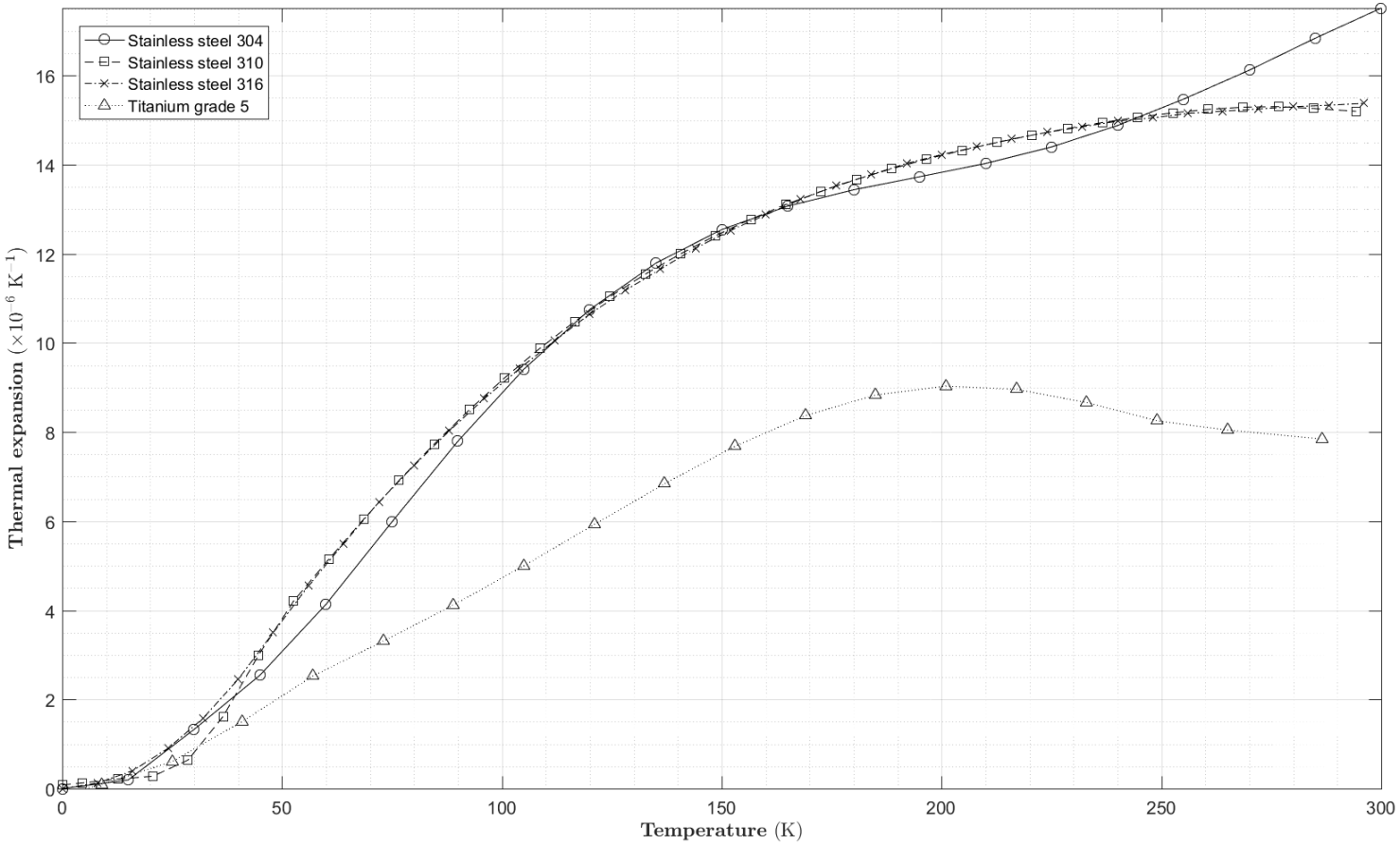

Figure G.2: Thermal Expansion

H

Precracked specimen

As briefly discussed in section 4.1 the starter notch in the initial drawings contained an error resulting in a shorter notch than desired. This was attempted to be corrected with the pre-cracking, to ensure a total crack depth which was equal to the minimum specified in the standards.

The pre-cracking of the specimen was performed at an external company, where they seemed to have encountered some difficulties realizing the pre-crack. Though no explanation was provided it can be assumed that some misalignment was present in the set-up used from the uneven crack depth on either sides of the specimen (as listed in Table H.1 and Table H.2).

H.1. Stainless steel

The initial crack depth is measured on both sides of the specimen from the pre-notch, for the images of the specimen refer to Figure H.1 through H.8, and for the measured depth see Table H.1.

Table H.1: Depth pre-crack 316LN specimen

specimen	**L**	**R**
316LN-1	1690 µm	1190 µm
316LN-2	1450 µm	550 µm

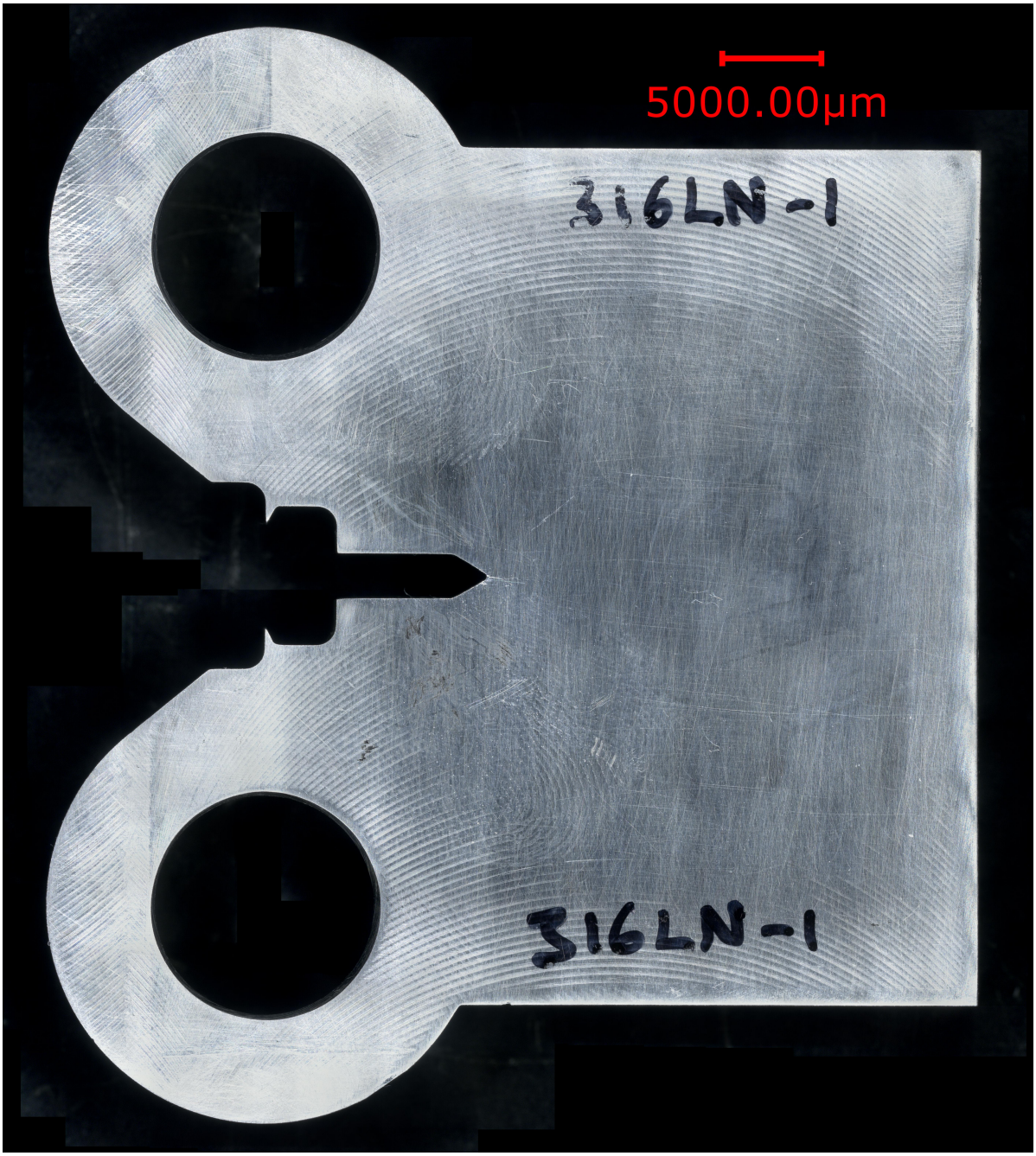

Figure H.1: 316LN specimen 1 - left side

Figure H.2: 316LN specimen 1 - right side

Figure H.3: 316LN specimen 1 - detail left side

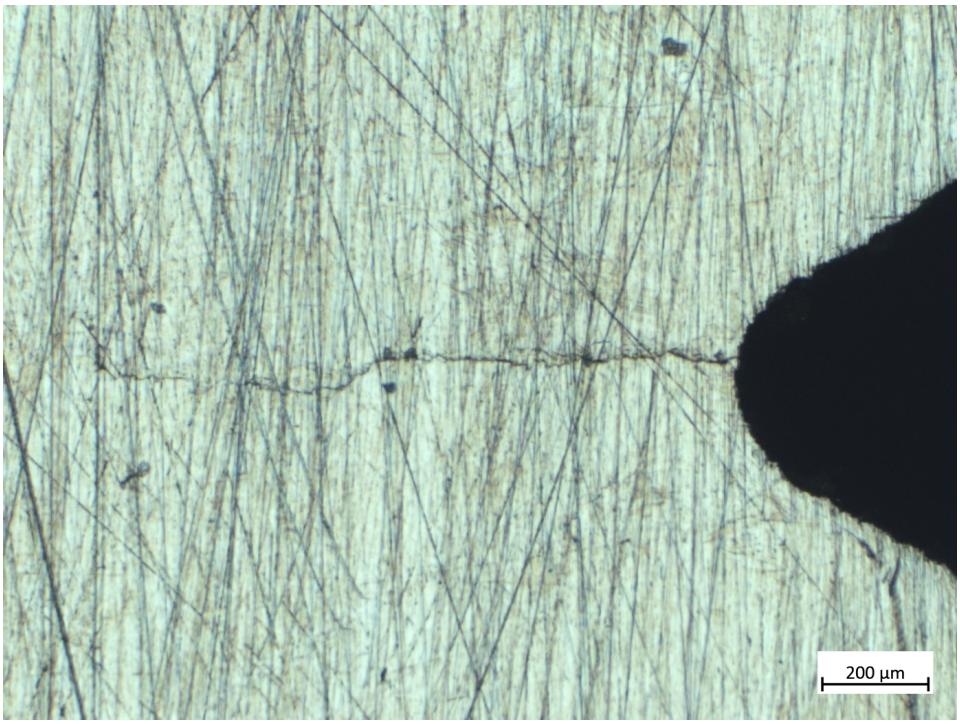

Figure H.4: 316LN specimen 1 - detail right side

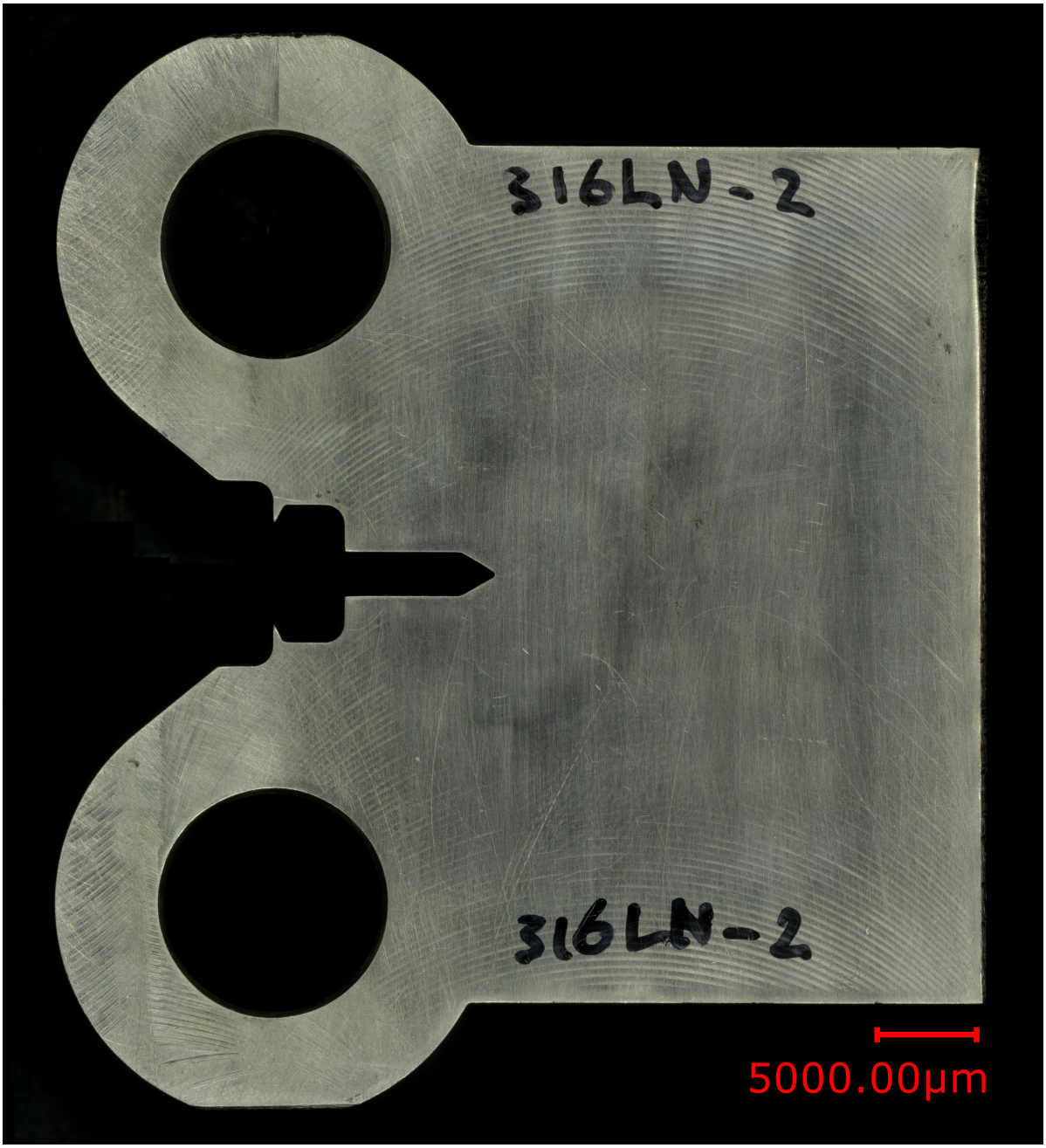

Figure H.5: 316LN specimen 2 - left side

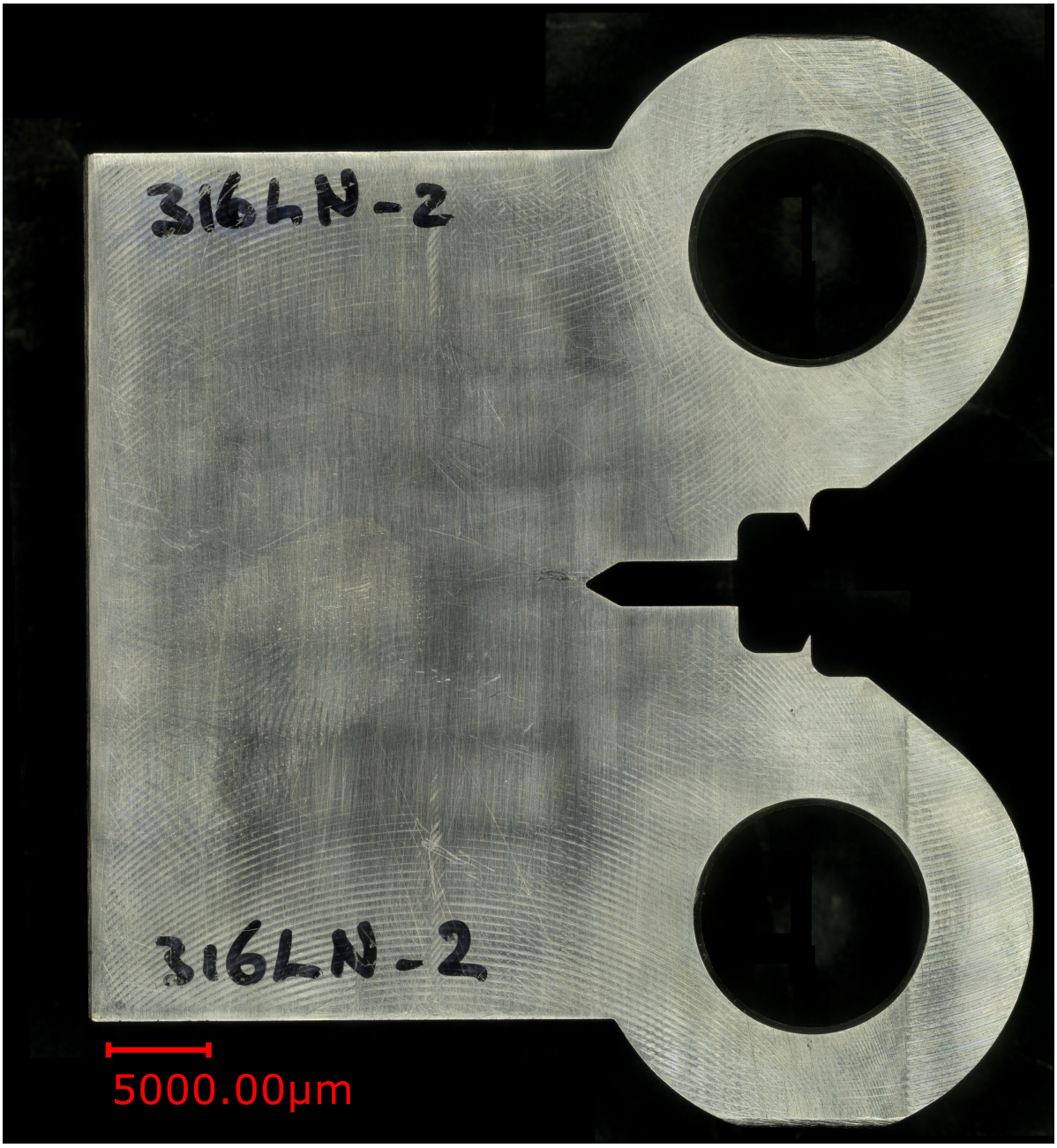

Figure H.6: 316LN specimen 2 - right side

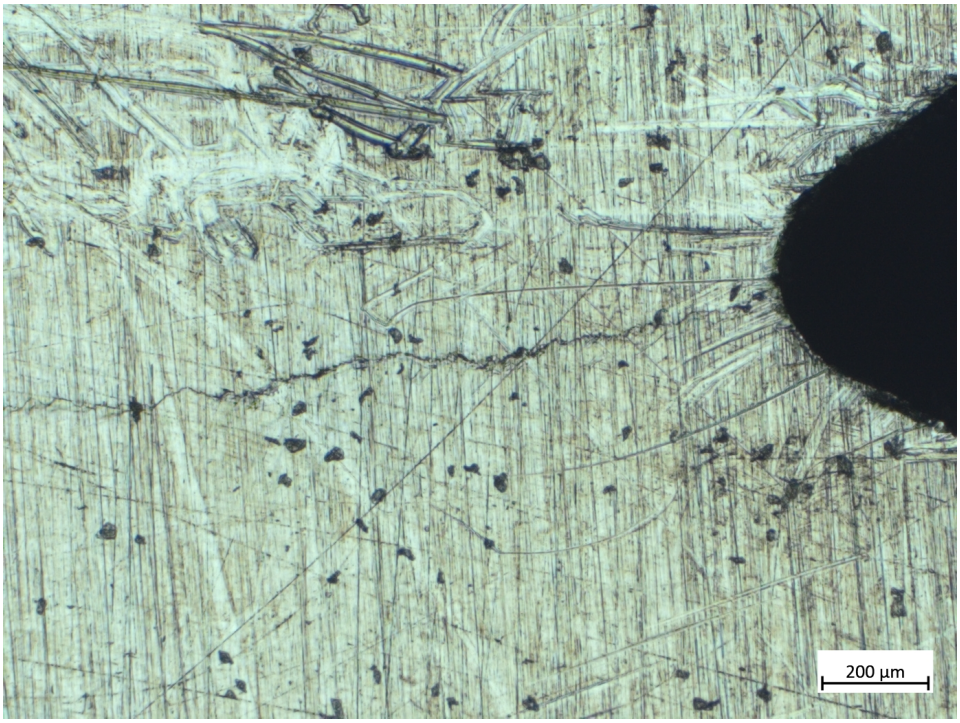

Figure H.7: 316LN specimen 2 - detail left side

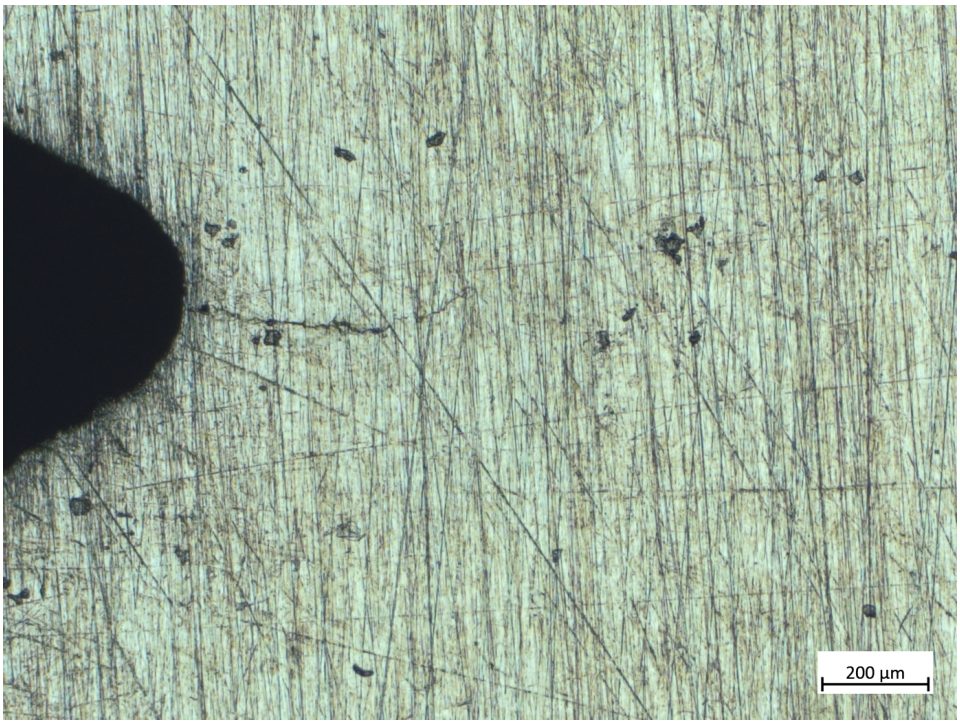

Figure H.8: 316LN specimen 2 - detail right side

H.2. Titanium grade 5

The initial crack depth is measured on both sides of the specimen from the pre-notch, for the images of the specimen refer to Figure H.9 through H.14, and for the measured depth see Table H.2.

Table H.2: Depth pre-crack Ti6Al4V specimen

specimen	L	R
Ti6Al4V-1	4180 µm	1802 µm
Ti6Al4V-2	11600 µm	10700 µm

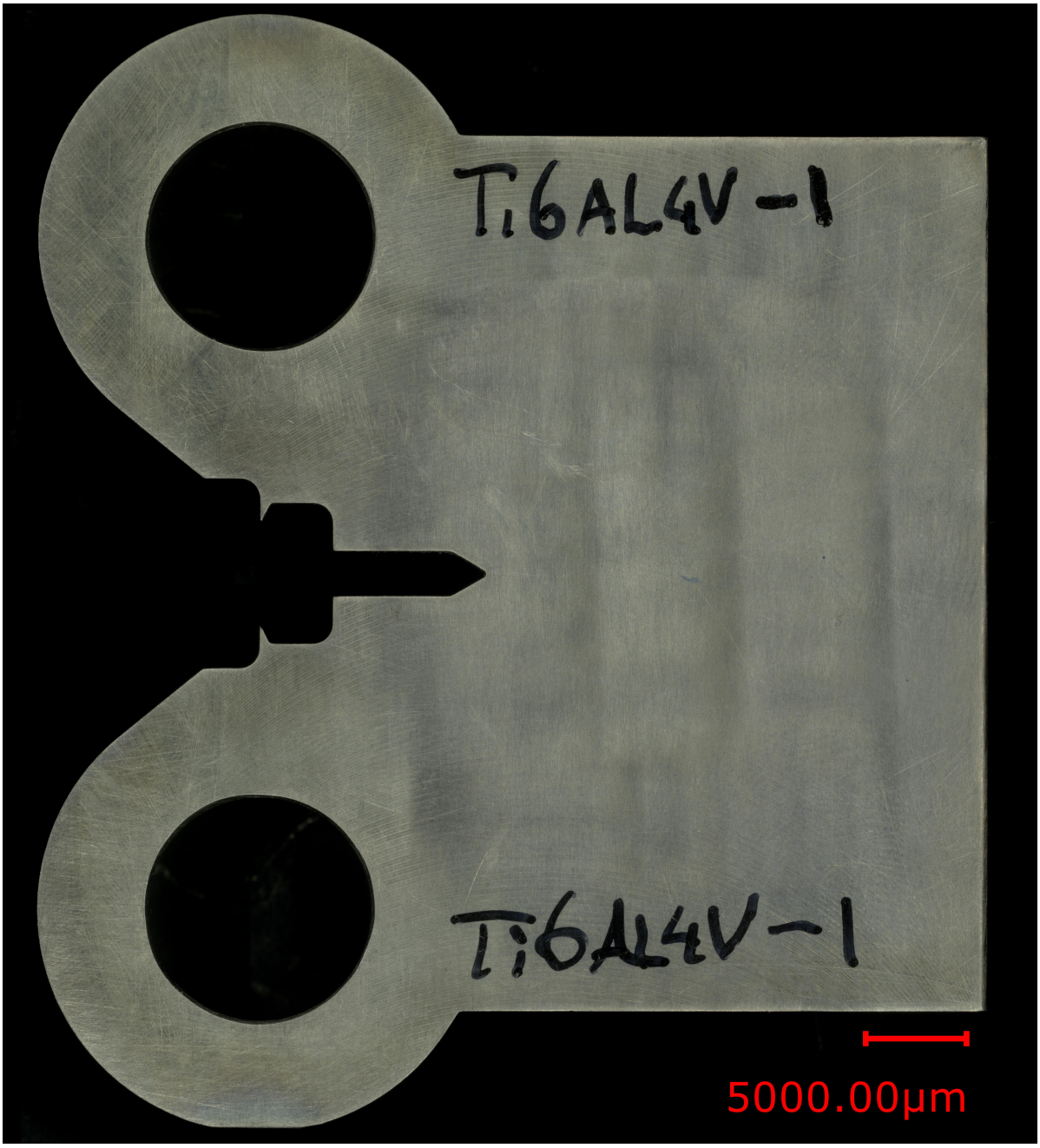

Figure H.9: Ti6Al4V specimen 1 - left side

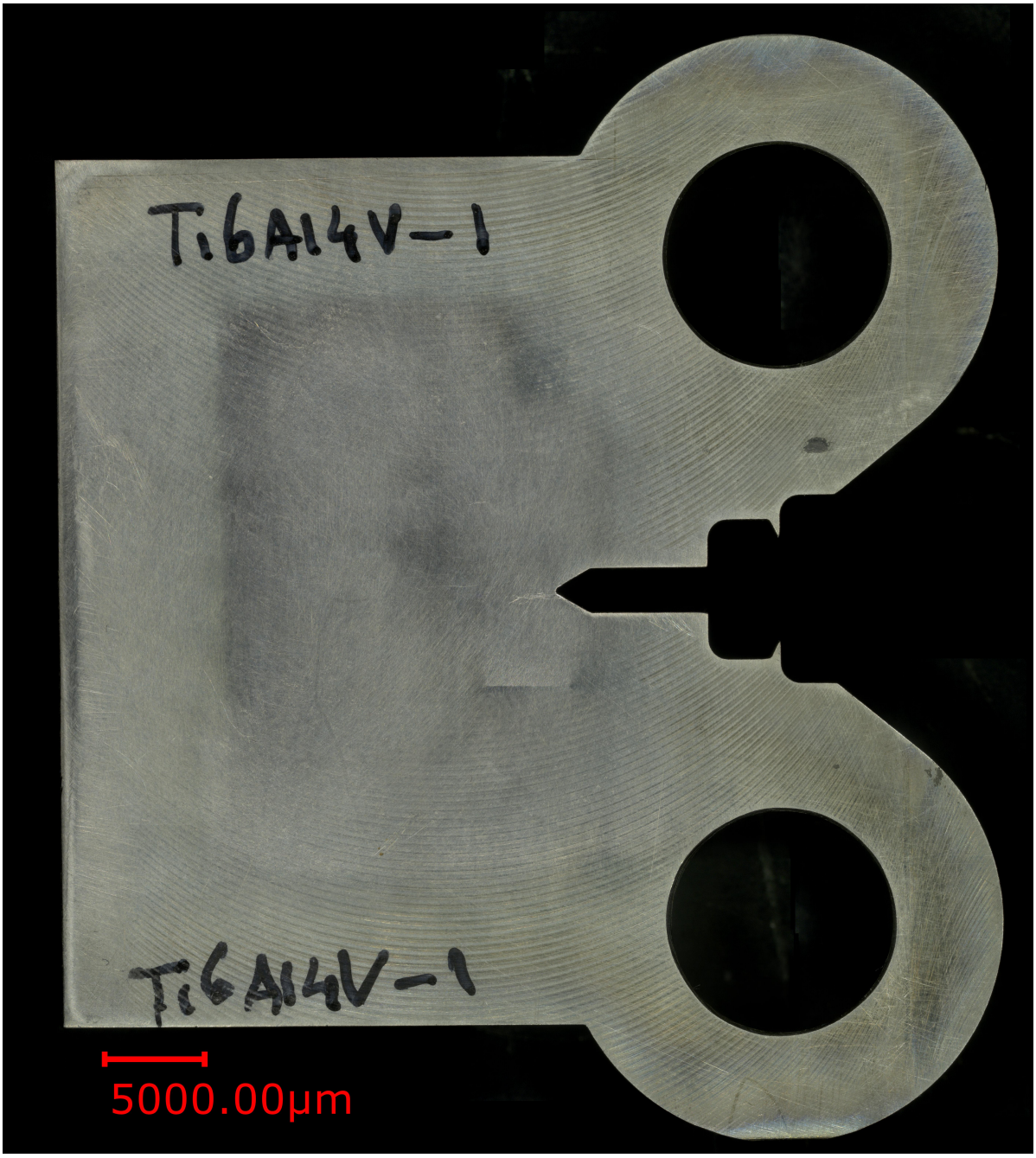

Figure H.10: Ti6Al4V specimen 1 - right side

Figure H.11: Ti6Al4V specimen 1 - detail left side

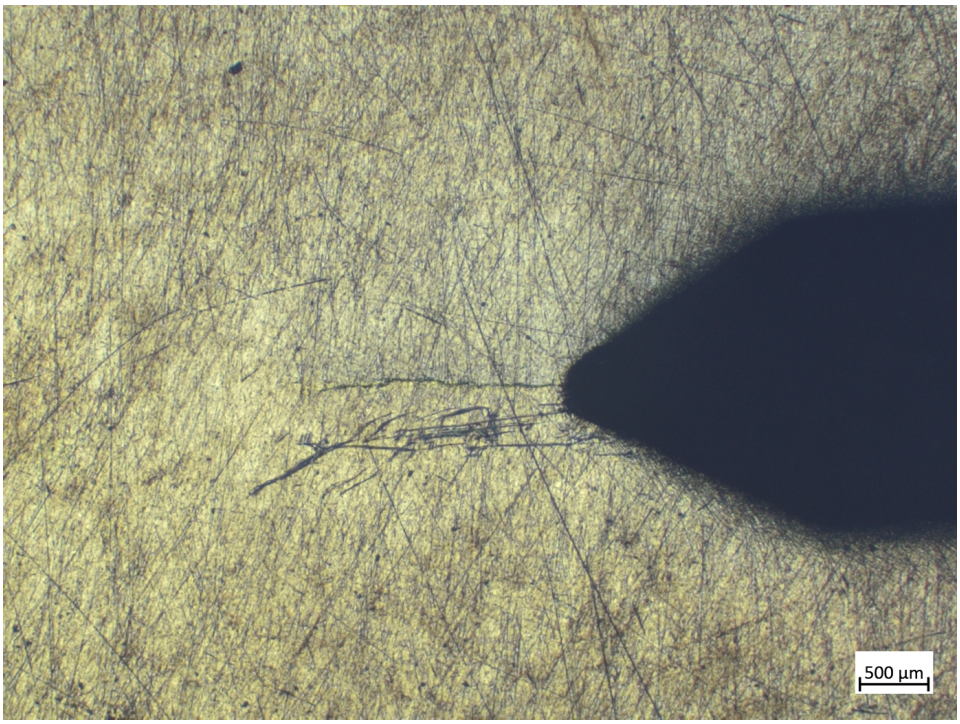

Figure H.12: Ti6Al4V specimen 1 - detail right side

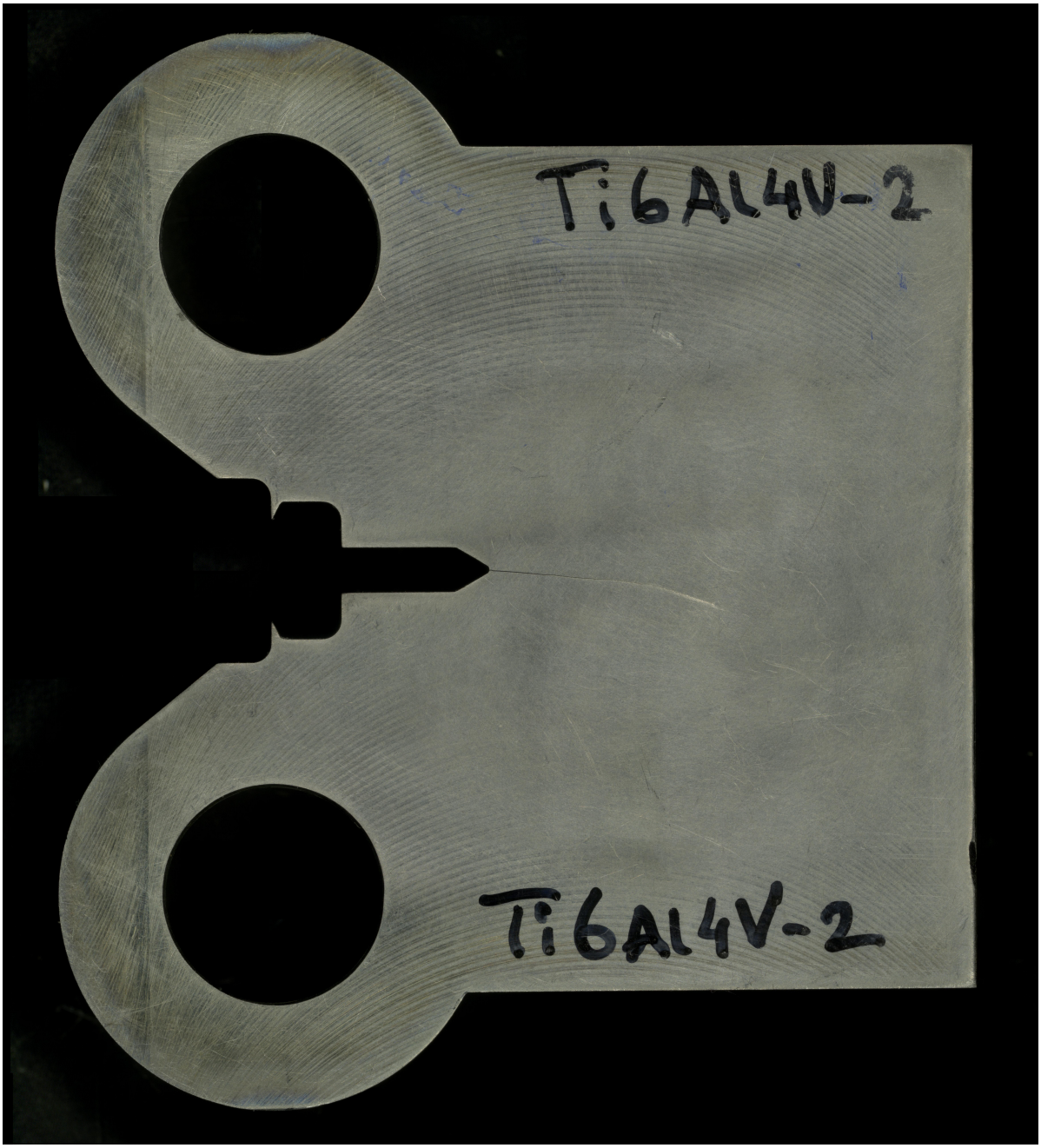

Figure H.13: Ti6Al4V specimen 2 - left side

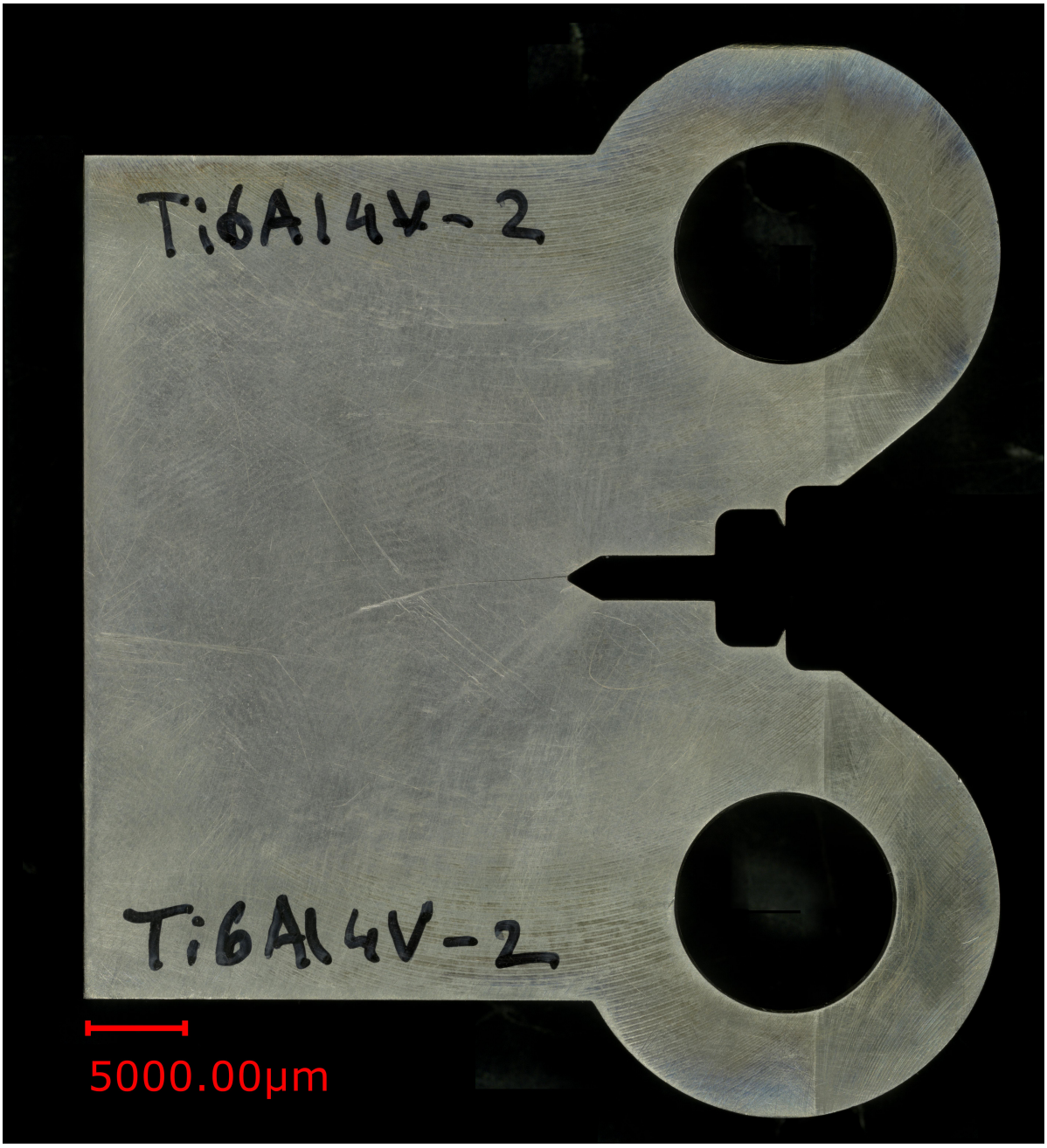

Figure H.14: Ti6Al4V specimen 2 - right side